HYDROGEOCHEMICAL ASSESSMENT, WATER TREATMENT AND REVALORIZATION OF DUMPS, TAILINGS AND DRAINAGES PRODUCED AT PHALABORWA INDUSTRIAL COMPLEX

Alba Gómez-Arias

Submitted in fulfillment of the requirements for the degree

Philosophiae Doctor

In the faculty of Natural and Agricultural Sciences

Institute for Ground Water Studies

University of the Free State

Bloemfontein, South Africa

In collaboration with the Faculty of Experimental Science

Department of Earth Sciences

University of Huelva

Huelva, Spain

2020

Promotors: Prof Danie Vermeulen and Prof Jose Miguel Nieto Liñán

Declaration

I, Alba Gómez Arias, hereby declare that the present thesis, submitted to the Institute for Groundwater Studies, Faculty of Natural and Agricultural Sciences, University of the Free State, Bloemfontein, South Africa, and to the Department of Earth Sciences, Faculty of Experimental Science, University of Huelva, Huelva, Spain, is my independent work and I have not previously submitted it for any degree or examination at any other university, and that all the sources used or quoted herein have been indicated and acknowledged in the text and in the list of references.

A mis padres,

Angela y Pepe.

A mis amores,

Julio y Delia.

“It always seems impossible until it's done.”

(Nelson Mandela)

AKNOWLEDGMENT

I would like to express my sincere gratitude to the people that contributed in some way to the success of this study:

To my supervisors, prof Danie Vermeulen and prof Jose Miguel Nieto, for their continuous support and assistance during this joint venture between two Universities, two countries, two continents.

To the person who sparked this study, prof Esta van Heerden, for being the first one believing in me, for the opportunity, for the lessons.

To Mark Surmon, Joseph Muhlarhi and Linda Desmest for the information and assistance during the samplings at Palabora Mining Company.

To Adolf Delport and his colleagues for the information and assistance during the samplings at Foskor.

To Emile Corradi and his colleagues for the information and assistance during the samplings at Bosveld Phosphate.

To Eelco Lukas for your inestimable lessons with WISH.

To Lore-Mari Deysel and Ayanda Hadebe for their help with the water analyses.

To each and every one of my lab-mates for their contributions, conversations, laughs and emotional support.

To Lola Yesares for your inestimable help with the sampling, the mineralogy and the articles, but most of all for your friendship over the years and over the countries.

To Manu Caraballo because your contributions improved each of the articles integrated in this manuscript.

To Jou-An Chen for your keenly awaited visits and unforgettable conversations.

To Maleke bis for your help during the sampling and your tolerance with my driving.

To my fantastic brothers Kay Kuloyo and Borja Linares for the fire and the strength that made me feel at home.

To Ana for your listening and your help when I needed it the most.

Last but not the least, I would like to thank my family for supporting me throughout writing this thesis, particularly my mum, Angela, thanks for everything you have done for me this difficult year. To my dad Pepe, thanks for your support throughout

my career. To my beloved Julio and Delia: Julio thanks for your support and your help, you're an inspiration to work hard and resiliently. Every piece of advice, every discussion, every word, every minute, every grain of rice got me closer to write the last word of this manuscript. And Delia, thanks for your understanding, your patience and your unvaluable time. I'm finally done, it's time for us to enjoy every minute this thesis has stolen from us.

This research was conducted under the ERAMIN project AMDREY -PCIN2015-242-256, financially supported by the Department of Science and Technology, South Africa. It was also partially financed by: The Department of Microbial, Biochemical and Food Biotechnology; project MOS (grant number CGL2016-79204-R), which is supported by the Spanish Government; CORFO and Codelco (project CORFO-16PTECME-66524); project CONICYT/PIA Project AFB180004; UNESCO (UNESCO-IUGS-IGCP-Project 682) and Science Foundation Ireland (grant number 18/IF/6347).

ABSTRACT

The Phalaborwa Industrial Complex is formed by several mines and factories that extract value out of the geological formation named Phalaborwa (or Palabora) Igneous Complex (PIC). The industrial activity started in 1950's with the extraction of phosphate rocks and Cu. Since then, more than 4500 Mt of solid waste enriched in magnetite, Zr, Ni, Au, Ag, Pt and rare earth elements (REE), the latter unexplored yet, have been accumulating in PIC area in the form of tailings and waste rock dumps, as well as above 3 Mm^3 of industrial wastewater, including rock drainages and process water, as described in chapter 1. Due to the industrial activities, the water quality of the aquifers underneath PIC has been deteriorated reaching up to 10 g/L of sulphate, particularly surrounding the impoundment dams of the phosphoric acid plant from the fertilizer industry. Chapter 2 introduces the study area and addresses the groundwater quality at PIC and the efforts to restrain the contamination plume by using abstraction boreholes, which resulted in a continuous rise of pollution within PIC facilities but it helped to control the migration of the plume beyond the industrial area. In addition, chapter 3 describes the state of the art in passive water treatments that might deal with such water pollution.

However, this study goes beyond the environmental assessment, it is a comprehensive evaluation of PIC's wastes, which led to the revalorization of the mining wastes as potential REE resources and as neutralization reagent and culminated with the design of a system that would bring benefit from both characteristics of the wastes. Chapter 4 encompasses a mineralogical and geochemical study of the PIC's mine wastes that assessed all the waste rock dumps and tailings. The study was conducted under the hypothesis that the abundance of REE from the ore and host rocks mined from PIC might be preserved or even enriched in the mining wastes. The abundance of REE minerals (mainly monazite) and REE-bearing minerals (mainly fluorapatite, calcite and dolomite) confirmed that hypothesis and suggests the economic potential of PIC wastes as secondary source of REE. The most profitable REE are Nd, Dy, Pr and Tb (87% of net value). The tailings are economically more attractive than the WRDs because the mineral

processing has generated tailings of mostly monomineralic particles enriched in REE.

The environmental characterization of PIC wastes, described in chapter 5, was carried out in order to evaluate its potential as neutralizing reagent for passive water treatment. The mining waste used to treat acid industrial wastewater (AIW) need to accomplish two main characteristics i) high neutralization potential and ii) low toxicity. National and international procedures were carried out to assess the neutralization potential and the toxicity of the leachate that could be released from each rock and each tailing. The results of this investigation showed that none of the PIC rocks have the potential to produce acid rock drainage. It also demonstrated that the carbonatite rocks and the tailings from the copper plant (herein named East tailing) exhibit the highest neutralization potential (up to 800 kg $CaCO_3$ eq/t). According to the National Environmental Management Waste Act (59/2008) of South Africa, PIC wastes classify as Type 3 waste (non-hazardous). PIC wastes would mostly release non-toxic elements such as Ca, Mg, SO_4, Na, P, K and Fe. Although there are radionuclides such as U and Th in the non-labile fraction of PIC wastes, leachable concentrations were always below 0.006 mg/L. Among PIC wastes, East tailing would the best option as alkaline reagent to neutralize AIW because of its neutralization potential and non-harmful leachate composition predicted.

The knowledge acquired at this point of the investigation served to develop a system that could remediate the extremely acidic wastewater from the neighbouring phosphoric acid plant. This system would be a near-zero waste if the substrate used get enriched in REE and become a marketable by-product. In chapter 6, the material from East tailing was selected for its abundance of REE minerals and REE-bearing minerals, as well as for its neutralization potential (reactor A). A BDAS reactor (Barium carbonate Dispersed Alkaline Substrate) was added to the system to reduce the hardness and to further improve the water quality (reactor B). The system, developed at bench scale, was able to remediate the extremely AIW from the phosphoric acid plant and, at the same time, to concentrate the REE contained in both the water and the tailing. The treated water complies with WHO (World Health Organization) guideline for drinking water for all the parameters except Ni,

Cd and occasionally Ba. Mineralogical and geochemical analyses showed that the REE concentration increased from the initial1.3 g/kg up to 2.1 g/kg in the central area of reactor A. Most REE precipitated as newly formed REE-rich Ca-Al-F phosphate. Minor concentrations of REE were found in reactor B, together with most of the radionuclides.

Altogether, the findings of the thesis bring to the table an eco-friendly and sustainable alternative to concentrate REE in a circular economy approach, while improving the quality of the extremely acidic wastewater. Therefore, the implementation of this system in PIC would have positive impacts to both the economy and the environment of Phalaborwa and the surroundings. This approach to an environmental problem caused by industries could be extrapolated to other carbonatite deposits in South Africa and abroad as a feasible environmental solution with little to none economic imbursement implications. Further feasibility studies of the marketable substrate are recommended in order to estimate if the remediation of acid water using East tailing could be a profitable and sustainable activity.

KEYWORDS: Phalaborwa, Palabora Complex, mine waste, environmental characterization, revalorization, mineralogy of tailing, waste rock dumps, water treatment, rare earth elements, barium carbonate dispersed alkaline substrate, circular economy.

RESUMEN

El Complejo Industrial de Phalaborwa, Sudáfrica, está formado por varias minas y fábricas que extraen valor de la formación geológica denominada Complejo Ígneo de Phalaborwa (o Palabora) (PIC, por sus siglas en inglés). La actividad industrial se inició en la década de 1950 con la extracción de rocas fosfatadas y Cu. Desde entonces, más de 4500 Mt de residuos sólidos enriquecidos en magnetita, Zr, Ni, Au, Ag, Pt y tierras raras (REE, por sus siglas en inglés), estos últimos inexplorados hasta ahora, se han ido acumulando en el área de PIC en forma de relaves y escombreras, así como más de 3 Mm^3 de aguas residuales industriales, incluidos drenajes de rocas y agua de las plantas de procesamiento, como se describe en el capítulo 1. Debido a las actividades industriales, la calidad del agua de los acuíferos subyacentes se ha deteriorado alcanzando hasta 10 g/L de sulfato, particularmente en el entorno de las balsas de fosfoyeso generados por la planta de ácido fosfórico de la fábrica de fertilizantes. El capítulo 2 describe la zona de estudio y aborda la calidad del agua subterránea en PIC y los esfuerzos para contener la pluma de contaminación mediante el uso de pozos de extracción que dieron como resultado un aumento continuo de la contaminación dentro de las instalaciones de PIC, pero ayudaron a controlar la migración de la pluma de contaminación más allá del área industrial. Por otro lado, el capítulo 3 describe los tratamientos de agua pasivos que podrían hacer frente a dicha contaminación.

Sin embargo, este estudio va más allá de la evaluación ambiental, se trata de una evaluación integral de los residuos industriales de PIC, que llevó a la revalorización de los residuos mineros alcalinos como potenciales recursos secundarios de REE y como agente de neutralización, y culminó con el diseño de un sistema que se beneficiaría de ambas características de los residuos. El Capítulo 4 abarca un estudio mineralógico y geoquímico de los residuos mineros de PIC que evaluó todos sus relaves y escombreras. El estudio se realizó bajo la hipótesis de que la abundancia REE del yacimiento podría preservarse o incluso enriquecerse en los residuos mineros. La abundancia de minerales de REE (principalmente monacita) y minerales enriquecidos en REE (principalmente fluorapatita, calcita y dolomita) confirmó esta hipótesis e incidió en el potencial económico de los residuos mineros

como fuente secundaria de REE. Las REE más rentables, en función de su precio y su abundancia en PIC, son Nd, Dy, Pr y Tb (87% del valor neto). Los relaves son económicamente más atractivos que las escombreras porque el procesamiento mineral ha generado relaves de partículas principalmente monominerales enriquecidas en REE.

La caracterización ambiental de los residuos de PIC, descrita en el capítulo 5, se llevó a cabo con el fin de evaluar su potencial como reactivo neutralizante para el tratamiento pasivo de aguas acidas. Los desechos mineros utilizados para tratar aguas industriales ácidas (AIW, por sus siglas en inglés) deben cumplir dos características principales: i) alto potencial de neutralización y ii) baja toxicidad. Para evaluar el potencial de neutralización y la toxicidad de los lixiviados que pudieran liberarse de cada roca y cada relave, se llevaron a cabo protocolos basados en regulaciones nacionales e internacionales. Los resultados de esta investigación demostraron que ninguno de los residuos mineros tiene el potencial de producir drenaje ácido de roca. También demostró que las carbonatitas y los relaves producidos por la planta de cobre (denominados East Tailing) exhiben el mayor potencial de neutralización (hasta 800 kg $CaCO_3$ eq /t). De acuerdo con la Ley Nacional de Gestión Ambiental de Residuos (59/2008) de Sudáfrica, los residuos mineros de PIC se clasifican como residuos de Tipo 3 (no peligrosos). Estos residuos liberarían principalmente elementos no tóxicos como Ca, Mg, SO_4, Na, P, K y Fe. Aunque hay radionucleidos como U y Th en la fracción no lábil de algunos residuos, las concentraciones en la fracción móvil siempre estuvieron por debajo de 0,006 mg/L. Entre los residuos de PIC, East tailing sería la mejor opción como reactivo alcalino para neutralizar AIW debido a su potencial de neutralización y a la composición inocua de su lixiviado.

El conocimiento adquirido en este punto de la investigación sirvió para desarrollar un sistema que podría remediar las aguas extremadamente ácidas de la planta de ácido fosfórico localizada en PIC. Este sistema sería un tratamiento de agua de bajo coste, si el sustrato utilizado se enriqueciera en REE y se convirtiera en un subproducto con valor comercial. En el capítulo 6, se seleccionó el material procedente de East tailing por su abundancia en minerales de REE y minerales alcalinos enriquecidos en tierras raras, así como por su potencial de neutralización

(reactor A). Se añadió al sistema un reactor BDAS (siglas en ingles de Sustrato Alcalino Disperso de carbonato de bario) para reducir la dureza y mejorar aún más la calidad del agua (reactor B). El sistema, desarrollado a escala de laboratorio, fue capaz de remediar el agua extremadamente acida de la planta de ácido fosfórico y, al mismo tiempo, concentrar la REE contenida tanto en el agua como en el material de relave. El agua tratada cumple con los requisitos de la Organización Mundial de la Salud (OMS) para agua potable en todos los parámetros excepto Ni, Cd y ocasionalmente Ba. Los análisis mineralógicos y geoquímicos del sustrato mostraron que la concentración de REE aumentó desde los 1.3 g/kg iniciales hasta 2.1 g/kg en la zona central del reactor A. La mayoría de las REE precipitaron como fosfato de Ca-Al-F rico en REE. Mientras que en la columna B se encontraron concentraciones menores de REE, junto con la mayoría de los radionucleidos.

En conjunto, los resultados de la tesis proporcionan una alternativa ecológica y sostenible para concentrar REE en un enfoque de economía circular, al tiempo que se mejora la calidad de las aguas extremadamente ácidas. Por lo tanto, la implementación de este sistema en PIC tendría impacto positivo tanto en la economía como en el medio ambiente de Phalaborwa y sus alrededores. Este enfoque dirigido a solucionar un problema ambiental causado por la actividad industrial podría extrapolarse a otros depósitos de carbonatita en Sudáfrica y el extranjero como una solución ambiental viable y quizá con poca o ninguna implicación económica. Finalmente, se recomienda realizar estudios adicionales para determinar el valor comercial del residuo generado y si la remediación de aguas acidas usando estos relaves alcalinos podría ser una actividad económicamente rentable y sostenible.

"Haz de la ciencia poesía,
de los sueños creaciones,
de los deseos ilusiones,
y de las aguas alegrías..."
(Rafael Fernández Rubio)

TABLE OF CONTENTS

LIST OF FIGURES

LIST OF TABLES

ACRONIMS

AMD	acid mine drainage
ALD	anoxic limestone drains
ABA	acid base accounting
ABACUS	acid base accounting cumulative screening tool
AIW	acid industrial wastewater
all	allanite
an	anzaite
ap	apatite group
AP	acid potential
ARD	acid rock drainage
ARDI	acid rock drainage index
arg	aragonite
ba	baddeleyite
bar	barite
bat	bastnäsite
B-carb	banded carbonatite
BCR	Community Bureau of Reference
BDAS	Barium carbonate Dispersed Alkaline Substrate
bdl	Below detection limit
bn	bornite
br	brushite
BSE	backscattered electron
bt	britholite
cal	calcite
cal	calcite
ch	chloritoid
chl	chlorite
cm	centimetre
COP	Cooper Open Pit
cp	chalcopyrite
cpx	clinopyroxene
CRM	critical raw material
cv	covellite
d	day
DAS	dispersed alkaline substrate
dio	diopside
DO	dissolved oxygen
dol	dolomite
EC	electric conductivity
EDAX	energy dispersive analysis of X-ray
EDS	energy dispersive spectroscopy
EPMA	electron probe micro-analyser

eq	equivalent
ETE	East Tailing eastern section
ETN	East Tailing northern section
ETS	East Tailing southern section
ETW	East Tailing western section
F1	fraction 1 of the sequential extraction
F2	fraction 2 of the sequential extraction
F3	fraction 3 of the sequential extraction
F4	fraction 4 of the sequential extraction
fap	fluorapatite
F-ap	fluorapatite
F-pyrox	feldspathic pyroxenite
g	gram
ha	hectare
HPLC	High Performance Liquid Chromatography
HREE	heavy rare earth elements
ICP-MS	inductively coupled plasma mass spectroscopy
ICP-OES	inductively coupled plasma optical emission spectroscopy
IGS	Institute for Groundwater Studies
ilm	ilmenite
IOCG	Iron-Oxide Copper-Gold
kg	kilogram
km	kilometre
KNP	Kruger National Park
L	litre
LCT	Leachable Concentration Threshold
LREE	light rare earth elements
m	metre
m	mass
m^2	square metre
m^3	cubic metre
mbs	meters below surface
mg	milligram
mgt	magnetite
mi	microcline
mo	monazite
M-pyrox	micaceous pyroxenite
MREE	medium rare earth elements
mS	milliSiemens
mV	millivolts
na	not analysed
NAG	net acid generation
NCV	net carbon value
NCV*	modified net carbon value
NP	neutralization potential

NPM	North Pyroxenite Mine
NPR	neutralization potential ratio
NSPP	New South Pyroxenite Pit
ol	olivine
ORP	oxidation-reduction potential
pa	parisite
PG	phosphogypsum
pH	hydrogen potential
phlo	phlogopite
Phosc	phoscorite (foskorite)
PIC	Phalaborwa Igneous Complex
PT	pseudo total
PTE	potentially toxic element
qtz	quartz
RAPS	reducing and alkalinity producing systems
REE	rare earth elements
REO	rare earth oxides
s	second
SDD	silicon drift detector
SE	sequential extraction
SEM	scanning electron microscope
SI	saturation index
STN	Selati Tailing North
STS	Selati Tailing South
T	temperature
t	ton
T-carb	transgressive carbonatite
TCT	Total Concentration Threshold
TDS	total dissolved solids
th	thorite
tho	thorianite
ulv	ulvospinel
USGS	United States geological survey
v	stock value
VO	vermiculite open pit
w	weight
WDS	wavelength-dispersive spectroscopy
wi	witherite
WRD	waste rock dump
XRD	X-ray diffraction
y	year
zi	Zircon

CHAPTER 1: INTRODUCTION

1.1. PREFACE

In the Ba-Phalaborwa Municipality of the Limpopo province, South Africa, there is an industrial complex where several mines and factories work synergically to extract value out of the geological formation named Phalaborwa (or Palabora) Igneous Complex (PIC). The industrial activity of that area started in the 1950's with extraction of phosphate rocks and Cu, and it has been increasing ever since. After more than six decades of production, more than 4500 Mt of waste have been accumulating in PIC area in the form of tailings and waste rock dumps. The environmental impact of the industrial activity in PIC has been widely reported by the scientific community as well as by pertinent governmental bodies and the officials of the nearby Kruger National Park.

There is only one main reason for any industry to pollute the environment; it is profitable. With that thought in mind, there are two options to help the industries avoid pollution:

i) Fine the companies that pollute, so that polluting is not profitable anymore. This option has been widely adopted by governments.

ii) Change the industrial chain from linear to circular: the recycling of industrial waste can increase the benefits of the companies, while decreasing their environmental impact. This option has been evaluated throughout this thesis for the industrial complex of Phalaborwa.

The recycling of industrial wastes is a common practice in certain sectors. That is the case of steel slags, which is an alkaline by-product of the steel industries that use the basic oxygen furnace technology (Oster, 1982). Such by-product has been used extensively in construction as road aggregates, Portland cement, roofing granules, etc. Recent studies showcase the use of this steel by-product in leach beds to neutralize acid mine drainage (AMD) (Kruse et al., 2019; Simmons et al., 2002). Other alkaline industrial wastes used for AMD neutralization are e.g. paper

mill sludge, sewage sludge (Moodley et al., 2018) and more recently overburden "phosphatic carbonated" wastes (Ouakibi et al., 2014).

Carbonatite and phoscorite rocks compose the core of PIC. Both are inherited in the mining wastes, which turn those into potential alkaline materials for AMD neutralization. However, before using any industrial waste to neutralize acid water, it is necessary to perform a detailed analysis to the waste and to the water-waste interaction, to ensure that no pollutants are released to the water during the water treatment process. As it is the case of red mud , an alkaline by-product of the alumina industry, that can only be used below 10%, because it increases the concentration of heavy metals and salts when used at 20% (Paradis et al., 2006).

On the other hand, the scarcity of economic REE deposits promoted the investigation of new REE sources worldwide. Secondary REE-resource investigations are focused on industrial wastes such as phosphogypsum stacks (fertilizer industry), red mud (aluminium industry), coal ash (thermal power plants), wastewater streams and mining wastes (slags, tailings and rock dumps) (Humsa and Srivastava, 2015; Jowitt et al., 2018; Zhang et al., 2014). Coincidently, most carbonatites and phosphate rocks deposits are REE bearing deposits. Indeed, previous petrogenetic studies examined the rare earth minerals of PIC as indicators. PIC has not been mined for REE up to now, but according to USGS (United States geological Survey) PIC has reserves of 652 Mt of at 0.15% REO cutoff (Orris and Grauch, 2002). Which might be inherited in PIC's tailings and waster rock dumps.

Currently there is no REE mining in South Africa. PIC could host the first REE mine in South Africa, if the potential of its wastes as a secondary resource of REE is proven. However "data and tools are needed to establish the recycling and reuse potential of these [mining waste] materials; geochemists and mineralogists have a significant role to play in this endeavour" (Bellenfant et al., 2013).

1.2. AIM AND OBJECTIVES

The circular economy is a concept that enables economic growth by turning waste into valuable materials, which benefits businesses, society and the environment. The main aim of this study is based in the application of "circular economy" concept to the mines and factories stablished in the industrial complex of Phalaborwa. Therefore, this study is focussed in the revalorization of the mining wastes as secondary resource of REE and as reagent to neutralize industrial wastewater. To achieve this, it is necessary to characterize mineralogically and geochemically the mining wastes generated from PIC, followed by the development of a novel water treatment system.

This thesis is based in the hypothesis that the mining wastes from PIC are enriched in REE and have enough neutralization potential to be used as reagent for a water treatment system that could neutralize the extremely acidic wastewater, while producing a REE-rich by-product that could defray the costs of the water treatment or even transform water remediation into a profitable activity.

To demonstrate this hypothesis, the following objectives need to be achieved:

- Mineralogical and geochemical characterization of mining wastes from PIC, focusing in the REE minerals and the alkaline REE-bearing minerals.
- Assessment of the neutralization potential and the leachates of the mining wastes towards their further options for recycling.
- Development of a novel water treatment based on alkaline mine waste to treat the acid wastewater from the phosphoric acid plant.
- Mineralogical and geochemical characterization of the water treatment residue, focussing in their REE concentration towards a possible reclassification as marketable by-product.

1.3. THESIS LAYOUT

Chapter 1 introduce the problem statement, aim, Objectives and the layout of the thesis dissertation.

Chapter 2 describes in detail the study area including the geographical location, climatology, hydrogeology, geology of Phalaborwa Igneous Complex (PIC) and the Industrial complex of Phalaborwa.

Chapter 3 describes the state of the art of the subjects relevant to this thesis such as critical raw materials, mine waste revalorization and water treatments.

Chapter 4 is based on the article submitted to Cleaner production entitled "Mine waste characterization of Phalaborwa Igneous Complex as a base for its potential as REE resource". It encompasses a mineralogical and geochemical characterization of PIC wastes with special attention to the REE content and the possibilities of revalorization of these wastes as secondary REE resource.

Chapter 5 is based on the article published in Geochemical Exploration entitled "Environmental and Geochemical Characterization of Alkaline Mine Wastes from Phalaborwa (Palabora) Complex, South Africa". It is a comprehensive characterization of the neutralization potential and the elemental composition of the leachates that might be produced by PIC wastes as a base for its potential as alkaline reagent for water treatment.

Chapter 6 is based on the article submitted to Journal of Hazardous of Materials entitled "Concentration of rare earth elements from acid wastewater using REE-rich alkaline mine waste: a novel approach of an acid wastewater neutralization system". It addressed the development of the prototype of a passive water treatment to neutralize acid water using PIC wastes and the characterization of REE-rich by-product obtained from the water treatment.

Chapter 7 provides overall conclusions and recommendations according to the results acquired during the development of the thesis.

CHAPTER 2: STUDY AREA

2.1. GEOGRAPHY, TOPOGRAPHY AND HYDROLOGY

The study area is located in Ba-Phalaborwa Municipality, within the Mopani district of the Limpopo province, Northeast of South Africa. The municipality encompasses 7462 Km^2, of which 27% are private farms (game, fruit and cattle farming), above 50% belongs to Kruger National Park (KNP), and the township of Phalaborwa is 9.4 Km^2. The study area comprise the tailings and waste rock dumps and dams generated by a group of mines and mineral-related companies settled on the Phalaborwa Igneous Complex (PIC). This industrial facility covers 115 Km^2, it is adjacent to the North with the town of Phalaborwa and to the West with the Kruger National Park.

PIC is located in the Lowveld region of Limpopo. The area is characterized by a smooth topography about 360 masl with a southward slope and spotted with conical hills rising 50 to 90 m above surface. The climatic zone is Subtropical with hot and rainy summers and template winters. The minimum temperatures throughout the year oscillates between 8 and 18°C, while the maximum are between 23 and 30°C. The mean annual rainfall is about 528 mm/year, while the evaporation is about 1550 mm/year. Both rainfall and evaporation are greater in summer (Vegter, 2003).

The study area is located in the hydrological area named Lower Olifants of the Olifants River Basin. This region is drained by the Olifants and Ga-Selati Rivers. Olifants watercourse flows near the Southern border of PIC, towards to KNP. Ga-Selati River is a tributary of Olifants River that flows through PIC for about 18 Km before flowing into Olifants River. Tshutshi Spruit is also a tributary of the Olifants River that flows near the North-eastern border of the PIC. The influence of the population and industrial activities, included those of PIC, in the water quality of all three watercourses have been widely reported, the environmental consequences have been assessed and closely monitored by the scientific community, as well as by the pertinent governmental institutions (e.g. Department of Water Affairs and Forestry, 2004; Valverde *et al.*, 2020).

2.2. GEOLOGY

Geologically, PIC is located in the North-western edge of the Kaapvaal Craton, over a series of alkaline magma that intruded the Craton during Paleoproterozoic Era (2060 Ma) first dated by Holmes and Cahen, 1957 (Figure 2.1). This geological event, coeval with the Bushveld granites (Vielreicher et al., 2000), was named Phalaborwa (Palabora) Igneous Complex (Aldous, 1986; Basson et al., 2017; Hanekom et al., 1965) or Palabora Carbonatitic Complex (Giebel et al., 2017; Heinrich, 1970).

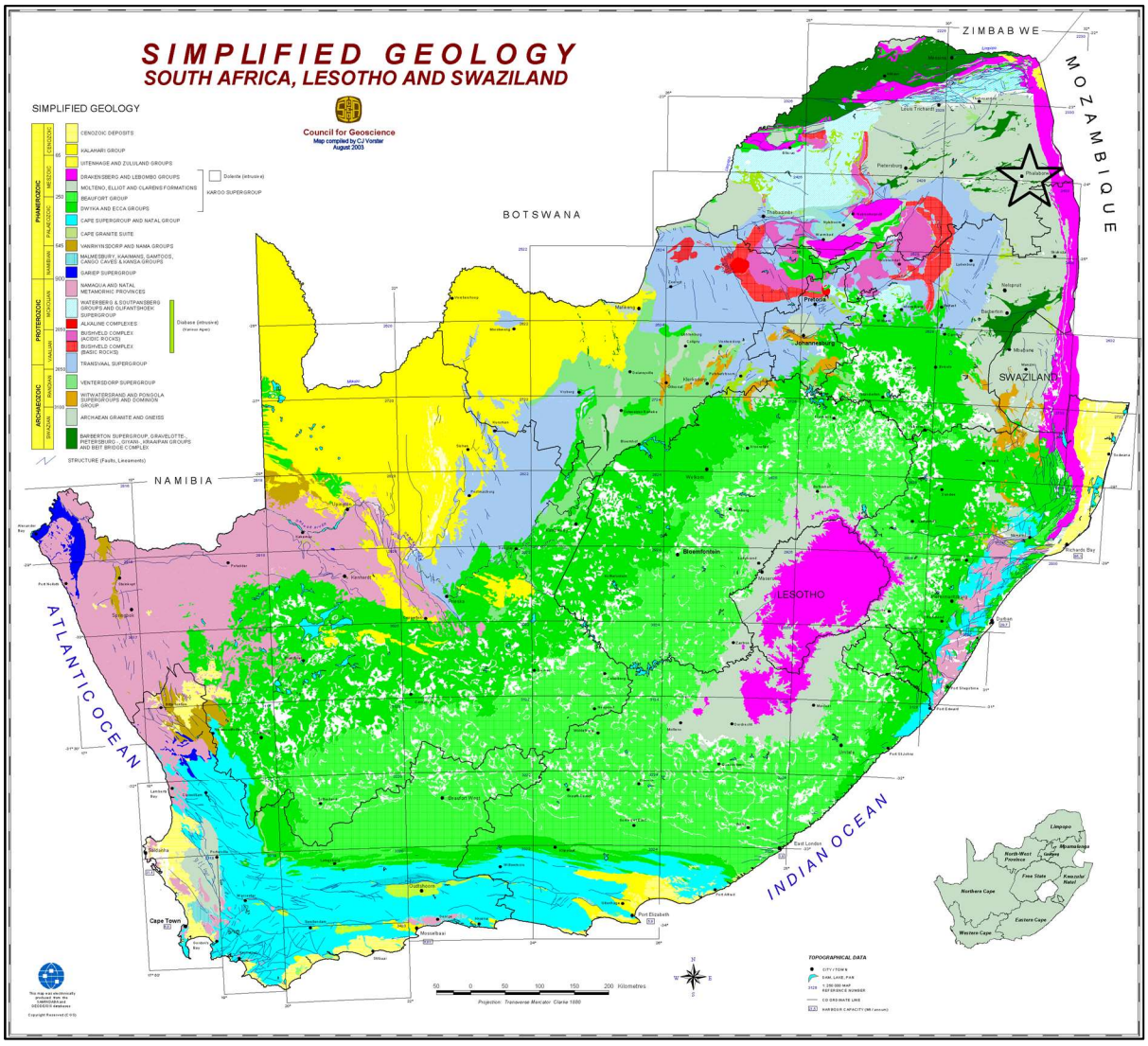

Figure 2.1 Simplified geological map of South Africa showing the location of the Study area (indicated with a star), Phalaborwa Igneous Complex (Council for Geoscience, 2003).

2.2.1. KAAPVAAL CRATON

Kaapvaal craton is one of the oldest and best preserved cratons on Earth; its emplacement started 3500 Ma ago and ended 2500 Ma ago (Poujol et al., 2003). Between 3600 and 3200 Ma ago started the magmatic accretion and tectonic amalgamation of protocontinental blocks that characterized the early stage of the craton formation (Figure 2.2a). Each block was an independent arc or greenstone belt. The magmatic accretion occurred in the south of the craton as a succession of overlapping of the magmatic arcs, while in the north of the craton there was tectonic accretion and collisional suturing of blocks of different ages (de Ronde and Kamo, 2000; Lowe and Byerly, 1999; Lowe, 1994; Poujol et al., 2003).

About 3100 Ma ago, the Mesoarchaean magmatism started, origin of the potassic granitoid batholiths that forms the current Kaapvaal Craton. The emplacement of theses granitoids started in the North-Eastern domain (on which the study area is located) and younger greenstone belts were formed along the juvenile arc in the contact area with younger segments of the craton due to the collision and/or subduction of the younger segment (Figure 2.2b) according to Poujol et al., 2003.

Between 3000 and 2800 Ma ago there was a continent-arc collision with post- or syntectonic emplacement of low-Ca (S-type) granitoid plutons (Meyer et al., 1994). The currently known as Witwatersrand basins were the typical foreland deposits of such event (Figure 2.2c).

Around 2700 Ma ago there was a late state continental collision in the west, while the north is characterized by a rifting episode responsible for the emplacement of the Gaborone Granite Complex and Kanye Volcanic Formation (Gambogi, 2016; Moore et al., 1993). Another rifting episode occurred in the centre of the craton, whose volcanic evidences can be seen in Ventersdorp Supergroup (Figure 2.2d).

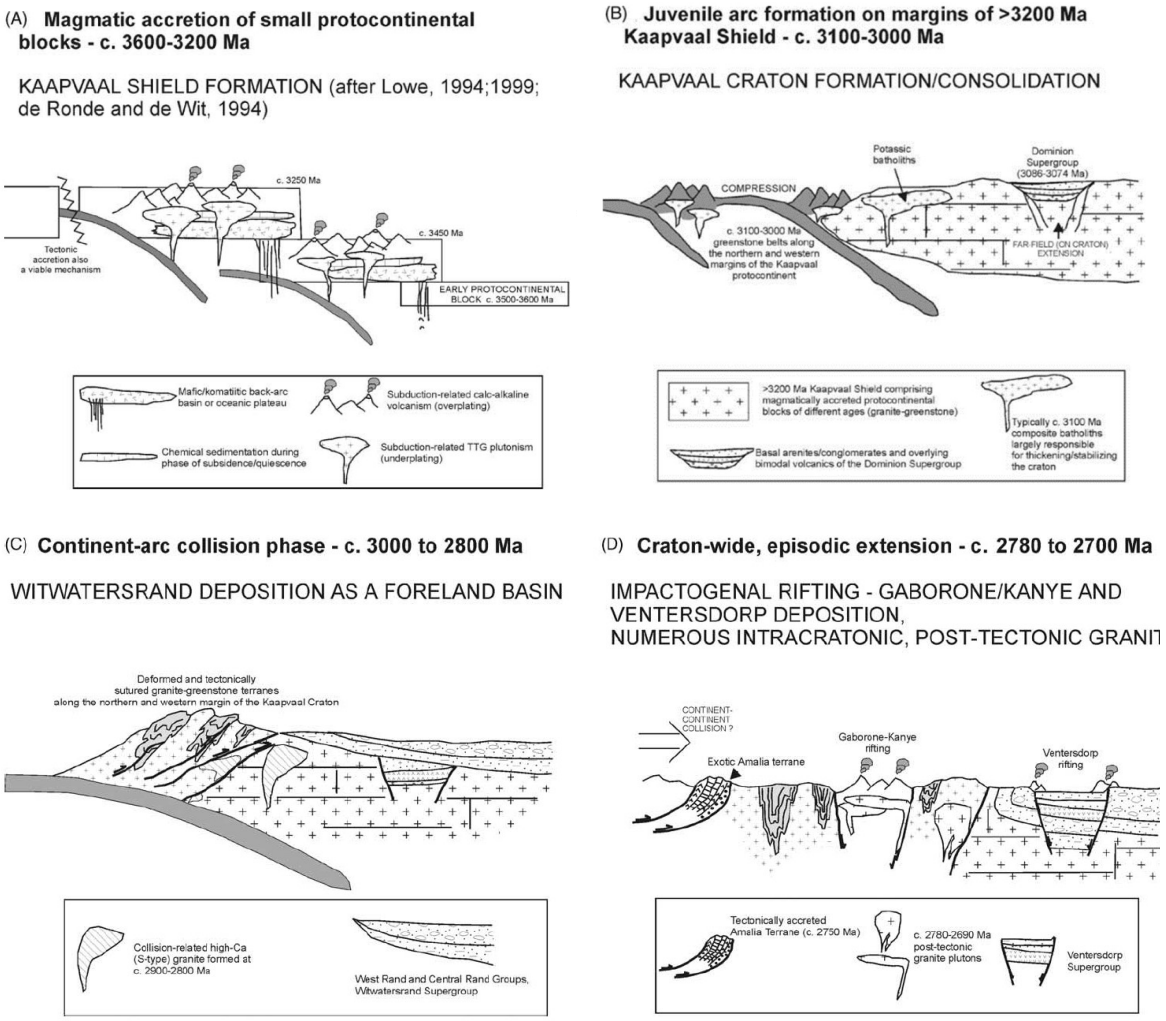

Figure2.2. Orogeny and evolution of the Kaapvaal kraton (Poujol et al., 2003)

2.2.2. MAKHUTSWI GNEISS

The study area is located in the Northeast of the Kaapvaal Craton. The tectonic accretion, that occurred in this area between 3228 and 3063 Ma (Poujol et al., 1996; Poujol and Robb, 1999), originated what is currently known as Makhutswi Gneiss. This is very complex composite gneiss from tonalitic to granodioritic composition which is found between the Murchison Greenstone Belt at north and Nelspruit Suite at South (Robb et al., 2006). Several plutons can be found within the Makhutswi Gneiss, whose emplacements took place between 3095±5 Ma (granodiorite dated from Harmony Granite) and 2671±8 M (granite dated from Mashishimale Granites Suite) (Poujol and Robb, 1999; Zeh et al., 2009).

An important magmatic activity occurred 2800 Ma, which affected this area promoting the crystallizations of pegmatitic dykes intrusive into the Makhutswi gneiss, the Willie Granite and the Lekkersmaak granite, both plutons of the Makhutswi gneiss (Jaguin et al., 2013). Other plutons close to the study area are the Harmony Granite, Mashishimale Granites Suite, Pompey Granite, and the Murchison Greenstone Belt.

2.2.3. PHALABORWA IGNEOUS COMPLEX

This magmatic plume intruded the Kaapvaal craton about 2060 Ma ago (Holmes and Cahen, 1957; Reischmann, 1995) and left a pipe-like intrusion with three well differentiated sections; northern pyroxenite (olivine-phlogopite pegmatoid altered to serpentine and vermiculite), central carbonatite (termed Loolekop pipe) and southern pyroxenite (phlogopite/vermiculite pegmatoid rich in apatite and pyroxene).

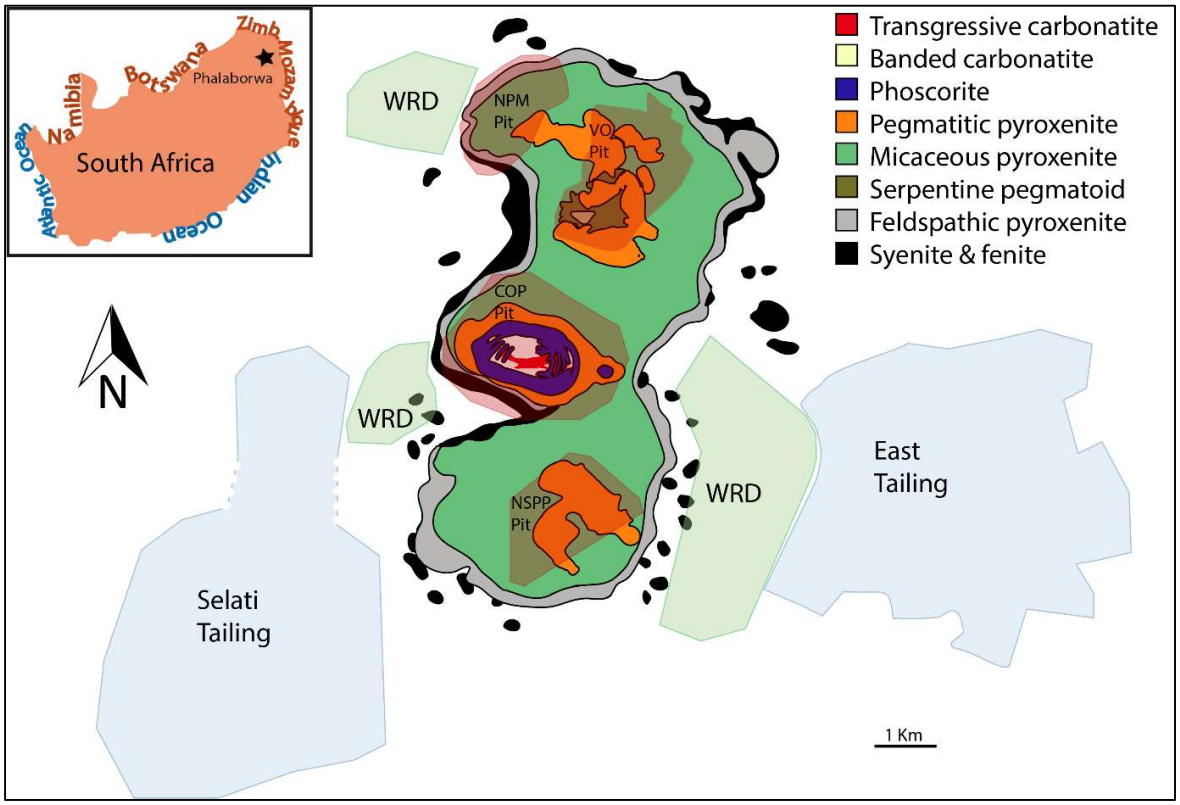

Figure 2.3. Geological map of Phalaborwa Igneous Complex (PIC) with the open pits shaded in red, WRD in green and tailings in blue Complex (modified from Giebel et al., 2019).

The Loolekop pipe has a concentric structure (ring-like morphology). From outside to the centre of the pipe is composed by phlogopite-pyroxene-apatite pegmatoid, followed by phoscorite (partially serpentinised olivine with apatite and magnetite) and finally the carbonatite core. There are two well differentiated carbonatites; the outer and older banded carbonatite with apatite, dolomite, chondrodite, olivine, phlogopite and biotite and the inner and younger transgressive carbonatite with off-shoots transgressing the earlier banding (Verwoerd and du Toit, 2006).

According to Henrich (1970) the emplacement of the PIC started as pyroxenitic pegmatoids, followed by pyroxenite, phoscorite, syenite coeval with feldspathic pyroxenite, banded carbonatite and finally the transgressive carbonatite.

The carbonatite of Loolekop hosts the only economic deposit of copper found in a carbonatitic complex. The previous genetic description of the Loolekop pipe (i.e. Heinrich, 1970) stated that the Cu mineralization was related with the carbonatitic magmatism. However, further studies suggested that PIC is coeval with Bushveld and therefore could follow the genetic model of IOCG deposits (Iron-Oxide Copper-Gold) (Groves and Vielreicher, 2001; Harmer, 2000; Vielreicher et al., 2000). Hence, the lithological differences of this concentric structure might be due to the heterogeneity of the mantle at the time that the mantle plume was active (more than 2000 Ma ago), which was affected by tensional stress and hydrothermal activity.

A recent study (Giebel et al., 2017) specifies that “PIC experienced at least two successive stages of intense fluid-rock interaction”. Giebel and co-authors analysed the rare earth minerals as petrogenetic indicators for the Loolekop formation; during the orthomagmatic crystallization, inclusions of fergusolite and REE-Ti-betafite were formed in magnetite, while bastnäsite was enclosed in calcite and dolomite. During the late magmatic to hydrothermal process, monzonite replaced primary apatite, while britholite precipitated as rims around serpentines and chondrodites. In the last stage, a postmagmatic ancylite is bound to fluid paths with secondary mineralization of carbonates.

No major faults are indicated on the 1:250000 geological maps of the area. However, minor fault zones, related to PIC emplacement have been described

(Basson et al., 2017). The Loolekop pipe occurs at the junction of five faults zones and, according to Basson et al. (2017) they drove the emplacement of phoscorite, as well as banded and transgressive carbonatites: i) the Mica fault zone is the oldest structure and it strikes N-S coincidently with the orientations of the entire PIC and the Eastern edge of the Kaapvaal; ii) the Tree fault zone is parallel to SW faults zone; iii) the SW fault zone is an anastomosing fault network; iv) the N-NW structural orientation, which includes the glimmerite fault and v) the youngest Central fault zone, which consists of narrow faults striking WNW in a stock-worked texture (Figure 2.4a to e).

After the emplacement of PIC, a group of vertical subparallel northeast dolerite dykes of Proterozoic to Jurassic age intruded PIC (Figure 2.4f and g). There are also some minor dykes of syenite, lamprophyre, diopsidic pyroxenite, as well as carbonatite and carbonatitic breccia (Briden, 1976; Hanekom et al., 1965; Heinrich, 1970; Stettler et al., 1989; Uken and Watkeys, 1997; Wu et al., 2011).

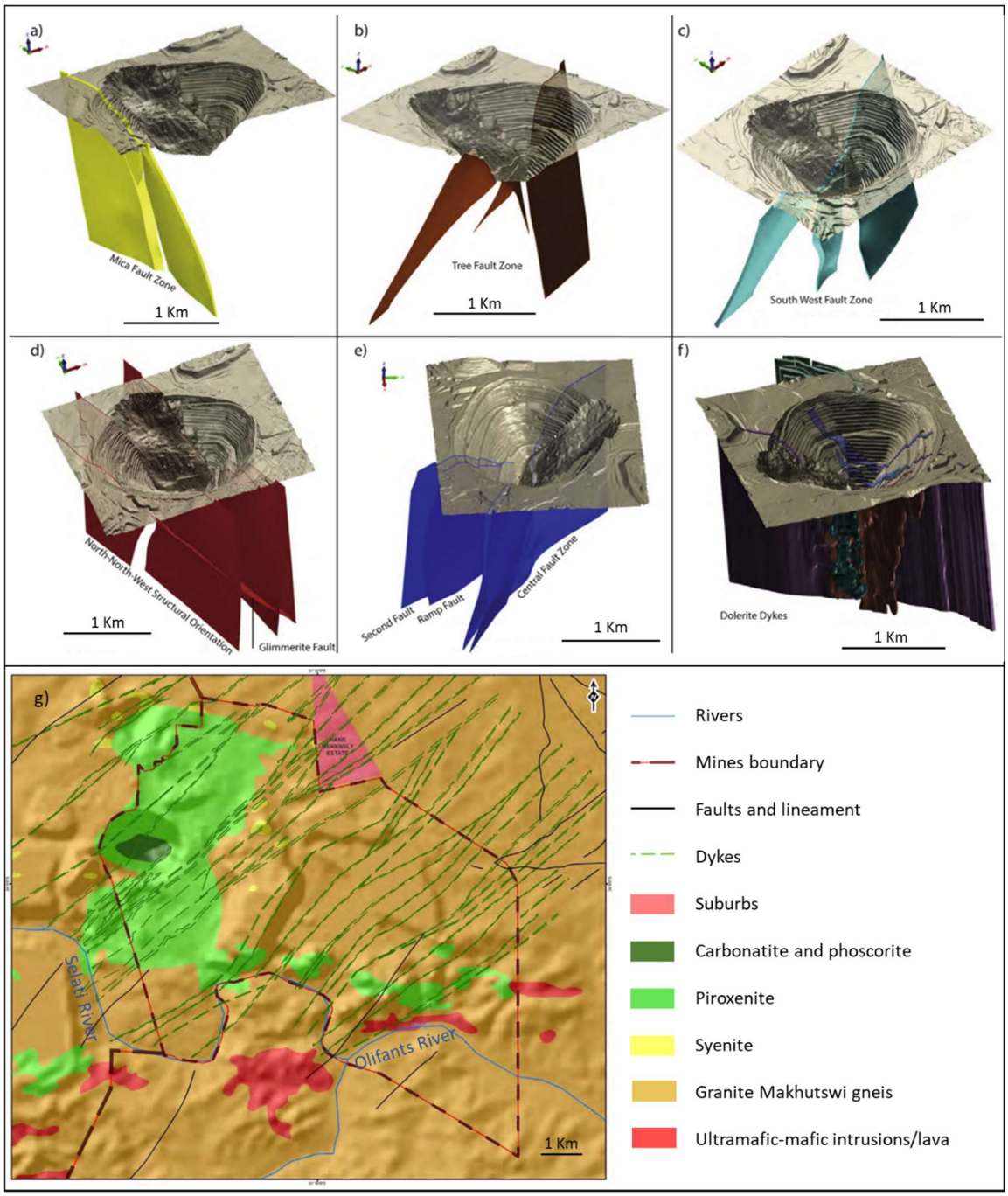

Figure 2.4 Regional geological map and 3D views of major structures and fault zones affecting Phalaborwa Igneous complex; a) Mica Fault Zone; b) Tree Fault Zone; c) South West Fault Zone; d) Faults in the NNW structural orientation; Glimmerite Fault; e) Central Fault Zone with Second and Ramp faults; f) Dolerite dykes, modified from (Basson et al., 2017); g) Regional geological map of Phalaborwa Igneous Complex showing dikes, faults and lineaments (Golder Associates, 2019).

2.3. PIC MINES AND INDUSTRIES

A primitive mining activity in PIC took place at about the seventh century when the tribes of the Mutapa Empire (also known as Mwenemutapa or Monomotapa) started producing utensils and ornaments using iron and copper from PIC (Roux et al., 1989). Nowadays, an intricate and synergic network of mining companies are currently mining PIC. They extract mainly copper, phosphate and vermiculite, as well as some by-products such as magnetite, zirconium, nickel sulphate and anode slimes with gold, silver and platinum. Mining activity on this area has generated multiple tailings and waste rock dumps (WRD) (Figure 2.3), mainly composed by the previously described mineralogy of PIC, except for the difference that will be further discussed in this thesis. Such differences are mainly due to the ore processing during the extraction of the mineral commodities from the gangue minerals, as well as the weathering processes affecting the tailings and WRD over time.

The ore processing in this area includes crushing, milling, flotation, filtration, drying, magnetic separation (for magnetite), smelting, converting, sulphuric acid attack, scrubbing, anode casting, electrolytic refinery (for copper), winnowing (for vermiculite) and drained for thickening (for phosphate) (Foskor, 2018; Steyl, 2011).

After processing, waste materials are pumped into the tailing dams. Selati tailing dam is the largest in the southern hemisphere, it covers an area of about 11 Km^2 and it is located South of Selati River (Foskor, 2018). North of Selati River there is a smaller tailing dam called Southern tailing. Both tailings collect the residue of the phosphate mine. Due to the similarity expected between both tailings, during the investigation described in this thesis they are considered as one tailing divided by the Selati River and from now on will be called Selati tailing north and south, respectively. On the other hand, the Cu mine stores the residues on the Eastern side of the industrial area, herein called East tailing, except for the residues that are rich in magnetite, which are stored at the north of this tailing and subdivided in Hi-Ti magnetite and Low-Ti magnetite piles for further commercialization.

In contrast, WRDs are associated with the open pits. The Copper Open Pit (COP) is the principal and the widest opencast pit in Africa. The so-called Main Waste Rock

Dump collected all the waste rocks from the COP (now decommissioned) and from the construction phase of the underground Cu mine (still active). Currently, the main WRD has a height of 105 m above ground level and is no longer operational (Golder Associates, 2013). Other minor WRD in the area are associated with the phosphate and the vermiculite mining operations. Some of them were completely reclaimed or are in the process to be reclaimed for the recovery of phosphate.

The leachates from the tailings and WRDs are collected and pumped into return water dams together with effluents and runoff from the plants. The main dam of the complex is surrounded by the East tailing and has about 2 Mm^3 capacity.

In PIC there are also several industries that process mine products and by-products. The fertilizer industry is the most noticeable of them. They process the phosphate rock extracted by the mine to produce phosphoric acid. This is a wet process in which the rock is attacked with sulphuric acid. This process generates two types of waste; an extremely acidic wastewater and a phosphogypsum (PG) slurry. The slurry is pumped to the phosphogypsum stacks and the industrial wastewater is recirculated between the impounding dams and ponds surrounding the PG stacks before to be reused in the plant.

2.3. HYDROGEOLOGY

Previous studies showcased the existence of a semi-confined aquifer system in the study area (Brink, 2011; DWAF, 1998; Golder Associates, 2012). This aquifer has an upper weathered zone (0-15 meters below surface (mbs)) followed by a fractured permeable horizon (15-25 mbs) and the deepest zone of the aquifer is composed by poorly fractured to fresh bedrock (25 – 180 mbs). The transmissivity for the upper area ranges from 0.15 to 1.5 m^2/day, except for the contact zones of the dykes where the transmissivity increases to 3 – 50 m^2/day, and the faults where transmissivity reach up to 60 m^2/day. The fractured horizon transmissivity is more variable, ranging from 1.1 m^2/day for the dolerite dykes, to 20 m^2/day for the granite gneiss and 75 m^2/day for pyroxenite. In this zone, the transmissivity of the contact zone of the dykes and the faults only reach up to 2.4 and 40 m^2/day, respectively. The deepest area of the aquifer has very low transmissivity (<0.03 m^2/day), except for the contact zone of the dykes and faults (up to 8 and 600

m²/day, respectively) (Golder Associates, 2012). In general terms, the yield of the study area oscillates between 0.1 and 2 l/s (Figure 2.5; DWAF, 2003).

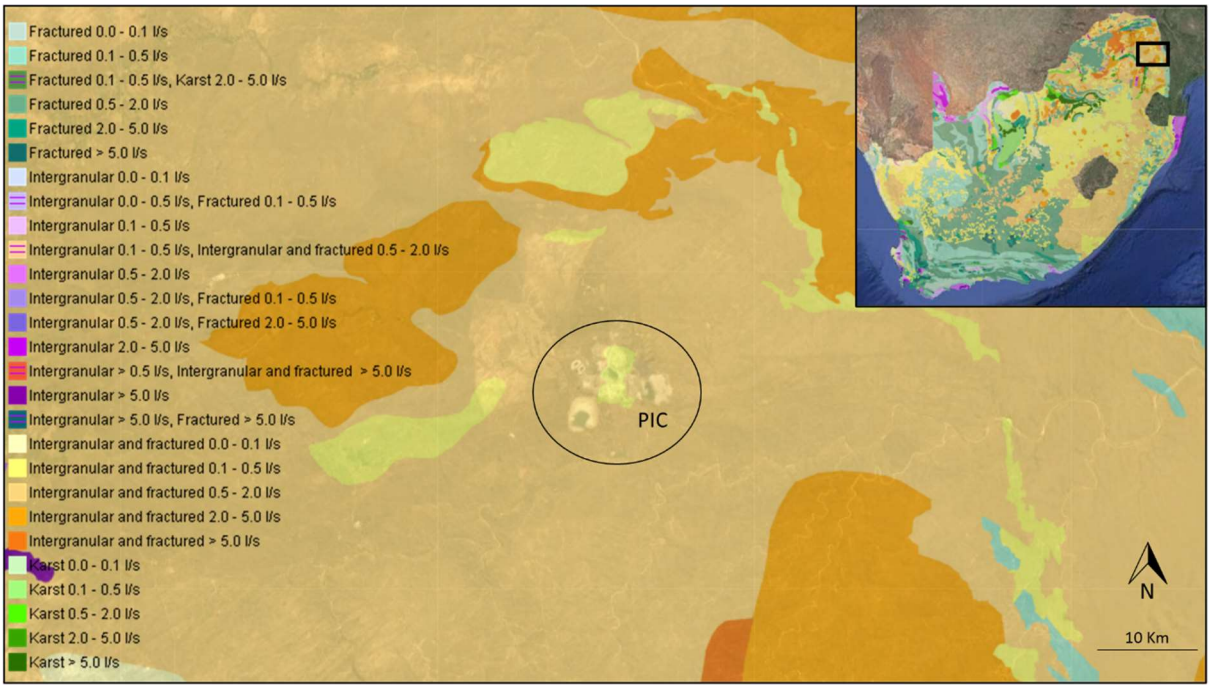

Figure 2.5 Aquifer classification and yield of both South Africa (Top right) and the area of Phalaborwa Igneous Complex (PIC), modified from DWAF (2003).

Particularly dolerite dykes act as natural barriers that compartmentalise the aquifer, while the contact zone in both sides of the dykes act as preferential groundwater pathways (Figure 2.6). Therefore, the distribution of dykes has a great influence in the aquifer recharge and in the distribution of pollution from surface to the aquifer compartments. Due to the influence of the dolerite dykes' orientation, the groundwater flows northeast or southwest locally. However, the regional groundwater flow direction is in general southward, towards the Selati and the Olifants rivers, whereas at the south of Selati River, the groundwater flows northeast towards the Selati River. Despite the influence of the dykes, the water table is pseudo-parallel to the topography of the site.

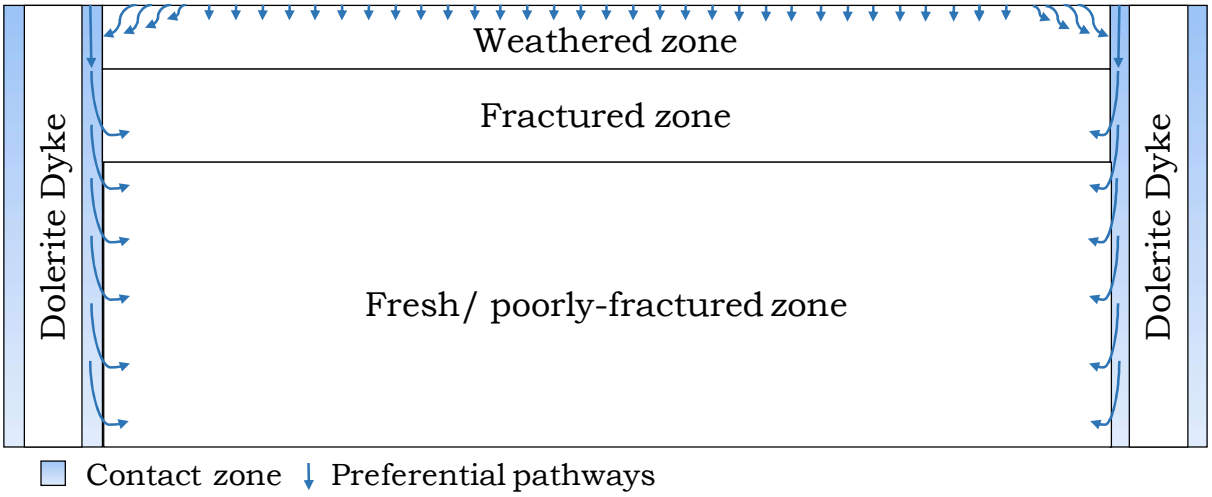

Figure 2.6. Simplified Cross Section representing the conceptual hydrogeological model of PIC.

The estimation of the seepage from PIC dams, tailings and WRD ranges from 6 to 24 m^3/day/ha. Such seepage has created over time a groundwater plume of contamination that is closely monitored and reported by each of the PIC's companies. The historical data from each company together with the analysis of the groundwater carried out during this thesis has been gathered to plot the spatial and temporal evolution of the groundwater contamination of PIC area. Each site produces a seepage with different chemical composition. All of them have in common high concentrations of sulphate. Therefore, the sulphate concentration is commonly used in the area to track the impact of the industrial activity in the groundwater, as well as the lakes and rivers surrounding PIC. The concentration of sulphate in groundwater reported since 1991 has been plotted herein (Figure 2.7) using Windows Interpretation System for Hydrologists (WISH). High concentrations of sulphate were found all around the study area (red dots in Figure 2.7). When the stiff diagram of each borehole is plotted (Figure 2.8), it exhibits a pattern that shows that the background of the aquifer is characterized by alkaline water with high concentrations of Mg and whose (K + Na) is higher than Ca, which gives to the Stiff diagram a characteristic arrow-like signature. On the other hand, the areas where groundwater have been impacted by the industries shows very high concentration of sulphate and low alkalinity, which produce a boot-like Stiff diagram (Figure 2.8). The boreholes around Selati tailing (Figure 2.8 empty circles)

are not represented because the analyses of Cl^- were not reported. In general terms, Magnesium is the dominant cation of the aquifer, while sulphate is the dominant anion. The high TDS detected in the sectors of the aquifer impacted by the industrial activity is related to the abundance of sulphate (SO_4^{2-}), Ca, Mg and Na.

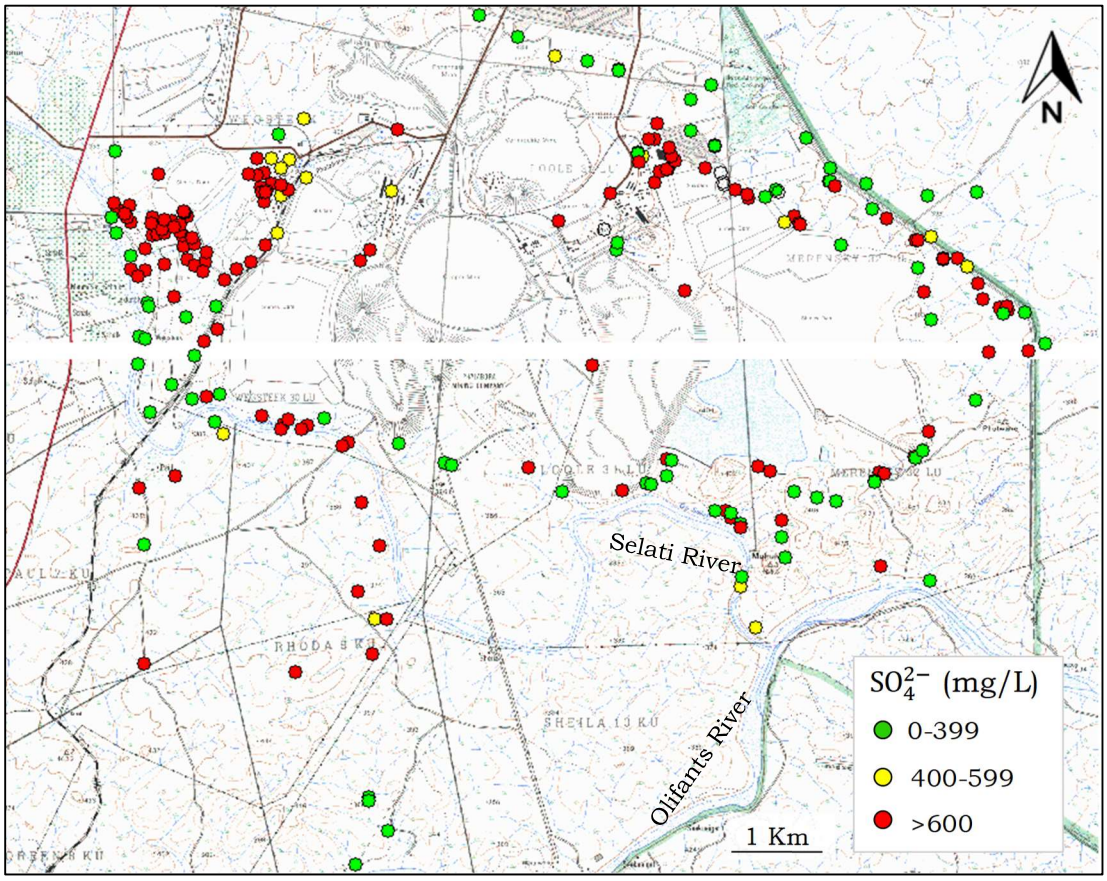

Figure 2.7. Sulphate concentration of groundwater, analysed from each sampling borehole of PIC industrial area.

Each tailing, WRD and dam from PIC influences the load and the chemistry of the leachates. This, together with the compartmentation of the aquifer produce an heterogeneous distribution of the pollutants in the groundwater. The concentration of Na, K, Ca Mg and Cl varies among the different polluted areas within PIC. The sulphate is the common pollutant for all the pollution sources (Figure 2.7 and 2.8).

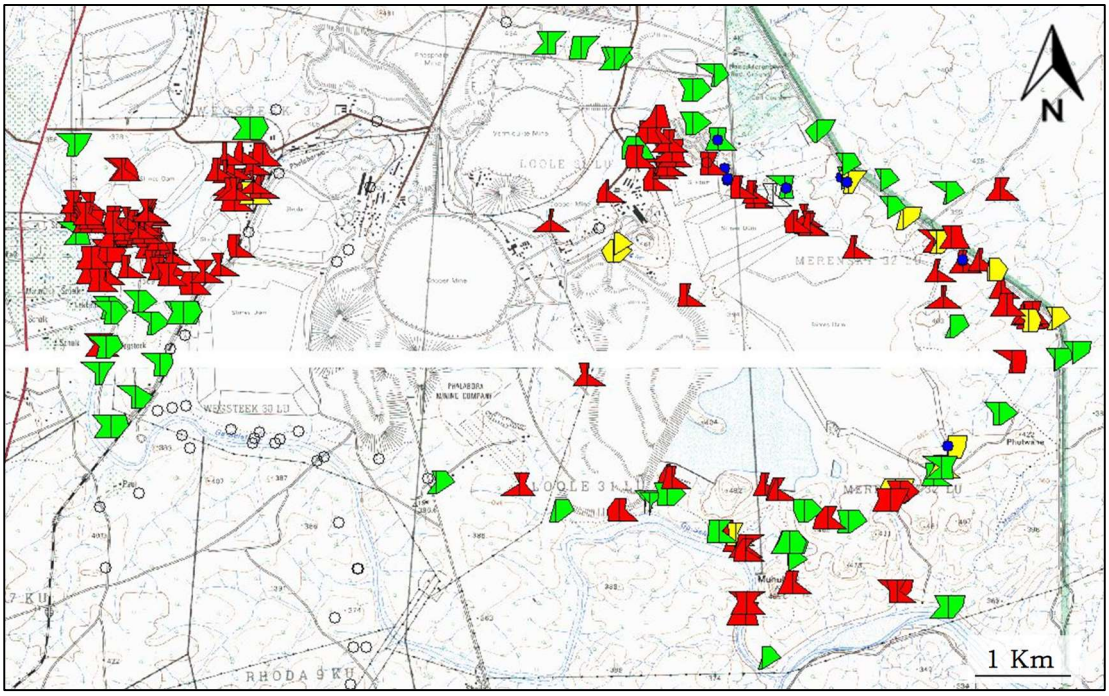

Figure 2.8. Stiff diagrams of PIC's borehole water. Circules represent the boreholes whose water analyses were incomplet and no diagram could be drawn.

The first groundwater analyses were reported by the phosphoric acid industry in 1991 (Figure 2.8), located in the northeast of PIC area. At that time the water analyses from the boreholes nearby the phosphogypsum stacks and particularly the so called FGM-B37 (by the southeast side of the newest phosphogypsum stack, near the train rail) had a sulphate concentration of about 6 g/L (Figure 2.9, map 1991).

In 1997, several abstraction boreholes were installed to contain the contamination plume within the boundaries of the company facilities and to limit its impact in the Selati River. As a result, the sulphate concentration of the boreholes downstream of the abstraction boreholes (towards Selati river) decreased. However, the water quality from the boreholes upstream worsen (Figure 2.9, maps 2000, 2005 and 2010). The concentration of sulphate near the impoundment dams kept on increasing over time, reaching up to 20 g/L by 2000 and surpassing 50 g/L by 2007. Since December 2013, the production of the phosphoric acid plant stopped. This, together with some measures put in place by the company to reduce their

impact to the aquifer, resulted in a decreasing of the sulphate concentration around the phosphogypsum stacks (Figure 2.9, 2015 and 2.10).

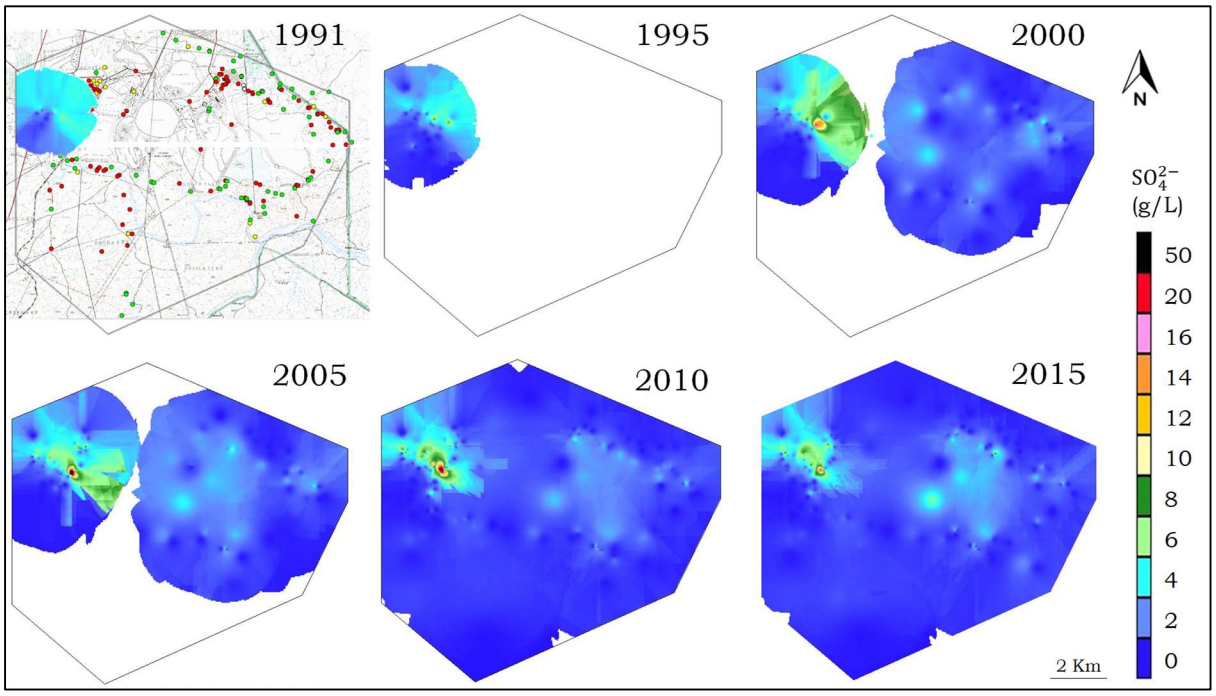

Figure 2.9. Temporal evolution of the contamination plume in the groundwater, in terms of sulphate concentration (mg/L) between 1991 and 2015.

Data collected from the mines since 2000 show an increment of sulphate between the main WRD, that collects the overburden of the Cu open pit, and the East tailing that collects the residue from the Cu plant (Figure 2.9). At the southeast tip of East tailing the concentration of sulphate also increased over time. However, the biggest concern of this sector is the area north of East tailing, next to the Hi-Ti magnetite reservoir where sulphate concentration of the groundwater reached 8 g/L (Figure 2.10). Nevertheless, Selati tailing, the open pits and the smaller WRDs do not seem to have a relevant impact on the groundwater quality (Figure 2.9 and 2.10).

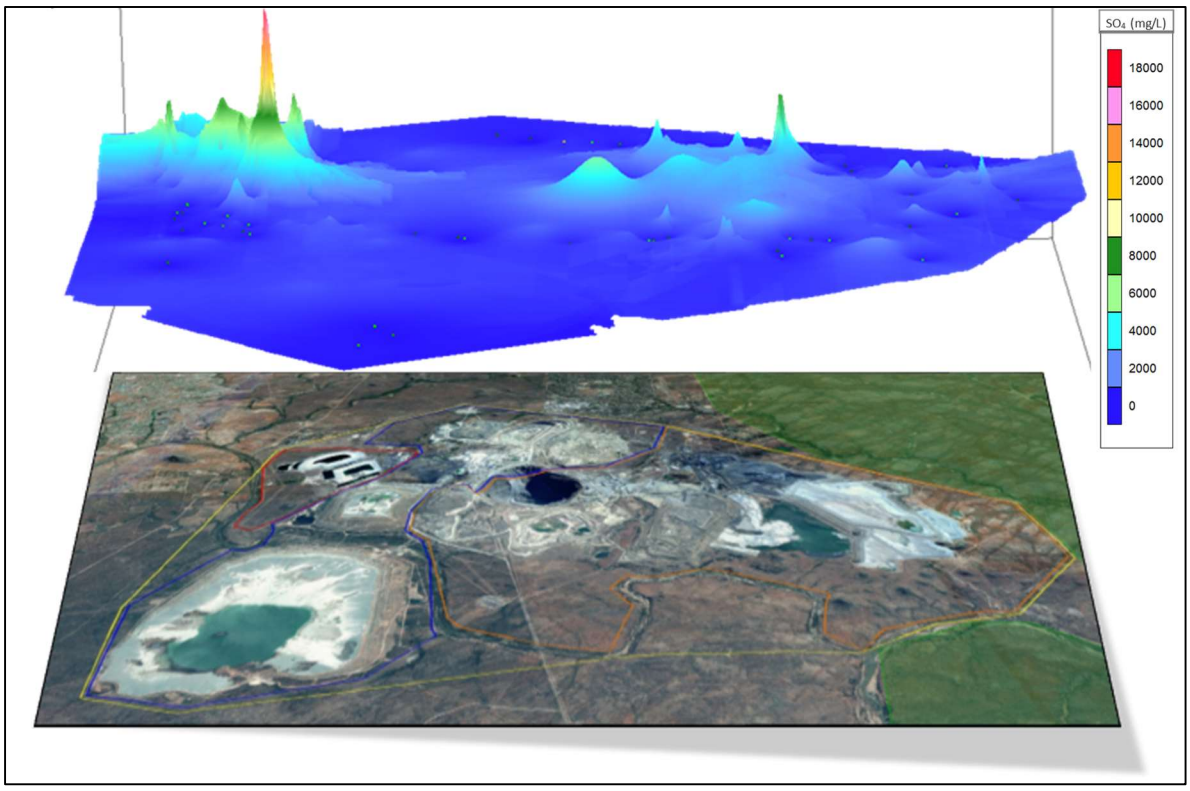

Figure 2.10. Areal picture of the industrial complex of Phalaborwa (in yellow). Delineated in red is the phosphoric acid industry (Bosveld), in blue is the phosphate rock mine (FOSKOR), in orange is the Cu mine (Palabora Mining Company). Shaded in green is the Kruger National Park. On top is the 3D representation of the concentration of sulphate in groundwater as per 2015.

CHAPTER 3: OPTIONS FOR PIC MINE WASTE REVALORIZATION

3.1. RARE EARTH ELEMENTS

3.1.1. DEFINITION

Rare Earth Elements (REE) are a group of elements composed of lanthanides, yttrium and scandium, essential for modern technological development and classified as Critical Raw Materials (CRM) (Haque et al., 2014; Hatch, 2011). Nowadays, most of the remining studies and operations are focused on the CRM. Those are raw materials that are of relevant economic importance and whose supply are at risk. The first list of critical raw materials was published in 2011 by the European Commission and included 14 materials. It was last updated in 2017 and now includes 27 materials (European Union, 2017) such as rare earth elements (REE), metals of the platinum group (PG), Barite ($BaSO_4$), and phosphate rocks, among others (Figure 3.1). The crustal abundance of REE ranges from 60 to 0.5 parts per million, but minable deposits are scarce (120 Mt of REE global reserves). The world annual production of rare earth oxides (REO) was estimated to be 170000 tons for 2018 (Gambogi, 2019), of which 70.6% was produced in China. REO prices ranged from 2 $/kg (Ce and La oxides, 99.5% min.) to 461 $/kg (Tb oxides, 99.99% min.) by 2019.

3.1.1. REE MINING

Most carbonatites are REE bearing deposits, such as Bayan Obo, China (largest REE resource with 57.4 Mt 4-6% REO cutoff); Mount Weld, Australia (11-17% REO); Mountain Pass, USA (5-12% REO); Tomtor, Russia (8-31 % REO); Aracha, Brazil (2.5-13% REO); Catalao, Brazil (1-12% REO); Maoniuping, China (1-8% REO); Lugin Gol, Mongolia (3.2% REO); Okorusu Complex, Namibia (2-7% REO); Amma Dongar, India (3% REO); Mrima Hill, Kenia (0.6-5% REO), among others (Gambogi, 2019).

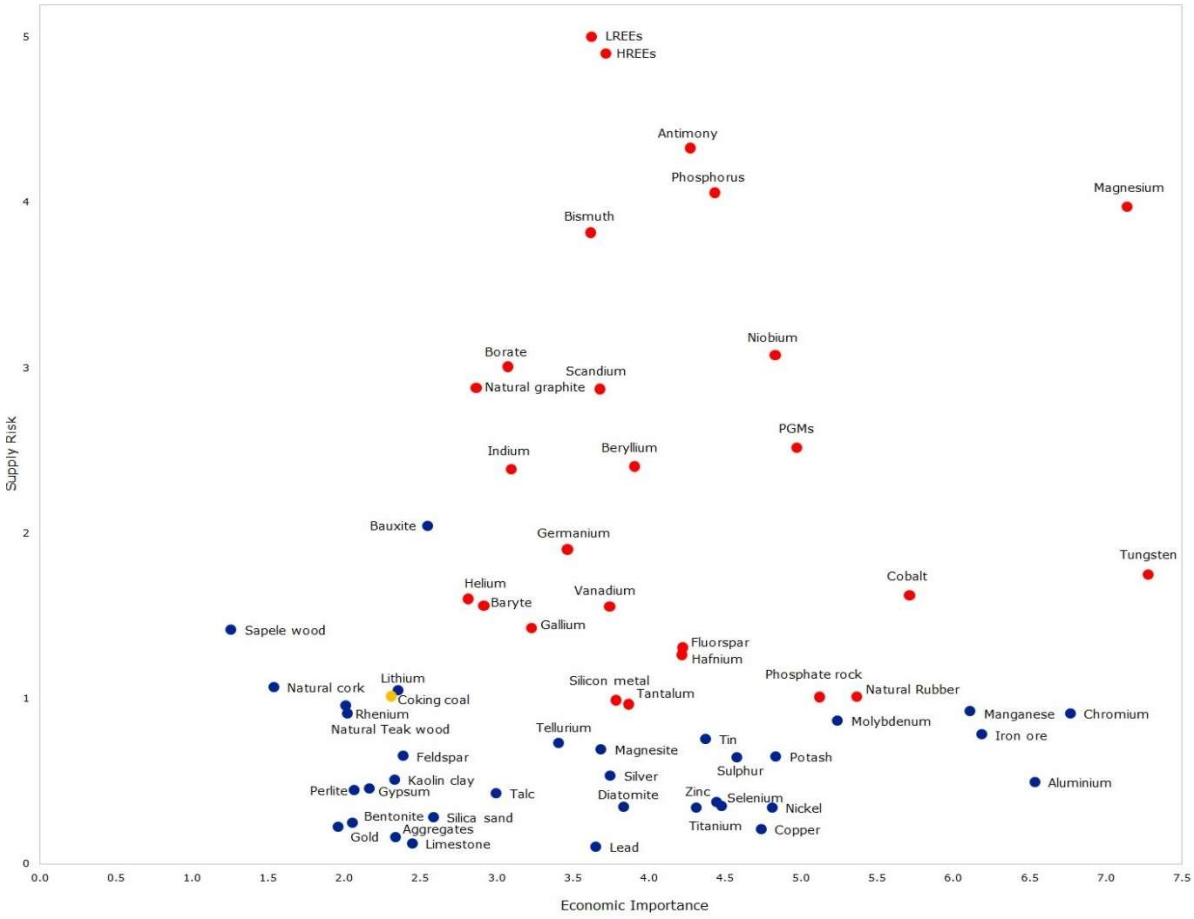

Figure 3.1 Criticality assessment of raw materials according to their economic importance and supply risk. Critical raw materials (red dots) and non-critical raw material (blue dots) (European Union, 2017).

The economic importance of carbonatites is well documented not only for been the main source of light rare earth elements (LREE), but also for been a source of P, U, Th, Sc, Nb, Ta, Fe, Ti, Fl, Zr, Ba, Cu, vermiculite, phlogopite, baddeleyite and bauxite, among others (i.e. Fan et al., 2016; Orris and Grauch, 2002; Simandl and Paradis, 2018; Woolley, 2001). Up to date, 527 carbonatite occurrences have been described worldwide. Africa has 40% of the known carbonatite deposits, of which 43 occurrences have been found in South Africa (Verwoerd, 1993; Woolley, 2001; Madugalla *et al.*, 2014). Palabora (Phalaborwa) Igneous Complex (PIC) is the most noticeable and the unique economic Cu deposit hosted by carbonatites. Previous studies examined the rare earth minerals of PIC as petrogenetic indicators of e.g. the Loolekop pipe formation of PIC (Giebel et al., 2019, 2017; Milani et al., 2017). They describe the occurrence of fergusonite and REE-Ti-betafite associated with

magnetite in transgressive carbonatites; bastnäsite enclosed in calcite and dolomite in transgressive carbonatites; monazite replacing primary apatite in transgressive carbonatites; britholite as rims around serpentines and chondrodites in both carbonatites and phoscorites —also known as foskorites, (Wall and Zaitsev, 2004) pag. 46); as well as parisite, synchysite, ancylite, cordylite and anzaite, particularly in carbonatite and phoscorite (Dawson and Hinton, 2003; Giebel et al., 2019; Milani et al., 2017).

Currently there is no REE mining in South Africa, but several project are on track, including the Steenkampskraal project in the Western Cape with 0.5 Mt of 1% REO cutoff, of which 86,900 tons have an average of 14.36% REO, and Zandkopsdrift project with 57 Mt of 1% REO cutoff (Gambogi, 2016; Harmer and Nex, 2016). PIC has not been mined for REE up to now, although it has reserves of 652 Mt at 0.15% REO cutoff (USGS, 2002). However, the large amount of residues in PIC associated to the extraction of copper and apatite could be mineable. In fact, due to the previous material processing, there might be an enrichment of REE during the beneficiation process and their extraction could be more cost-effective.

3.2. MINE WASTE REVALORIZATION AND REUSE

Before the end of 20th century, each mine used to extract only one to two commodities at high cut off. Therefore, valuable materials were left behind in the mining wastes (Blengini et al., 2019). The current scarcity of mineral resources, the increasing demand and price, and the technological advances are the main driving forces towards mine waste revalorization and re-mining. The mineral waste reprocessing of old tailings and waste rock dumps (WRDs) has become a common practice lately. Although it is almost as old as mining itself, as Lebre and co-authors illustrated with a tailing reprocessing case dating from 1905 (Lèbre *et al.*, 2017). A more recently case is Penouta Mine; a Spanish tin mine that closed down in 1985 and reopens again in 2018 to recover Tantalum and Niobium from its tailings (Lèbre *et al.*, 2017). Mining companies are mining either their own tailings and WRDs or those from neighboring mines to recover either the same commodity, or a different one.

3.2.1. REE-RECYCLING AND MINE WASTE REPROCESSING

The scarcity of economic REE deposits promoted the investigation of new REE sources such as recycling, currently limited to batteries, magnets, catalysts and fluorescent lamps. Furthermore, secondary REE-resource investigation has gained momentum on the last years, focused on industrial wastes such as phosphogypsum stacks (fertilizer industry), red mud (aluminum industry), coal ash (thermal power plants), wastewater streams and mining wastes (slags, tailings and rock dumps) (Humsa and Srivastava, 2015; Jowitt et al., 2018; Zhang et al., 2014). Those mines whose ore were extracted from REE-bearing deposits, such as carbonatites, peralkaline igneous deposits, kimberlites, laterites, ion-adsorption clays and placer deposits, among others, are potential sources of REE (Jowitt et al., 2018). Also in REE mines, the inefficiency of the rare earth ores beneficiation produce tailings with substantial concentration of rare earth elements. That is the case of Bayan Obo with only 10% REE recovery and Mountain pass, whose tailing has more than 3% of REE. Indeed, the tailing of the latter is the second largest rare earth deposit in the United States (Binnemans et al., 2015). The application of circular economy model to REE industry is the main geopolitical strategy to ensure the security supply. This includes the reprocessing of mining and industrial wastes with REE content, as well as the recycling of REE-rich products such as electronic waste (e-waste).

Even though the decision of reprocessing waste is exclusively based on economic factors, there is a clear environmental benefit since the commodities recovered from the waste will no longer be released to the environment (Hansen *et al.*, 2005). This is especially relevant for the present case study since PIC is located on the border of the Kruger National Park, the biggest natural reserve of South Africa (19,485 km^2) and declared a biosphere reserve by UNESCO in 2001. In addition, it is part of the Great Limpopo Transfrontier Park (35,000 km^2) since 2000, one of the biggest parks worldwide (K2C, 2014).

Although ore reprocessing is not novel, and REE scarcity is pushing the searching for alternative sources, no previous studies have addressed the revalorization potential of the mining waste produced at PIC as secondary source of REE. The present study is a comprehensive mineralogical and geochemical characterization

of rare earth minerals and rare earth-bearing minerals from PIC's tailings and waste rock dumps. This study addresses the first steps towards the revalorization and reclassification of the mining residues as possible REE resource. In addition, the mineralogical characterization of REE occurrence in these residues could assist for future mineral processing design in this industrial complex and elsewhere.

3.2.2. MINE WASTE RECYCLING AS ALKALINE MATERIAL

Alkaline wastes such as fly ash, paper mills and red mud, among other, has been widely studied for their application as reagent to neutralize acid drainage and acid wastewater (Millán-Becerro et al., 2019; Paradis et al., 2006; Pérez-López et al., 2011; Surender, 2009). However, the knowledge about the potential of alkaline mine wastes as reagent for water treatment is scarce. Certainly, most mining wastes produce acid mine drainage (AMD), mainly due to the content of iron sulphide minerals such as pyrite. However, some mines extract commodities hosted by alkaline rocks such as carbonatites and phoscorites that are the main source of light REE (LREE) and phosphate, respectively (Gambogi, 2019). The high concentration in carbonates, mainly calcite, are transferred to the wastes. Therefore, the mine wastes of such mines become an attractive source of neutralizing reagent. Also, the characteristics of the material that, in the case of tailings, are already milled, contributes to the low cost and efficiency of alkaline mine waste for acid wastewater treatment. The use of alkaline mine waste to neutralize acid wastewater would have a double environmental benefit; i) a reduction of the solid waste produced by mines and ii) the improvement of the industrial wastewater quality, reducing their impact in the surroundings.

3.3. WATER TREATMENTS

The water treatments available for acid mine or industrial wastewater are subdivided according to the water flow, energy and maintenance requirements in; i) Active water treatments: capable to treat high volume of water using external source of power and industrial reagents involving high CAPEX and OPEX; and ii) Passive water treatments: treat smaller volume of water with naturally-available energy sources, in gravity-flow treatment systems which require low maintenance, with the bulk cost associated with the commissioning of the plant as CAPEX. It is

worth mentioning that nowadays novel hybrid systems, so called semi-passive, have been under trial.

Many passive treatment methods have been developed over the past three decades, such as aerobic and anaerobic wetlands, Anoxic Limestone Drains (ALD), limestone sands, beds, ponds and open channels, diversion wells, reducing and alkalinity producing systems (RAPS) and ReRAPS, among others (e.g. Watzlaf, 2004). More recently, a new system called Dispersed Alkaline Substrate (DAS) has been developed to neutralize acid mine drainages and remove trivalent metals with the aim to solve the clogging problem caused by the Al^{3+} and Fe^{3+} precipitation that has been documented in many of the previously mentioned systems (Cravotta III and Trahan, 1999; Robbins et al., 1996; Skousen et al., 2017; Watzlaf et al., 2002, 2000; Ziemkiewicz et al., 2003). This new system consists of an inert matrix of wood chips, which provide high permeability and reduce clogging problems, mixed with a fine-grained alkaline material such as limestone sand and magnesia (MgO) (Rötting et al., 2007; 2008). This system has been implemented at full scale in Huelva, Spain in two different sites; Mina Esperanza (Caraballo et al., 2011) and, more recently, Mina Concepcion (Figure 3.1). However, the main disadvantage of the limestone is that the calcite only increases the pH up to 5 or 6, thus only promoting the precipitation of trivalent metals. Even though, the co-precipitation of divalent metals may take place during the removal of trivalent metals such as Al3+ and Fe3+, there are divalent metal such as Mn and Zn that require high pH (around 8 to 9) to be removed as a hydroxides or carbonate from solution (Cortina et al., 2003). Magnesia-DAS was proposed as a solution in order to fully remove those divalent metals (Rötting *et al.*, 2008). However, high concentrations of Mg were released into the treated water. These disadvantages of calcite- and magnesia-DAS, together with the high incidence of alkaline mine in South Africa, promoted the development of an improved water treatment named BDAS system. This system is based on DAS technology and was developed by the University of the Free State, South Africa (van Heerden et al., 2015). BDAS has the capacity to remove di- and trivalent metals, as well as sulphate using witherite ($BaCO_3$). The interaction $BaCO_3$ - water can be described in the following equations (Gomez-Arias et al., 2015):

1. $BaCO_3$ is dissolved in contact with wastewater:

$$BaCO_3 + H_2O \rightarrow Ba^{2+} + HCO_3^- + OH^- \quad 3.1$$

2. Sulphates dissolved in the wastewater precipitate as barium sulphates:

$$BaCO_3 + H_2SO_4 \rightarrow BaSO_4 + H_2CO_3 \quad 3.2$$

3. The pH increases above 8 by consuming protons and releasing bicarbonate anions:

$$BaCO_3 + H^+ \rightarrow Ba^{2+} + HCO_3^- \quad 3.3$$

4. The high pH and the presence of bicarbonate anions promote metal precipitation as carbonates:

$$Me^{2+} + HCO_3^- \rightarrow MeCO_3 + H^+ \quad 3.4$$

This system has been successfully used to treat acid and alkaline wastewater from mines and other industries at both bench and pilot scales (Castillo et al., 2015; Gomez-Arias et al., 2015; Torres et al., 2018).

Figure 3.2 Aerial image of a passive water treatment plant using dispersed alkaline substrate (DAS) technology to remediate acid mine drainage in Huelva, Spain (Google Earth Pro, 2020).

For instance, in 2014, a first attempt to neutralize extremely acid water, generated from the phosphoric acid plant of the Fertilizer industry located in PIC, was carried out using a BDAS system. However, the extremely acidic conditions (net acidity of 52 g/L as $CaCO_3$) and the high concentration of anions and cations depleted the efficiency of the system within three months. The need to optimize the system prolonging the life cycle of the water treatment and decreasing its operational costs, lead the assessment of other alkaline materials that could be used as a pre-treatment for BDAS system. In fact, the alkaline mine waste from PIC might represent a source of neutralizing reagent, as well as a secondary resource of REE, both aspects unexplored so far.

CHAPTER 4: MINE WASTE FROM CARBONATITE DEPOSITS AS POTENTIAL RARE EARTH RESOURCE: INSIGHT INTO PHALABORWA (PALABORA) COMPLEX

ABSTRACT

Phalaborwa (Palabora) Igneous Complex (PIC), South Africa, has been mined for the last six decades for copper and phosphate, among others commodities. As a result, more than 4,500 Mt of mining wastes have been dumped in waste rock dumps (WRDs) and tailing impoundments. This study aims to investigate the potential of the PIC wastes as a secondary resource of rare earth elements (REE) and its possible processing options, by means of both mineralogical and geochemical determinations. Phoscorites and carbonatites are major lithologies in the WRDs and contain a notable concentration of REE, of which 0.2 and 0.1 wt%, respectively, would be easily extractable. The mineralogical results show monazite as the main REE-mineral (∑REE 60 wt%), while fluorapatite and calcite are the most important REE-bearing minerals (∑REE 1 and 0.5 wt%, respectively) for their abundance. On the other hand, the tailings are comprised mostly by monomineralic particles of calcite, dolomite, pyroxene, fluorapatite, magnetite and phlogopite. Based on the geochemical results, the extraction of REE from monazite, fluorapatite, calcite and dolomite, from tailings produced by both the Cu and the phosphate mines, might produce up to 5.65 and 1.75 kg of REE per ton, respectively. Therefore, tailings from PIC have the potential to become an asset. An approach to circular economy by re-processing mining wastes would extend the lifetime of PIC mines and their benefits, while reducing the waste of resources and their environmental impact.

4.1. INTRODUCTION

Rare Earth Elements (REE), including lanthanides, yttrium and scandium, can be subdivided into light REE (LREE) for La, Ce, Pr and Nd; medium REE (MREE) for Sm, Eu and Gd; and heavy REE (HREE) for Tb, Dy, Ho, Er, Tm Yb, Lu, Y and Sc. All of them are classified as critical raw materials (CRM) (EC-DG ENTR, 2014). Nassar et al. (2020) has shown how REE disruption potential (understood as a producing country's ability and willingness to supply the U.S.) has decreased in the past few years thanks to the increased production diversification, particularly outside of China. However, REE still pose the greatest supply risk for the manufacturing sector. Resulting from this recent economic and supply risk assessment, the ability to diversify the REE supply sources and include new alternative resources and strategies (e.g., mine wastes revalorization and reprocessing) are of paramount importance for both world´s economy and geopolitical stability.

REE crustal abundance typically range from 0.5 to 60 ppm, but minable deposits are scarce comprising only 120 Mt of the global reserves (Krishnamurthy and Gupta, 2015). Economic REE concentrations are mainly associated with carbonatites, peralkaline igneous deposits and REE-bearing clays and placer deposits (Gambogi, 2019). Carbonatites are the main source of light rare earth elements (LREE) and Sc. Currently, 527 carbonatite occurrences have been reported worldwide, of which 43 deposits have been found in South Africa (Madugalla et al., 2014; Owen and Madari, 2009; Verwoerd, 1993; Woolley, 2001). Among them, Phalaborwa Igneous Complex (PIC) is the most noticeable and unique economic carbonatitic-hosted Cu deposit on Earth (Hanekom et al., 1965). Previous petrogenetic studies of PIC have highlighted the occurrence of REE-minerals, particularly in fresh carbonatite and phoscorite rocks (Dawson and Hinton, 2003; Giebel et al., 2019, 2017; Milani et al., 2017).

Mine residues reprocessing is widely studied nowadays around the world. At PIC, the intense mining of Cu and phosphate generate about 18 and 29 Mt of waste per year, respectively (Foskor, 2018; Golder Associates, 2019). Part of it is reprocessed to extract magnetite, Zr, Ni and anode slimes with Au, Ag and Pt (Foskor, 2018; Valderrama et al., 2011; Zhang et al., 2014). However, no previous studies have

addressed the potential revalorization of PIC's waste rock dumps (WRD) and tailings as secondary source of REE.

The present study encompasses a comprehensive mineralogical and geochemical characterization of REE content in PIC's tailings and WRDs, as well as envisages the first estimation for the revalorization and reclassification of these mining residues as a possible REE resource. In addition, the mineralogical characterization of REE occurrences in these residues could assist in future mineral processing in this industrial complex.

4.2. SITE DESCRIPTION

4.2.1. GEOLOGICAL SETTING

Phalaborwa (Palabora) Igneous Complex (PIC) is located in the North-Western edge of the Kaapvaal Craton, associated with a series of intrusions of Paleoproterozoic alkaline magmas (Aldous, 1986; Basson et al., 2017; Hanekom et al., 1965). This complex is a pipe-like intrusion with three well-differentiated sections (Figure 4.1); (1) the Northern Pyroxenite, formed mainly of olivine and phlogopite. It shows pegmatite-like textures and pervasive alteration to serpentine and vermiculite; (2) the Southern Pyroxenite comprised mostly by coarse grained phlogopite and vermiculite and subordinated apatite and pyroxene; and (3) the Central Carbonatite, also known as the Loolekop pipe, constitutes a concentric structure made of three ring–like bodies. From outside inwards, they are: i) the outermost pegmatitic-pyroxenite body, composed by pyroxene, phlogopite and fluorapatite; ii) the intermediate phoscorite, which is mainly formed by hydroxyapatite and fluorapatite, partially serpentinized olivine and magnetite; and iii) the carbonatite core mainly composed of carbonates (calcite and dolomite), fluorapatite, chondrodite, olivine, phlogopite and biotite. This carbonatite core includes two facies; the outer and older, banded carbonatite (B-carbonatite) and the inner and younger, transgressive carbonatite (T-carbonatite). The main phosphate ore is associated to the intermediate phoscorite whereas the Cu mineralization is linked to the carbonatitic core (Briden, 1976; Giebel et al., 2019, 2017; Hanekom et al., 1965; Heinrich, 1970; Stettler et al., 1989; Uken and Watkeys, 1997; Verwoerd, 1993; Wilkin and Barnes, 1997; Wu et al., 2011).

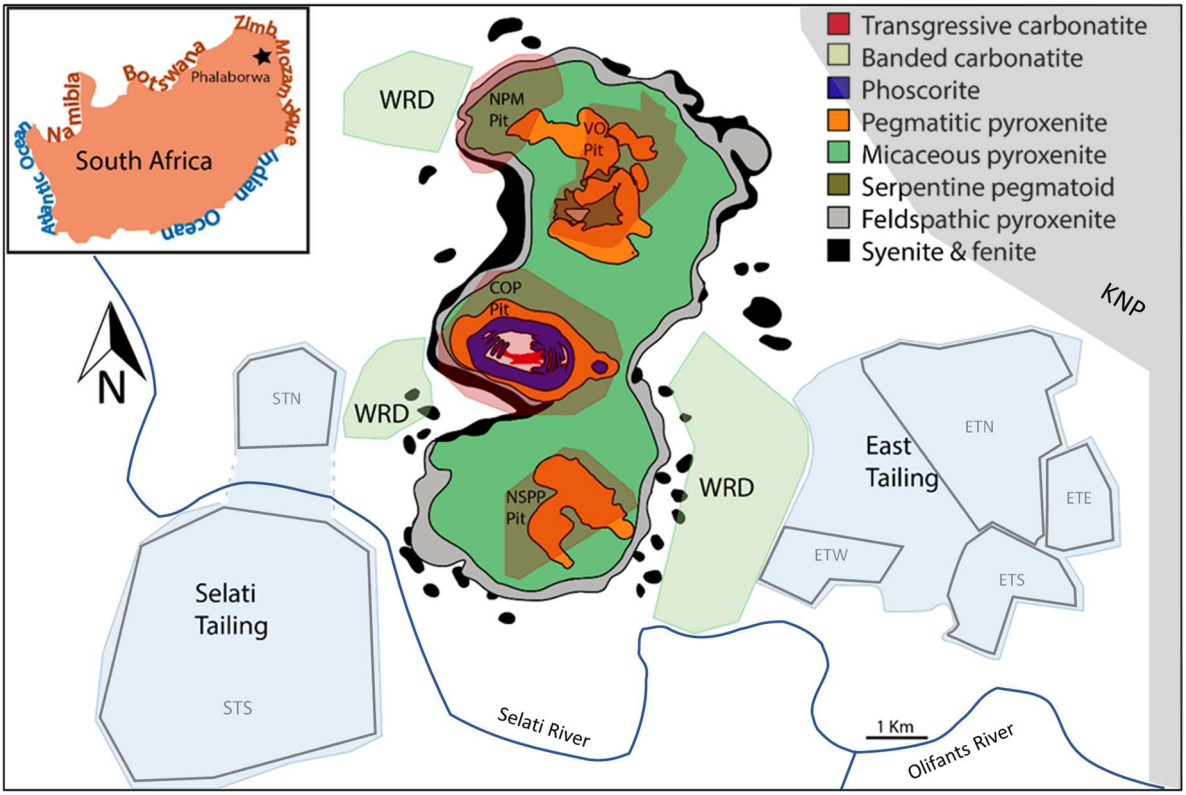

Figure 4.1. Simplified geological map of Phalaborwa Igneous Complex (modified from Giebel et al., 2019). Red shadows include the Cu open pit (COP), the North Pyroxenite Mine (NPM) pit, the New South Pyroxenite Pit (NSPP) and Vermiculite Open (VO) Pit; Blue shadows represent the East and Selati tailing dams with each tailing sector marked in grey ; and shaded in green are represented the waste rock dumps (WRDs).

4.2.2. LOCATION AND INDUSTRIAL OPERATIONS

The complex is located in the Limpopo province of South Africa, adjacent to the town of Phalaborwa and the Kruger National Park. The mining activities began in the 1950s with the extraction of phosphate and Cu minerals. Currently, 50 km^2 of the complex is occupied by a synergic network of mining companies dedicated mainly to the extraction of Cu, phosphate and vermiculite (Brink, 2011; Foskor, 2018; Steyl, 2011). Decades of mining activity in this area has generated multiple WRDs and tailings (Figure 4.1). The main WRD of PIC is located east of the Cu open pit (COP) (both decommissioned) and collected the removal of COP overburden. It has a height of 105 m above ground level and piles about 1,085 Mt of mainly barren carbonatites, and minor barren phoscorites and pyroxenites. Two smaller WRDs,

located southwest (decommissioned) and northwest (active) of COP, collect mainly barren pyroxenites and phoscorites from North Pyroxenite Mine (NSPP), New South Pyroxenite Pit (NPM) and Vermiculite Open (VO) pit (Figure 4.1) (Brink, 2011; Moukodi, 2008). Selati tailing is located in the southern most area of PIC, intersected by the Ga-Selati River. This has been the largest tailing in the southern hemisphere, with about 2,830 Mt of processed material from the phosphate plant (Foskor, 2018). The East tailing is located in the eastern most part of PIC, which collects about 575 Mt of the residues after carbonatite froth-flotation from the Cu beneficiation (Hu et al., 2017; Moukodi, 2008).

4.3. SAMPLES AND METHODS

4.3.1. WASTE ROCK AND TAILING SAMPLING

A set of 60 samples, ranging from 1 to 12 kg each, were collected from the PIC's WRDs, including all the representative lithological-type fragments. Tailing samples were collected from 6 different sectors. A composite of approximately 5 kg and up to 2m depth, were taken from each section (Figure 4.1), including six samples of recently piled tailings and 14 samples of different ages. The description and coordinates of the sampling points for both WRD and tailings are displayed in table B.1 of the supplementary material.

Rock samples were split, half-samples were crashed, milled, homogeneously mixed and representative subsamples were collected using a sampler splitter for sequential extraction assays. The remaining rocks were used for mineralogical characterization. Tailing samples were homogeneously mixed and split for further chemical and mineralogical analysis.

4.3.2. MINERALOGICAL CHARACTERIZATION

Detailed mineralogical and micro-textural studies were undertaken at the University of Huelva (Spain). Fourteen polished thin sections from the main lithologies were studied by both petrographic microscope and scanning electron microscope coupled with energy dispersive spectroscopy (SEM–EDS) Fei-QUANTA 200 equipped with a microanalyzer EDAX Genesis 2000. Ten thin sections

containing carbonates, silicates, phosphates, oxides and sulphides were selected for electron microprobe analyses (EPMA). The chemical compositions were determined using a JEOL JXA-8200 Super Probe Electron Probe Micro-Analyzer. The measurements were performed on carbon-coated polished sections using an acceleration voltage of 20 kV, 20 nA beam current, 30 s counting time for the peak and 10 s for the background. The analysis spots were selected using backscattered electron (BSE) images. Concentrations of FeO, CaO, MgO, MnO_2, SrO, BaO, CuO, ZnO, PbO, TiO_2, CuO and ZnO in carbonates and Fe-oxyhydroxides, as well as Ag, Sb, Mn, Cd, Bi, As, Sn, Co, Se, Ni, Au, Cu, Zn, Fe, Pb, Hg and S elements in sulphides and sulfosalts were determined by wavelength-dispersive spectroscopy (WDS). Up to 73 successful EPMA analyses on phosphates, 19 on carbonates, 12 on oxides and 29 on silicates have been obtained. Routine data reductions, including full matrix (ZAF) corrections, were performed. In addition, in order to perform semiquantitative mineralogical analyses on waste rock dump samples, 14 samples were investigated by X-ray diffraction (XRD) using a Broker D8 Advance Powder Diffractometer with Cu–Kα radiation.

The mineralogy and textures of tailings were also investigated on ten polished sections by both petrographic microscope and SEM-EDS JEOL JMS-5410 equipped with a Link Oxford microanalyzer from the University College Dublin. Compositional mapping of SEM was undertaken by silicon drift detector (SDD), followed by semiquantitative mineralogical analyses by ImageJ software (https://imagej.nih.gov/ij).

4.3.3. MINERAL DISSOLUTION BY SEQUENTIAL EXTRACTION ASSAYS AND CHEMICAL ANALYSIS

Samples were submitted to a REE leachability assay based in a sequential extraction procedure (described in supplementary material, appendix A.1) designed to contact the residues with different chemical reagents to release the elements hosted on the different mineral phases. The selection of the following four fractions of the sequential extraction is based on the main mineralogy of these mine residues (i.e. phosphates, carbonates, Fe-oxides, sulphides and silicates); fraction 1 (F1) induces dissolution of water/acid soluble minerals and release of exchangeable elements by the use of 0.11 mol/l acetic acid, fraction 2 (F2) attacks the reducible

fraction by the use of 0.1 mol/l hydroxylamine hydrochloride, fraction 3 (F3) tackled the oxidizable fraction by the use of 8.8 mol/l H_2O_2, temperature (85°C) and 1.0 mol/l ammonium acetate and fraction 4 (F4) digests the residual fraction by the use of aqua regia (a mixture of 12 mol/l HCl and 15.8 mol/l HNO3 in the ratio 3:1) at 100°C.

Table 4.1. Simplified BCR-sequential extraction procedure (Pérez-López et al., 2011)

Step	Fraction	Reagents	Procedures
F1	Easily soluble	0.11 M CH_3COOH	40 mLCH_3COOH + 1 g sample shaken for 16 h
F2	Reducible	0.5 M $NH_2OH{\cdot}HCl$ (pH 2)	40 mL $NH_2OH{\cdot}HCl$ + residue from step 1 shaken for 16h
F3	Oxidizable	8.8 M H_2O_2	10 mL H_2O_2 + residue from step 2 at 85˚C to almost dryness
		1 M $NH_4C_2H_3O_2$ (pH2)	50 mL $NH_4C_2H_3O_2$ shaken for 16 h
F4	Residual	Aqua Regia 3:1	10 mL aqua regia + residue from step 3 (first 20 h and then 1 h at 100˚C)
		(12 M HCl:15.8 M HNO_3)	

Additionally, sub-samples of all the studied residues were independently submitted to an aqua regia digestion to obtain the pseudo total bulk chemistry of the samples. Specific details about the sequential extraction procedure are offered in the Supplementary Information. The extractants of the sequential extractions were analysed at the University of the Free State by Inductively Coupled Plasma Mass Spectrometry (ICP-MS) PerkinElmer NexIon 2000c, inductively coupled plasma optical emission spectroscopy (ICP-OES) Teledyneleemanlabs Prodigy and High-Performance Liquid Chromatography (HPLC) Shimadzu prominence (analytical details included in the supplementary materials, appendix A.2). In addition, 20 subsamples were also analysed by an accredited laboratory at the Institute for Groundwater Studies at the University of Free Sate in order to validate the results.

4.4. RESULTS

4.4.1. WASTE ROCK DUMPS

Rock fragments of diverse lithologies were observed unevenly distributed, regarding size and mineralogical composition, along all the main slopes of the WRDs. Most common fragments include (Figure 4.1 and 4.2):

T-carbonatite is mainly comprised of calcite, magnetite, dolomite, enstatite and fluorapatite. The subordinated mineralogy consists of variable amounts of phlogopite, muscovite, chalcopyrite, bornite, chalcocite, pyrite, monazite, zircon, rutile, bastnäsite-(Ce) and anzaite-(Ce). The T-carbonatite shows phaneritic texture characterized by coarse magnetite associated with euhedral aggregates of calcite and dolomite and Cu-sulphides filling interstices (Figure 4.2a).

B-carbonatite is mostly composed of calcite, dolomite, magnetite, enstatite, fluorapatite and phlogopite. The minor mineralogy consisted of chalcopyrite, chalcocite, pyrite, pentlandite, olivine, serpentine, chlorite and parisite. These minerals have been observed distributed in inequigranular, euhedral to subhedral aggregates forming mm-to-cm rhythmic banding (Figure 4.2b).

Phoscorite is mostly formed of fluorapatite and phlogopite, and minor magnetite, ilmenite, ulvospinel, olivine, serpentine, calcite, dolomite and bornite. These minerals show phaneritic textures characterized by inequigranular euhedral fluorapatite aggregates with phlogopite and calcite filling open spaces (Figure 4.2c).
F-pyroxenite is mainly comprised of microcline, diopside, hydroxyapatite, fluorapatite, and subordinated amounts of calcite, magnetite, chalcopyrite, bornite and allanite. Clinopyroxenes and feldspars appear as coarse euhedral aggregates, including pegmatoid texture, whereas apatite group minerals have been observed as fine-grained euhedral to subhedral aggregates (Figure 4.2d).

M-pyroxenite is mainly composed of fine-grained diopside and phlogopite. The subordinated mineralogy consists of variable proportions of interstitial microcline, magnetite, hydroxyapatite, thorite and baddeleyite (Figure 4.2e).

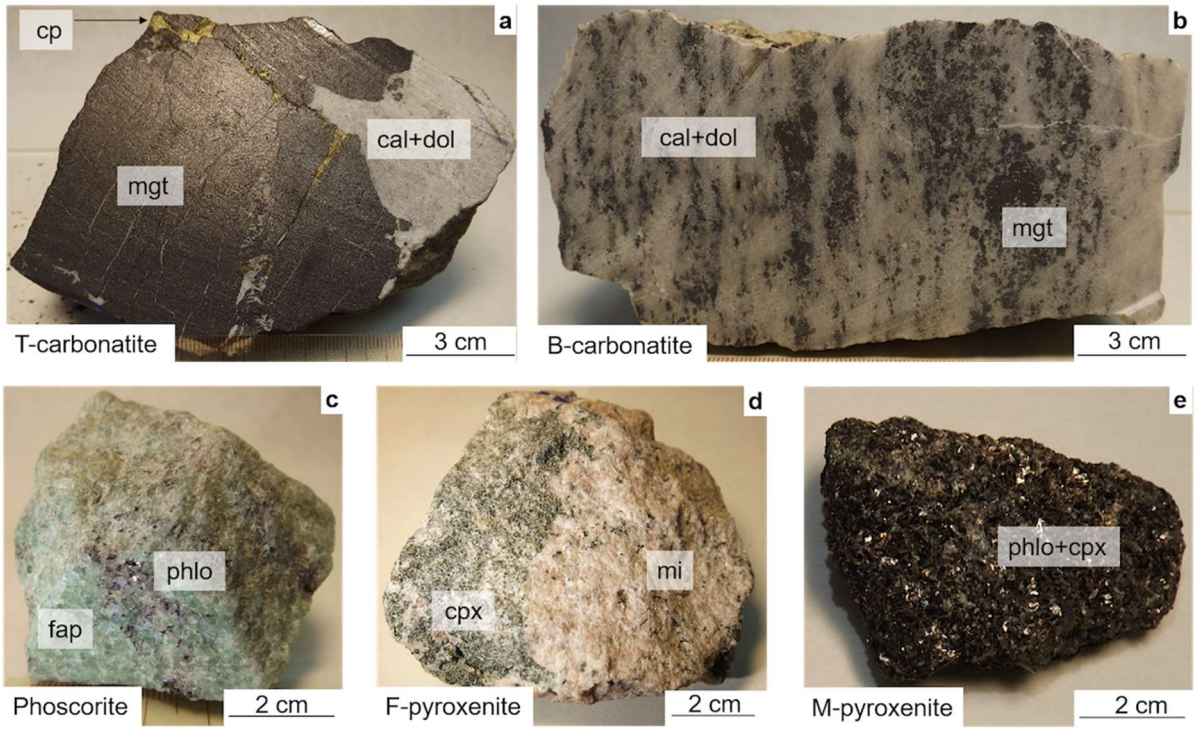

Figure 4.2 Rocks fragment from the waste rock dumps of Phalaborwa Igneous Complex; B-carbonatite formed of alternating band of magnetite (mgt) and calcite (cal) associated with dolomite (dol); (b) T-carbonatite composed by magnetite, calcite, dolomite and chalcopyrite (cp) filling fractures; (c) phoscorite comprised of fluorapatite (fap) associated with phlogopite (phlo); d) F-pyroxenite formed by microcline (mi) and clinopyroxene (cpx); and e) M-pyroxenite composed by phlogopite and clinopyroxene.

4.4.2. MINERALOGICAL ANALYSIS OF THE WASTE ROCK DUMPS

PHOSPHATES

Several minerals from the apatite group have been identified as a major component in all the WRDs (Figure 4.1). Fluorapatite have been recognized in both carbonatites (Figure 4.3a and h) and phoscorites (Figure 4.3b), whereas hydroxyapatite is most common in pyroxenite fragments (Figure 4.3c and e).

Fluorapatites and hydroxyapatites occur as euhedral to anhedral aggregates showing a wide range of grain sizes, between a few µm to 2 mm in both carbonatites (Figure 4.3a and h) and pyroxenites (Figure 4.3c and e), and up to 4 mm in phoscorites (Figure 4.2c). Both hydroxyapatite and fluorapatite have been observed

associated mainly with carbonates (Figure 4.3a), micas (Figure 4.3b), pyroxenes and feldspars in all the waste rock samples (Figure 4.3c and d).

Fluorapatite from both carbonatites and phoscorites shows similar high REE contents (mean values of 1.03 and 0.93 wt% respectively), being relatively enriched in LREE (mean values of 0.83 and 0.66 wt%, respectively) (Figure 4.4a). Fluorapatite grains from both carbonatites and phoscorites exhibit internal heterogeneous composition related to its REE distribution. Fluorapatite from carbonatites shows an enrichment in REE at the crystal boundaries (Figure 4.3a), whereas fluorapatite from phoscorites exhibits an opposite REE distribution (Figure 4.3b).

CARBONATES

Calcite and dolomite have been identified in all the WRDs (Figure 4.2a, b, Figure 4.3a, g, h, k, l and o). They are most abundant in carbonatites with a 3:1 ratio. These minerals occur with large variability of textures, such as coarse calcite and dolomite groundmasses in transgressive carbonatites (Figure 4.2b), alternating mm-to-cm bands in banded carbonatites (Figure 4.2a), calcite with dolomite inclusions disseminated in banded carbonatites (Figure 4.2a) and fine interstitial infilling in phoscorites and pyroxenites. Calcite exhibits higher REE contents than dolomite, showing mean values of 0.52 and 0.22 wt%, respectively. Both carbonates are relatively enriched in LREE (mean values of 0.35 and 0.13 wt%, respectively) (Figure 4.4b).

SILICATES

Pyroxenes have been found widely distributed throughout the WRDs (Figure 4.2d, e, 3c and d). In carbonatites and phoscorites, enstatite has been recognized as the most common orthopyroxene, whereas in pyroxenites, diopside is the most abundant clinopyroxene. Enstatite occurs as subhedral aggregates between a 2 μm to 2 mm. Diopside appear as euhedral aggregates which is usually replaced by chlorite and showing a wide range of grain sizes, up to 10 cm (Figure 4.2d, e, 4.3c and d). Diopside from F- and M-pyroxenites show similar low REE contents (mean values of 0.05 and 0.06 wt%, respectively), being both slightly enriched in HREE (both mean values of 0.03 wt%) (Figure 4.4c).

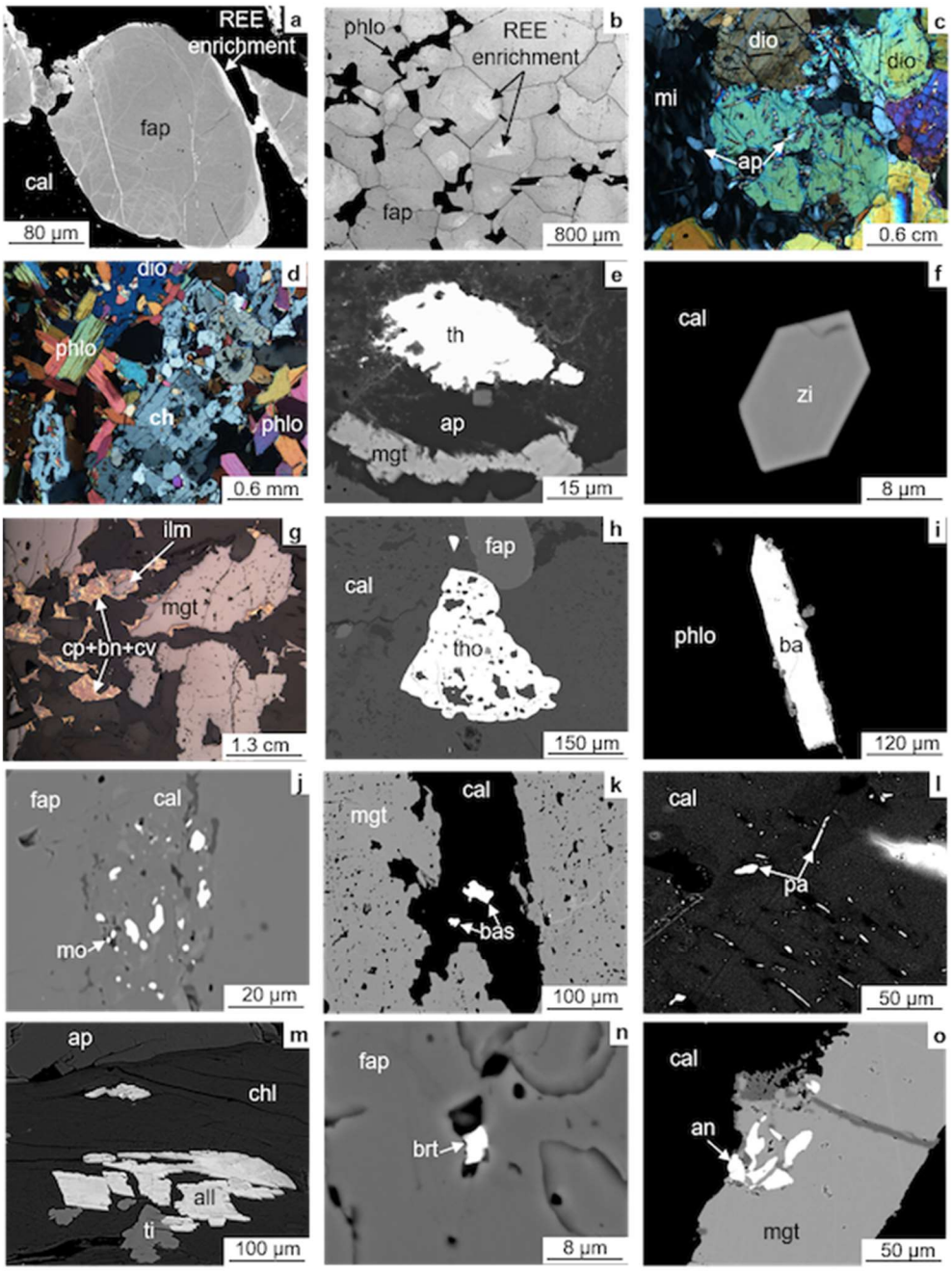

Figure 4.3 Reflected light and backscattered electron (BSE) images of the waste rocks; a) LREE enrichment along grain boundaries of subhedral fluorapatite (fap) included in calcite (cal); b) phlogopite (phlo) filling interstices in fluorapatite aggregate with LREE enrichment in the core grains; c) diopside (dio) aggregate with apatite (ap) inclusions and microcline (mi) filling open spaces; (d) phlogopite aggregate associated with chloritoid (ch) and diopside; e) thorite (th) filling spaces in apatite and magnetite

(mgt); f) euhedral zircon (zi) grain included in calcite; g) chalcopyrite (cp), bornite (bn) and covellite (cv) filling open space in magnetite, ilmenite (ilm) and calcite crystals; h) thorianite (tho) replacing calcite; i) acicular baddeleyite (ba) crystal filling interstices in phlogopite; j) monazite (mo) inclusions in fluorapatite; (k) bastnäsite (bat) grains in calcite; (l) parasite (pa) crystals associated with calcite; (m) allanite (all) interbedded with chlorite (chl); (n) britholite (bt) inclusions in fluorapatite; (o) anzaite (an) included in magnetite.

Phlogopite is the most common mica. It is broadly distributed (Figure 4.2c, e, and 4.3d) but particularly abundant in M-pyroxenites (Figure 4.2e and 4.3d). This is mainly associated with calcite, fluorapatite and magnetite in carbonatites and phoscorites (Figure 4.2c and 4.3b), whereas in pyroxenites, phlogopite is linked to diopside and microcline (Figure 4.2d). Phlogopite shows a wide range of textures and grain sizes, including coarse euhedral aggregates forming mica-pyroxenites (Figure 4.2e); fine aggregates filling interstices in fluorapatite and calcite in both phoscorites and carbonatites (Figure 4.3b).

Microcline has been recognized as the most common feldspar, unevenly distributed throughout WRDs and linked mostly to M-pyroxenites (Figure 4.1d). Microcline was observed as subhedral aggregates, up to 1 cm, associated mostly with diopside and hydroxyapatite (Figure 4.2d and 4.3c).

Thorite has been recognized as a minor mineral in both M-pyroxenite and T-carbonatite rocks fragments. Thorite has been mainly identified as micrometric inclusions in hydroxyapatite and associated with thorianite and magnetite (Figure 4.3e). Based on SEM-EDAX analyses, thorite shows a high REE homogeneous composition (mean value of 3.9 wt%), being relatively enriched in LREE and MREE (mean values of 2.5 and 1 wt% respectively).

Zircon is a minor but common silicate found in all the waste rock samples. It occurs as <10 μm euhedral crystals associated with pyroxenes, carbonates and hydroxyapatite (Figure 4.3f). Based on SEM-EDAX analyses, zircons show a homogeneous high REE distribution, with mean values of 6 wt%.

OXIDES

Magnetite is the most common oxide in all the waste rocks samples but mainly linked to both B- and T-carbonatite (Figure 4.2a, b and 4.3g). Magnetite shows a wide range of textures, grain sizes and an intricate relationship with other minerals. Overall, magnetite shows textures such as infilling of fractures, skeletal crystals included in pyroxenes and coarse aggregates (Figure 4.3e and g). Magnetite is closely associated with **ilmenite** and **ulvospinel**, showing exsolutions and intergrowth textures (Figure 4.3g). Moreover, magnetite is linked to the Cu-sulphides suite, showing textures such as Cu-sulphides replacing and filling interstices in magnetite aggregates (Figure 4.3g).

Both magnetite and ilmenite in T-carbonatite present a slightly high REE concentration (REE mean values of 0.07 and 0.06 wt%, respectively). Magnetite is relatively enriched in LREE and HREE and depleted in MREE, whereas ilmenite is enriched in HREE and MREE (Figure 4.4d and Table A.1 of supplementary material).

Thorianite has been identified as a minor but common oxide in T-carbonatite. It appears as micrometric grains associated systematically with magnetite, and to a lesser extent, with thorite (Figure 4.3h). Based on SEM-EDAX analyses, thorianite shows a homogeneous high REE distribution, with mean values of 10 wt%.

Baddeleyite occurs as a rare mineral in M-pyroxenite. It has been observed as 400 μm euhedral crystals embedded in phlogopite (Figure 4.3i). Baddeleyite SEM analyses reveal low REE concentration (mean value of 0.6 wt%).

SULPHIDES

Chalcopyrite, bornite, covellite, chalcocite, pyrite and millerite are common phases along WRDs, but mainly linked to carbonatite fragments (Figure 4.2a and b). These are in close relationship with magnetite (Figure 4.2b and 4.3g), and show complex textural features such as intergrowth, exsolutions, replacements and veinlets (Figure 4.3g).

REE MINERALS

Monazite is the most common REE. It is widely distributed throughout all the waste rocks, but linked mostly to both transgressive and banded carbonatites (Figure 4.4a and b). It has been observed as fine euhedral aggregates (1 to 50 μm in thickness) included in fluorapatite and calcite (Figure 4.3j). Monazite shows higher REE content in B-carbonatites than in T-carbonatite (mean values of 60.7 and 47.9 wt%, respectively), being both relatively enriched in LREE (mean values of 56.4 and 44.3 wt%, respectively) (Figure 4.4e).

Bastnäsite-(Ce,La) has been identified in T-carbonatites. It occurs mostly as 5-50 μm anhedral grains embedded in late calcite veins (Figure 4.3k). Ce-bastnäsite in T-carbonatite exhibits a mean REE values of 70.3, of which 62.0 wt% are LREE (Figure 4.4e).

Parisite has been only recognized in T-carbonatite. It occurs as elongated 1-20 μm crystals included in calcite (Figure 4.3l). Parisite exhibits a homogeneous REE compositions, with mean values of 53.6 wt% and enrichment in LREE up to 49.5 wt % (Figure 4.4e).

Allanite-(Ce) has been recognized in F-pyroxenites as 5-250 μm grains associated with titanite and included in chlorite (Figure 4.3m). It shows a mean REE concentration of 21.0 wt%, being relatively enriched in LREE (mean value of 18.2 wt%) (Figure 4.4e).

Britholite-(Ce) is mainly present in both F-pyroxenite and T-carbonatite. It has been observed as >40 μm crystals filling interstices in chlorites within pyroxenites, whereas in carbonatites occurs as 5 μm inclusions in fluorapatite (Figure 4.3n). It has a mean REE content of 38 wt% and enrichment in LREE up to 36 wt%.

Anzaite-(Ce) has been recognized in T-carbonatite. It appears as < 120 μm sized grains replaced by magnetite and ilmenite (Figure 4.3o). It shows mean REE contents of 52.3 wt %, being enriched in LREE (mean values of 40.6 wt%) (Figure 4.4e).

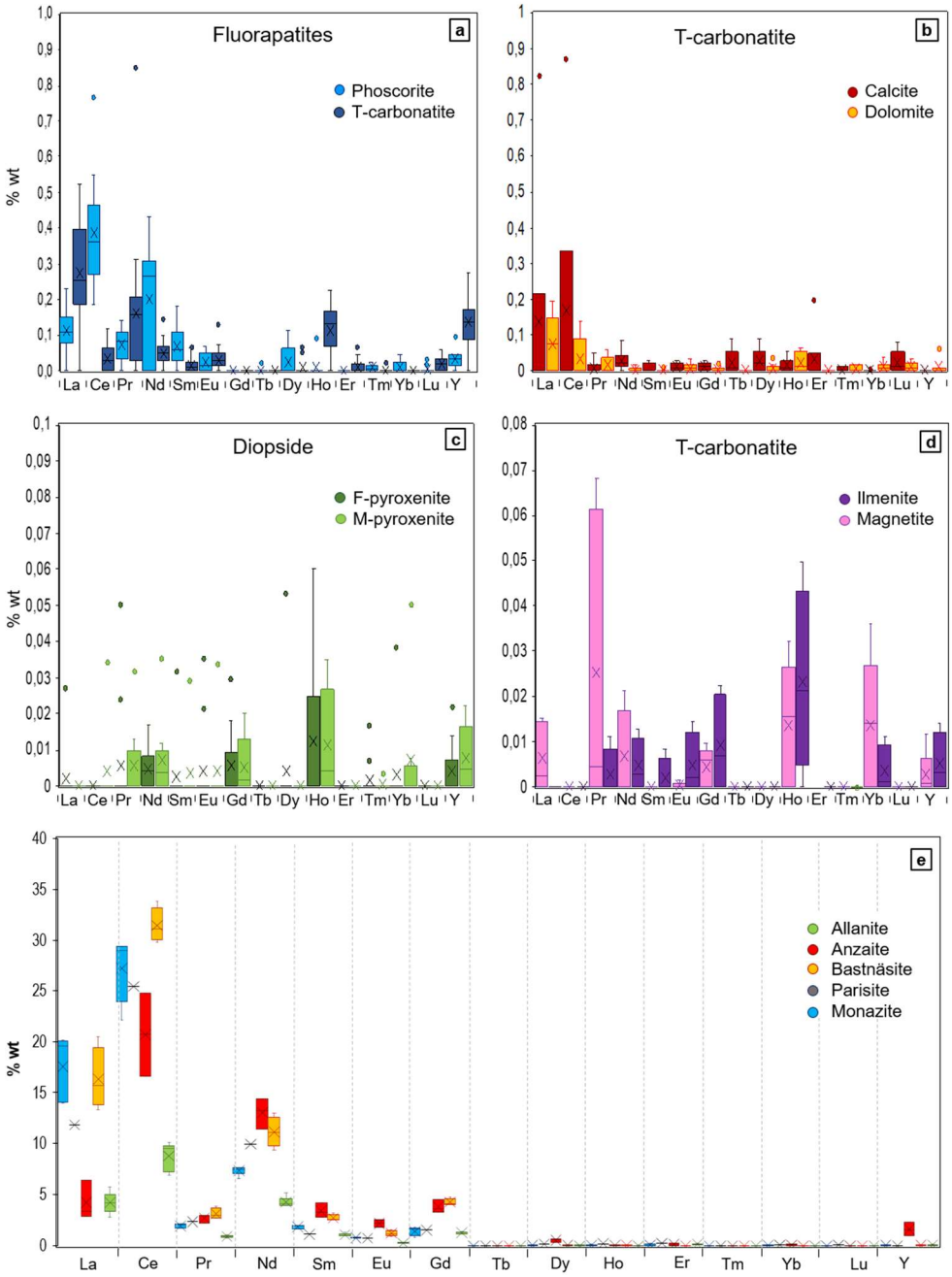

Figure 4.4 Rare earth elements distribution in both REE-bearing minerals and REE-minerals in waste rock dumps based on electron microprobe analyses (EPMA) analyses; a) Fluorapatite from phoscorites and T-carbonatite; b) Calcite and dolomite from T-carbonatite; c) Diopside from F-pyroxenite and M-pyroxenite; d) Ilmenite and magnetite from T-carbonatite; and e) REE content in allanite, anzaite, bastnäsite, parasite, monazite both phoscorites and T-carbonatite rocks. Extended data included in Table A.1 of supplementary material.

4.4.3. MINERALOGY OF TAILING PONDS

EAST TAILING

The main mineralogy is formed by calcite, dolomite, orthopyroxene, fluorapatite, magnetite, phlogopite, clinopyroxene and zircon. The minor mineralogy consists of chalcopyrite, ilmenite, pyrite, monazite, covellite, bornite, millerite, thorianite, ulvospinel and newly-formed Cu- sulphates (Figure 4.5a to e). In general terms, the mineralogy throughout East Tailing shows a homogeneous distribution, except for zircon that has only been recognized as a major component in the easternmost area (Figure 4.6).

Approximately, 90% of these minerals occur as monomineralic fragments, ranging from a few microns to 3 mm in diameter, most of them from 200 to 500 microns (Figure 4.5a and b). Some minor polymineralic fragments have been identified (Figure 4.5c, d and e), for example dolomite inclusions in calcite; fluorapatite and forsterite intergrowths; magnetite and ilmenite aggregates among phlogopite; micron-sized monazite inclusions in fluorapatite; and chalcopyrite associated with bornite and covellite, partially replaced by newly formed Cu-sulphate.

Monazite was a minor but common REE mineral showing a mean LREE value of 55.3 wt%. REE-bearing minerals identified in East Tailing are fluorapatite, zircon and thorianite (Figure 4.5). Fluorapatite has been recognized as the main REE-bearing mineral. Based on SEM-EDS analyses, most fluorapatite crystals show an enrichment in LREE in its grain boundaries reaching up to 5 wt% (Figure 4.5c). Zircon and thorianite-bearing REE have been punctually recognized showing a LREE concentration up to 13.2 and 10.2 wt% respectively.

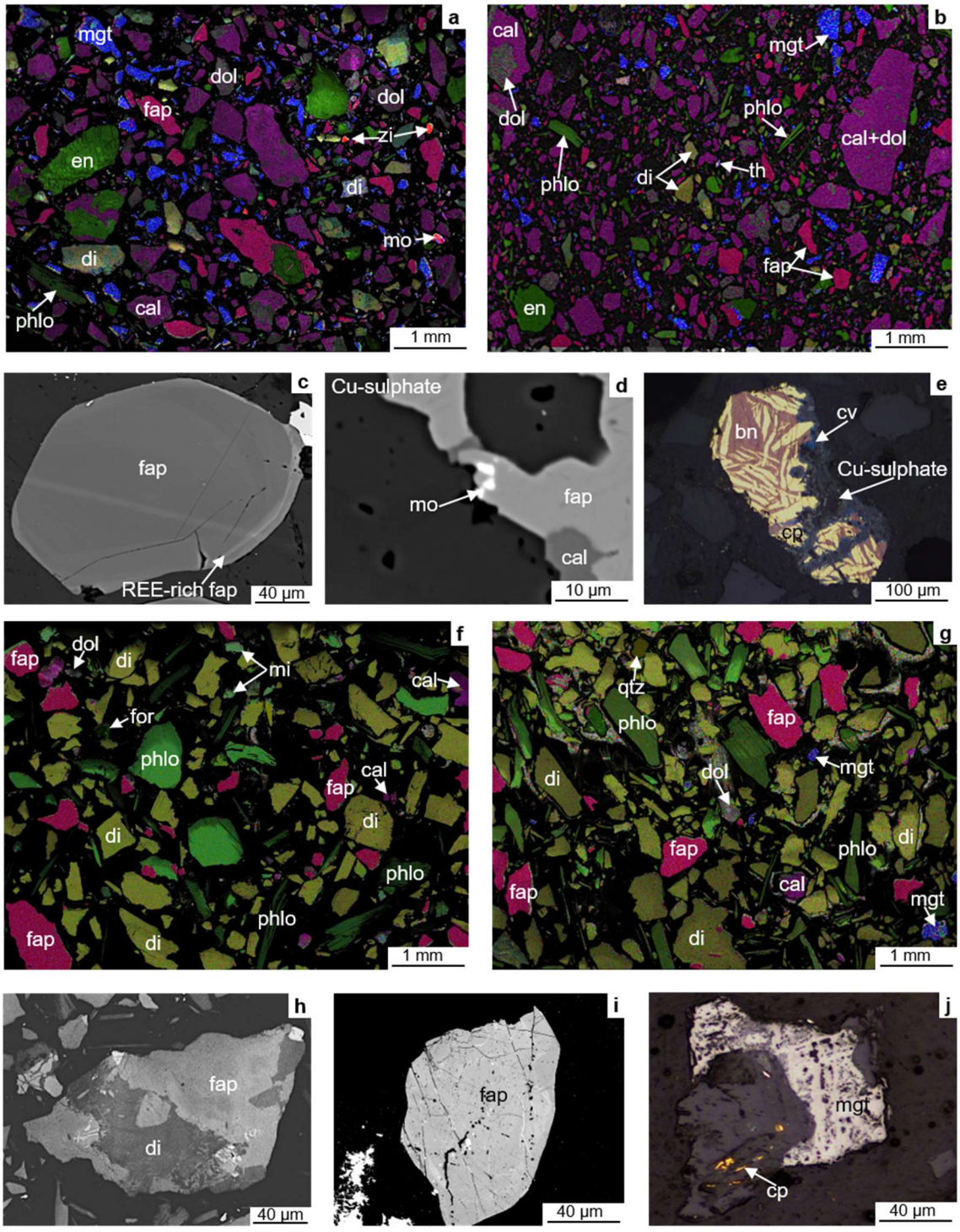

Figure 4.5 False-colour compositional scanning electron microscope (SEM) maps, petrographic microscope and backscattered electron (BSE) images of tailings samples. (a) and (b) Compositional SEM maps from East tailing showing the major mineralogy, including calcite (cal), dolomite (dol), enstatite (en), fluorapatite (fap), diopside (di),

phlogopite (phl), magnetite (mgt), zircon (zi) and monazite (mo); (c) fluorapatite showing a REE enrichment along grain boundaries; (d) monazite inclusions in fluorapatite; e) mixed-fragment formed by chalcopyrite (cp), bornite (bn), covellite (cv) and newly-formed Cu-sulphate; (f) and (g) compositional SEM maps from Selati tailing showing the major mineralogy, such as calcite, dolomite, fluorapatite, diopside, phlogopite, magnetite, microcline (mi) and quartz (qtz); (h) mixed fragment composed by diopside and fluorapatite; (i) subhedral fluorapatite included in calcite; (j) chalcopyrite and magnetite filling open spaces in calcite.

SELATI TAILINGS

The Selati tailing is mostly comprised of phlogopite, orthopyroxene, fluorapatite, calcite, quartz, dolomite, magnetite and microcline. These minerals show a homogenous distribution throughout the tailing. The subordinated mineralogy consists of variable amounts of chalcopyrite, ilmenite, hematite, pyrite and forsterite (Figure 4.5f to j), although quartz and magnetite have only been identified as a major phase in the southern area and forsterite in the northern (Figure 4.6).

In general terms, the minerals forming the tailing show a high liberation grade (~ 95%). These mainly occur as monomineralic fragments, from a few μm to 2 mm, most of them being between 300 and 800 μm (Figure 4.5f and g). Some minor polymineralic fragments have been identified (Figure 4.5h, I, and j), for example ilmenite inclusions in magnetite; fluorapatite associa ted with enstatite; intergrowths between dolomite and calcite; and chalcopyrite and magnetite filling open spaces in calcite.

Fluorapatite is the only REE-bearing mineral identified in the Selati tailing. Based on SEM-EDS analyses, fluorapatite exhibits an uneven REE distribution reaching up 10 wt% ∑LREE (Figure 4.5i).

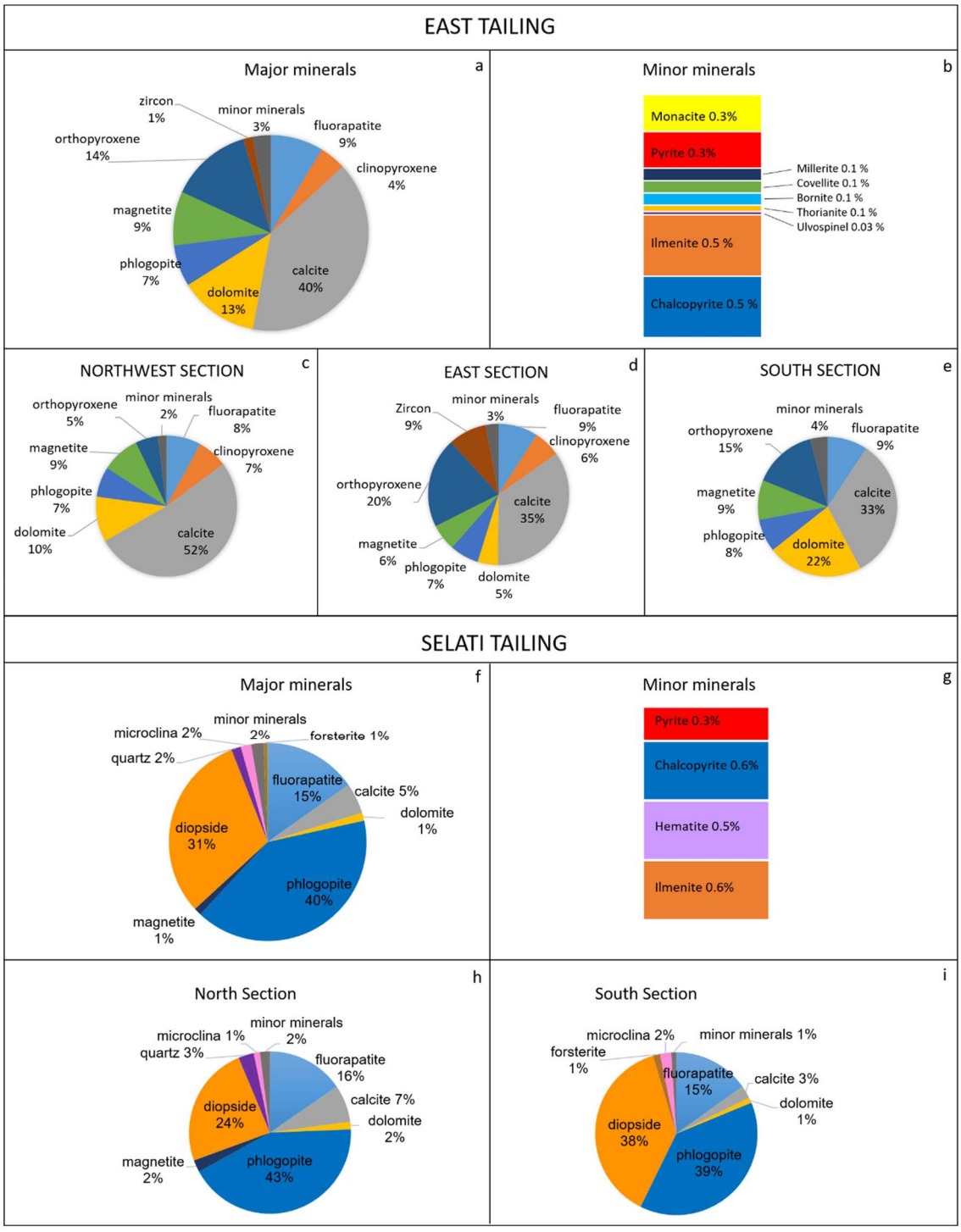

Figure 4.6 Mineralogical semi-quantification based on image analysis of scanning electron microscope (SEM) compositional maps of the East tailing; (a) major minerals, (b) minor minerals, (c) major minerals of northwest section, (d) of east section, (e) of south section; and the Selati tailing (f) major minerals, (g) minor minerals, (h) major minerals of north section and (i) south section.

4.4.4. REE SEQUENTIAL EXTRACTION TESTS

The sequential extraction efficiency, for the WRD and tailing composites, was calculated by weighting the samples before and after the extraction procedure (before F1 and after F4), obtaining the following results: B-carbonatite, T-carbonatite, phoscorite, F-pyroxenite, M-pyroxenite, East tailing and Selati tailing were dissolved in 98.2, 99.9, 9.8, 45.5, 42.6, 89.1 and 27.0 wt%, respectively.

CARBONATITES

Both T- and B- carbonatites showed a similar sequential dissolution behaviour (Figure 4.7). As previously mentioned, these two types of rocks are mainly comprised by carbonates (i.e. calcite and dolomite), magnetite, apatite and minor amounts of Cu sulphides. This mineralogical composition corresponded with the main elements released by the pseudo total (PT) digestion of both rocks (PT columns on Figure 4.7) since Ca>Fe>Mg>P>S>Cu. However, it is important to notice, that the dissolution of the carbonates (marked by the release of Ca and Mg) was not restricted to the first digestion step (F1), it also occurred at F2, F3 and to a less extent at F4, whereas the dissolution of magnetite did not happen during F2 and took place at F4. The former behavior can be attributed to an oversaturation of the extractant respect to calcite and the concomitant impossibility to keep on dissolving more carbonates, whereas the latter is due to the inability of the reagent used to dissolve highly crystalline Fe minerals like magnetite (Caraballo et al., 2018).

T-carbonatites and B-carbonatites have ∑REE average extracted contents of 0.12 and 0.15 wt%, respectively (Figure 4.7b). Some differences can be observed on the REE release patterns for both types of carbonatites. Despite the progressive dissolution of carbonates from F1 to F3 in T-carbonatites, REE showed a tendency to remain in the mineral phases until F3; whereas REE release from B-carbonatites tends to remain in the mineral phase even further and they are mostly extracted in F4.

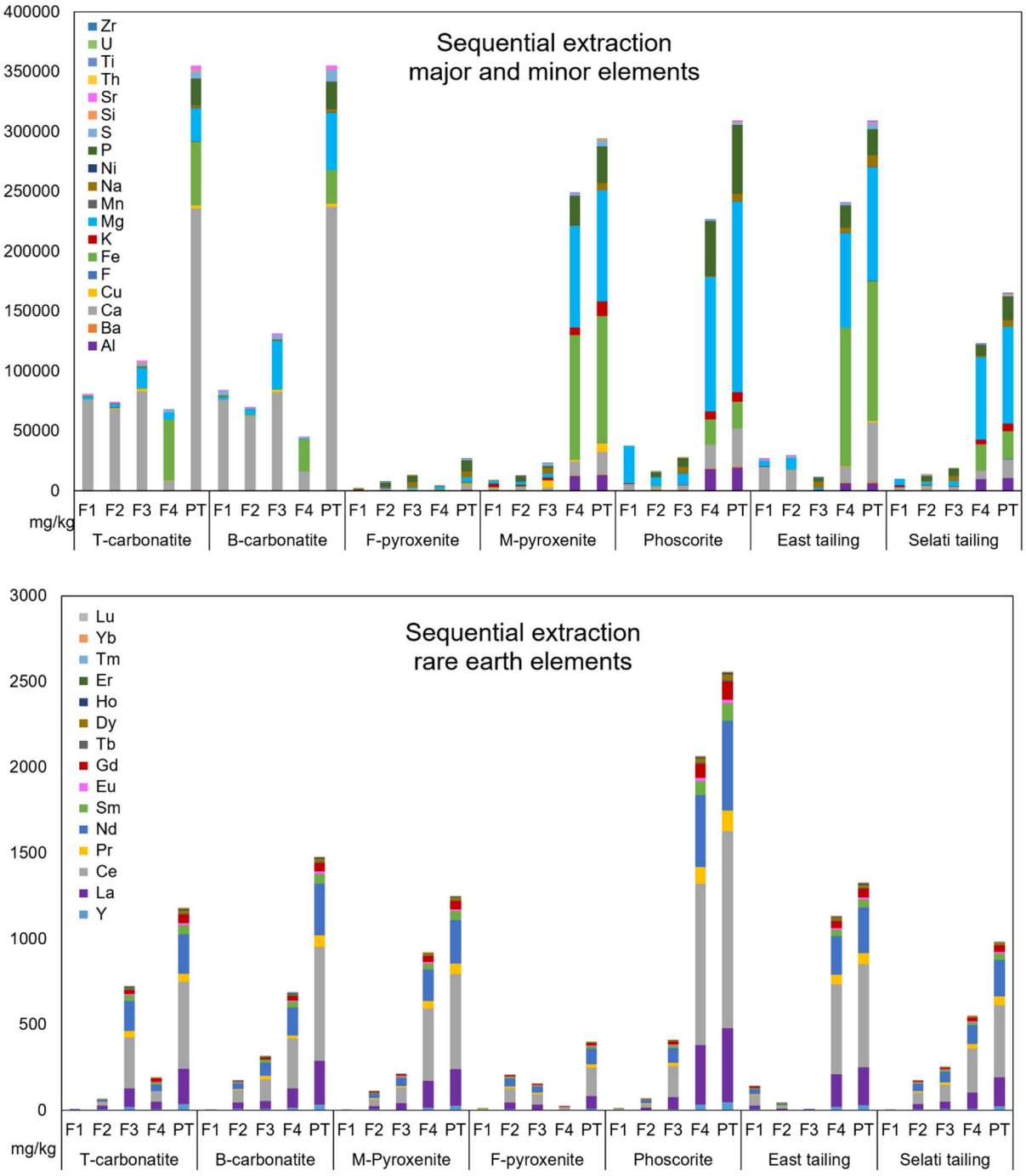

Figure 4.7 Elemental distribution of PIC's main lithologies and tailings in each step of the sequential extractions (F1, F2 F3 and F4) and the pseudo-total concentration in the aqua regia digestion (PT).

PHOSCORITES

As previously shown, this type of residue is mainly composed by fluorapatite and phlogopite. A small fraction of the fluorapatite (shown by P and Ca concentrations) was dissolved during F2 and F3 (Figure 4.7), while phlogopite (marked by Mg, K and Al) was poorly dissolved during F1, F2 and F3. The dissolution of spinel mineral group and forsterite contributes with the high concentration of Mg. The vast majority of the sample was dissolved during the aqua regia digestion (F4), including most of the fluorapatite, phlogopite and forsterite. Despite this poor dissolution efficiency (42.6%), the phoscorite is the most REE enriched lithology (0.23 wt% on average). Higher ∑REE concentrations might be anticipated if/when a complete sample dissolution is achieved. Ce, Nd and La were the most abundant REE released (1150, 524.1 and 430.7 mg/kg, respectively).

PYROXENITES

F- and M-pyroxenite show different mineral contents, with the former characterized by the presence of microcline, diopside, hydroxyapatite and the latter mainly comprised by diopside and phlogopite. As a result, they show different behaviors when underwent to the sequential dissolution protocol. F-pyroxenite only showed some dissolution of the hydroxyapatites, marked by P and Ca release, in F3 or PT, whereas all other mineral phases were not disassociated. As a result of these poor dissolution, almost no discernible ∑REE was released. The dissolution of M-pyroxenite was mostly restricted to the aqua regia steps (F4 and PT). The low solubility of the minerals comprising this residue induced a low ∑REE recovery. Nevertheless, concentrations as high as 0.11 wt% of ∑REE were observed.

EAST TAILING

This residue was comprised mainly by carbonates, enstatite, magnetite, phlogopite and diopside. Some carbonates were dissolved during F1 and F2 (marked by Ca release) but most minerals were not dissolved until the aqua regia digestion (F4). The ∑REE recovery showed similar behavior to the release of the major element, the main recovery took place during the aqua regia digestion. An average concentration of 0.14 wt% was achieved, where Ce, Nd and La were the most abundant REEs (602.3, 266.2 and 221.5 mg/kg, respectively) (Figure 4.7).

SELATI TAILING

A poor dissolution efficiency (27.0 wt%) was achieved for this residue. This could be anticipated from its original mineralogy, comprised mainly by phlogopite, diopside and fluorapatite, all minerals with low solubility. As a result, most of the mineral dissolution was limited to the aqua regia extractions (F4 and PT). The concentration of ∑REE was 0.1 wt% on average, showing some progressive release from F2 to F4, with its maximum recovery in F4.

4.5. DISCUSSION

4.5.1. REE POTENTIAL OF WRDS

Phosphate minerals, such as monazite and fluorapatite included in both carbonatites and phoscorite fragments, could be considered as the most interesting REE-source in PIC WRDs due to its abundance and remarkable REE concentration (Figure 4.3a, b, c, e, h, j, m, n, 4.4a and e). In this regard, monazite is the most common REE mineral in carbonatites. Fluorapatite in carbonatites has higher REE concentration than fluorapatite in phoscorite (Figure 4.4a), however, fluorapatite is less abundant in carbonatites (7-35 wt%) than in phoscorites (70 wt%) (Giebel et al., 2017; Milani et al., 2017; Vielreicher et al., 2000). The association of phosphate minerals and REE concentrations was demonstrated by merging mineralogical analyses with the elemental composition obtain after sequential extraction protocol implemented; EPMA results of monazite and fluorapatite show a REE concentration of 64 and 1 wt%, respectively (Figure 4.4a and e); while 87% of P were released during F4 —the digestion of phosphate minerals in F4 by the reaction with HCl has been previously reported (Ruttenberg, 1992)— together with 89% of REE, in phoscorite samples. Common carbonates forming the PIC WRDs may also be considered as a REE source owing to both its high abundance and its REE concentration (mean ∑REE of 0.5 wt% in calcite and 0.2 wt% in dolomite) (Figure 4.4b). Significantly, B-carbonatite has higher abundance of both carbonate minerals than T-carbonatite.

Minerals previously analyzed from fresh phoscorite and carbonatite samples (Dawson and Hinton, 2003; Giebel et al., 2016; Hornig-Kjarsgaard, 1998) presented lower concentration of REE than those analyzed herein from WRD fragments. For example, REE on fluorapatite, calcite and dolomite were reported in ranges of 0.5-3.9, 0.03-0.17 and 0.04-0.07 wt%, respectively, while in this study, WRD samples reach up to 4.8, 2.9 and 0.8 wt%, respectively. The lower REE contents of in-situ outcrop samples can be related to magmatic differentiation processes. According to Giebel et al. (2017), most REE minerals, fluorapatite, calcite and dolomite crystalized during either orto- or late-magmatic stages in phoscorite and carbonatites. However, Cu is mostly found in the PIC core which was affected by a high sulfidation stage. Therefore, the selective extraction of Cu-rich rocks might have left relatively REE enriched rock fragments in WRDs.

Diopside is the most abundant REE-bearing mineral in both M- and F-pyroxenites from WRDs (Figure 4.2c, d and 4.3d). Heinrich (1970) described the PIC fresh pyroxenites with diopside content up to 61%. Based on EPMA analyses, diopside REE concentration from both pyroxenite types shows an average of 0.06 and maximum content of 0.3 wt%, r espectively (Figure 4.4c). However, diopside is quite resistant and its dissolution did not begin until the last step of the sequential digestion (F4), as shown by the digestion of phoscorite and M-Pyroxenite samples (Figure 4.7). As a result, in M-pyroxenite, most REE were released in F4, also matching with high P extraction rates, probably related to monazite and hydroxyapatite dissolution (Figure 4.7). In contrast, most REE in F-pyroxenite were extracted in F2 and F3 associated with sulphides and oxides, such as magnetite, ilmenite and ulvospinel (with average REE concentration of 0.15 wt%), thorianite (10 wt%) and baddelayite (0.6 wt%) (Figure 4.3 and 4.7b). Taking into account that M-pyroxenite has a higher REE concentration than F-pyroxenite (average of 0.1 vs 0.05 wt%), this lithology might be considered as a secondary source of REE in PIC WRDs.

It is worth noting that resistant REE-rich minerals, such as allanite, britholite and thorite, are expected to be poorly digested during the sequential extraction. In that sense, geochemical analyses are expected to show lower REE concentration than mineralogical analyses.

4.5.2. REE POTENTIAL OF TAILING PONDS

Tailings can be considered as quite homogeneous anthropogenic deposits if compared with ore deposits that can show significant spatial geochemical and mineralogical changes along the multiple geological zones of the deposit. However, tailings may show some grain-size and specific-gravity driven segregations, as well as some enriched or depleted pseudo horizontal alteration fronts (Brodie et al., 1991; Chen et al., 2020; Smuda et al., 2014). Thus, a more detailed tailing sampling would enhance the reliability of the economic implications. However, they are adequate to obtain a first insight into their economic potential due to the expected homogeneity of these deposits, and to offer some light into the REE-bearing mineral phases that a possible metallurgical extraction process will have to handle.

In general terms, the tailing mineralogical composition is comparable with those identified in WRDs (Figure 4.6). In addition, newly-formed Cu-sulphates have been identified in the East tailing (Figure 4.5 and 4.6). Geochemical analyses showed that ∑REE of East tailing is 0.14 wt%, of which 0.11 wt% are LREE (Figure 4.7), while mineralogical analyses showed similar REE distribution pattern but with higher concentrations (∑REE is 0.56, of which 0.38 wt% are LREE). This pattern has been identified in fluorapatite, monazite, zircon and thorianite, from the tailing and the WRD samples, matching with the REE distribution reported for core samples from PIC (Bulakh et al., 1998; Dawson and Hinton, 2003; Giebel et al., 2019, 2017; Milani et al., 2017). Assuming that minerals from tailings would preserve the REE concentration of the original rock, the concentration of REE of the monazite in East tailing (∑REE 65 wt%) suggests that it is probably coming from the processing of mostly B-carbonatite (∑REE 61 wt%), whereas ∑REE of T-carbonatite is 48 wt% (Figure 4.5). Pålsson et al. (2014) also described a similar REE distribution between Fe ore deposits and their tailings.

Selati tailing also shows a homogeneous mineralogical distribution, except for quartz and magnetite (Figure 4.6h, i). The low abundance of calcite and dolomite (5 and 1%, respectively), together with the high abundance of phlogopite and diopside (40 and 31%, respectively), suggest that most tailing material comes from

the processing of pyroxenite, particularly mica-pyroxenite, which is also pointed by the abundance of microcline (2%) (Figure 4.5). Fluorapatite is the major REE-bearing mineral in Selati tailing (16% abundance). The scarcity of other REE-bearing minerals and REE minerals contribute to the low REE grade of this tailing (0.10 wt% according to geochemical analyses, 0.18% according to mineralogy) (Figure 4.6f, g, 4.7). Although, the proportion of LREE was also similar to the East tailing.

4.5.3. WASTE REVALORIZATION

The lithologies of PIC present a REE abundance below the cut-off of current active mines, such as Bayan Obo, Mount Weld and Mountain Pass (H. R. Fan et al., 2016; Gambogi, 2019; Kanazawa and Kamitani, 2006; Orris and Grauch, 2002; Simandl and Paradis, 2018; Woolley, 2001). However, their WRDs are depleted in REE with respect to the ore, while PIC WRDs shows an opposite pattern. Thus, PIC tailings are also enriched in REE due to the extraction of other commodities. Nevertheless, hydrometallurgy studies to recover REE from Bayan Obo tailings are in progress (Zhang *et al.*, 2014; Zheng, Wu and Bian, 2017).

This study suggests that WRDs and tailings could have economical potential for REE. The WRDs show an average of easily extractable REO of 0.17 wt%, similar to East and Selati tailings (0.15 and 0.11 wt%, respectively) (Figure 4.7). In both WRDs and tailings, monazite, fluorapatite and calcite are the most interesting minerals because of their high abundance and high concentration of REE (Figure 4.3, 4.4a, b, 4.5 and 4.6). According to Gambogi (2019) and Orris and Grauch (2002), deposits with over 0.1 wt% REO are considered a potential REE resource (i.e., Matamula deposit, Spain, with 0.1% REO) (Vergara, 2018). In this regard, East and Selati tailings have 4.1 and 6.6 Mt of REO at 0.69 and 0.23 wt%, respectively, distributed mainly in monomineralic fragments of fluorapatite, calcite, dolomite, pyroxenes, magnetite and, in East tailing, monazite released during the mineral processing. The nature of these material, REE-rich and already milled, contributes to the feasibility of its reprocessing and benefit.

Selati tailing has about 3.3 to 4.6 Mt of REO, based on sequential extraction and EPMA results (Figure 4.5, 4.6 and 4.7), that could be recovered from apatite group

minerals at an average of 1.6 kg REO/ton. In addition, East tailing has up to 1.1 kg REO/ton that could be recovered from fluorapatite, along with 3.6 kg REO/ton from calcite and dolomite via flotation (Cui, 2015) and 1.9 kg REO per ton from monazite by flotation, gravity separation, electrostatic separation and/or magnetic processes (e.g. Krishnamurthy & Gupta, 2015). Bioleaching has also been recently explored as an alternative to recover REE from tailings (e.g. Ibrahim & El-Sheikh, 2011; Maleke et al., 2019). For instance, up to 95% recovery of REO from apatite of an Fe ore tailing has been previously reported using chemical methods (Peelman et al., 2018; Vierrether and Cornell, 1993).

Overall, beneficiation of REO from monazite, fluorapatite, calcite and dolomite, according to the mineralogical results, could generate up to 6.61 and 2.05 kg REO per ton from East and Selati tailings, respectively. The monetary value of each tailing has been calculated using equation 4.1; taking into account the amount of waste accumulated in each tailing (m in tons), the average concentration of each REO ($\overline{x_i}$ in kg REO/t) and their individual stock value (v_i in \$/kg) in February 2020. Based on the geochemical and mineralogical results, East tailing has a REO content valued between 18 and 77 billion dollars; while Selati tailing value range between 61 and 123 billion dollars. The most profitable REOs of the tailings are Nd_2O_3, Dy_2O_3, Pr_2O_3 and Tb_4O_7, which represent 87% of the net value (Table A.5 of supplementary material).

$$Value\ (\$) = \sum_{i=L_a}^{i=Y} (\overline{x_i} \cdot v_i) \cdot m \cdot 10^{-9} \qquad 4.1$$

The main WRD reach up to 665 Mt of rock fragments, which together with the high concentration of REE in major minerals such as fluorapatite and calcite, suggest an economic potential for REE. However, due to the heterogeneity of the WRD, a more detailed study on a comprehensive drilling campaign is recommended for a reliable feasibility study.

4.6. CONCLUSIONS

The study suggests that PIC possess a large volume of wastes, including waste rocks and tailings, that are enriched in REE with respect to the ore deposit. The abundance of REE minerals (manly monazite), and REE-bearing minerals (mainly fluorapatite, calcite and dolomite) confirm the economic potential of PIC wastes as secondary source of REE. The most profitable REE are Nd, Dy, Pr and Tb (87% of net value). The tailings are economically more attractive than the WRDs because the mineral processing of the carbonatites and phoscorites to extract Cu and P has produced tailings of mostly monomineralic particles enriched in REE.

4.7. ACKNOWLEDGMENT

The authors thank the staff of Palabora Mining Company and Foskor for their assistance with the sampling. This research was conducted under the ERAMIN project AMDREY -PCIN2015-242-256, financially supported by the Department of Science and Technology, South Africa. It was also partially financed by: project MOS (grant number CGL2016-79204-R), which is supported by the Spanish Government, CORFO and Codelco (project CORFO-16PTECME-66524), project CONICYT/PIA Project AFB180004, UNESCO (UNESCO-IUGS-IGCP-Project 682) and Science Foundation Ireland (grant number 18/IF/6347).

CHAPTER 5: ENVIRONMENTAL AND GEOCHEMICAL CHARACTERIZATION OF ALKALINE MINE WASTES FROM PHALABORWA (PALABORA) COMPLEX, SOUTH AFRICA

ABSTRACT

A detailed characterization of alkaline tailing ponds and waste rock dumps from Phalaborwa Igneous Complex (PIC) South Africa, has been accomplished. The study goes beyond the environmental characterization of mining wastes, offering the first insight towards the recycling of the wastes as alkaline reagent to neutralize acid industrial wastewater. To achieve these aims, tailings and waste rocks were characterized using a combination of conventional, novel and modified Acid Rock Drainage (ARD) prediction methodologies, as well as South African leachate tests, sequential extractions and pseudo-total digestions. The scarcity of Fe-sulphide minerals and the abundance of alkaline minerals indicated that PIC wastes are not ARD producers. The highest neutralization potential was found in the carbonatite rocks and East tailing samples (range between 289 – 801 kg $CaCO_3$ eq/t). According to the National Environmental Management Waste Act (59/2008) of South Africa, tailing ponds and waste rock dumps from PIC classify as non-hazardous (Type 3 waste). The sequential extractions showed that the different fractions from most of the samples would mostly release sulphate and non-toxic elements, such as Ca, Mg, Na and K, which might be a concern if leached in high concentration. In addition, relatively high concentrations of radionuclides, such as U and Th (average of 6.7 and 36.3 mg/kg, respectively) are present in the non-labile fraction of PIC wastes, while the leachable concentrations were always below 0.006 mg/L. Among PIC wastes, East tailing would be the best option as alkaline reagent to neutralize acid wastewater because of its high neutralization potential and non-harmful leachate composition. In general, this study exposes the shortcomings in mine waste characterization, particularly for alkaline mine wastes and introduces the assessment of potential revalorization as a novel practice in mine waste characterization that, if extended as a regular practice, would facilitate a circular

economy approach to the mining industry with its consequent economic and environmental benefits.

5.1. INTRODUCTION

Alkaline mine wastes are usually classified as inert material because this type of waste has the capacity to neutralize acid leachates leading to the immobilization of cations and anions (e.g., metal precipitation as hydroxides or oxyhydroxy-sulphates). However, the near neutral–slightly alkaline pH reached in leachates generated from this type of waste may not be enough to induce the complete precipitation and removal of divalent metals such as Zn and Mn, as well as anions such as sulphate, phosphate, fluoride and chloride (Hiller et al., 2013). In addition, the alkali metals (e.g. Na and K) and alkaline earth cations (e.g. Ca, Mg and Ba) commonly released from alkaline mine wastes, which are not considered as toxic elements, might drastically affect the aquatic environments if they are leached in high concentrations.

The potential environmental problems caused by alkaline wastes have not been well-investigated (Kauppila et al., 2008; Kirby and Cravotta 2005; Pettit et al. 1999). Several studies have attempted to describe the negative environmental impact caused by alkaline mine tailings in aquatic systems of Finland and Tunisia (Heikkinen et al., 2009; Souissi et al., 2013), while other studies denied its impact (Hiller et al., 2013; Moukodi, 2008) based on current standards and protocols that indicate that samples classified as non-acid forming (e.g. sulphide absent, neutral paste pH and positive net neutralization potential) do not require further testing (e.g., Usher et al., 2003 and references therein). This assumption has provoked that the environmental impact of large alkaline tailings such as those from Bayan Obo Deposit in China and Phalaborwa igneous complex (PIC) in South Africa, among others, have been overlooked. In the case of PIC is worrisome because of its proximity to the renowned Kruger National Park (KNP) and the negative impact that it might have on its biodiversity.

On the other hand, most of the regulations for mine wastes are currently aimed to predict only acid mine drainage (AMD) generation and their toxicity, focusing on chemical test such as ABA (acid base accounting) and leachate test (Parbhakar-

Fox and Lottermoser, 2015a; Usher et al., 2003). However, recent studies agree that a detailed mineralogical approach should be included to improve the interpretation and prediction of leachates (Becker et al., 2015; Dold, 2017) not only to prevent the generation of AMD, but also the generation of neutral/alkaline mine drainage (NAMD). In the case of South Africa, NAMD occurrence is particularly high (Castillo et al., 2015). Although no specific regulation for extractive waste disposal has been developed in South Africa, the general landfill disposal regulation, which includes mining wastes, is stricter than elsewhere regulations (e.g., Australia and USA) including the elements commonly present in alkaline mine drainage. For instance the South African protocols and threshold stablished that are based on the USA standard for Toxicity Characteristic Leaching Procedure (1311-TCLP) test (USEPA, 1998) and the Australian Standard method AS-4439 (Standards Australia, 1997), with similar Leachable Concentration Thresholds (LCT) and Total Concentration Thresholds (TCT) (Department of Environmental Affairs, 2013), certain parameters such as B, Ba, Cl, Co, Mn, Sb, V, sulphate (SO_4) and total dissolved solids (TDS) have been included. Despite these efforts, conventional protocols overlook the speciation, and thereby mobility and long term bioavailability of the leachate compounds (Rodgers et al., 2015). Thus, although sequential extraction procedures (SEP) (Rauret et al., 1999) are not part of the protocol for landfill disposal, it has been included herein since it is a more comprehensive tool to address the leachates that wastes may produce under different circumstances; weathering (bioaccessible fraction (F1)), anaerobic conditions (reducible fraction (F2)) and aerobic conditions (oxidizable fraction (F3)).

On the other hand, alkaline mine waste from PIC might have the potential to be used as neutralizing reagent to remediate acid industrial wastewater (AIW). Other alkaline wastes such as fly ash, paper mill waste and bauxite tailing (red mud), among others, have been widely studied as a substitute for alkaline materials to neutralize AIW (Paradis et al., 2006; Pérez-López et al., 2011; Surender, 2009). Even though these alkaline wastes are a cheaper option and they may contribute to the neutralization process, quite often these wastes contain toxic elements that could be released into the treated water. Before recycling any alkaline waste as neutralizing reagent, or for any other purpose, a preliminary characterization of the

leachates that a waste may produce, such as those suggested herein, should be addressed.

Therefore, this study goes beyond conventional environmental characterization of mine wastes and seeks to achieve two aims; i) overcome the limitations of traditional protocols that are aimed to predict AMD by including novel and modified procedures, and ii) provide the first insight about the potential revalorization of PIC wastes based on its environmental characterization. The latter approach would enhance a circular economy strategy for the mining industry with its consequent economic and environmental benefits.

Phalaborwa Igneous Complex (PIC), South Africa, is an alkaline complex comprised by pyroxenite, phoscorite and the only carbonatite primarily mined for Cu in the world (**Error! Reference source not found.**; Giebel (2019)). Mining activities commenced in PIC between 1930s and 1960s to recover apatite, vermiculite and copper, among other by-products (Southwood and Cairncross, 2017). After 60 years of intensive mineral extraction and processing, more than 4500 Mt of mining wastes (rocks and tailings) have been disposed of on several dumps and ponds (FOSKOR, 2018; Moukodi, 2008). Indeed, PIC host one, if not, the largest tailing in the southern hemisphere (approx., 2830 Mt). This tailing, hereinafter referred to as Selati tailing (Fig. 1), consists of the processed material from the phosphate plant (FOSKOR, 2018) and is located in the southern most area of PIC. Smaller tailings grouped in the easternmost part of PIC, collect the carbonatite froth-flotation from the Cu beneficiation (Hu et al., 2017; Moukodi, 2008), hereinafter referred to as East tailing. In addition, PIC also host more than 1085 Mt of waste rocks piled in dumps and comprised of mainly barren carbonatites, phoscorites and pyroxenites (Brink, 2011; Moukodi, 2008). These mining wastes exposed to the rainwater leachate alkaline drainages that have deteriorated the water quality of surrounding aquatic ecosystems (i.e. surface and groundwater). In that sense, the Kruger National Park (KNP), which is the biggest natural reserve of South Africa (19,485 km^2) and declared a biosphere reserve by UNESCO in 2001 (K2C, 2014), is of especial concern, due to its proximity to the mining wastes of PIC (Fig. 1). Indeed, the Department of Environmental Affairs (2009) reported that “Olifants River, from the Selati [River] confluence to downstream border in the Kruger National Park …

is negatively impacted by poor water quality of the Selati River as a result of mining activities at Phalaborwa".

5.2. METHODOLOGY

5.2.1. SAMPLING AND SAMPLES PREPARATION

The sampling of mining waste from PIC includes 60 rock samples collected from the WRDs (approx. 1 to 12 kg/each) and tailing samples from up to 2m-deep trench (approx. 5 kg/each) from 16 sampling points, collected with shovels and soil samplers (Fig. 4.1, sample geolocation data in appendix B.1 and Table B.1). Polished thin sections and polished blocks were prepared at the University of Huelva from each rock and tailing sample for further mineralogical and textural determinations. For the sake of clarity, the results discussed herein are the average of mineralogical and textural determinations of each of the seven main lithologies, i.e. phoscorite, banded carbonatite (B-carbonatite), transgressive carbonatite (T-carbonatite), pegmatoidal pyroxenite (P-pyroxenite), micaceous pyroxenite (M-pyroxenite), feldspathic pyroxenite (F-pyroxenite) and syenite; as well as of each of the six tailing sectors, i.e. Selati tailing S, Selati tailing N, East tailing S, East tailing N, East tailing E and East tailing W (see chapter 4 and Fig 4.1 for lithologies classification and tailings description).

5.2.2. MINERALOGICAL AND TEXTURAL ANALYSES

Mineralogical determinations on both WRDs and tailings samples were carried out at the University of Huelva (Spain) and the University College Dublin (Ireland). Detailed mineralogical and micro-textural analyses on polished thin section were performed by both petrographic microscope and scanning electron microscope coupled with energy dispersive spectroscopy and SEM-EDS JEOL JMS-5410 equipped with a microanalyzer Link Oxford.

Semi-quantification of main mineralogy on WRD samples were estimated using the X-powder software on X-ray diffraction (XRD) analyses using a Broker D8 Advance Powder Diffractometer with Cu–Kα radiation. In addition, an estimation of minor

minerals abundances in the tailing samples was carried out by petrographic observations. Silicon drift detector (SDD) were used for elemental mapping of tailing samples, followed by semiquantitative mineralogical analyses by ImageJ software (https://imagej.nih.gov/ij).

5.2.3. ACID ROCK DRAINAGE (ARD) PREDICTION

Over the last decades different ARD protocols have been developed to assess the potential of mine waste to produce acid drainage. Current protocols are imprecise and they tend to differ among themselves in the prediction of the potential of mine waste to produce or neutralize acidity. The Water Reasearch Commission (WRC) of South Africa (WRC, 2011) recommends to follow the acid-base accounting (ABA) procedure described by Usher et al. (2003). This protocol includes, paste pH, net acid generation (NAG), net neutralization potential (NNP) and neutralization potential ratio (NPR), and uses a spreadsheet tool named ABACUS to standardise the interpretation of the results. In order to increase the accuracy of the predictions, mineralogical methods such as the traditional net carbon value (NCV, Bucknam, 1997) and the novel textural acid rock drainage index (ARDI, Parbhakar-Fox et al., 2011) are included in this study.

The results of the mineral and textural analysis were used to determine the **Net Carbon Value** (NCV) (Bucknam, 1997) and the textural acid rock drainage index (ARDI) as described in Parbhakar-Fox et al. (2011). NCV is based in the percentage of CO_2 of common carbonates, which is 44, 48, 44 and 38 CO_2% for calcite, dolomite, ankerite and siderite, respectively. These, multiplied by their abundance (in %), account altogether as the neutralization potential. The acid potential of a given sample is determined by the stoichiometric equivalence of one mole of sulphide being oxidised to sulphuric acid, consuming one mole of carbon dioxide, times -1.37 the percentage of sulphide present in each mineral, which is 53 and 20% for pyrite and arsenopyrite, respectively (eq. 5.1).

$$\text{NCV} = 0.44 \times \text{calcite} + 0.48 \times \text{dolomite} + 0.44\ \text{ankerite} + 0.38 \times \text{siderite} - 1.37 \times 0.53\ \text{pyrite} - 1.37 \times 0.20\ \text{arsenopyrite} \quad (5.1)$$

Since the most abundant Fe-sulphide in PIC waste was expected to be chalcopyrite (Chapter 4), a modified NCV (NCV*) is proposed herein (equation 5.2).

$$NCV^* = 0.44 \times \text{calcite} + 0.48 \times \text{dolomite} + 0.44 \text{ ankerite} + 0.38 \times \text{siderite} - 1.37 \times 0.53 \text{ pyrite} - 1.37 \times 0.20 \text{ arsenopyrite} - 1.37 \times 0.35 \text{ chalcopyrite} \quad (5.2)$$

The results are expressed in CO_2%. Negative values are indicative of the acid generation potential, while positive values are indicative of the acid neutralization potential. It is worth noticing that this method does not take into account the reactivity of each mineral.

On the other hand, the **textural ARDI** uses five parameters (A-E) to evaluate the acid generation potential of a given rock. Parameter A refers to the contents of acid forming phases (Fe-sulphides); parameter B is related to the degree of alteration of those sulphide minerals; parameter C evaluates the morphology of sulphides according to the available surface area for sulphide oxidation; parameter D is the amount of neutralizing minerals that surrounds the sulphides; and parameter E evaluated the spatial relationship between acid forming and acid consuming phases. Each parameter is evaluated in both mesoscale (using equation 5.3) and microscale (using equation 5.5) for each WRD sample. However, the tailing samples only allow microscale evaluation. Therefore, ARDI for WRD samples has been calculated as the average of meso- and microscale (equation 5.7), while ARDI for tailing samples correspond to the microscale evaluation (equation 5.5). Negative ARDI results are indicative of acid consuming capacity, while positive values are indicative of acid generating capacity (Table 5.2).

$$Me = [A_{0\text{-}10} + B_{0\text{-}10} + C_{0\text{-}10} + D_{\text{-}5\text{-}10} + E_{\text{-}5\text{-}10}] = X \quad (5.3)$$

$$X^1 = \sum X \,/\, \text{no. of Me phases} \quad (5.4)$$

$$Mi = [A_{0\text{-}10} + B_{0\text{-}10} + C_{0\text{-}10} + D_{\text{-}5\text{-}10} + E_{\text{-}5\text{-}10}] = Y \quad (5.5)$$

$$Y^1 = \sum Y \,/\, \text{no. of Mi phases} \quad (5.6)$$

$$ARDI = (X^1 + Y^1) \,/\, 2 \quad (5.7)$$

On the other hand, representative pulverized composite samples (ø < 75 μm) from tailings and WRD (13 samples in total) were analysed using the **Acid Base**

Accounting (ABA) procedure, described by Usher et al. (2003). Each assay was performed in triplicate. The procedure includes:

- Paste pH-Conductivity 1:1 (w/w) assess the readily available acidity/alkalinity of a sample. This procedure provides no indication of the sample's total acidity/alkalinity, but determines the immediate pH and electrical conductivity (EC) of the drainages produced by the wastes during the initial stage of the waste-water interaction. Each paste was stirred for 5 seconds and then pH and EC were measured after 10 minutes, 12 h, 24h and 48h. Paste EC values were converted to total dissolved solids (TDS) according to the equations 5.8 and 5.9 (modified from Hubert and Wolkersdorfer, 2015):

If EC < 5 (mS/cm) → TDS (mg/L) = EC x 970 5.8

If EC > 5 (mS/cm) → TDS (mg/L) = EC x 850 5.9

- Net Acid Generation (NAG) tests the reactivity of minerals, particularly Fe-sulphides, using hydrogen peroxide (H_2O_2) to determine the final NAG pH. Afterward, sodium hydroxide (NaOH) is used to titrate the solution up to pH 4.5, in order to determine the potential acidity of the samples as kg of sulphuric acid per tonne (kg H_2SO_4/t). Initial paste pH and final NAG pH are compared and discussed as an estimation of the evolution of the alkalinity or acidity of the drainage released from the wastes (Weber et al., 2006).

Sobek procedure was used to determine both the neutralization potential (NP) and the acid potential (AP) of each sample (equations 5.10 and 5.11, respectively). NP is related to the abundance of carbonates, bases and alkaline earth metals that are available to neutralize acidity, while AP is related to the abundance of sulphides, main precursor of acidity in mine residues (Usher et al., 2003). Due to the complexity of the samples, the acid potential (AP) has been calculated using the S% obtained from the fraction 3 of the sequential extraction as sulphide S% (Pérez-López et al., 2007). The results of both NP and AP are expressed as kg of $CaCO_3$ equivalent per ton (kg $CaCO_3$/t).

$$\text{NP (kg } CaCO_3/t) = \frac{[(N\ x\ vol\ (mL)\ of\ HCl) - (N\ x\ vol\ (\text{mL})\ of\ NaOH)\ x\ 50}{[Weight\ of\ sample\ (g)]} \quad 5.10$$

$$\text{AP (kg } CaCO_3/t) = S\% \text{ x } 31.25 \quad 5.11$$

AP and NP values were used to calculate the net neutralization potential (NNP) and the neutralization potential ratio (NPR) of each sample (equation 5.12 and 5.13, respectively). The results are expressed as kg of $CaCO_3$ equivalent per ton.

$$\text{NNP (kg } CaCO_3/t) = NP - AP \quad 5.12$$

$$NPR = NP / AP \quad 5.13$$

The results of each ARD assessment has been interpreted using the Acid Base Accounting Cumulative Screening Tool (ABACUS) developed by the Institute for Groundwater Studies of the University of the Free State, South Africa (Usher et al., 2003). ABACUS is a tool that provides consistency in the application and interpretation of the diverse ABA procedures used worldwide. Also, the program takes into consideration the presence or absence of gas phases. When carbon dioxide is present, the solubility of calcite increases. This occurs in "open systems" such as surface water bodies or pore water in contact with a gas phase. If the water is not in contact with a gas phase, which is the case of groundwater below the water table or the bottom of tailing ponds, it is considered as a "close system" with lower dissolution rate of calcite. Therefore, ABACUS offers two verdicts for each sample analysed based on the values of NNP close system and NNP open system.

5.2.4. PREDICTION OF DRAINAGE'S ELEMENTAL COMPOSITION

The toxicity of the leachates has been assessed using 0.5N acetic acid, as described in the Australian Standard method AS-4439 (Standards Australia, 1997) for solid wastes and contaminated soils. South African regulation stipulates the use of AS-4439 to assess the suitability of wastes for disposal in a landfill, including extractive waste. The results have been compared with the South African Leachable Concentration Thresholds (LCT) for landfill disposal of waste (Department of Environmental Affairs, 2013), which are similar to the Australian EPA 448.3 thresholds (EPA Victoria, 2007) (Appendix B.1 and Table B.2 of supplementary

material). In addition, the total concentration (TC) of the pollutants present in the solid wastes have been assessed and compared with South African total concentration thresholds (TCT) as described in GNR 635 (Department of Environmental Affairs, 2013). Each element has four LTC thresholds; LTC0 (inert), LTC1 (non-hazardous), LTC2 (hazardous) and LTC3 (extreme hazardous), and three TC thresholds; TCT0 (inert), TCT1 (hazardous) and TCT2 (extreme hazardous). Each waste can be classified according to the highest threshold overcame by any of the elements assessed from Type 0 waste (unsuitable for land fill disposal) up to Type 4 (inert) following the criteria of the National Environmental Management Waste Act (59/2008) of South Africa (DEA, 2013) (more details in supplementary material, Appendix B.2 and Table B.2).

In addition, the potentially toxic elements (PTEs) contained in PIC's wastes were assessed using sequential extractions following the BCR procedure described by Rauret et al. (1999) (Details in Appendix A.1). This methodology has been previously applied to assess metal mobility in mining wastes (e.g. Álvarez-Valero et al., 2009; Pérez-López et al., 2008). However, a recent study (Caraballo et al., 2018) has recommend to be precautious at the time of interpreting the results, because the high metallic concentrations of the mine residues frequently induce oversaturation of the leaching solutions and the concomitant inefficiency of the extraction step. The sequential extraction includes three steps or fractions; each fraction represents a different mobile phase of the waste. Fraction 1 (F1) or bioavailable refers to metals associated with phosphate and sulphate evaporitic salts. Fraction 2 or reducible refers to metals bound to Fe and Mn oxides; and Fraction 3 or oxidizable refers to metals associated to sulphides and organic matter (Pérez-López et al., 2007). In addition, the residual fraction (F4) represents the phase of non-mobile metals, which has been digested with aqua regia. The sum of each fraction (F1, F2, F3 and F4) comprises the pseudo-total composition. To verify reproducibility of the experiment, a pseudo-total digestion of each sample has also been performed using aqua regia. The high dissolution rate of alkaline materials in the pseudo-total digestions favours its comparison with total concentration thresholds (TCT), as described in GNR 635 (Department of Environmental Affairs, 2013).

The concentration of cations and S of the leachates, as well as the sequential extraction and the pseudo-total digestion were analysed by inductively coupled plasma optical emission spectroscopy (ICP-OES) Teledyne Prodigy; P and F were analysed by the discrete analyzer Easy Chem 200; and Cl was analysed using the spectrophotometer HACH DR3900. All the analyses were performed by an accredited laboratory at the Institute for Groundwater Studies at the University of Free Sate (South Africa) (Analytical details can be found in supplementary materials, appendix B.3).

5.3. RESULTS

5.3.1. MINERALOGY

The mineralogical characterization is focused in those minerals with known acidification or neutralization potential, such as sulphides and carbonates, among others. Sulphide minerals in the waste rocks and tailings are scarce. Semi-quantified analysis by elemental mapping show contents below 1 wt% (supplementary material Table B.3). Sulphide phases are mainly concentrated in both carbonatite rock fragments (Figure 5.1c to f) and East tailing (Figure 5.1j to l). The main acid-forming-sulphide minerals found in PIC wastes were chalcopyrite and, to a lesser extent, pyrite (Figure 5.1d to f and j to l). Both sulphides are strongly associated with calcite ($CaCO_3$), dolomite ($CaMg(CO_3)_2$), magnetite (Fe_3O_4), ilmenite ($FeTiO_3$) s(Figure 5.1a, b and g to i) and other minor sulphide minerals such us bornite (Cu_5FeS_4), covellite (CuS), chalcocite (Cu_2S), cubanite ($CuFe_2S_3$), millerite (NiS) and vallerite ($(Fe,Cu)_4(Mg,Al)_3S_4(OH,O)_6$) (Figure 5.1c, d, e, f, j and l), as well as newformed Cu-sulphate (Figure 5.2k).

Alkaline minerals in both the waste rocks dumps and tailings are highly abundant (supplementary material, Table B.3). Among them, calcite and dolomite are the most abundant (Figure 5.1a, b and h), followed by diopside($MgCaSi_2O_6$), phlogopite ($KMg_3AlSi_3O_{10}(F,OH)_2$), microcline ($KAlSi_3O_8$) and apatite ($Ca_5(PO_4)_3(Cl/F/OH)$ group minerals (Figure 5.1a, b, g and h). Calcite contents in carbonatite fragments and East tailing range between 25 and 67 wt%, determined by XRD and elemental mapping, whereas dolomite is particularly abundant in the East tailing (average value of 13 wt%). Diopside concentration in pyroxenite fragments ranges from 10

to 30 wt%. Selati tailing exhibits the highest concentration of diopside with mean values of 31 wt%, particularly enriched on its southernmost area (38 wt%, on average). Phlogopite content in pyroxenite fragments ranges between 5 and 55 wt%, and is particularly abundant in Selati tailing (with mean value of 40 wt%). Microcline is particularly abundant in F- pyroxenite (55 wt%) and represents 2 wt% of the Selati tailing. In addition, apatite mean content in phoscorite fragments are 70.5 wt%, whereas in both tailings (East and Selati) are 9 and 15 wt%, respectively.

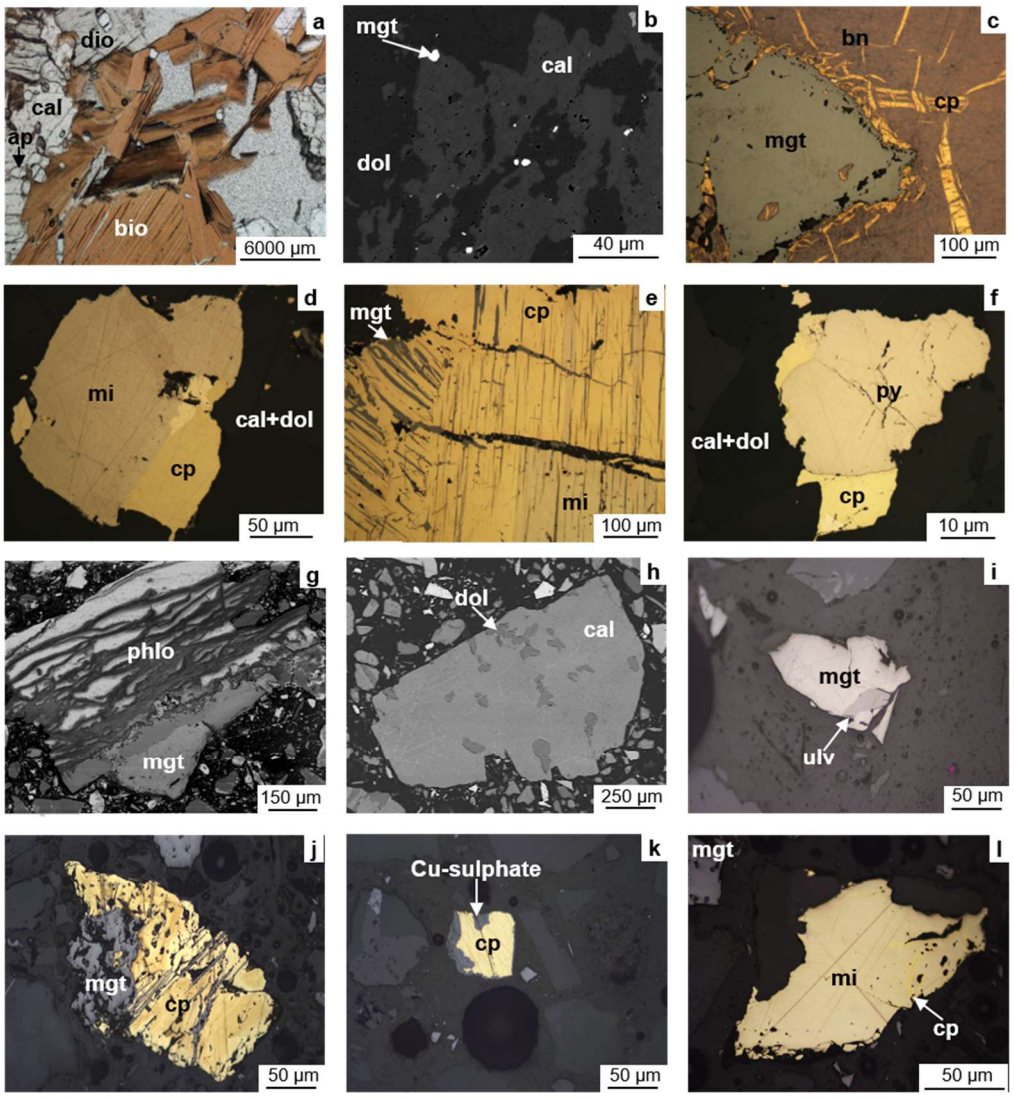

Figure 5.1 Transmitted, reflected light and backscattered electron (BSE) images from the Palabora WRD (images a to f) and tailings (images g to l). a) biotite (bio) aggregate associated with calcite (cal), diopside (dio) and apatite (ap); b) calcite and dolomite

(dol) including fine grained magnetite (mgt); c) chalcopyrite (cp) and bornite (bn) filling open space and replacing in magnetite; d) Interstitial millerite (mi) and chalcopyrite included in calcite and dolomite; e) Magnetite replaced by chalcopyrite and millerite; f) pyrite and chalcopyrite locked in cal and dolomite; g)mixed-fragment forms of phlogopite (phlo) and magnetite (mgt); h) Calcite (cal) grain showing fine grainded dolomite (dol) inclusions; i) magnetite grain including ulvospinel (ulv); j) Grain comprises of chalcopyrite (cp) and magnetite; k) mixed-fragment formed by chalcopyrite and a newly-formed Cu-sulphate; l) Millerite (mi) and chalcopyrite forming a mixed grain.

5.3.2. ACID ROCK DRAINAGE (ARD) PREDICTION

MINERALOGICAL APPROACH

Both ARDI and NCV mineralogical approaches indicate that none of the PIC wastes have potential to generate acid drainage (ARDI < 10, NCV > 0) (Table 5.1). According to ARDI, all the waste rock samples ranged between 5 and 10, reflecting non-acid forming to acid consuming conditions (more details in supplementary material, Table A.4), while NCV of carbonatites, phoscorite and East tailing fall under the classification of high potential for acid neutralization (NCV > 5).

PASTE PH/EC

The ultrapure water used for the paste pH/EC tests and as a (dH_2O, Figure 5.2). had an initial pH of 8.26 and no significant variations were observed throughout the experiment. In general terms, all the lithologies assessed showed a similar behaviour; they increased their pH within 10 minutes, but they decreased gradually over time without reaching the initial pH. The exception is B-carbonatite that showed a slight decreased of pH after 10 min, but it increased thereafter recovering initial values. In particular, the highest pH was achieved by syenite and pyroxenites (Figure 5.2).

On the other hand, the EC of the ultrapure water increased in every test performed. Among lithologies, the highest EC was produced by B-carbonatite (5.02 mS/cm), while sections west and south of the East tailing showed the highest EC (6.96 and 4.74 mS/cm, respectively) among the assessed tailing samples.

Table 5.1 Acid rock drainage (ARD) tests using traditional chemical procedures and novel mineralogical approaches. Units for NAG rate (pH 4.5) are given in kg H2SO4/t; AP, NP, NNP are in kg CaCO3 eq/t; units for NCV are in %CO2. Potential acid rock drainage (ARD) thresholds adapted from previous studies (* Bucknam, 1997; +Parbhakar-Fox et al., 2011; ^Usher et al., 2003).

	CHEMICAL^								MINERALOGICAL	
Samples	Initial pH (24h)	Final pH (NAG)	NAG rate	S%	AP	NP	NNP	NPR	ARDI+	NCV*
T-carbonatite	8.69	9.83	0	0.25	7.74	680	671.9	87.8	8.2	17.01
B-carbonatite	8.24	9.37	0	0.37	11.6	801	789	69	9.67	17.21
East tailing S	8.39	7.35	0	0.07	2.3	336	333.4	145	5.1	25.01
East tailing N	8.58	8.64	0	0.07	2.1	390	387.8	184	3.69	27.62
East tailing W	8.53	8.78	0	0.07	2.3	663	660.7	295	5.2	21.58
East tailing E	8.65	8.67	0	0.06	2.1	289	268	138	6.58	18.16
Selati tailing N	9.1	6.5	0	b.d.l	–	54.6	54.6	–	5.6	3.9
Selati tailing S	9.11	5.83	0	b.d.l	–	59.2	59.2	–	6.1	1.66
F-Pyroxenite	9.32	4.05	1.5	b.d.l	–	12.3	12.3	–	7.56	3.12
P-pyroxenite	9.27	7.35	0	0.47	12.5	72	43.9	4.9	7.66	2.94
Syenite	9.48	4.95	0	b.d.l	–	10.2	10.2	–	7.8	2.2
M-Pyroxenite	9.72	5.39	0	b.d.l	–	25.4	18.1	–	7.57	1.99
Phoscorite	8.82	5.38	0	b.d.l	–	113	112.8	–	6.27	7.04
	ARD Classification									
Potential acid forming-High	< 3.5	< 3.5					< (-20)		41–50	< (-5)
Potential acid forming			> 0	> 0.3				< 1	31 – 40	(-5) – (-1)
Potential acid forming-Low	3.5 – 5	3.5 – 4.5*					(-20) – 0	1 – 2	21 – 30	(-1) – (-0.1)
Not acid Forming/ acid consuming	> 5	> 4.5	0	< 0.3			0 – 20	2 – 4	(-10) – 20	(-0.1) – 5
High acid Consuming							> 20	> 4		> 5

*The NAG threshold for not acid forming was stablished at pH 4 by Miller et al. (1990) and at 5.5 by Usher et al. (2003). An intermediate value of 4.5 is used herein for ARD classification.

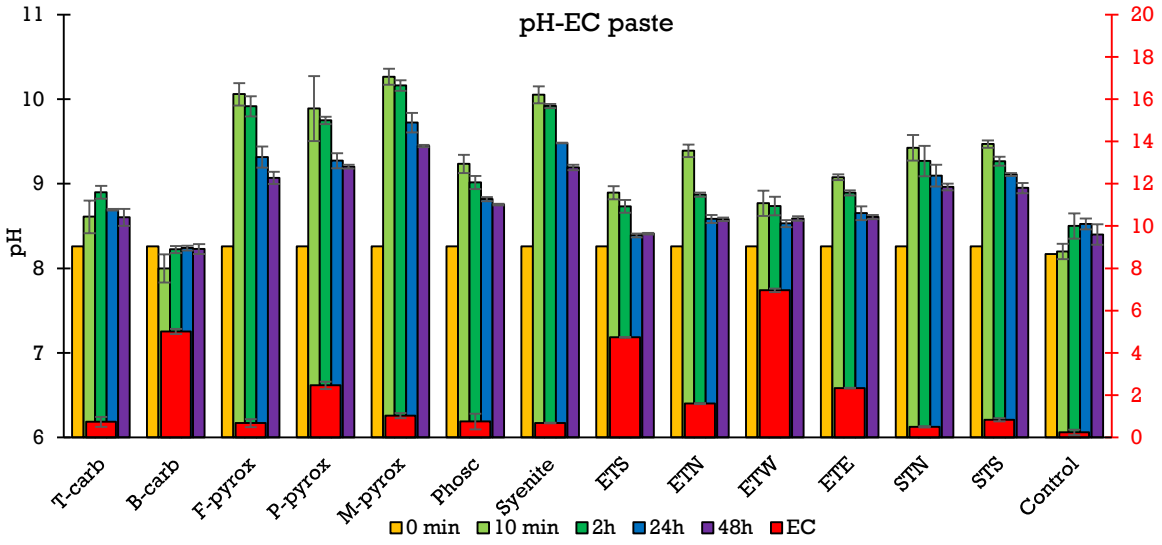

Figure 5.2 Graphic of paste pH-EC. pH measured after 10 min, 2 h, 24 h and 48 h. Electrical conductivity measured after 48 h. Samples analysed; transgressive carbonatite (T-carb), banded-carbonatite (B-carb), feldspathic pyroxenite (F-pyrox), pegmatoidal pyroxenite (P-pyrox), micaceous pyroxenite (M-pyrox), phoscorite (Phosc), syenite, East tailing S (ETS), East tailing N (ETN), East tailing W (ETW), East tailing E (ETE), Selati tailing N (STN), Selati tailing S (STS) and ultrapure water as control. Errors bars correspond to standard deviations of triplicates.

NET ACID GENERATION

According to the net acid generation (NAG) procedure both tailings would be classified as material with non-acid-generation capacity (final pH > 4.5). Also, the WRD are composed of non-acid-generating rock fragments, with the exception of F-pyroxenite that represents low risk to generate acid drainage, as shown by a final pH of 4.05 and NAG rate of 1.5 kg H_2SO_4/t (Table 5.1).

NET NEUTRALIZATION POTENTIAL AND NEUTRALIZATION POTENTIAL RATIO

The average of the neutralization potential (NP) of each lithology and tailing samples are shown in Table 5.1. B-carbonatite resulted in the highest NP range, followed by T-carbonatite and East tailing samples (801, 680 and 663 kg $CaCO_3$/t, respectively), while F-pyroxenite and syenite had the lowest NP range (10.2 and 12.3 kg $CaCO_3$/t, respectively).

Most lithologies contained less than 0.3 S%, resulting in an acidification potential (AP) ≤ 9.4 kg $CaCO_3$ eq/t. In contrast, some B-carbonatite and P-pyroxenite samples showed average values of 0.4 and 0.5 S% (11.6 and 12.5 kg $CaCO_3$ eq/t), respectively. The tailing samples also had low concentration of S, and therefore low AP, particularly the Selati tailing whose S content was below detection limit.

The high NP of all the samples analysed, together with their relatively low AP, confer positive values of NNP, hence falling under the classification of acid consuming material. Most NNP values are far above 20 kg $CaCO_3$ eq/t, hence they have high acid consuming capacity, except for syenite, F- and M-pyroxenites (10.2, 12.3, 18.1 kg $CaCO_3$ eq/t, respectively). In addition, all NPR values are also above high acid consuming threshold (4 kg $CaCO_3$ eq/t), with P-pyroxenite showing the lowest NPR value (4.9 kg $CaCO_3$ eq/t).

5.3.3. PREDICTION OF ELEMENTAL COMPOSITION

LEACHING TESTS AS PER WASTE DISPOSAL REGULATION

Every leaching test performed on tailing samples and waste rocks showed values below TCLP limits (US standard for Toxicity Characteristic Leaching Procedure, Table B.2 of supplementary material). They were also below LTC0 (South African threshold for inert waste, Table B.2 of supplementary material) for B, Cl, Co, Cr, Mo, Sb, V and Zn (Figure 5.3, top graphs). However, some of the samples from the WRDs reached or exceed LTC0 for As, Ba, Cd, Cu, F, Hg, Mn, Ni, S, and/or TDS (Figure 5.3). East tailing samples were above LTC0 for As, Ba, Cu, Mn, Ni, Se and TDS, while Selati tailing exceeded LTC0 for Ba, F, Ni, and Pb. It is worth noting that none of PIC wastes overcame LTC1 (threshold for non-hazardous material).

In addition, all the wastes surpassed TCT0 for at least 1 analyte. For example, Cu was above TCT0 at every waste characterized, except for M-pyroxenite (Fig. 4, bottom left graph). Other elements above TCT0 were, in order of occurrence, Ba, As, Se, F, Ni and Pb (Figure 5.3, bottom graphs). However, TCT1 thresholds were never exceeded.

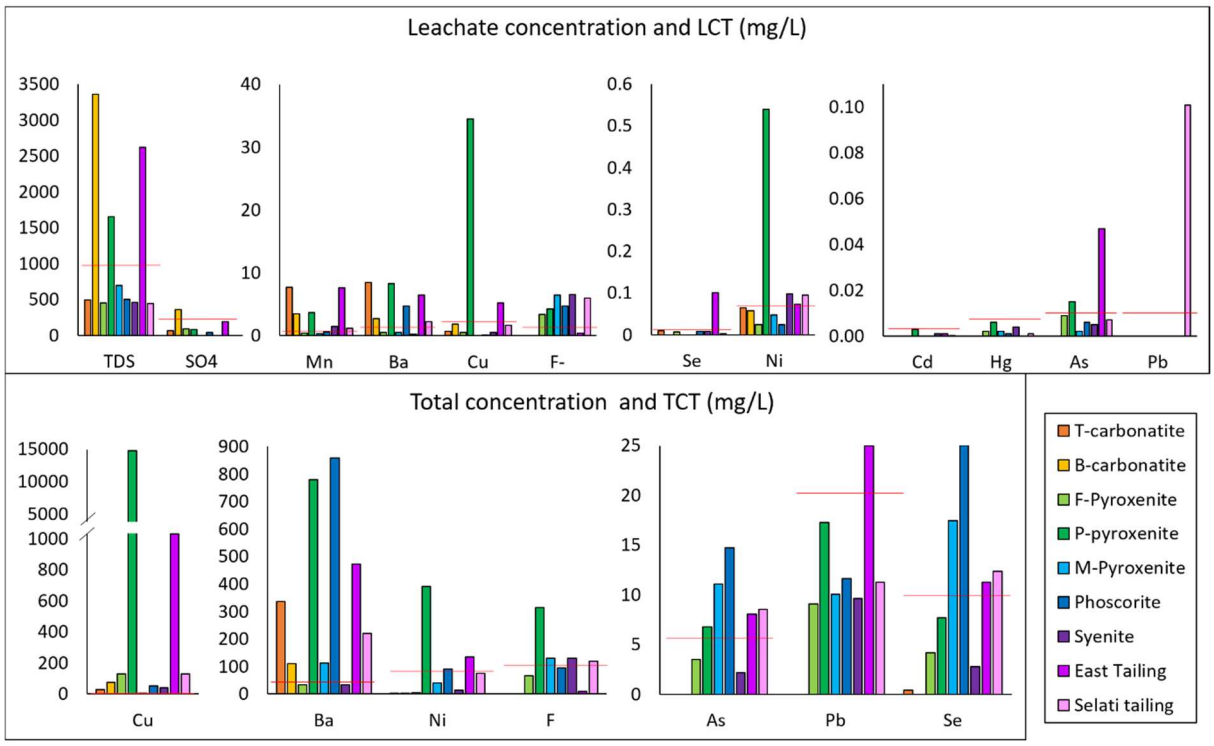

Figure 5.3 Leachates and total elemental composition of main lithologies from the waste rock dumps and tailings. PIC samples submitted to the Australian Standard method AS-4439 following the South African procedures for leaching tests (top), Leachable Concentration Thresholds for inert material (LTC0) are marked in red, and total concentration of elements (bottom) obtained from the sum of fractions 1, 2, 3 and 4 of the sequential extraction, Total Concentration Thresholds for inert material (TCT0) are marked in red. Only elements that are closed or above LTC0 or TCT0 are shown.

SEQUENTIAL EXTRACTION

In general, mean concentrations of S and Cu were predominant among the leachates of PIC wastes (waste rocks and tailings), particularly in fraction 3 (Figure 5.4) where the oxidative dissolution of Cu-sulphides (Fig. 1) take place. However, none of the samples overcame the threshold LTC0 in any of the fractions for S, as well as for B, Cd, Co, Cr, F, Mo, Sb, V and Zn, while Mn was above LTC0 but below LTC1 for every fraction.

In the bioavailable fraction (F1), S, Mn and Ba were predominant in most waste rocks and East tailing, while no S was bioavailable for syenite, M-pyroxenite and Selati tailing. In this fraction, only Ba, Cu and Mn overcame LCT0. The reducible

fraction (F2) also showed high concentrations of S for T- and B-carbonatite, F-pyroxenite and phoscorite samples, as well as for both tailings. However, Cl was predominant in F2 for syenite, P- and M-pyroxenite. In F2, As was above LTC0 in all the samples analysed; Ba and Mn were above LTC0 for some tailing samples, as well as for phoscorite, T- and B-carbonatites. Pb and Se were above LTC0 for all three pyroxenites, syenite and Selati tailing. The oxidizable fraction (F3) was characterized by high concentrations of S, Cu and Mn and, to a lesser extent, Ba, Ni, Pb, Se and As. Cu was above LTC0 for T- and B-carbonatite, F-pyroxenite, and East tailing, while one of the pyroxenites analysed (P-pyroxenite) reached up to 210 mg/L, which is above LTC2. Only carbonatites released Mn concentrations above LTC0 in F3. Although most Ba were released during F1 and F2, in F3 the concentration of Ba also overcame LTC0 in phoscorite, carbonatites and P-pyroxenite, together with Ni.

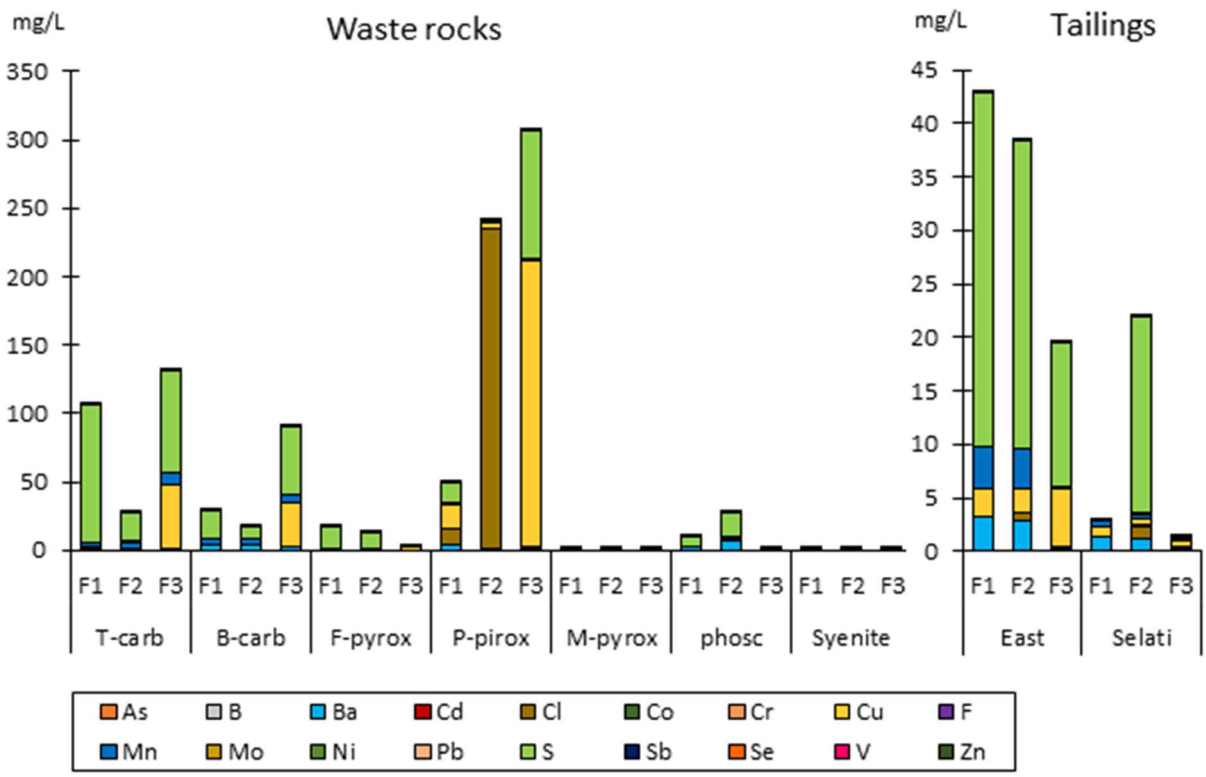

Figure 5.4. Leachates elemental composition of the bioavailable (F1), reducible (F2) and oxidizable (F3) fractions of the sequential extraction of PIC's waste rocks and tailings. The results showed herein correspond to the average of the elements regulated by the South African Department of Environmental Affairs (2013).

In addition, As was also above LTC0 in all the pyroxenites, phoscorite and Selati tailing samples. Se was above LTC0 for all the samples except syenite. Concentrations of Pb were above LTC0 for all the rocks analysed, except for T-carbonatite.

The occurrence of no regulated elements such as Ca, Mg, Na and K were high in the labile fraction of most waste rocks and tailing samples (Table 5.2). The highest concentration of Ca and Mg were released from carbonatite samples, while their concentrations of Na and K were particularly low. The concentration of trivalent metals such as Fe and Al were also relatively high, particularly in the labile fraction of P-pyroxenite and syenite. In addition, the total concentration of radionuclides such as U and Th reach up to 46.7 and 159.7 mg/kg, respectively (supplementary material, Table B.6); although the labile fractions of all PIC samples were always below 0.031 and 0.013 mg/L, respectively (Table 5.2).

Table 5.2 Mean concentration of non-regulated elements in the labile fraction of the sequential extraction (F1+F2+F3) performed to PIC wastes.

Analyte (mg/L)	B-carb	T-carb	F-pyrox	P-pyrox	M-pyrox	phosc	syenite	East tailing	Selati tailing
Ca	5273.54	5111.14	90.10	181.78	136.14	274.43	18.90	434.68	194.91
Mg	461.112	970.276	33.082	214.291	154.809	1127.899	33.564	380.417	283.487
Na	44.482	44.344	89.899	108.107	85.807	114.642	87.850	105.375	87.077
K	8.057	4.139	15.818	214.608	69.313	37.648	18.051	3.735	61.651
Fe	48.364	36.312	13.140	52.889	20.030	22.154	54.479	20.016	33.084
Al	2.913	4.656	12.195	21.764	19.848	28.568	24.733	1.280	19.875
Th	0.000	0.000	0.004	0.002	0.003	0.002	0.001	0.005	0.013
U	0.000	0.000	0.008	0.013	0.013	0.011	0.002	0.004	0.031

5.4. DISCUSSION

Alkaline mine wastes are not well understood and the scarce investigation on these wastes is traduced in lack of specific regulation and assessment for its disposal and its potential reuse worldwide. That is the case of the South African Phalaborwa Igneous Complex (PIC) where more than 4500 Mt of alkaline mining wastes have been disposed in tailing dams and waste rock dumps (FOSKOR, 2018; Moukodi, 2008). This study uses current protocols designed typically for sulphidic mine

wastes and alternative methods that might enhance the characterization of alkaline mine wastes, the prediction of alkaline mine drainage composition and, at the same time, shed some light about its potential reuse as alkaline reagent.

5.4.1. ASSESSMENT OF ALKALINE MINE WASTES.

The acid-base account (ABA) is one of the most commonly used methods in the assessment of sulphidic mine wastes to characterize acid-forming materials (INAP, 2009). However, this method also evaluates acid-neutralizing processes (dissolution of carbonates, displacement of exchangeable bases, and weathering of alkaline silicates). Therefore, somehow it can be useful when evaluating alkaline wastes. Nevertheless, the ABA method present significant limitations such as; a) the neutralization potential of a waste is measured according to rapidly dissolving sources of neutralisation, such as carbonates, and do not take into account the long term neutralisation capacity of other sources of neutralization, such as silicates (Gerson et al., 2019); and b) the acid potential (AP) calculation assumes that all sulphur measured by the total S method can be oxidized to produce 1 mol of sulphuric acid per mole of sulphur (Bouzahzah et al., 2015; Lawrence and Wang, 1996; Sobek et al., 1978; Usher et al., 2003), which occurs during the oxidation of pyrite. However, this assumption is invalid for many mine wastes whose main sulphide minerals are not pyrite and/or the sulphur is present in other phases such as sulphates.

The sequential extraction has been used herein to partially resolve the overestimation of AP (Figure 5.3); the sulphates present in the samples were extracted in the first step of the sequential extraction (F1), the sulphur contained in oxide minerals were extracted in the second step (F2) and finally, in the third step (F3) hydrogen peroxide/ammonium acetate (H_2O_2/NH_4OAc) mixture was able to oxidize sulphides (Du Laing, 2010), even though it is still not able to distinguish among sulphide species that are acid-forming or not. For example, for T-carbonatite and East tailing above 60% of total S belonged to sulphate and oxide species (Figure 5.4). Previous study (Caraballo et al., 2018) stated that the fractions could be oversaturated when used in sulphidic mine waste, which means that part of the sulphates, S-oxides and sulphide species could remain undigested after F1, F2 and F3, respectively, and get digested thereafter. Therefore, the concentration of S

digested in F4, which ranged 10 to 30% of the total S for PIC wastes, add uncertainty to the sulphide S results obtained from F3. It should however be noted that the concentration of sulphide in PIC wastes is low, compared to the sulphidic mine wastes and, therefore unlikely to oversaturate the F3 of the sequential extraction. Other authors have stressed the importance of mineralogical characterization in the prediction of ARD (Dold, 2017; Parbhakar-Fox and Lottermoser, 2015). In this study, the mineralogical characterization showed the presence of 7 different sulphide minerals, as well as sulphate compounds, (Figure 5.1) from which only two of them, i.e. chalcopyrite and anecdotic pyrite are identified as acidity producers (e.g. Dold, 2017; Stumm and Morgan, 1981). In general, the PIC wastes contain below 0.3% pyrite and 0.6% chalcopyrite (Table B3 of supplementary material), which supports the findings of the sequential extraction. Thus, the PIC wastes do not have enough Fe-sulphide minerals to sustain acid drainage generation.

In order to further improve ABA method, a mineralogical approach has been introduced in this study using NCV and textural ARDI (Bucknam, 1997; Parbhakar-Fox et al., 2011). This approach, together with semiquantitive mineralogical analysis give a more realistic information about the constituents of the samples and foster a better understanding of the minerals that are able to produce acidity or generate alkalinity. In that sense, abundant alkalinity-producing minerals were found throughout PIC wastes, including fast-dissolving minerals such as calcite and dolomite, as well as long term alkalinity-producing minerals such as diopside, phlogopite and microcline (Sverdrup, 1990). According to Kwong, (1993), there is an effective neutralizing capacity if the abundance of diopside and biotite exceeds 5 and 10%, respectively. Such is the case of all the pyroxenites and Selati tailing samples analysed (Table B3 of supplementary material). In addition, the high concentration of Si in fractions 2 and 3 (Table B6 of supplementary material) suggest that relatively-easy soluble silicates are present in PIC wastes. Therefore, the long-term neutralization potential may be higher than the results determined by ABA (Table 5.3). The combination of BCR and mineralogical characterization undeniably enhanced the characterization of alkaline wastes and the prediction of NAMD.

Although both tailings and WRDs from PIC have neutralization potential, the magnitude of the neutralization potential obtained differed depending on the procedure used. For example, according to NCV and NPR, East tailing has the highest neutralization potential (23.1 %CO_2 and 190.5, respectively), followed by both carbonatites and phoscorite (Table 5.1). This differs from NNP results, which indicate that both carbonatites have the highest neutralization potential, followed by East tailing and phoscorite (Table 5.1). The discrepancies between the methods are mostly because both carbonatites have the highest concentration of sulphide and carbonate minerals. Therefore, those methods in which AP values weight more than NP will underestimate the neutralization potential of the carbonatite, and vice versa.

Similar discrepancies were observed in the analysis of syenite and pyroxenite samples. The highest paste pH values were achieved by those lithologies (Table 5.1). However, according to NNP and NCV, they are not classified as high acid consuming materials. Furthermore, F-pyroxenite would fall under low-potential of acid forming, according to NAG (Table 5.1). Such discrepancies might be related to the low concentration of carbonate and sulphide minerals, except for P-pyroxenite (Figure 1 and table 5.1). This resulted in an initial alkaline pH due to minor fast-dissolving alkaline minerals (paste-pH above 9, table 5.1, Figure 5.2), followed by a pH dropping after carbonates are consumed and the sulphides start been oxidized (NAG pH 4-7, table 5.1). Once the scarce sulphides are consumed, no acid mine drainage would be produced, and low alkalinity is expected to be generated afterwards (NP and NCV classification, table 5.1), which is consistent with the alkaline mineral content (Figure 5.1 and table B.3 of supplementary material). The most abundant alkaline minerals of these lithologies are diopside and phlogopite whose NP are below 10 kg $CaCO_3$ eq/t and their reactivity at pH 5 range between 10 and15 Keq/ha/year, which is 40-60% of the carbonate 25 Keq/Ha/year (Blowes et al., 2003; Brough et al., 2013; Global Acid Rock Drainage, 2014; Sverdrup, 1990).

ABACUS verdict, according to the NNP values, is that most of the samples probably have an excess of neutralizing minerals (Tables B.7 and B.8 of supplementary material), which suggests the potential of PIC wastes to generate NAMD. Although

the comparison between NPR and S% leaves P-pyroxenite and B-carbonatite in the uncertainty area (Figure 5.5b), only P-pyroxenites could produce acidity under certain conditions, according to the S% and NPR values for both, open and closed systems (Figure 5.5a). Taking into account that the S% is an overestimation because it does not discern among sulphur species, and the neutralization potential is underestimated because it only assesses rapidly dissolving sources of neutralization, the ABACUS veridic can be considered as a conservative evaluation of the potential generation/neutralization of acid rock drainage. The limitations of ABA procedures and ABACUS tool affect both acid and alkaline mine waste characterizations.

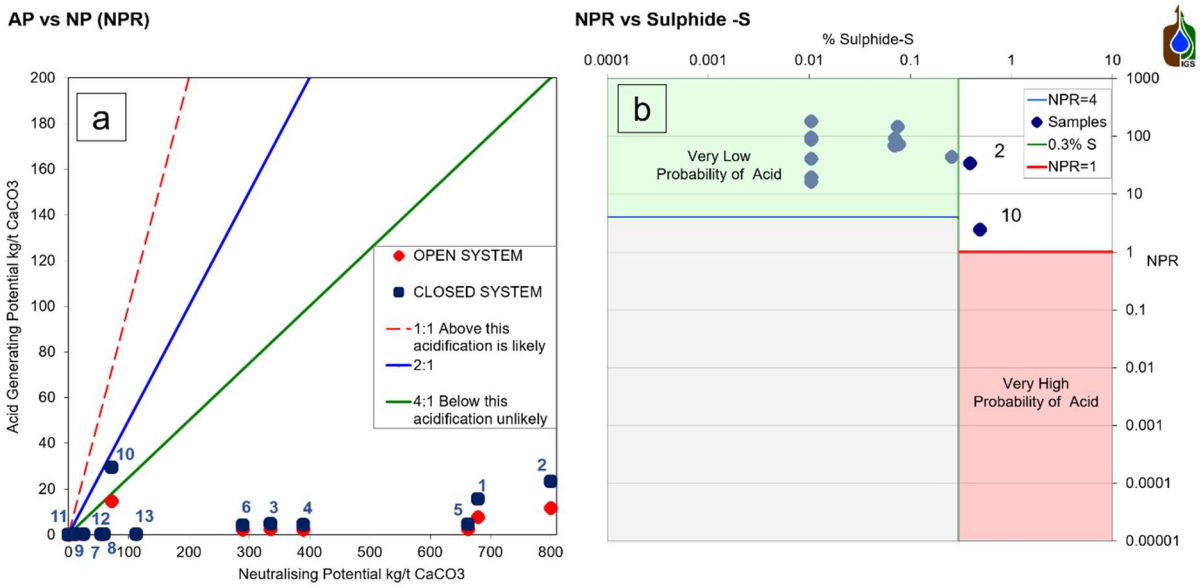

Figure 5.5 Abacus charts showing the average of each lithology (1: T-carbonatite, 2: B-carbonatite, 9: F-pyroxenite, 10: P-pyroxenite, 11: Syenite, 12: M-pyroxenite and 13: Phoscorite) and each tailing sector (3: East tailing S, 4: East tailing N, 5: East tailing W, 6: East tailing E, 7: Selati tailing N and 8: Selati tailing S); a) Acid Potential (AP) versus Neutralization Potential (NP) and b) Neutralization Potential Ratio (NPR) versus sulphide content expressed as S% under closed conditions. Note that in order to represent the samples with S% below detection limit (0.01 S%), the value of 0.01 S% has been used.

EC values does not play a role in the ABACUS verdict. However, it indicates the elemental load in the leachate, which is crucial when predicting the AMD or NMD formation. Current tests highlight the problems related to heavy metals present in

AMD ignoring the high concentrations of alkali and alkaline metals in solution. It is worthy of mention that the leachable concentration test of the South African regulation is stricter in this regard and it includes TDS and SO_4^{2-} Cl, B, Ba, Co, Mn, Sb and V thresholds for the classification of the waste (Department of Environmental Affairs, 2013). In this study, high concentrations of no regulated elements such as Ca, Mg, Na and K are released from the labile fraction. This corresponds with the high EC values of the leachates, and altogether indicates the potential of these type of wastes to generate saline NAMD.

On the other hand, the leaching tests show that all the rocks and tailing samples have at least one element above LTC0 and/or TCT0 (Thresholds for inert material), but none of them overcame LCT1 nor TCT1 (thresholds for non-hazardous waste). Therefore, the drainages produced by PIC wastes would classify as non-hazardous. However, the sequential extractions indicate that under oxidizing conditions (F3) P-pyroxenite have the capacity to release concentration of Cu above the limit LTC2, assigned for harmful material. This exposes the limitations of the leachate test to predict the release of toxic elements in the long term, as the F3 of the sequential extraction simulates the complete oxidation of sulphide minerals, in this case mostly chalcopyrite.

Even though pseudo-total digestion is compared with total digestion thresholds, all the elements regulated were far below TCT1 for all the samples analysed, being the closest Se, Cu and Ba whose concentrations were, on average, 5, 8 and 18 times smaller than TCT1 threshold (Table A6 in supplementary material). Therefore, all the mining residues classify as non-harmful material (type 3 waste) according to the National Environmental Management Waste Act (59/2008) of South Africa, in spite of their capacity to generate saline NAMD.

5.4.2. ALKALINE MINE WASTES REUSE.

These non-harmful wastes, and in particular the tailings, can substitute the limestone sand typically used in passive water treatments such as DAS (dispersed alkaline substrate; Caraballo et al., 2011). Even though carbonatite rocks have more calcite, their relatively high content in Fe-sulphide minerals (mainly chalcopyrite) might be a concern. However, the mineral processing of the

carbonatites to concentrate Cu sulphide minerals, including chalcopyrite, has produced a tailing (East tailing) rich in carbonates and poor in sulphides. Indeed, all the methods described herein concur on classifying East tailing as high acid consuming material (table 1 and Figure 5.5). Therefore, it is reasonable to assume that wastes from East tailing have the capacity to neutralize acid industrial wastewater and is a better option than Selati tailing and WRD. However, the released of Ca > Mg > Na > SO_4 > K > Fe could be detrimental to the treatment´s efficiency because they can interfere with the precipitation of the mineral phases responsible for the metal removal within the treatment (i.e., schwertmannite, hydrobasaluminite and gypsum). These elements (with the exception of SO_4 and Fe) are not typically included in any regulation for landfill or extractive waste disposal around the world, but they are present in water regulations, as they would increase hardness and ionic strength of the water, which could have a detrimental impact on the surrounding environment.

Furthermore, the radionuclides, such as U and Th, do not belong to the routine of elements to screen for in waste characterization protocols. However, carbonatitic deposits are known to often concentrate them (13% of carbonatite deposits have thorite and 12% have thorianite and/or U-thorianite (Berger et al., 2009). On average, the pseudo-total concentrations of U and Th in PIC wastes were 6.7 and 36.3 mg/kg, respectively (supplementary material, Table B.6). Nevertheless, the labile fractions of those radionuclides were, on average, 0.003 and 0.006 mg/L for Th and U, respectively (Table 5.2), which is far below the limit stablished by the World Health Organization (WHO) for drinking water (0.03 mg of U/L; WHO, 2017). The low leachability of the U and Th might be because the main source of these radionuclides in PIC are silicates, such as thorite, and therefore they belong to the non-labile fraction of the residues (refer to chapter 4, section 4.4.2). Both thorite and thorianite have been identified in PIC as micrometric inclusion in apatite and strongly associated with magnetite (Dawson et al., 1996; Giebel et al., 2017; Milani et al., 2017). Therefore, if the material from East tailing is used as alkaline reagent, the concentration of U in the treated water would presumably comply with drinking water standards (WHO, 2017).

In addition, the characteristics of East tailing are better in comparison with other alkaline wastes used to neutralize acid industrial wastewater such as fly ash and red mud (Table 4). The neutralization potential of East tailing (662.9 kg $CaCO_3$/t) are 2 to 30 times higher than fly ash (20 – 275 kg $CaCO_3$/t) (Qureshi et al., 2016) and 7 times higher than red mud (~91.6 $CaCO_3$/t) (Paradis et al., 2006). On the other hand, the highest concentrations of potentially toxic elements in East tailing are only represented by Fe, Al and Mn, while in red mud and fly ash, in addition to those metals, high concentrations of Cr, Zn, Pb, and As, are present (Table 5.3).

Table 5.3 Neutralization potential (NP, expressed in kg CaCO3), paste pH and the concentration of toxic elements (mg/kg) of several red mud and fly ash studies are compared with PIC waste from East tailing.

Waste	NP	pH	Fe	Al	Mn	Cr	Zn	Pb	As	Location	References
Red mud	~91.6 (Doye and Duchesn, 2003)	10.00 - 12.56 (Tanez and Hurel, 2019)	261000	65700	406000	1350000	80000	50000	1000	Alcoa (Spain)	(Rubinos and Barral, 2013)
Red mud			560000	200000	1180000	1120000	n.r.	230000	213000	Ajka (Hungary)	(Milačič et al., 2012)
Red mud			550000	106000	3850000	580000	300000	230000	75000	BB Alumina (Bosnia and Herzegivina)	(Smicikl as et al., 2015)
Fly ash	20 – 275 (Qureshi et al., 2016)	9.5-13.48 (Qureshi et al., 2016)	312000	179000	700	168	218	18.9	7.49	Power plant-West Bengal (India)	(Qureshi et al., 2016)
Fly ash			132153	33394	232.34	20.5	46.7	110	44.2	Atikokan Thermal Power (Canada)	(Yeheyis et al., 2009)
Fly ash			22503	147918	309	n.r	42.09	56.56	49.1	Eskom power station (South Africa)	(Mainganye et al., 2013)
Tailing	662.9	8.53	116204	6578	913	31.5	6.2	24.9	8.1	East tailing	This study

n.r.=not reported

The determination of the mobility of metals plays an important role in the mine waste characterization. In that sense, the sequential extractions brough benefits to both the characterization of the alkaline mine waste and the assessment of its revalorization potential; i) the determination of the bioavailable fraction (F1) is similar to conventional leachate test, and ii) determines the pollutants that might be released under reducing (F2) and oxidative (F3) conditions. Such information is

also relevant for the preliminary evaluation of any alkaline material subject to be used as a reagent for water treatments in either anaerobic or aerobic reactors (F2 and F3, respectively). In addition, kinetic experiments such as column percolation tests, suggested for extractive waste management measures by EU regulations (Commission Decision 2009/360/CE), could be used to simulate short-term geochemical behaviour of the alkaline waste, which combined with geochemical modelling could enhance long term prediction.

5.5. CONCLUSIONS

The combination of traditional technique such as ABA with mineralogical analyses, as well as the combination of leachate test with BCR-sequential extractions enhanced the characterization and led to have a better understanding of the alkaline waste, from its neutralization capacity to its toxicity, shedding some light on its recycling potential.

Despite the discrepancies between methods, it was concluded that the residues produced by the mining activity in PIC have no potential to sustain acid drainage generation due to the scarcity of Fe-sulphide and the abundance of alkaline minerals. Indeed, the identification of soluble carbonates and relatively fast-dissolving silicates (diopside, phlogopite and microcline) in the samples suggests long term generation of NAMD.

Although the sequential extractions demonstrated that under oxidizing conditions some waste rocks (P- pyroxenites) have the capacity to release concentrations of Cu above the limit assigned for harmful material, all the samples would classify as non-harmful material according to national and international regulations for solid waste and contaminated soil, which demonstrates its limitations for alkaline mine waste characterization. In addition, current regulations do not include alkali/alkaline elements (Ca, Ba, Na, Cl, among others) and radionuclides, which are present in both waste rocks and tailings. Indeed, these elements are present in water regulations, as they would increase hardness and ionic strength of the water, which could have a negative impact on the aquatic environment. Therefore, this study highlights the need to include them in current regulations in order to consider the potential risk of alkaline mine waste to the environment.

The environmental characterization of PIC wastes also offered the first insight toward their recycling potential as alkaline reagent to neutralize AIW. Among PIC wastes**,** East tailing is the most feasible alternative to neutralize acid industrial wastewater because of its high neutralization potential and its low concentrations of potentially toxic elements. Despite the high concentrations of some alkali/alkaline elements, which could be detrimental to the final quality of the treated water.

In conclusion, this study stresses the need to enhance mine waste characterization procedures and set the ground for the inclusion of options of revalorization as part of the protocols for mine waste characterization, which would decrease the environmental impact of mine waste, and is aligned with the global circular economy strategy.

5.6. ACKNOWLEDGMENT

This work was supported by the Department of Science and Technology (South Africa) through the ERAMIN project AMDREY -PCIN2015-242-256. It was also partially financed by: UNESCO (UNESCO-IUGS-IGCP-Project 682), project MOS (grant number CGL2016-79204-R), CORFO and Codelco (project CORFO-16PTECME-66524), project CONICYT/PIA AFB180004 and Science Foundation Ireland (grant number 18/IF/6347). Special thanks are due to the staff of Palabora Mining Company and Foskor for their assistance during the sampling. The authors would like to thank the reviewers for their thoughtful comments and efforts towards improving the manuscript.

CHAPTER 6: CONCENTRATION OF RARE EARTH ELEMENTS FROM ACID WASTEWATER USING REE-RICH ALKALINE MINE WASTE: A NOVEL APPROACH OF AN ACID WASTEWATER NEUTRALIZATION SYSTEM.

ABSTRACT

The capacity of an alkaline REE-rich tailing from Phalaborwa complex to neutralize extreme acid wastewater from the fertilizer industry and, at the same time, to concentrate REE from both wastes were assessed in a sequential passive system. The results showed that the water quality improved substantially; the removal efficiency of anions such as fluor > sulphate > phosphate, trivalent (i.e. Fe, Al and Cr) and divalent metals (i.e. Cu, Cd and Mn) and radionuclides were removed up to 100% throughout the experiment. Interestingly, approx. 90% of REE were removed in the alkaline tailing column, while 5% were immobilized in the witherite column, opposite to U that was removed mainly in the latter. According to the geochemical model the immobilization of the anions and cations were mainly controlled by the precipitation of phosphate minerals in both columns. This result is in agreement with the sequential extraction, where most potentially toxic elements and REE were concentrated in the fraction associated to phosphate minerals in both columns. The mineralogical characterization identified brushite and an unidentified CaAlF-phosphate as major minerals. The later acts as a sink for REE in the tailing column. To the best of our knowledge, this is the first study that describes the formation of this phosphate mineral and its activity as a sink of REE in ambient conditions. Minor REE sorption by oxide minerals cannot be ruled out. The concentration of REE in the substrate reached up to 2.1 g/kg in the middle of the column. Newly formed gypsum and oxide minerals were found throughout the system and they were mainly associated to the removal of Fe > Al > Cr > Cu > Cd > Mn > Ni > As. Even though the water quality does not reach drinking water standards because of the salinity-related compounds that still remained in water, the water improvements after treatment and the enrichment of REE with

marketable values suggest that the use of alkaline tailing can be an attractive alternative to create a self-sustainable and environmentally-friendly water treatment that mitigates the contamination of acid wastewater from the fertilizer industry.

6.1. INTRODUCTION

The Phalaborwa Industrial Complex (PIC), located in the central Lowveld of Limpopo province, is well known for hosting the only economic copper sulphide carbonatite orebody in the world (Giebel et al., 2019; Heinrich, 1970). It also represents one of the major sources of phosphate in Southern Africa. The phosphate rock is mined since 1950's, which promoted the establishment of a fertilizer industry at PIC in the early 1960's (Roux et al., 1989). The igneous phosphate rock, phoscorite, is mainly composed by Mg (15.9 wt% on average), followed by P, Ca, Fe, Al, K and Na (average of 5.7 wt%, 3.1 wt%, 2.2 wt%, 1.9 wt%, 0.8 wt% and 0.6 wt%, respectively), as well as, minor concentrations of rare earth elements (REE) and radionuclides (0.23 and 0.006 wt%, respectively) (refer to chapter 4). It is worth mentioning that, in general, igneous phosphate rocks contain lower concentration of radionuclides and higher concentration of REE than sedimentary phosphate deposits (Pufahl and Groat, 2017). As a result of the phosphate ore processing for phosphoric acid production (equation 6.1), industrial waste/by-products such as phosphogypsum and extremely acidic wastewater were generated and accumulated on PIC by approx. 54 years.

$$Ca_{10}(PO_4)_6F_2 + 10H_2SO_4 + 2H_2O \rightarrow 10CaSO_4.2H_2O + 6H_3PO_4 + 2HF \qquad 6.1$$

After the chemical processing, residual phosphoric, sulphuric and hydrofluoric acids as well as most of the valuable (e.g. REE and Au), heavy metals (such as Al, Fe, Ni, Mn, among others) and radionuclides (i.e. Th and U) contained in the phosphate rock are disposed along with the phosphogypsum and, to a lesser extent, in the wastewater (Msila et al., 2016; Saadaoui et al., 2017). For every tonne of phosphoric acid produced, 4 to 6 tonnes of dry mass of phosphogypsum are generated (Saadaoui et al., 2017). Around 540000 tons of phosphogypsum are estimated to be dumped in PIC and the exposure to continuous weathering has triggered the generation of leachates with high concentrations of potentially toxic

elements (Pérez-lópez et al., 2015). This leachate, together with the processed water from the plant, is accumulated in impoundments upon and surrounding the phosphogypsum stacks (. Due to its proximity to the Kruger National Park (KNP), the negative environmental impact caused by the phosphogypsum stacks and the impoundments to the surrounding ground- and surface water bodies have elucidated public concern in South Africa (e.g. Kings, 2014; Mbombela, 2014).

Alkaline reagents and industrial wastes have been extensively used in passive and active strategies to remediate extremely acidic wastewaters (Castillo et al., 2012). For example, recent studies (Millán-Becerro et al., 2020, 2019) demonstrated that the Disperse Alkaline System (DAS) treatments are sustainable solutions to treat wastewaters from the fertilizer industry. These studies tested several DAS systems using different alkaline reagents such as limestone, biomass ash, fly ash, magnesia, magnesium hydroxide, calcium hydroxide and barium carbonate (BDAS). They proved to effectively remove phosphates, fluorides, Fe, Zn, Al, Cr, Cu, Cd and U from solution. However, these treatments were not completely effective for both As and SO_4, remaining in high concentrations at the end of the treatment. In this sense, better results have been obtained using BDAS to treat acid and alkaline mine drainages with high sulphate concentration (Castillo et al., 2015; Gomez-Arias et al., 2016, 2015; Torres et al., 2018). On the other hand, *Ayora et al.*, (2016) has reported that limestone DAS are able to remediate acid mine drainage and concentrate traces of REE (including lanthanides, yttrium and scandium) in Al-rich residues. Therefore, it is hypothesized that the treatment of acid REE-rich industrial wastewater (AIW) through a passive system based on REE-rich alkaline mine tailing (1.4 kg/t, refer to chapter 4) would be a cost-effective alternative whose residue might be considered as a secondary resource of REE

The alkaline tailings generated during the extraction of Cu from the carbonatite rocks are located in the Easternmost side of PIC (herein East tailing). Therefore, this alkaline residue might represent a suitable and cost-effective solution for the neutralization of the AIW produced by the neighbouring industry. This study aims to prove that the use of alkaline tailings from PIC as reagent for a DAS system is an affordable solution to treat the AIW from the fertilizer industry and, at the same time, can lead to the concentration of REE from both industrial wastes in a

particular section of the system. Due to the high concentration of phosphate and sulphate that characterizes the AIW from the fertilizer industry, a BDAS reactor have been added to further improve the quality of the water.

6.2. METHODOLOGY

6.2.1. STARTING MATERIAL

Extremely acidic wastewater

Approx. 300L of wastewaters from the impoundments (Figure 6.1) surrounding the main phosphogypsum stack at the Phalaborwa Industrial Complex (PIC) were collected using an Integra Bladder Pump Model 407 (Solinst Canada Ltd) and polyethylene containers (25L). The containers were rinsed three time with wastewater, and then slowly and fully filled. The drums were transported within 24 hours to the lab and stored at 4°C.

Alkaline material

A sampling was carried out in the East tailing and around 80 kg of samples were collected from the surface of the tailing. The samples were homogeneously mixed and a sampler splitter was used to obtain representative and homogeneous subsamples that would be used as reagent for further batch experiments and bench-scale prototype. Commercial witherite powder (88.6% $BaCO_3$) from Protea chemicals was also used as reagent for the second column of the prototype.

6.2.2. BATCH EXPERIMENTS

Preliminary batch experiments were performed in order to optimize the amount of tailing required to neutralize the AIW in a continuous system. The interactions were performed between a mixture of AIW and alkaline waste at different ratios; 16.6 and 4g of tailing in 40 mL AIW, respectively (1:6 and 1:10). The interactions were carried out in triplicates in 50 mL Falcon tubes and placed on an orbital shaker at room temperature and 12 rpm. Each batch experiment included 10 different samples which were removed from the rotor at designated time intervals of 0.5, 1, 3, 6, 12, 24, 48, 72, 96 and 144 hours. Thereafter, each sample was centrifuged at 3000 rpm for 20 min and different physicochemical parameters such as pH and

Electrical Conductivity (EC) in the supernatant of each sample were monitored using an ExStix®II multi-probe.

6.2.3. BENCH-SCALE PROTOTYPE

The bench-scale prototype consisted of 2 reactors connected in series (Figure C.1 of supplementary material). Each reactor consists in a PVC column (10 cm inner diameter, height 50 cm) with four sampling ports every 10 cm height, which were connected to internal perforated drain pipes. An outlet port was located at the bottom of each column, covered with a 2.5 cm layer of quartz gravel (particle size: ~5-8 mm). The reactors were filled with 40 cm of reactive material composed of a mixture of alkaline material and wood shavings. Based in the results and modelling of the batch experiments, the first reactor (column A) was filled with 2 kg of alkaline waste from East tailing. Following the BDAS system specifications (van Heerden et al., 2015), the second reactor (column B) was packed using 0.7 kg of witherite ($BaCO_3$). Witherite was selected due to its ability to remove divalent metals and sulphate (Gomez-Arias et al., 2015). The witherite used was purchased from Protea Chemicals Company and it contains 88.6% $BaCO_3$ and traces of Fe and SO_4.

The down-flow reactors had supernatant open to the atmosphere in order to maximize Fe oxidation and minimize Fe^{2+} solubility in the reactor. The wastewater was pumped to the top using a peristaltic pump with an inflow rate of 0.9 mL/min to allow a residence time of approximately 24 hours in each column. A porosity of 32.6 and 44.4% was volumetrically calculated for the columns A and B, respectively. Water samples of the reactors for temporal and spatial analyses were taken daily and weekly, respectively. Then each sample was filtered with Teflon filters 0.45 µm, acidified with 65% HNO_3 and stored until their chemical analysis.

6.2.4. MINERALOGICAL CHARACTERIZATION

At the end of the bench-scale experiment, both reactors were drained, opened and solid samples of the substrate were collected from the top, middle and bottom of each reactor. The samples were freeze dried overnight and prepared for their mineralogical characterization. The characterization was undertaken at the University of Huelva (Spain) and The University of the Free State (South Africa). Polished thin sections were prepared for the mineralogical determination of the

substrate from column A. To avoid the dissolution problems during the preparation of the polished section of the substrate from column B, the samples were mounted in a stub and coated with carbon. The mineralogical and microtextural characterization of the substrates were performed by a scanning electron microscope coupled with energy dispersive spectroscopy (SEM–EDS) Fei-QUANTA 200 equipped with a microanalyzer EDAX Genesis 2000 and SEM-EDS JEOL JMS-5410 equipped with a microanalyzer Link Oxford. In addition, the reagents (tailing and witherite), as well as substrate samples from the top, middle and bottom of both columns were analysed using X-ray diffraction (XRD) with a Broker D8 Advance Powder Diffractometer with Cu–Kα radiation. Crystalline phases were identified using XPowder Software with PDF2.DAT database of the International Centre for Diffraction Data (ICDD).

6.2.5. SEQUENTIAL EXTRACTION

Geochemical speciation of elements in the alkaline tailing and the reactors substrate (every 8 cm) was carried out using the optimized three-steps sequential extraction procedure proposed by the Community Bureau of Reference (BCR) as described in Rauret et al. (1999), performed in triplicate. The first step of the sequential extraction uses 0.11 mol/L acetic acid to extract water/acid soluble minerals and release exchangeable elements, the extractant is referred herein as fraction 1 (F1). The second step use 0.1 mol/L hydroxylamine hydrochloride to extract the reducible fraction, referred as fraction 2 (F2). The third step involves both reagents 8.8 mol/L H_2O_2 and 1.0 mol/L ammonium acetate to tackle the oxidizable fraction, referred as fraction 3 (F3). Additionally, pseudo-total digestions (with aqua regia) were performed in triplicate to all the samples (more details in table 4.1 and appendix A.1 of supplementary material).

6.2.6. HYDROCHEMICAL ANALYSIS

The physicochemical parameters of the samples from the batch and bench-scale experiments were analysed immediately after sampling to avoid the effects of the CO_2(g) and O_2(g) dissolution. Physicochemical parameters such as dissolved oxygen (DO), temperature (T), pH, electrical conductivity (EC) and total dissolved solids (TDS) were measured in all samples with an ExStix®II multi-probe, and oxidation-

reduction potential (ORP) was measured with an ExStix®II ORP (Pt and Ag/AgCl electrodes) probe. ORP measurements were corrected to standard hydrogen electrode.

The chemical composition of the water and the sequential extractions' extractants was analysed at the University of the Free State. Major and minor constituents such as Al, As, B, Ba, Be, Ca, Cd, Co, Cr, Cu, Fe, K, Li, Mg, Mn, Mo, Na, Ni, Pb, S, Sb, Se, Si, Sn, Sr, U, V and Zn were analysed by inductively coupled plasma optical emission spectroscopy (ICP-OES) Teledyne leeman labs Prodigy, while rare earth elements (REE), including lanthanides, Sc and Y were analysed by Inductively Coupled Plasma Mass Spectrometry (ICP-MS) PerkinElmer NexIon 2000c. Anions such as P and F were analysed by the discrete analyzer Easy Chem 200. Analytical details are displayed in appendix B.3 of supplementary materials.

6.2.7. MODELLING AND STATISTICAL ANALYSIS

The speciation of elements and saturation indices of waters were predicted by using the thermodynamic computer program PHREEQC v3.4, based on equilibrium chemistry of aqueous solutions interacting with minerals, gases, solid solutions, exchangers, and sorption surfaces (Parkhurst & Appelo, 2013). Although, the wastewater had a high ionic strength (1.6 mol/kgw), solutions from both batch and column experiments exhibited ionic strength values lower than 0.7 (interquartile range between 0.2 and 0.6 mol/kgw). For this reason, the database provided by Lawrence Livermore National Laboratory (llnl.dat), and MINTEQ thermodynamic database (Allison et al., 1991) were used. Zero, negative or positive SI values indicate that the solutions are in equilibrium, undersaturated and supersaturated respectively, with regards to a certain solid phase.

Statistical analyses were performed using R software (http://www.r-project.org/), version 3.6.1. Correlation matrix was performed using the Hmisc package and Pearson and Spearman correlations. The principal correlation analysis (PCoA) was used to observe multiple inter-correlated quantitative variables. Correlation matrix. This analysis was used to determine the correlation between the physicochemical parameters and the elemental composition of the IAW, in column A and column B. The principal component analysis (PCA) was carried out using FactoMineR &

factoextra package. Biplot was used in order observed the individual (water samples) and varibles (Metals).

6.3. RESULTS

6.3.1. CHARACTERISTICS OF STARTING MATERIALS:

Characteristics of the alkaline material

According to the mineralogical characterization, the alkaline tailing was mainly comprised of calcite > dolomite > pyroxene > f-apatite > magnetite > phlogopite > zircon > monazite (Table 6.1).

Table 6.1 Mineralogical and elemental characterization of alkaline material.

Mineralogical characterization				
East tailing	**Calcite**	**Dolomite**	**F-apatite**	**Monazite**
Abundance (%)	40	13	9	0.3
REE (%)	0.8	0.3	1.2	67.3
Elemental composition				
Major elements (mg/Kg)	**Fe**	**Mg**	**Ca**	**P**
	146716	110131	49885	20912
	Al	**S**	**Na**	**Sr**
	3772.4	3536.7	1770.3	1327.5
	Mn	**Cu**	**Ti**	**Ni**
	1010.4	587.8	204.4	144.5
	Ba	**U**	**Si**	**Zr**
	77.9	61.2	29.6	0.7
	K	**F**		
	0.1	0.01		
Rare earth elements (mg/Kg)	**Ce**	**Nd**	**La**	**Pr**
	556	246	203	59
	Gd	**Sm**	**Y**	**Dy**
	47.60	45.03	28.02	18.43
	Eu	**Er**	**Tb**	**Sc**
	10.57	4.65	4.56	3.92
	Ho	**Yb**	**Tm**	**Lu**
	2.48	2.31	0.47	0.18
	∑REE			
	1332.32			

The chemical composition of the alkaline tailing is characterised by high concentrations of Fe, Mg, Ca and P, in this order of abundance, with appreciable concentrations of Al, S, Na, Sr and Mn (Table 6.1). Among trace elements, Cu, Ti, Ni, Ba and U are the most abundant. The average concentration of REE in the tailing is 1332 mg/kg, of which 75% belongs to the Ce, La and Nd, altogether.

Characteristics of the wastewater

The physicochemical parameters indicated extremely acidic (pH 1.3) and oxidative conditions (542.3 mV). High EC values corresponded with the high concentrations of cations and anions present in solution (Table 6.2).

Table 6.2 Physicochemical characterization of the wastewater.

Physicochemical characteristics						
Parameters	**pH**	**T (°C)**	**TDS (g/l)**	**EC (mS/cm)**	**Eh (mV)**	**Net acidity (mg/L $CaCO_3$)**
	1.3	23.0	24.9	29.3	542.3	52000
Elemental composition						
Major elements (mg/L)	**Ca**	**K**	**Mg**	**Na**	**Al**	**Cu**
	860.0	330.0	1865.4	225.7	447.62	63.80
	Fe	**Mn**				
	211.83	47.05				
Anions (mg/L)	**Fluoride**	**Phosphate**	**Sulphate**			
	1099	7450	11911			
Minor elements (mg/L)	**Zn**	**B**	**V**	**Ni**	**Se**	**Cr**
	4.05	3.61	3.11	3.56	2.84	2.73
	Co	**Ba**	**Be**	**Cd**		
	1.42	0.55	0.09	0.09		
Rare earth elements (mg/L)	**Nd**	**La**	**Ce**	**Y**	**Sm**	**Sc**
	1.66	1.61	1.43	0.69	0.41	0.29
	Er	**Tm**	**Dy**	**Gd**	**Pr**	**Yb**
	0.18	0.17	0.16	0.14	0.12	0.10
	Eu	**Tb**	**Lu**	**Ho**	**∑REE**	
	0.09	0.07	0.03	0.02	7.2	
Radionuclides (mg/L)	**U**					
	1.04					

The AIW was particularly enriched in anions such as sulphate > phosphate > fluoride > chloride. The concentrations of Nd, La and Ce were the highest amongst REE in the AIW, coincidently with East tailing and phoscorite ratios (refer to

chapter 4), whereby we can infer that such concentrations of REE elements came from the processed phosphoric rocks.

6.3.2. BATCH EXPERIMENTS: OPTIMIZATION OF NEUTRALIZATION PROCESS

In order to determine the most effective dose of alkaline waste to treat the water, the modeling was performed using the REACTION command in the PHREEQC code. For the sake of simplicity, only those minerals included in the waste that dissolve at a fast pace in acidic conditions were included (i.e. calcite, dolomite and fluorapatite), while those less reactive minerals (i.e. silicates or magnetite) or found at very low concentrations (e.g. sulphide) were not considered.

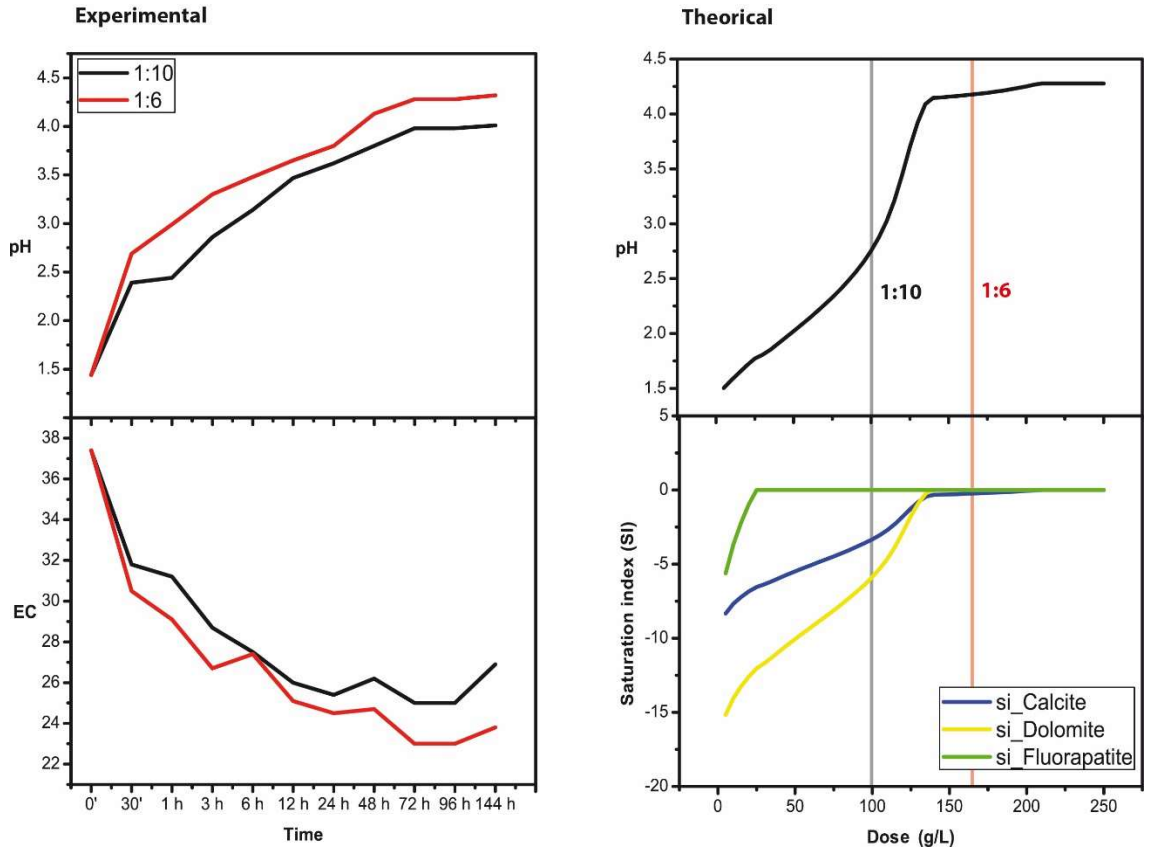

Figure 6.1 Evolution of pH and conductivity (EC) during the interaction between tailing and acidic wastewater (left). Modelled pH and saturation indices (SI) during the reaction of the tailing with the acidic waste waters (right).

To accomplish this, the solid reacting with the waters was defined stoichiometrically to reflect accurately the waste mineralogy. As can be seen in Figure 6.1, the pH of the solution increases progressively concomitant to the addition of alkaline wastes due to the dissolution of calcite, dolomite and fluorapatite.

A steady state is observed at values around 4.28, after adding a total of 210 g/L of alkaline waste. However, an amount of 150 g/L (1:6) was enough to increase the pH values around 4.2, which can be considered as the optimal dose for water treatment as it was confirmed at experimental results. From this point on, waters become oversaturated with respect to calcite, which is the main mineral phase responsible of acidity neutralization during the reaction.

6.3.3. BENCH SCALE PROTOTYPE

WATER ANALYSIS

Temporal and spatial evolution of hydrogeochemistry of treated AIW

Overall, it can be observed that the matrix of columns A (based on alkaline waste) releases potentially toxic elements, which are mostly reprecipitated within the same column leading to waters with concentrations below initial values (Figure 6.3 and 6.4). Column B (based on barium carbonate) met its purposes enhancing the removal of divalent metals and anions from water, and improving the physicochemical parameters (Figure 6.2, 6.3 and 6.4).

According to the evolution of physicochemical parameters (Figure 6.2), the best results were achieved during the first five weeks, when the pH of the AIW increased from 1.4 to 5.4 and EC decreased from 28.3 to 9.4 mS/cm, on average. The concentration of anions was associated not only with the polluted AIW, but also to the dissolution of the matrix in column A. For instance, the concentration of dissolved phosphate increased at the top of column A, particularly at the beginning of the experiment, and kept fluctuating thereafter throughout column A (Figure 6.3).

The fluctuations smoothed overtime as the apatite group minerals ($Ca_{10}(PO_4)_6(OH,F,Cl)_2$, originally present in the matrix, may have been dissolved

over time. Column B was very efficient removing phosphates at the beginning of the experiment but its removal capacity dropped over time. This can be observed in Figure 6.3 where the concentration of phosphate dropped from about 40000 to 10000 mg/L at the top of column B (port B1) during the first three weeks. As a result, the highest removal percentage of phosphate took place at the beginning and at the end of the experiment. Unlike phosphate, sulphate and fluoride were immobilized throughout the whole duration of the experiment, reaching an overall removal efficiency between 90 and 100% (Figure 6.3).

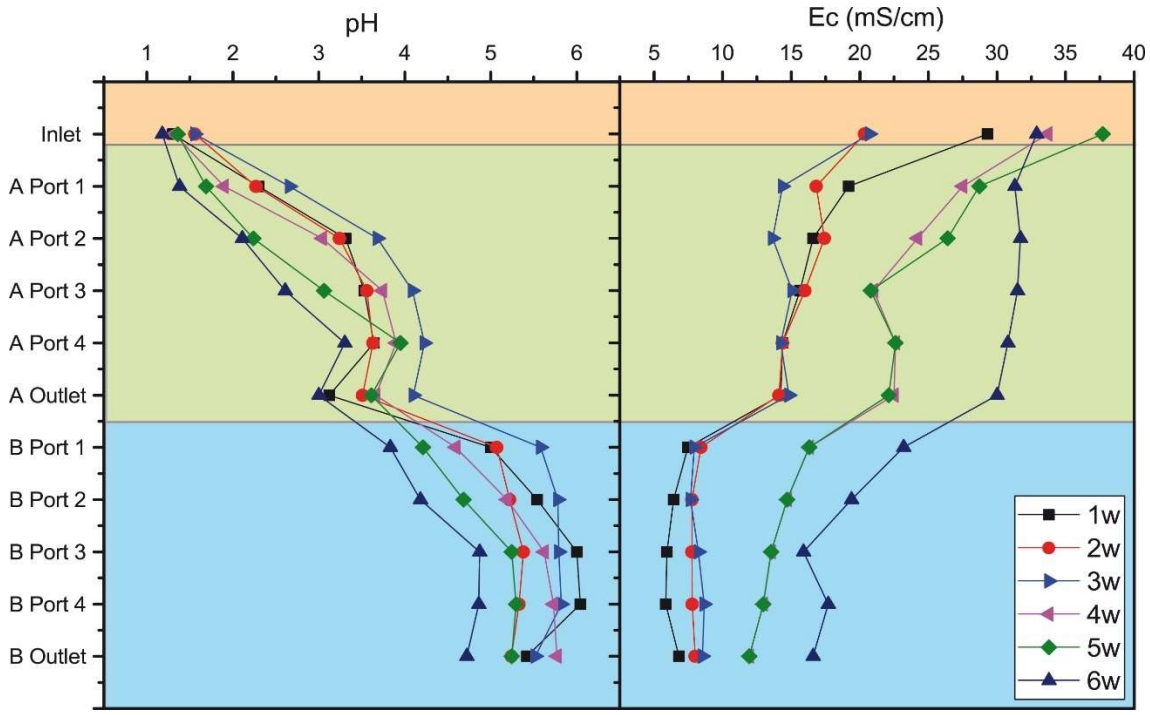

Figure 6.2 Spatial evolution of the physicochemical parameters of the extremely acidic wastewater throughout the system, including the inlet (orange shade), column A (green shade) and column B (blue shade), from week 1 (1w) to week 6 (6w).

The AIW was enriched in Mg and Ca through column A, while column B removed between 70 and 90% of Mg and Ca, respectively, until the fifth week (Figure 6.3). Similar trend was observed for divalent metals such as Ni, Mn and U reaching a removal efficiency between 80 and 100% in column B (Figure 6.4). Column A contributed to a total removal of Fe, Al and Cr between 85 and 100% (Figure 6.3), while the removal efficiency of most divalent metals (i.e. Cu, Cd and Zn) ranged from 25 to 80%, decreasing gradually over time (Figure 6.4). Originally, the more

abundant REE of the AIW were Ce, La and Nd, which accounted for more than 50% of all REE (7.16 mg/L) (Figure 6.4 and table C.1 of supplementary material).

The concentration of dissolved REE in the top of column A oscillated (Figure 6.4 port A1), with a rise in REE concentration in weeks 1, 4 and 6, mostly due to the increment of dissolved Ce, La, Nd, Gd, Pr and Ho. Thereafter, REE concentration decrease drastically from port A2 downwards reaching up to 90% of REE removal, which remained almost constant throughout the system (column A and B) with no significant temporal variations. In particular, about 95% of Ce, La, Nd and Y were removed from solution, as well as 89, 80, 71 and 65% of Gd, Sm, Pr and Eu, respectively. By contrast, the AIW was enriched in As and Ba reaching concentrations of up to 0.78 and 80.3 mg/L, respectively (Figure 6.3 and 6.4).

As expected, the efficiency of the system dropped over time as the reagents were consumed. Over the sixth week of the experiment, pH only increased up to 4 and EC was reduced only 50% (Figure 6.2), while the removal of Ca and Mg also dropped to 36 and 19%, respectively (Figure 6.3). It is worth noting that the removal of di- and trivalent metals such as Al, Fe, Cu, Cr and Mn remained above 98% throughout the experiment (Figure 6.3 and 6.4) despite the reagent consumption.

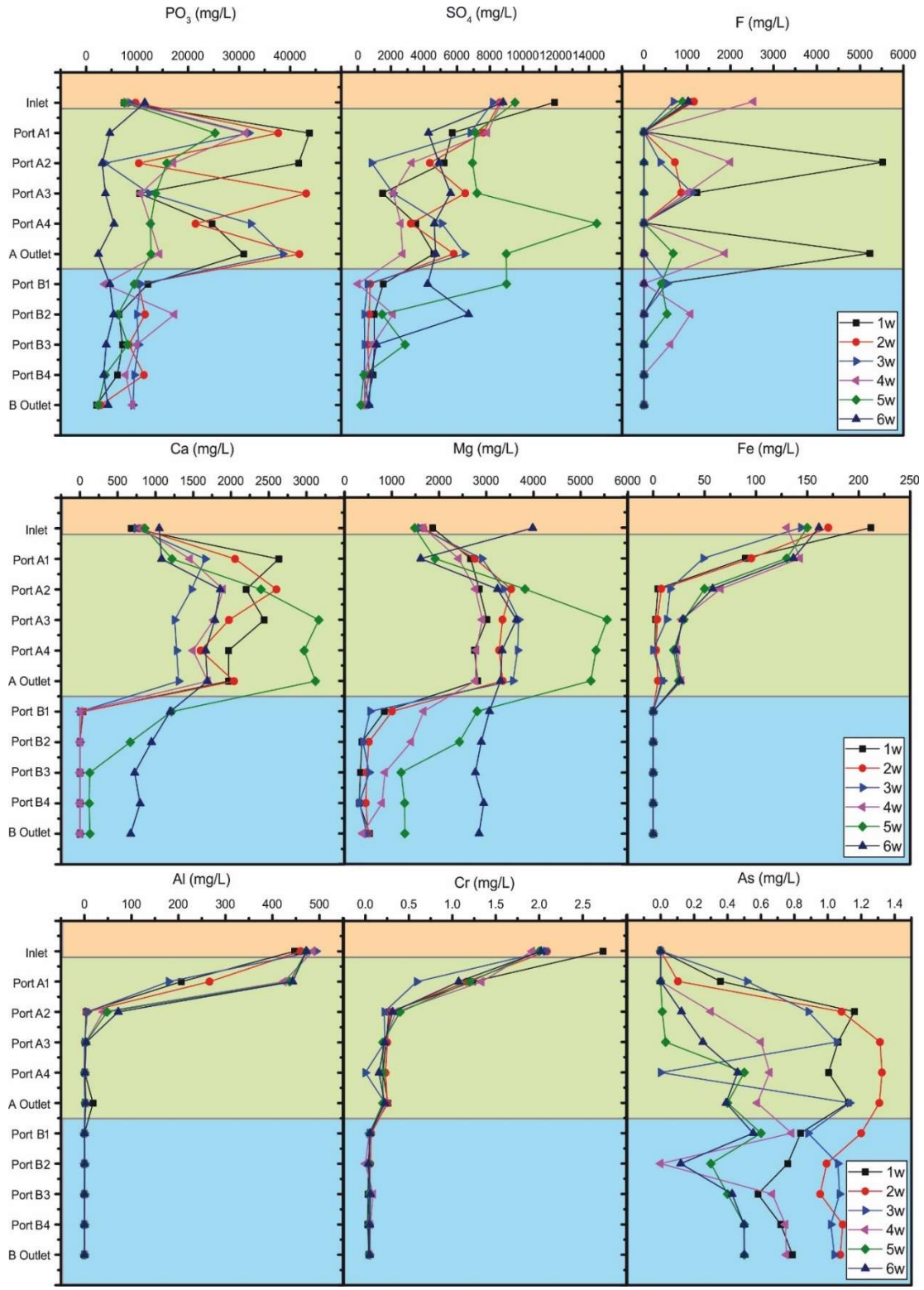

Figure 6.3 Spatial evolution of anions (sulphate, phosphate and fluoride) and cations (Ca, Mg, Fe, Al, Cr and As) throughout the system, including the inlet (orange shade), column A (green shade) and column B (blue shade), from week 1 (1w) to week 6 (6w).

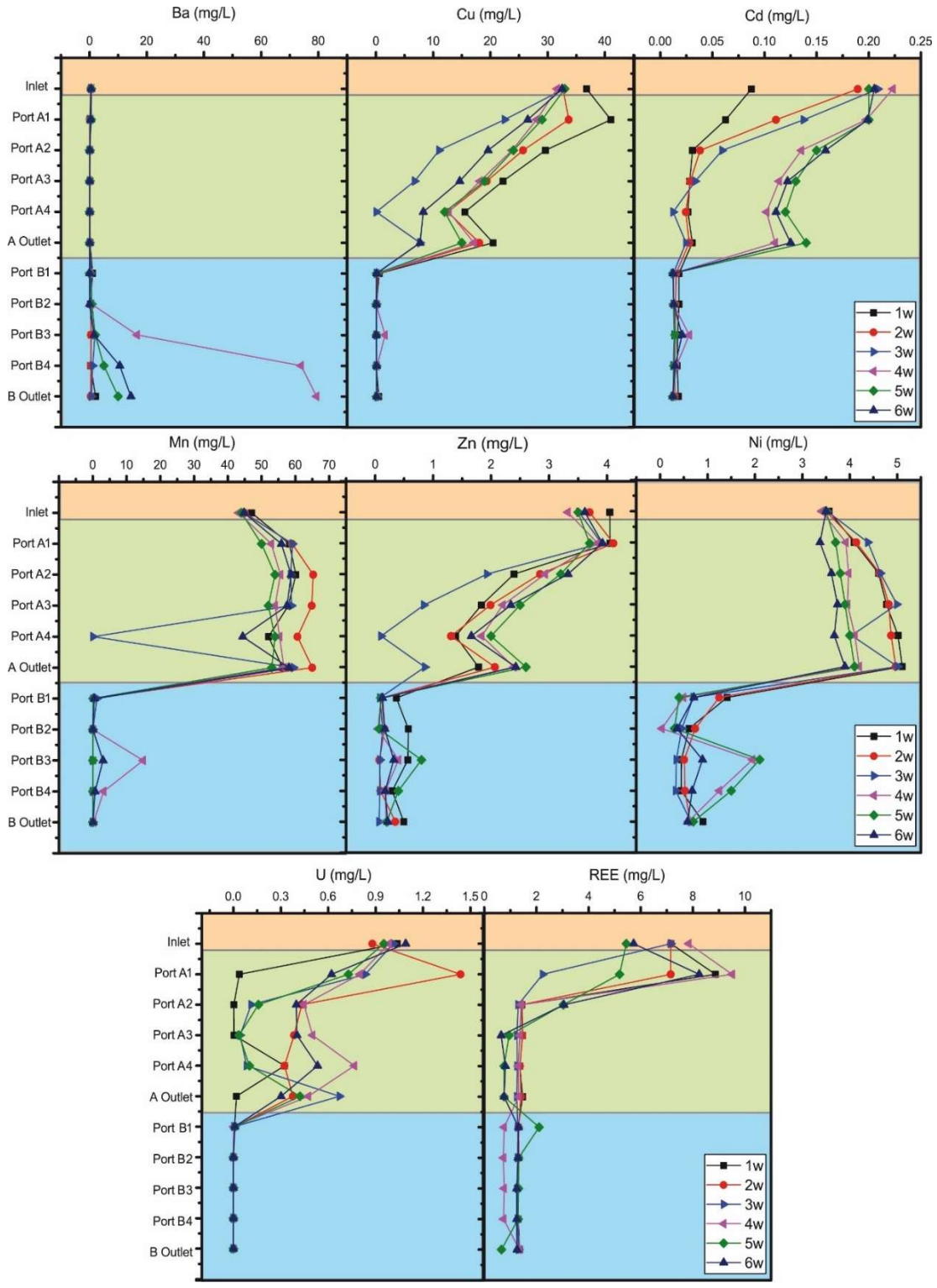

Figure 6.4 Spatial evolution of cations (Ba, Cu, Cd, Mn, Zn, Ni and U) and the summatory of rare earth elements (REE, i.e. lanthanides, Y and Sc) throughout the system, including the inlet (orange shade), column A (green shade) and column B (blue shade), from week 1 (1w) to week 6 (6w).

The results of the Principal Component Analysis (PCA) indicated that the temporal and spatial evolution of pH and chemical composition of the AIW accounts for 71% of all data variations (Figure 6.5). The PCA1 represents 53.4% of the total variance and it is most likely correlated with the quality of the AIW and its spatial evolution within the columns. The pH is the factor with more positive loading in PCA1, while most metals (except Ba and As) have a strong negative loading. The PCA2 explains 17.6% of the total variance and it might be related to the temporal variations of the performance of the water treatment. In fact, REE, Fe, Cr and Al have the highest positive loads for PCA2, which are the elements with lowest temporal variations, while Ca, Mg, and phosphate have higher negative loading for PCA2, which are the compounds with broader temporal variations. It is worth noting that pH, Zn, Cu and sulphate have no significant influence on PCA2.

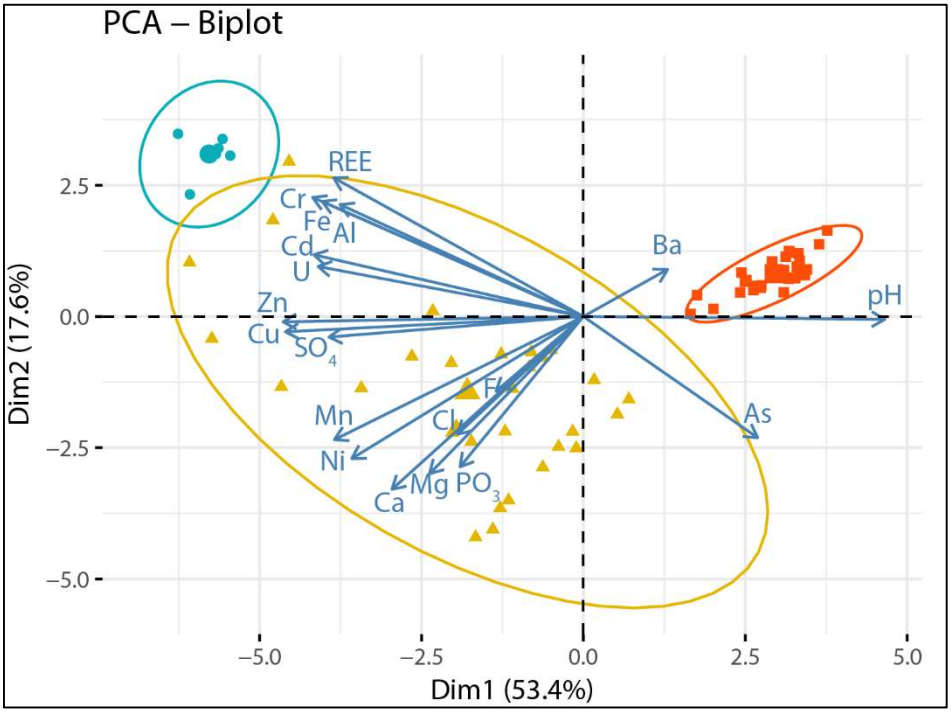

Figure 6.5 Principal component analysis biplot of water analysis from Inlet (blue dots) and from each sampling port of column A (yellow triangles) and column B (red squares).

The analysis of the AIW before treatment (inlet) are closely clustered (Figure 6.5 blue markers). On the other hand, the samples from column A present high dispersion of the data (Figure 6.5 and Figure C.2 of the supplementary material). This showcases the complexity of geochemical processes (precipitation of pollutants, dissolution of tailing minerals and reprecipitation of secondary minerals) involved in column A (Figure 6.5, yellow markers). The opposite trend is observed in column B, where all the data is closely clustered and highly correlated with Ba and pH (Figure 6.5, red markers).

In column A, REE are correlated with Cu, Cr, Al, Fe and, to a lesser extent, with Ba, U, Cd, Zn and sulphate. However, they appear to be inversely correlated to pH, Ca, Mg, Ni and As (Figure 6.5). In column B, pH is inversely proportional to the concentration of all the elements analysed, except for As and REE (Figure 6.2 and 6.5).

GEOCHEMICAL MODEL:

The geochemical model (Figure 6.6) predicted that phosphate minerals such as fluorapatite ($Ca_5(PO_4)_3F$) would be oversaturated throughout the system, but they would precipitate mostly in column A. Also, it can be seen the oversaturation of Mn phosphate and REE-phosphate minerals throughout the system (from port A2 downwards). In addition, the removal of Al from IAW at pH below 3 suggests that it could have coprecipitated with phosphate minerals and rules out its precipitation as both hydroxide and oxyhydroxide minerals. On the other hand, the model suggested the precipitation of fluorite and LaF_3 as alternative mechanisms to remove F and REE from solution (Figure 6.6).

Regarding oxy-hydroxide minerals, column B was oversaturated in Zn-ferrite ($ZnFe_2O_4$) and Cu-ferrite ($CuZnFe_2O_4$) only during the first week of the experiment. Column B was also oversaturated in goethite and chromite at the beginning of the experiment, but the saturation index decreased over time, reaching undersaturation conditions in weeks 3 and 5, respectively. The AIW was oversaturated in eskolaite (Cr_2O_3) and delafossite ($CuFeO_2$), which could start precipitating at the bottom of column A at the beginning of the experiment, but mostly in column B throughout the experiment (Figure 6.6).

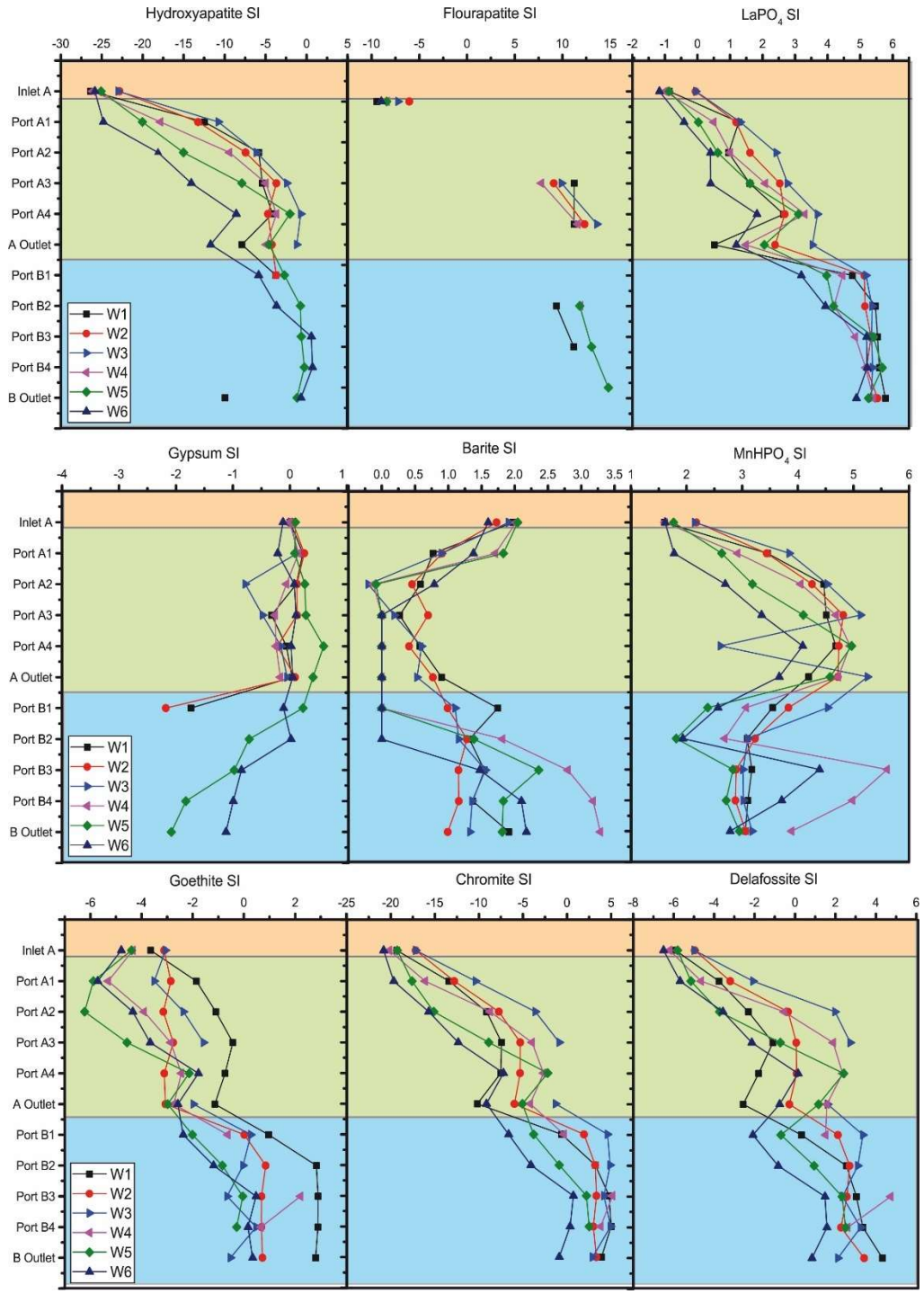

Figure 6.6 Evolution of the saturation index (SI) for phosphate, sulphate and oxyhydroxide minerals calculated with PHREEQC using the physicochemical parameters and chemical composition of the water throughout the system.

MATRIX ANALYSES

Sequential extraction:

The sequential extraction shows that the original tailing had above 20000 mg/kg of P (Figure 6.7), mostly in the residual fraction (F4). The precipitation of phosphate minerals increased the concentration of P in column A, particularly in middle and mainly in the residual fraction, although the proportion of the mobile fractions (F2 > F1> F3) also increased. However, the highest P concentrations were found in column B, where the enhanced dissolved levels of P from column A may be massively precipitated, and are mainly concentrated in the reducible fraction. Like P, F was also concentrated in the middle of column A, however, this compound was immobilized mostly in column A and accumulated mainly in the residual (F4) and reducible (F2) fractions (Figure 6.7). The low concentration of F and S in the tailing suggests that their presence in the substrate was mainly associated to their removal from the AIW. S was drastically accumulated in the top of column A and its concentration decreases gradually downwards. Thereafter, the remaining S was mostly immobilized in the top of column B decreasing downward the column. Interestingly, sulphate was mostly accumulated in the soluble (F1) and reducible (F2) fractions (Figure 6.7).

The original tailing had a homogeneous distribution of Ca between F1, F2 and F4 (Figure 6.7). Once the substrate interacted with the AIW, the concentration of Ca increased gradually from top to bottom of column A, particularly in the residual fraction (F4). The calcium remaining in solution was retained in column B. The concentration of Ca decreased from top to bottom of column B and their distribution among fractions varied; at the top of the column, Ca was found mostly in F1, while in the middle Ca was distributed between F2 and F4, and at the bottom Ca was present mostly in F2. Unlike Ca, the high concentration of Mg of the original tailing (Figure 6.7) was mostly in F4 and after the interaction with the AIW, such concentration was drastically depleted in the top of column A and, to a lesser extent, in the middle and bottom. This correlates with the increasing of dissolved Mg in de water (Figure 6.3). The Mg dissolved seems to have re-precipitated in column B, as the sequential extraction shows a gradual increment of Mg from top to bottom of column B, mostly in F1 and 2.

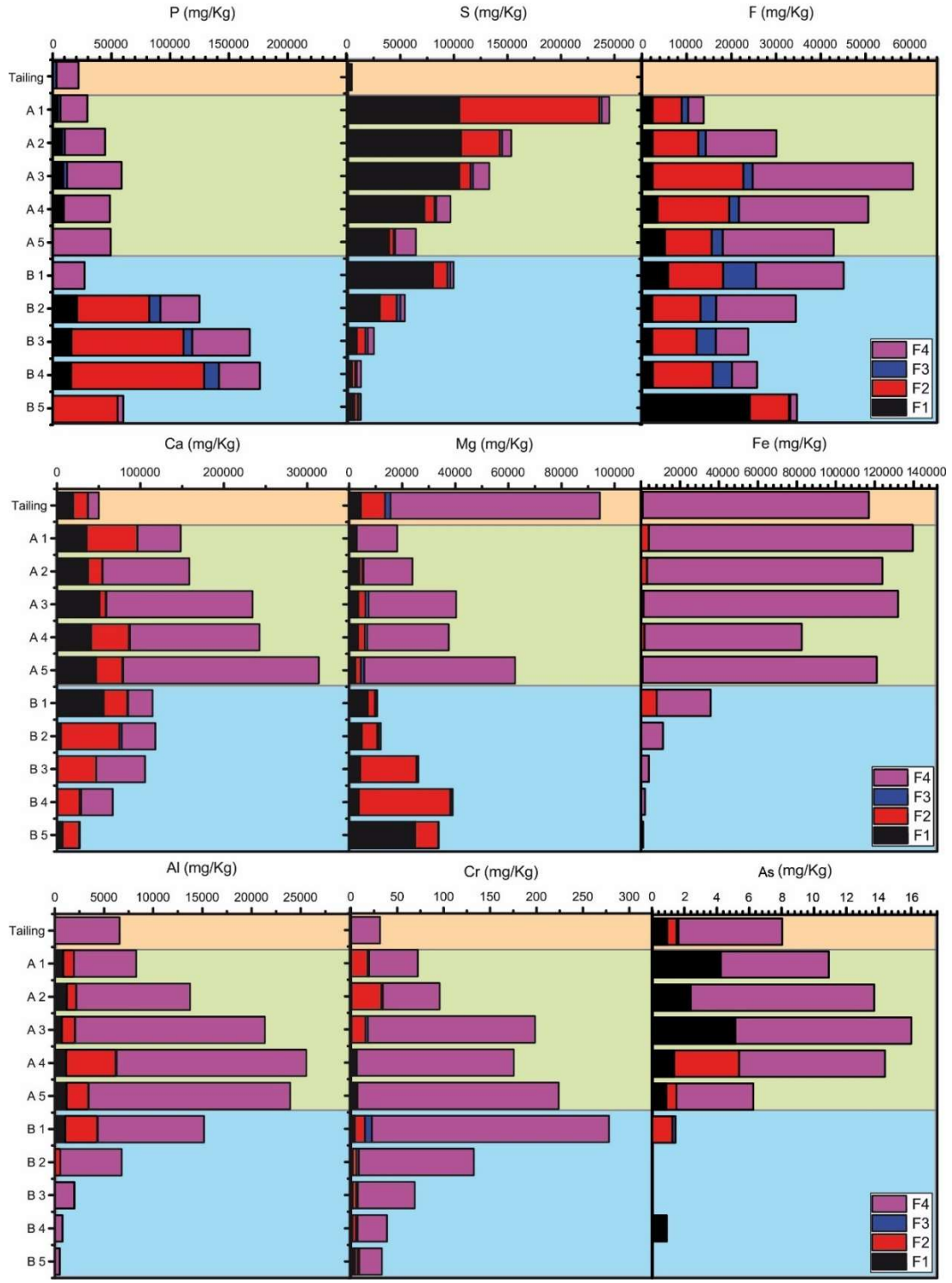

Figure 6.7 Average of the anions (S, P and F) and cations (Ca, Mg, Fe, Al, Cr and As) in fraction 1 (F1), fraction 2 (F2), fraction 3 (F3) and fraction 4 (F4) of the sequential extraction performed to the tailing (orange shade), column A from top to bottom (A1 to A5, green shade) and column B (from B1 to B5, blue shade).

Overall, it can be inferred that the matrix of column A and B is enriched by heavy metals load from the AIW, except in the case of Ni (Figure 6.8). Most Al has been extracted in F4 from the tailing, as well as from both columns (Figure 6.7). The rise of Al in column A after the interaction with the AIW corresponds with their removal from solution (Figure 6.3). Also, the low concentration of Al in the substrate of column B correlates with the low concentration of dissolved Al in the AIW that was reaching column B.

The accumulation of Cr and Cd in the profile of the columns correlates positively with the distribution of Al (Figure 6.5, 6.7 and 6.8). Furthermore, all these metals were present mostly in the residual fraction (F4). Opposite to As, which does not correlate with any of the elements analysed (Figure 6.5) in the water nor in the matrix. The concentration of As increased from top to bottom of column and it was present mostly in F4 and F1, although the sample A5 has more As in F2 than F1. The content of As in column B was very low and it was limited to the top, mostly in F2, and to the bottom, mostly in F1 (Figure 6.7).

The precipitation of Fe in the substrate is clearly observed in F1 and F2 of column A (Figure 6.7 and Figure C.2 of the supplementary material), where the concentration of Fe increased from 0 to 136 mg/kg in F1 and from 784 to 10835 mg/kg in F2 (average of column A substrate before and after the interaction). However, the concentration of Fe in the AIW is too low, compared with original concentration of Fe in the tailing, to produce a significant difference in the pseudo-total concentration of Fe. Opposite to column B, where the precipitation of Fe is clearly observed, particularly at the top of the column. The concentration of Fe reached up to 35716 mg/kg of which 78% was detected in F4 and 22% in F2 (Figure 6.7).

Similar to Fe, divalent metals such as Cu, Mn, Ni and Zn were clearly immobilized in column B (Figure 6.8). The concentration of Cu was unevenly distributed between the residual (F4) and the mobile (F1, F2 and F3) fractions, particularly high in the oxydizable fraction (F3) in column A and in the reducible fraction (F2) in column B. However, Mn and Ni were concentrated mainly in the mobile fraction of column B, while, Zn was mainly extracted from the residual fraction (F4).

In addition to the inherent concentration of Ba in column B, the matrix of column A as well as the AIW also contributed to the concentrations of Ba (472.96 mg/Kg and 0.5 mg/L, respectively) in the system (Figure 6.8 and 6.4). This explains the slow rise of Ba throughout column A, while the concentration of Ba in column B, originally comprised of witherite ($BaCO_3$), was higher at the bottom than the top, suggesting that the interaction with the AIW dissolved the $BaCO_3$ in the top of the column. In general, Ba was extracted in F4 throughout the system. However, significant concentration of Ba was found in F2 and, to a lesser extent, in F3 at the bottom of column B (ports B4 and B5 in Figure 6.8).

Most of the U dissolved in the AIW precipitated in column B, following a similar pattern to the Ba (Figure 6.8); both U and Ba were found mostly in the residual fraction (F4) throughout the system. However, at the bottom of column B (ports B4 and B5 in Figure 6.8) they were found also in the reducible (F2) and, to a lesser extent, in the oxidizable (F3) fractions.

Finally, the concentration of REE decreased in the top of column A after the interaction with the AIW (Figure 6.8), particularly in the soluble (F1) and residual (F4) fractions. The concentration REE increased thereafter reaching the highest concentration in the middle of column A. Most REE remained in column A in the residual fraction (F4), followed by the reducible fraction (F2). In detail, the more abundant REE were Nd, Ce, La, Sm, Y, Sc, Pr, Gd and Dy (655.7, 434.5, 432.1, 175.1, 119.0, 73.1, 51.6, 36.5 and 25.8 mg/Kg in the middle of column A). It is worth noting that Sc was the most abundant REE in F3 and F2 and the second most abundant in F1 after Nd.

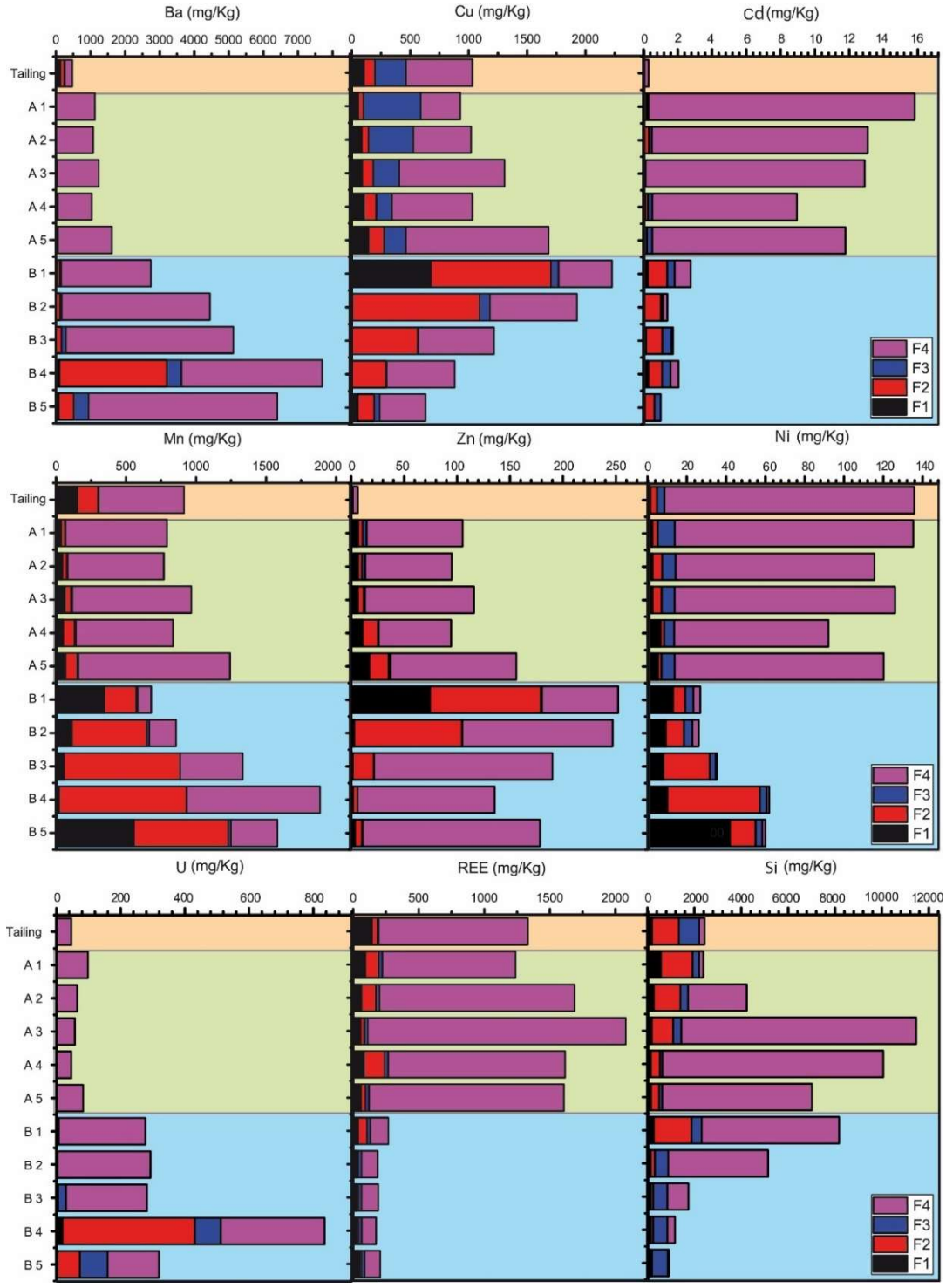

Figure 6.8 Average of the cations (Ba, Cu, Cd, Mn, Zn, Ni, U and Si) and the summatory of rare earth elements (REE, including lanthanides, Y and Sc) in fraction 1 (F1), fraction 2 (F2), fraction 3 (F3) and fraction 4 (F4) of the sequential extraction performed to the tailing (orange shade), column A from top to bottom (A1 to A5, green shade) and column B from top to bottom (B1 to B5, blue shade).

MINERALOGICAL CHARACTERIZATION:

According to XRD and SEM results, the main mineralogical composition of the substrate of column A is phlogopite ($KMg_3AlSi_3O_{10}(F,OH)_2$), calcite ($CaCO_3$) , dolomite ($CaMg(CO_3)_2$, magnetite ($Fe_3O_4$), fluorapatite ($Ca_5(PO_4)_3F$), and enstatite ($MgSiO_3$) (Figure 6.9 and 6.10). Minor mineralogy includes chalcopyrite ($CuFeS_2$), zircons ($ZrSiO_4$), barite ($BaSO_4$), quartz (SiO_4), ilmenite ($FeTiO_3$), thorianite (ThO_2) and a variety of oxyhydroxides of Fe, Cr, Ni and Ti (Figure 6.10). These minerals show a complex textural relationship, being the general pattern partial dissolution of tailing-forming phases, which in some cases, are replaced by newly-formed minerals (Figure 6.10d, e and f). Newly-formed phases have been also identified as common components, such as gypsum, brushite and unidentified Ca-Al-F-phosphate and Fe-Cr-Ni-oxyhydroxides, (Figure 6.9 and 6.10d, e, f, g and h).

Calcite and dolomite show a high degree of dissolution including corroded edges and replacement along with cleavage (Figure 6.10d, e and f). Dissolution of more resistant minerals such as magnetite, fluorapatite, enstatite and phlogopite exhibit low to none degree of dissolution, showing in some cases partially corroded grain boundaries (Figure 6.10d, e, f; and Figures C.3a, C.4a, b and C.5b of supplementary material).

Main newly-formed phases include porous groundmasses of Ca-Al-F phosphate, with up to 0.5% of REE (Figure 6.10d, e, f and i). This phase appears as botryoids, from 100 to 400 μm in diameter, which systematically are cementing multiple fragments of common tailing forming minerals (Figure 6.10a to f). Main micro-textural relationships with former mineralogy include dissolution-replacement of calcite and dolomite (Figure 6.10d and f), and nucleation around magnetite, fluorapatite, silicate grain boundaries (Figure 6.10a to f) and wood fragments (Figure 6.10h and g). It is noteworthy that a mixture of very fine grains (minor than 1 μm in diameter) was often observed within the Ca-Al-F phosphate botryoids. Therefore, cannot be ruled out that an aggregation of nano-minerals forms these groundmasses. Another common newly-formed mineral is the Fe-Cr-Ni oxyhydroxide that has been found often between the exfoliation of phlogopite minerals and in wood fragments as aggregates of 1 to 20 μm (Figure 6.10a, g and h). This mineral often contains traces of Ca, Cl, Cu, S, Si and Zn.

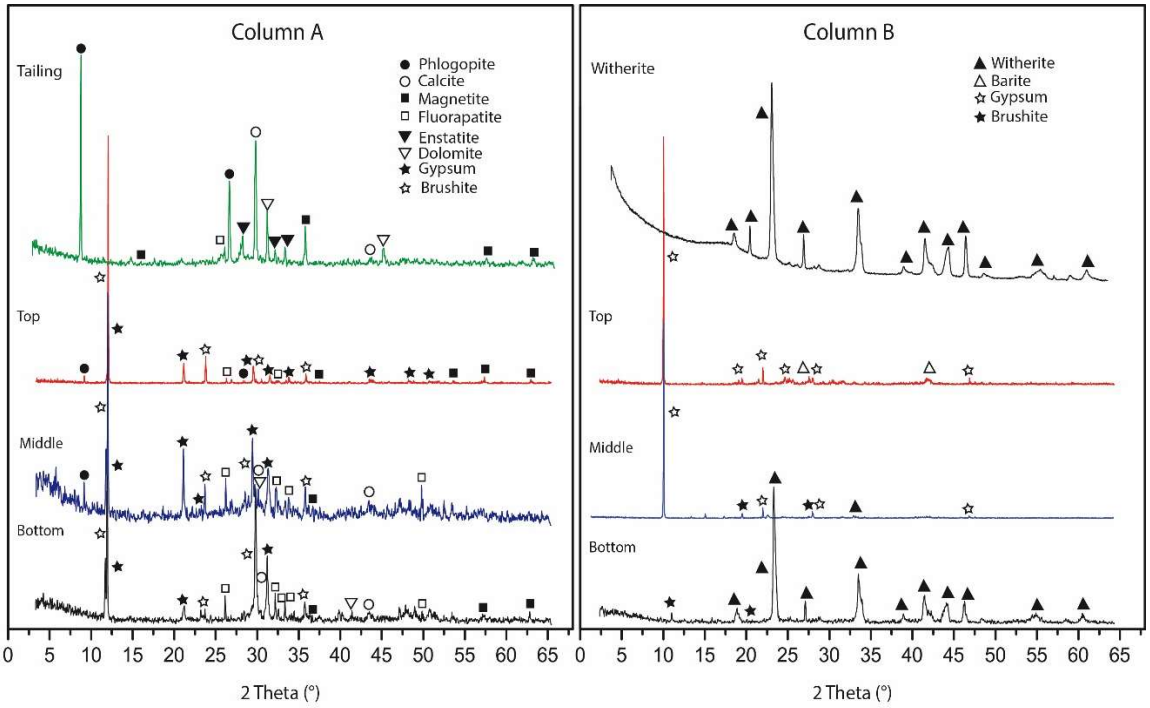

Figure 6.9 XRD analysis of the tailing and the witherite ($BaCO_3$) before the interaction with AIW (green), and the substrates after the interaction with AIW from the top (red), middle (blue) and bottom (black) of column A (left) and column B (right). Phlogopite (Ph), magnetite (Mt), Fluorapatite (F), enstatite (E), calcite (C), dolomite (D), britholite (Br), gypsum (G), witherite (W) and barite (B).

Column a

Mineralogy in column A is heterogeneous. In that sense, calcite and dolomite were about 95 and 90% consumed at the top of column A (according to XRD semi-quantification, Figure 6.9, 6.10a and d), remaining some relicts (22 and 77% of calcite and dolomite, respectively) in the middle section (Figure 6.9, 6.10b and e) and barely consumed towards the bottom (Figure 6.9, 6.10c and f).

Newly-formed Ca-Al-F phosphate (Figure 6.10a to f) was similarly distributed and abundant throughout the column, although showing variable chemical composition. In that sense, Ca-Al-F phosphate increase its Mg content towards the bottom of the column, while it shows the highest REE concentrations towards the top of the column, reaching up 0.5% wt (Figure 6.10i). However newly-formed Fe-Cr-Ni oxyhydroxide minerals were only found in the top section of the column,

while newly-formed brushite and gypsum were found throughout the column, but more abundant in the top of column A (Figure 6.9).

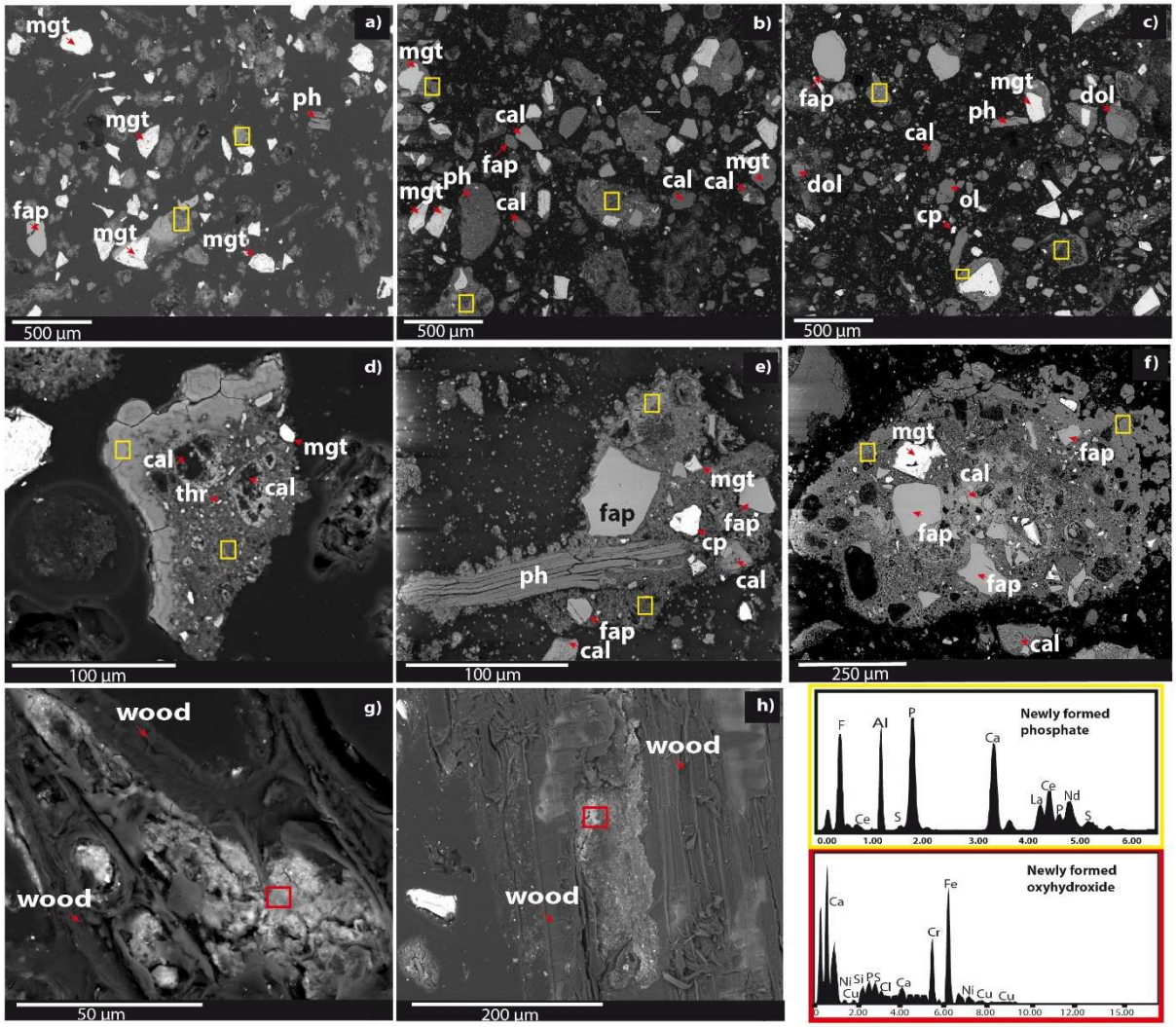

Figure 6.10 Scanning electron microscope (SEM) images and energy dispersive spectroscopy (EDS) spectrums of the column A substrate; a), b) and c) general view of the column A top, middle and bottom, respectively. These are mainly formed by magnetite (mgt), fluorapatite (fap), phlogopite (ph) calcite (cal), dolomite (dol), chalcopyrite (cp) and olivine (ol); d), e) and f) Newly-formed Ca-Al-F phosphate from the column A top, middle and bottom, respectively, embedding fragments of calcite, fluorapatite, phlogopite, magnetite, chalcopyrite, thorianite (thr) and calcite; (g) and (h) Fe-Cr-Ni oxyhydroxide filling open spaces in wood fragments; and (i) representative EDS spectrums of newly-formed REE-rich Ca-Al-F phosphate (in yellow) identified in images d, e and f; and newly-formed Fe-Cr-Ni oxyhydroxides (in red) identified in images g and h.

Column B

According to XRD and SEM results, the original witherite ($BaCO_3$) of column B was partially consumed during the interaction with the AIW (Figure 6.9). The main mineralogical composition of column B is formed by witherite and newly-formed gypsum, brushite and barite (Figure 6.9, 6.11a, b and c). Minor mineralogy includes newly-formed minerals such as aragonite, apatite, kaolinite and non-identified oxides, oxyhydroxides and sulphates of Cu, Fe, Al, As and U, (Figure 6.11c, e, f).

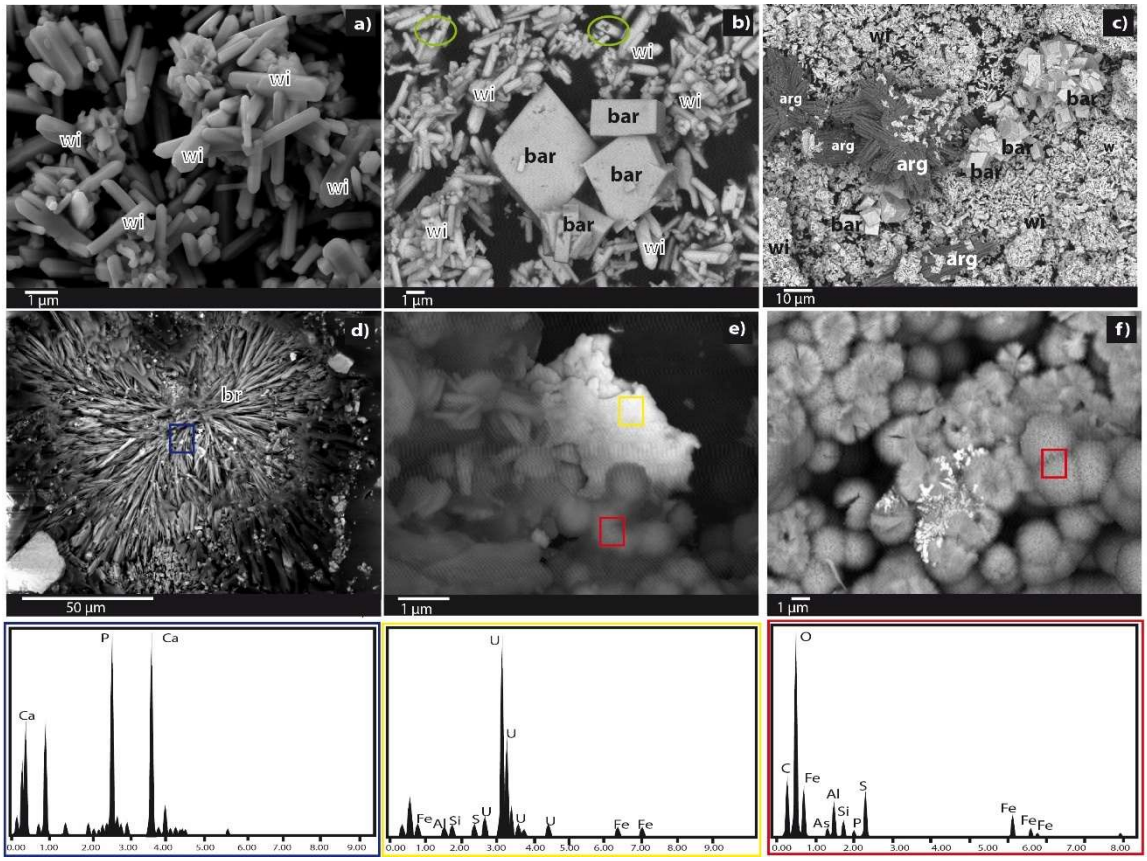

Figure 6.11 Scanning electron microscope (SEM) images and representative energy dispersive spectroscopy (EDS) spectrums of the column B substrate; a) prismatic witherite (w) aggregates from the bottom of column B; b) Euhedral barite (b) crystals associate with witherites from the top of the column; c) radial aragonite (a) aggregates included in a matrix formed by barite and witherite; d) radial brushite (br) aggregates from the middle section of column B; e) Fe-sulphate aggregates including a U-oxyhydroxide; f) fine-grained skeletal Cu-sulphates growing on radial aggregates of Fe- oxyhydroxysulphate.

Euhedral crystals of witherite (Figure 6.11a, b and c, and Figure C.7b of supplementary material), mostly 1 to 3 μm, show several degrees of dissolution including partially corroded grain boundaries, holes and dissolution along C axis. The degree of dissolution is inversely proportional to the size of the crystals, crystals above 10 μm only developed superficial corrosion textures.

Euhedral and subhedral barite crystals range between 1 and 10 μm. They often present twins and traces Al, Fe, Si, Ca and/or Ni, identified by SEM-EDS (Figure 6.11b and c). Aragonite crystals of up to 60 μm have developed acicular structure in bunch or radial distribution and often show traces of S (Figure 6.11c). Sulphates and oxyhydroxysulphates of Fe, Al, Cu and As are found as radial aggregates with a diameter range between 0.5 and 3 μm (Figure 6.11e and f). Fine-grained of Cu sulphates (<1 μm) were observed in the surface of those aggregates (Figure 6.11f), as well as on wood (Figure C.6a of supplementary material).

The heterogenous mineralogical distribution throughout column B is marked by the dissolution of the witherite crystals (Figure 6.9 and 6.11b) and the precipitation of newly-formed minerals (Figure 6.9 and 6.11b to f). Dissolution marks are present in most witherite crystals from the top, but their alteration decreases downwards (Figure 6.11a and b). Newly-formed barite and aragonite crystals were mostly found in the top of the column (Figure 6.9 and 6.11b and c). Newly-formed brushite crystals are the most abundant minerals found in the top, as well as in the middle of column B (Figure 6.9 and 6.11d), meanwhile aggregates of radial Fe-oxyhydroxysulphate were also found evenly distributed throughout the column and associated occasionally with skeletal Cu-sulphate and amorphous U-oxyhydroxide (Figure 6.11e, f and Figure C.6a of supplementary material).

6.4. DISCUSSION:

The results from the preliminary batch experiments were used to design the bench scale prototype. In the first reactor (column A), 2 kg of carbonatite-rich tailing from Phalaborwa Industrial Complex (PIC) was used as an alkaline reagent. According to the model that reactor could increase the pH from 1.3 up to 4 for 15L of IAW. Since the column works in continuo, the capacity of this reactor to neutralize would progressively decrease overtime as the carbonates are consumed. The second

reactor (column B) was filled with 700 g of witherite, based on the Barium carbonate Dispersed Alkaline Substrate (BDAS) System (van Heerden et al., 2015). The water treatment was kept running until the final treated water dropped below pH 5, which occurred after week 6 and 100 L of IAW was treated.

6.4.1. COLUMN A (TAILING REACTOR)

The interaction between the tailing and the AIW increased the quality of the AIW by increasing its alkalinity and reducing the concentration of Al, Fe, Cr, Cu, U and sulphate by 100, 88 87, 38, 40 and 43%, respectively (Figure 6.2, 6.3 and 6.4). However, As concentration increased and no significant removal of Ni was observed (Figure 6.3 and 6.4). In addition, the concentration of Ca, Mg, Mn and phosphate increased, particularly at the beginning of the experiment (Figure 6.3). Similar results were reported by (Millán-Becerro et al., 2020) by using limestone, fly and biomass ash-DAS to remediate the drainage from a phosphogypsum pile (solid residue from phosphoric acid plants).

The alkalinity of the tailing (420 kg $CaCO_3$ eq/t, refer to chapter 5) is mostly due to the high content in calcite and dolomite. Dissolution textures were observed by SEM in column A in calcite and dolomite crystals, (Figure 6.10d, e and f) which are indicative of advance corrosion (Andò et al., 2012) as result of the interaction with the AIW. This textural pattern matches with the XRD analyses, which detect only 3% of carbonates (calcite and dolomite) at the top of column A, 26% in the middle and 36% at the bottom (Figure 6.9). These results clearly mark the high consumption of carbonate minerals in column A, which decreases gradually downwards the column.

Both calcite and dolomite from PIC have been described as REE-bearing minerals (Dawson & Hinton, 2003; Giebel, 2019; refer to chapter 4). Thus, their released REE and divalent metals (M^{2+}, reaction 6.2) to the AIW. The interaction increased the concentration of Ca, Mg, Mn and REE in solution (Figure 6.3 and 6.4), as well as phosphate, Ni and As from the incipient dissolution of other minerals present in the tailing, such as fluorapatite. On the other hand, the AIW was the main source of sulphate, fluoride, Al, Cu, Cr and Zn.

$$MCO_3 + H^+ \rightarrow M^{2+} + HCO_3^- \quad 6.2$$

The dissolution of the apatite group minerals (Figure 6.6) was predicted by the geochemical model and it was also observed throughout the column during the early stage of the experiment, as indicated by the increment of phosphate concentrations in the treated water on that period (Figure 6.3). In fact, at the end of the experiment most of the fluorapatite was dissolved at the top of column A (Figure 6.9). The apatite group minerals from PIC tailings have been described as REE-bearing minerals (refer to chapter 4). Therefore, the dissolution of the apatite group minerals contributed with the rise of REE in solution, particularly at the top of column A (Figure 6.4, sampling port 1). However, according to the geochemical model, saturation index (SI) of REE-phosphate minerals increases from port A2 downwards (Figure 6.6), which match with the identification by SEM-EDS of newly-formed REE-rich phosphate homogeneously distributed throughout the column (Figure 6.10a to f), but mostly concentrated in the middle section (Figure 6.7 and 6.8). Indeed, in this section of the column an enrichment of REE, Al, Ca, F and P can be observed in the substrate, particularly in the residual fraction (F4) (Figure 6.7 and 6.8). To the best of our knowledge, this is the first study that describes the formation of this phosphate compound and its activity as a sink of REE in ambient conditions. Significantly, REE were removed up to 83% in column A, which corresponds with the high concentration of REE extracted from the residual fraction (F4) of the column, mostly in the middle section. In addition, the model suggests precipitation of fluor as fluorapatite and fluorite, but it seems that F was mainly incorporated to the Ca-Al-F-phosphate. Once again, the highest concentration of F was extracted mostly from the residual fraction (F4) of middle section of the column. In addition, F shows an opposite behaviour to U, which precipitated mostly in the middle-bottom of column B (Figure 6.8). As a result, the newly-formed phosphate was enriched in REE and depleted in U.

The dissolution of both carbonates (equation 6.2) increased the pH of the water from 1.2 up to a range of 3.2 to 4.2, depending on the week of operation (Figure 6.2). The raising of pH induced the precipitation of oxide and sulphate minerals, which likely contribute to the co-precipitation of Cu, Zn, Cd, Cr, As and REE (Figure 6.10g and h). The precipitation of Fe-Al-oxy-hydroxy-sulphates such as

basaluminite has been previously associated with the immobilization of REE (Ayora et al., 2016). However, in this experiment most REE were detected in the newly-formed phosphate (Figure 6.10d, e, f and i), which is supported by the sequential extractions data that extracted only 10% of the REE in the mobile fraction, (F1, F2 and F3) (Figure 6.8) commonly associated to soluble, oxy-hydroxy-sulphate and sulphide minerals (Macías et al., 2017), while the remaining 90% were extracted in F4, together with 83% of P (Figure 6.7). On the other hand, schwertmannite has been correlated with the uptake of Cu, Zn, As, Cr and Cd (Ayora et al., 2016) and, even though the model indicated that the system was undersaturated in schwertmannite, Fe-oxyhydroxysulphate minerals have been identified in column B (Figure 6.1). In addition, the results of the sequential extraction showed enrichment of Cu, Zn, As, Cr, Cd, Fe and Al in the middle-bottom of column A in the F4 (Figure 6.7 and 6.8), likely associated to phosphate minerals. Indeed, Millan-Becerro *et al.* (2020) stated that phosphate minerals precipitation could act as a sink for As, Fe, U, Zn, Cr, and Cu, although, the excess of phosphate in solution could inhibit the adsorption of As, since As-oxyanions compete with phosphate for sorption sites on phosphate minerals such as hydroxylapatite (Bibi et al., 2017; Huang et al., 2020).

The solution was predicted to be oversaturated in sulphate minerals such as gypsum in the middle-bottom of column A, which corresponded with partial removal of sulphate (approx. 40%) in this column and its accumulation mainly in the F1 and F2 associated to the sulphate and oxide minerals, respectively. This is also consistent with the high concentration of gypsum detected by XRD in the middle and bottom samples and the presence of oxy-hydroxy-sulphate minerals observed by SEM (Figure 6.10g, h and i).

6.4.2. COLUMN B (BDAS REACTOR)

The interaction between witherite ($BaCO_3$) and the water outflowing from column A resulted in an increase of pH values up to around 6 at the beginning of the experiment (Figure 6.2), Although, as the witherite was being consumed, the performance of the reactor decreased and the pH at the outlet of column B was 4.7 (Figure 6.2). At the end of the experiment, no witherite was detected by XRD

analyses at the top of the column, while 0.5% remained in the middle and 40% at the bottom.

Under this range of pH, the precipitation of oxy/hydroxide minerals control the complete immobilization of the remaining Fe, Al, Cu, Cd, Cr and As in the system (Figure 6.11e, f and Figure C.6a of supplementary material). In addition to oxy/hydroxides minerals, abundant phosphate, carbonate and sulfate minerals precipitated in column B as it was observed by SEM and detected by XRD (Figure 6.9, 6.11b, c, d, and Figures C6b, C7a and C7b of supplementary material). In detail, brushite ($CaHPO_4{\cdot}2H_2O$) was detected abundantly in the top and middle of column B (Figure 6.9 and 6.11d), minor aragonite crystals ($CaCO_3$) were also observed at the bottom of column B, associated with barite ($BaSO_4$) (Figure 6.9 and 6.11c). The precipitation of those minerals corresponds with the removal of sulphate, phosphate, Ca and Mg from the water (Figure 6.3).

The capacity of the BDAS reactor to remove Al, Cr, Cu, Fe, Mn and U was maintained during the entire experimental period above 98% (Figure 6.3 and 6.4), While the removal of Ni, Zn and Cd oscillated between 80-90%, 88-100% and 87-93%, respectively. However, the precipitation of Ca and Mg decreased over time. Previous studies showcased that the solubility of $BaCO_3$ decreases substantially with the presence of Ba^{2+} ions in solution (Hlabela *et al.*, 2007) and the molar ratio between Ca^{2+} and SO_4^{2-} (Torres *et al.*, 2018). Therefore, the imbalance of those ions in the inflowing wastewater could be detrimental for the optimal functioning of the BDAS reactor (column B). Those ions are removed from solution during the precipitation of $BaSO_4$ and $CaCO_3$ (reaction 6.3). This reaction is limited by the concentration of Ca and/or sulphate dissolved in the wastewater (reactions 6.4 and 6.5, Torres *et al.*, 2018). Therefore, the reactor will achieve a better performance if the molar ratio between Ca^{2+} and SO_4^{2-} is closer to 1 and vice versa. The inflowing wastewater in column B has an average molar ratio Ca^{2+}/SO_4^{2-} of 0.92. The highest ratio (1.50) was achieved during the fourth week, coincidently with the peak of Ba^{2+} detected at the outlet of column B in the same period (Figure 6.4). Unlike Millan-Becerro et al. (2020), the removal efficiency of sulphate was maintained at 95% throughout the experiment. However, the concentration of dissolved Ba increased in this column. The Sequential extraction shows a decrease in the concentration of

Ba, particularly high at the top-middle of the column, which might by indicative of the dissolution of the $BaCO_3$ in that section. This reaction promoted an increment of dissolved Ba from port B3 downwards (Figure 6.4), which might inhibit the dissolution of the $BaCO_3$ in the middle-bottom section of the BDAS reactor (Figure 6.7 and 6.8). This would explain the remaining 40% of witherite at the bottom of the column, despite the low pH achieved at the end of the experiment.

$$BaCO_{3(s)} + Ca^{2+} + SO_4^{2-} \rightarrow CaCO_{3(s)} + BaSO_{4(s)} \quad 6.3$$

$$\frac{x}{y} > 1: x\,Ca2^{+} + y\,SO_4^{2-} + x\,BaCO_{3(s)} \rightarrow x\,CaCO_{3(s)} + y\,BaSO_{4(s)} + (x-y)\,Ba^{2+} \quad 6.4$$

$$\frac{x}{y} < 1: x\,Ca2^{+} + y\,SO_4^{2-} + y\,BaCO_{3(s)} \rightarrow x\,CaCO_{3(s)} + y\,BaSO_{4(s)} + (x-y)\,CO_3^{2-} \quad 6.5$$

In addition, As was scarcely removed. The increase of HCO_3^- (bicarbonate) and carbonate (CO_3^{2-}) produced by the dissolution of carbonate minerals ($CaCO_3$ and $CaMg(CO_3)_2$ in reactor A and $BaCO_3$ in reactor B), together with the remaining phosphate in dissolution, might be an inhibitor factor during the arsenic adsorption. (Maiti *et al.*, 2012; Millán-Becerro *et al.*, 2020)

Finally, the treated water complies with WHO guideline for drinking water (WHO, 2011) for all the parameters except As, Ni, Cd and occasionally Ba. In addition to the WHO parameters, South African guideline SANS:241 (SABS, 2015) introduces thresholds for pH, TDS, EC, sulphate, Na, Al, Fe, Mn and Zn. The treated water complies also with SANS:241 for all the above-mentioned parameters expect for those related with salinity, such as Na, TDS and EC.

6.4.3. SUBSTRATE VALORISATION

Approx. 100 L of AIW containing 7.2 mg of REE/L (Table 6.2 and Figure 6.4) was treated at 1.8 ml/min for 6 weeks. Hence, the amount of REE introduced by the drainage was about 720 mg. The removal efficiency of REE reach up to 83% in column A, while column B contribute only with the 7%, hence the column A was enriched with 597.6 mg and column B with 50.4 mg of REE. The fertilizer industry from PIC has about 1356097 m^3 of AIW storage capacity. The remediation of all that water could produce about 9764 tons of REE that otherwise would be lost through seepage. The seepage has been estimated in 40 m^3/day and is responsible

for a contamination plume that is currently contained with abstraction boreholes (Inprocon, 2013).

The sequential extraction indicated that the tailing had originally an average of 1332 mg of REE/kg of sample (Table 6.1 and Figure 6.8). After the interaction with the REE-rich wastewater, the REE concentration in the substrate increased to an average of 1646 mg/kg (Figure 6.7). This means an increasing of about 313 mg of REE/kg of substrate. Since reactor A has 2 kg of tailing, about 627 mg of REE have been added to the matrix. Therefore, by the end of the experiment, the matrix of the reactor A has about 3292 mg of REE. Minor amount of REE reached reactor B, about 145 mg of REE. The estimated increasing of REE in the entire system (627 + 145 = 772 mg REE) is similar to the average concentration of REE introduced by the AIW.

REE-bearing carbonates were dissolved by the acid wastewater, particularly at the top of column A, which is corroborated by the decrease of calcite minerals (Figure 6.9) and drop of REE extracted in F1 of the sequential extraction (Figure 6.7). In column B, the concentration of REE extracted in F1 (Figure 6.7) indicates that minor REE-bearing carbonate precipitated in the top that column. The oxy-/hydroxide minerals precipitated, mostly in the top of both columns A and B, have traces of REE, as it was detected in F2 of the sequential extractions.

In the original tailing, most REE were dissolved in F4 (1138mg/kg, on average). Such amount increases substantially after the interaction with the wastewater reaching up to 1967 mg/kg in the middle of the column A. This corresponds with the precipitation of the newly-formed Ca-Al-F phosphate mineral with 0.5% REE content, which perhaps could be recovered via flotation together with the REE content from the pre-existent REE-bearing minerals, such as the fluorapatite, calcite and dolomite (Cui, 2015) that remains in the substrate. Previous studies about the reprocessing of Fe ore tailings showcased up to 95% recovery of rare earth oxides from apatite group minerals using chemical methods (Peelman et al., 2018; Vierrether and Cornell, 1993). Bioleaching has also been recently explored as an alternative to recover REE from tailings (e.g. (Ibrahim and El-Sheikh, 2011; Maleke et al., 2019).

The cooccurrence and coprecipitation of REE and U have been widely documented (e.g. Balaram, 2019; René, 2018). However, the system developed herein has been able to precipitate most of the REE in column A, while most U precipitated in column B (Figure 6.4 and 6.8), leaving a substrate enriched in REE and depleted in radionuclides.

6.5. CONCLUSIONS

The bench scale prototype was designed to treat extremely acidic water and concentrate rare earth elements (REE) as a feasible and sustainable solution to an environmental problem with the lowest economic implications. The use of alkaline mining waste to neutralize the acidity would drive down cost of the treatment. In addition, the precipitation of REE present in both the mining waste and the water, could produce a REE-enriched substrate potentially sealable that might defray the treatment cost and perhaps turn it into a profitable process.

The system was able to neutralize the extremely acidic water increasing the pH from 1.3 up to 6. It also showed an efficient removal of up to 100% of toxic elements such as Al, Cr, Cu, F, Fe, Mn, U and Zn; while the removal of alkali and alkaline earth metals such as Ca, Mg, K and Na ranged 40 – 100%. It is worth mentioning that the system was able to precipitate up to 12 and 40 g/L of sulfate an phosphate, respectively. The installation of this system at full scale would prevent that more than 800 kg/day of pollutants would infiltrate to the aquifers. This includes anions (39, 223 and 428 kg/day of fluoride, phosphate and sulphate, respectively) and cations (16.114, 30.960, 0.003, 0.098, 2.526, 7.626, 5.280, 52.231, 1.694, 3.611, 0.114, 0.042 and 0.122 kg/day of Al, Ca, Cd, Cr, Cu, Fe, K, Mg, Mn, Na, Ni, U and Zn, respectively).

The accumulation of REE from both the tailing and the industrial wastewater occurred as REE-rich Ca-Al-F phosphate minerals, particularly in the middle section of reactor A where an enrichment of 2.1 g of REE/kg of substrate was obtained. The implementation of this system could recover up to 7 tons of REE from the water and 71 tons of REE from the substrate. In addition, the Cu plant produces about 18 Mt of tailing per year. This means that the reprocessing of East

tailing could sustain a yearly production of up to 25000 tons of REE per year, which would be above 10% of the global REE production.

Further feasibility studies need to be performed in order to evaluate the upscaling of the system and to estimate the marketability of the REE-rich by-product.

CHAPTER 7: GENERAL CONCLUSIONS

The renown Phalaborwa Igneous Complex (PIC) hosts an intricate industrial complex with a particular synergy among the different companies that operates there. The industrial activity started in PIC in the 1950s, when no environmental restrictions were enforced. Six decades later, the legacy of such long industrial activity includes 4500 Mt of waste rocks and tailings, and about 1Mm^3 of extremely acidic industrial wastewater, all of them enriched in REE. The Environment Conservation Act introduced in 1989 (South Africa, 1989) what is often considered as the first environmental legal obligations for industries (Linde, 2013). This act regulated the environmental impact of the industrial activity of PIC, which has been closely monitored by law enforcement officials and SANSPark personnel of the neighbouring Kruger National Park.

Due to the complexity and synergy among PIC industries, this investigation evaluated the best option to improve the environmental footprint of PIC as a whole. This study goes beyond a prevention strategy and proposes an eco-friendly and self-sustainable water treatment developed following a proper mineralogical, geochemical and hydrochemical study of REE-rich wastes produced at PIC. Such treatment has been able to remediate the extremely acidic water produced by the phosphoric acid plant and, at the same time, it concentrates REE in a particular section of the system.

The chapter 4 entitled “Mine waste from carbonatite deposits as potential rare earth resource: insight into Phalaborwa (Palabora) Complex” seeks to shed light on the mineralogical and geochemical composition of the waste rocks and the tailings from PIC in order to reclassify them as secondary resource of REE. In view of the results, it can be concluded that:

The abundance of REE minerals and REE-bearing minerals demonstrated that REE are preserved and, in some instance, concentrated in the mine waste, with respect to the REE concentration of the original deposit. Phoscorites and carbonatites are major lithologies in the WRDs and contain significant concentration of REE, of

which 0.23 and 0.14 wt%, respectively, would be easily extractable. The mineralogical results show monazite as the main REE-mineral with an average of 60 wt% of ∑REE, while calcite and fluorapatite are the most abundant REE-bearing minerals, whose ∑REE range between 0.5 and 1 wt%. On the other hand, the tailings are comprised mostly by monomineralic particles of calcite, dolomite, pyroxene, fluorapatite, magnetite and phlogopite. According to the geochemical results, the extraction of REE from monazite, fluorapatite, calcite and dolomite, from tailings produced by the Cu mine, might produce up to 5.65 kg of REE per ton. Although calcite has relatively low concentration of REE, due to its high abundance, it would be the main source of REE, followed by monazite and fluorapatite (3.2, 2.0 and 1.1 kg of REE per ton of tailing, respectively). The most profitable REE are Nd, Dy, Pr and Tb which represent 87% of net value. Therefore, PIC wastes and particularly the Cu tailing, have the potential to be reclassified as secondary resource of REE. An approach to circular economy by re-processing mining waste would extend the lifetime of PIC mines and their benefits, while reducing the waste of resources and their environmental impact.

The chapter 5 entitled "Environmental and Geochemical Characterization of Alkaline Mine Wastes from Phalaborwa (Palabora) Complex, South Africa" goes beyond the traditional environmental characterization of mining wastes. It aims to evaluate the potential of the mining wastes from PIC as alkaline reagent to neutralize acid industrial wastewater. Based on the results, it can be concluded that:

Both the tailing ponds and the waste rock dumps of PIC are comprised by abundant alkaline minerals, while the Fe-sulphide minerals are scarce. Which means that none of the mine wastes from PIC have the potential to sustain the production acid mine drainage. Furthermore, most of them felt under the classification of neutral to alkaline drainage producers. The highest neutralization potential was found in the carbonatite rocks and East tailing samples (range between 289 – 801 kg $CaCO_3$ eq/t). Regarding the toxicity of the leachates that they might produce, the PIC's mine wastes classify as Type 3 waste (non-hazardous), according to the National Environmental Management Waste Act (59/2008) of South Africa. Also, the sequential extractions showed that they would release mostly non-toxic elements

such as Ca, Mg, SO_4, Na, P, K and Fe. However, relatively high concentrations of radionuclides, such as U and Th (average of 6.7 and 36.3 mg/kg, respectively) are present in the non-labile fraction of PIC wastes, while the leachable concentrations were always below 0.006 mg/L. Among PIC wastes, the results of this section encourage to consider PIC tailing from the Cu mine as feasible alkaline reagents to be used during the treatment of acid industrial water within a circular economy strategy that would tackle at the same time the environmental impact caused by the mine residue and by the acid industrial water.

The chapter 6 entitled "Concentration of rare earth elements from acid wastewater using REE-rich alkaline mine waste: a novel approach of an acid wastewater neutralization system" aims to prove that alkaline material from PIC tailings can be use as reagent for a DAS system as an affordable solution to treat the acid wastewater from the phosphoric acid plant and, at the same time, can lead to the concentration of REE from both industrial wastes. Based on the results, it can be concluded that:

The system composed of two reactors in series, the first reactor (reactor A) with tailing material from the Cu mine and second reactor (reactor B) with commercial barium carbonate, improved substantially water quality. The removal efficiency of anions such as fluor > sulphate > phosphate, reached up to 100%, also trivalent (i.e. Fe and Al), divalent metals (i.e. Cu, Cd, Ni, Mn, Ni, Cr and As) and radionuclides were removed up to 100% throughout the experiment. The industrial wastewater contains high concentration of REE about 7.2 mg/L. Approx. 90% of REE were removed from solution in reactor A, while 5% were immobilized in reactor B, opposite to U that was removed mainly in reactor B.

The Mineralogical characterization of the substrate identified mayor brushite and an unidentified Ca-Al-F-phosphate that acts as a sink for REE in reactor A. To the best of our knowledge, this is the first study that describes the formation of this compound and its activity as a sink of REE in ambient conditions. The concentration of REE in the substrate of column A (original concentration in the tailing of 1.3g of REE/kg of tailing) reached up to 2.1 g of REE/kg in the middle of the reactor. Newly formed phosphate, gypsum and oxide minerals were found throughout the system and they were mainly associated to the removal of Fe, Al,

Cr, Cu, Cd, Mn, Ni and As. The improvement of the water quality after the treatment and the enrichment of REE suggest that the use of alkaline tailing can be an attractive alternative to create a water treatment self-sustainable that a) mitigates the contamination produced by acid wastewater, b) reduces the waste of critical resources and c) decreases the mining waste. Consequently, the low-cost system developed herein could reduce the environmental impact of PIC's industrial activity and be used as an eco-friendly technology to concentrate REE.

This thesis provides valuable information on the revalorization of alkaline mining waste enriched in REE from its mineralogical, geochemical and hydrochemical characterization and finalise with its use as reagent for a self-sustainable water treatment. This system could recover up to 0.4 Mt of REE from both the water and the tailing. In addition, every year the Cu plant produces about 18 Mt of tailing that is dumped in East tailing. This means that the reprocessing of East tailing could generate up to 25000 tons of REE per year, which would be above 10% of the global REE production.

CONCLUSIONES GENERALES

El reconocido Complejo Ígneo de Phalaborwa (PIC) alberga un intrincado complejo industrial con una sinergia particular entre las diferentes empresas que allí operan. La actividad industrial comenzó en PIC en la década de 1950, cuando no se imponían aun restricciones ambientales. Seis décadas después, el legado de una actividad industrial que aun continua ha dejado 4500 Mt de residuos mineros en escombreras y relaves, y aproximadamente 1 millón de m3 de aguas residuales industriales extremadamente ácidas, todas ellas enriquecidas con tierras raras (REE, por sus siglas en inglés). La Ley de Conservación del Medio Ambiente introducida en 1989 (Sudáfrica, 1989), es considerada como las primeras obligaciones legales ambientales para las industrias (Linde, 2013). Esta ley reguló el impacto ambiental de la actividad industrial de PIC, que ha sido monitoreada de cerca por funcionarios encargados de hacer cumplir la ley y por personal de SANSPark del aledaño Parque Nacional Kruger.

Debido a la complejidad y sinergia entre las industrias de PIC, esta investigación evaluó la mejor opción para mejorar la huella ambiental de PIC en su conjunto. Este estudio va más allá de una estrategia de prevención y propone un tratamiento de agua ecológico y autosostenible desarrollado a partir de un adecuado estudio mineralógico, geoquímico e hidroquímico de los residuos ricos en REE producidos en el PIC. Dicho tratamiento podría remediar el agua extremadamente ácida producida por la planta de ácido fosfórico y, al mismo tiempo, concentrar REE en una sección particular del propio sistema.

El capítulo 4 titulado “Residuos mineros de depósitos de carbonatita como potencial recurso de tierras raras: conocimiento del complejo Phalaborwa (Palabora)” busca arrojar luz sobre la composición mineralógica y geoquímica de las escombreras y los relaves del PIC para reclasificarlos como recursos secundarios REE. A la vista de los resultados, se puede concluir que:

La abundancia de minerales de REE y minerales que contienen REE demostró que las REE se conservan y, en algunos casos, se concentran en los residuos mineros, con respecto a la concentración de REE del depósito original. Las foscoritas y las carbonatitas son litologías importantes en las escombreras y contienen una

concentración significativa de REE, de la cual el 0,23 y el 0,14% en peso, respectivamente, serían fácilmente extraíbles. Los resultados mineralógicos muestran a la monacita como el principal mineral de REE con un promedio de 60% en peso de ∑REE, mientras que la calcita y la fluorapatita son los minerales ricos en REE más abundantes, cuyo ∑REE varía entre 0.5 y 1% en peso. Por otro lado, los relaves están compuestos mayoritariamente por partículas monominerales de calcita, dolomita, piroxeno, fluorapatita, magnetita y flogopita. De acuerdo con los resultados geoquímicos, la extracción de REE de monacita, fluorapatita, calcita y dolomita, de los relaves producidos por la mina de cobre, podría producir hasta 5.65 kg de REE por tonelada. Aunque la calcita tiene una concentración relativamente baja de REE, debido a su gran abundancia, sería la principal fuente de REE, seguida de la monacita y la fluorapatita (3.2, 2.0 y 1.1 kg de REE por tonelada de relaves, respectivamente). Los REE más rentables son Nd, Dy, Pr y Tb que representan el 87% del valor neto. Por lo tanto, los desechos de PIC y, en particular, los relaves de Cu, tienen potencial para ser reclasificados como recurso secundario de REE. Un enfoque hacia la economía circular mediante el reprocesamiento de los residuos mineros prolongaría la vida útil de las minas PIC y sus beneficios, al tiempo que aumentaría el aprovechamiento de recursos y disminuiría su impacto ambiental.

El capítulo 5, titulado “Caracterización medioambiental y geoquímica de los residuos mineros alcalinos del complejo Phalaborwa (Palabora), Sudáfrica” va más allá de la caracterización medioambiental tradicional de los residuos mineros. Tiene como objetivo evaluar el potencial de los residuos mineros del PIC como reactivo alcalino para neutralizar las aguas residuales industriales ácidas. En base a los resultados, se puede concluir que:

Tanto los relaves como las escombreras de PIC están compuestos por abundantes minerales alcalinos, mientras que los minerales de sulfuro de Fe son escasos. Lo que significa que ninguno de los residuos mineros de PIC tiene el potencial de producir drenaje ácido de la mina. Además, la mayoría de ellos entran en la clasificación de productores de drenaje neutros a alcalinos. El mayor potencial de neutralización se encontró en las rocas de carbonatita y las muestras de relaves del ‘East Tailing’ (289 - 801 kg CaCO3 eq / t). Con respecto a la toxicidad de los

lixiviados que podrían producir, los residuos mineros de PIC se clasifican como residuos Tipo 3 (no peligrosos), de acuerdo con la Ley Nacional de Desechos de Gestión Ambiental (59/2008) de Sudáfrica. Además, las extracciones secuenciales mostraron que liberarían principalmente elementos no tóxicos como Ca, Mg, SO4, Na, P, K y Fe. Sin embargo, concentraciones relativamente altas de radionucleidos, como U y Th (promedio de 6,7 y 36,3 mg/kg, respectivamente) están presentes en la fracción no lábil de los residuos, mientras que las concentraciones lixiviables siempre estuvieron por debajo de 0,006 mg/L. Los resultados de este capítulo indican que los relaves de la mina de cobre son reactivos alcalinos viables para ser utilizados durante el tratamiento de aguas industriales ácidas dentro de una estrategia de economía circular que abordaría al mismo tiempo el impacto ambiental causado por los residuos de minas y por el agua industrial ácida producidos en PIC.

El capítulo 6 titulado "Concentración de elementos de tierras raras de aguas residuales ácidas utilizando residuos de minas alcalinas ricas en REE: un enfoque novedoso de un sistema de neutralización de aguas residuales ácidas" tiene como objetivo demostrar que el material alcalino de los relaves de PIC puede utilizarse como reactivo para un sistema DAS. Una solución asequible para tratar las aguas residuales extremadamente ácidas de la planta de ácido fosfórico y, al mismo tiempo, puede conducir a la concentración de las REE que se encuentran en ambos residuos industriales. En base a los resultados, se puede concluir que:

El sistema compuesto por dos reactores en serie, el primer reactor (reactor A) con material de relaves de la mina de Cu y el segundo reactor (reactor B) con carbonato de bario comercial, mejoró sustancialmente la calidad del agua. La eficiencia de eliminación de aniones como flúor> sulfato> fosfato alcanzó hasta el 100%, también se eliminaron metales trivalentes (como Fe y Al), divalentes (como Cu, Cd, Ni, Mn, Ni, Cr y As) y radionucleidos. Las aguas residuales industriales contienen una alta concentración de REE de aproximadamente 7,2 mg/L. Aprox. El 90% de REE se eliminó de la solución en el reactor A, mientras que el 5% se inmovilizó en el reactor B, frente a U que se eliminó principalmente en el reactor B.

La caracterización mineralógica del sustrato identificó abundantes minerales neoformados de brushita y de Ca-Al-F-fosfato no identificado que actúa como

sumidero de REE en el reactor A. Hasta donde sabemos, este es el primer estudio que describe la formación de este compuesto y su actividad como sumidero de REE en condiciones ambientales. La concentración de REE en el sustrato de la columna A (concentración original del relave 1,3 g de REE/kg) incrementó hasta 2,1 g de REE/kg en el centro del reactor. Se encontraron minerales de fosfato, yeso y óxido neoformados en todo el sistema y se asociaron principalmente a la eliminación de Fe, Al, Cr, Cu, Cd, Mn, Ni y As. La mejora de la calidad del agua tras el tratamiento y el enriquecimiento de REE del sustrato sugieren que el uso de relaves alcalinos puede ser una alternativa atractiva para crear un tratamiento de agua autosostenible que a) mitigue la contaminación producida por aguas residuales ácidas, b) incremente el aprovechamiento de recursos críticos y c) disminuya los residuos mineros. En consecuencia, el sistema de bajo costo desarrollado aquí podría reducir el impacto ambiental de la actividad industrial de PIC y ser utilizado como una tecnología ecológica para concentrar REE.

Esta tesis aporta información valiosa sobre la revalorización de residuos mineros alcalinos enriquecidos en REE a partir de su caracterización mineralógica, geoquímica e hidroquímica, y finaliza con su uso como reactivo para un tratamiento de aguas autosostenible y posiblemente rentable. Este sistema podría recuperar hasta 0.4 Mt de REE tanto del agua como del relave de cobre. Además, cada año la planta de Cu produce alrededor de 18 Mt de relaves que se vierten en el Este. Esto significa que el reprocesamiento del relave podría generar hasta 25.000 toneladas de REE por año, lo que estaría por encima del 10% de la producción mundial de REE.

REFERENCES

Aldous, R.T.H., 1986. Copper-rich fluid inclusions in pyroxenes from the Guide copper mine, a satellite intrusion of the Palabora igneous complex, South Africa. Econ. Geol. 81, 143–155. https://doi.org/10.2113/gsecongeo.81.1.143

Allison, J.D., Brown, D.S., Novo-Gradac, K.J., 1991. MINTEQA2/PRODEFA2—A geochemical assessment model for environmental systems—Version 3.0 user's manual.

Ayora, C., Macías, F., Torres, E., Lozano, A., Carrero, S., Nieto, J.M., Pérez-López, R., Fernández-Martínez, A., Castillo-Michel, H., 2016. Recovery of Rare Earth Elements and Yttrium from Passive-Remediation Systems of Acid Mine Drainage. Environ. Sci. Technol. 50, 8255–8262. https://doi.org/10.1021/acs.est.6b02084

Balaram, V., 2019. Rare earth elements: A review of applications, occurrence, exploration, analysis, recycling, and environmental impact. Geosci. Front. 10, 1285–1303. https://doi.org/10.1016/j.gsf.2018.12.005

Basson, I., Lourens, P., Paetzold, H.D., Thomas, S., Brazier, R., Molabe, P., 2017. Structural analysis and 3D modelling of major mineralizing structures at the Phalaborwa copper deposit. Ore Geol. Rev. 83, 30–42. https://doi.org/10.1016/j.oregeorev.2016.12.002

Becker, M., Dyantyi, N., Broadhurst, J.L., Harrison, S.T.L., Franzidis, J.P., 2015. A mineralogical approach to evaluating laboratory scale acid rock drainage characterisation tests. Miner. Eng. 80, 33–36. https://doi.org/10.1016/j.mineng.2015.06.015

Bellenfant, G., Guezennec, A., Bodénan, F., Hugues, D., Cassard, D., Bellenfant, G., Guezennec, A., Bodénan, F., Hugues, P.D., Cassard, D., 2013. Re-processing of mining waste : Combining environmental management and metal recovery ? To cite this version : HAL Id : hal-00849984.

Berger, V.I., Singer, D.A., Orris, G.J., 2009. Carbonatites of the world, explored deposits of Nb and REE; database and grade and tonnage models: U.S.

Geological Survey Open-File Report 2009-1139, 17 p. and database. Open File Rep. 2009-1139.

Bibi, S., Kamran, M.A., Sultana, J., Farooqi, A., 2017. Occurrence and methods to remove arsenic and fluoride contamination in water. Environ. Chem. Lett. 15, 125–149. https://doi.org/10.1007/s10311-016-0590-2

Binnemans, K., Jones, P.T., Blanpain, B., Van Gerven, T., Pontikes, Y., 2015. Towards zero-waste valorisation of rare-earth-containing industrial process residues: A critical review. J. Clean. Prod. 99, 17–38. https://doi.org/10.1016/j.jclepro.2015.02.089

Blengini, G.A., Mathieux, F., Mancini, L., Nyberg, M., Cavaco Viegas, H., Salminen, J., Garbarino, E., Orveillion, G., Saveyn, H., 2019. Recovery of critical and other raw materials from mining waste and landfills, EUR 29744. ed. Publications Office of the European. JRC116131., Luxembourg. https://doi.org/10.2760/174367

Blowes, D.W., Ptacek, C.J., Jambor, J.L., Weisener, C.G., 2003. The Geochemistry of Acid Mine Drainage, in: Treatise on Geochemistry. Elsevier, pp. 149–204. https://doi.org/10.1016/B0-08-043751-6/09137-4

Briden, J.C., 1976. Application of Palaeomagnetism to Proterozoic Tectonics. Philos. Trans. R. Soc. A Math. Phys. Eng. Sci. 280, 405–416. https://doi.org/10.1098/rsta.1976.0004

Brink, D., 2011. Occurrence of Groundwater in Phalaborwa Igneous Complex. University of the Free State, Bloemfontein.

Brodie, M.J., Broughton, L.M., Robertson, A.M., 1991. A Conceptual Rock Classification System For Waste Management And A Laboratory Method For ARD Prediction From Rock Piles, in: Second International Conference on the Abatement of Acidic Drainage. Vancouver, p. 17.

Brough, C.P., Warrender, R., Bowell, R.J., Barnes, A., Parbhakar-Fox, A., 2013. The process mineralogy of mine wastes. Miner. Eng. 52, 125–135. https://doi.org/10.1016/j.mineng.2013.05.003

Bucknam, C.H., 1997. Net Carbonate Value (NCV) for Acid–Base Accounting. [WWW Document]. Net Carbonate Value Acid–Base Accounting. URL

http://www.bucknam.com/ncv.html

Bulakh, A.G., Le Bas, M.J., Wall, F., Zaitsev, A.N., 1998. Ancylite-bearing carbonatites of the Seblyavr massif, Kola Peninsula, Russia. Neues Jahrb. für Mineral. Monatshefte 171–192.

Bulletin, I., 2007. Epa Publication 448 Classification of Wastes 1–12.

Caraballo, M.A., Macias, F., Nieto, J.M., Castillo, J., Quispe, D., Ayora, C., 2011. Hydrochemical performance and mineralogical evolution of a dispersed alkaline substrate (DAS) remediating the highly polluted acid mine drainage in the full-scale passive treatment of Mina Esperanza (SW Spain). Am. Mineral. 96, 1270–1277. https://doi.org/10.2138/am.2011.3752

Caraballo, M.A., Serna, A., Macías, F., Pérez-López, R., Ruiz-Cánovas, C., Richter, P., Becerra-Herrera, M., 2018. Uncertainty in the measurement of toxic metals mobility in mining/mineral wastes by standardized BCR®SEP. J. Hazard. Mater. 360, 587–593. https://doi.org/10.1016/j.jhazmat.2018.08.046

Castillo, J., Gomez-Arias, A., Posthumus, J.J., Welman-Purchase, M.D., Van Heerden, E., 2015. Geochemical study of the interaction of acid and alkaline mine drainage with BaCO3, in: Brown, A., Bucknam, C., Burgess, J., Carballo, M., Castendyk, D., Figueroa, L., Kirk, L., McLemore, V., McPhee, J., O'Kane, M., Seal, R., Wiertz, J., Williams, D., Wilson, W., Wolkersdorfer, C. (Eds.), 10th ICARD | IMWA 2015 Conference – Agreeing on Solutions for More Sustainable Mine Water Management. Santiago de Chile, p. paper 290. https://doi.org/ISBN 978-956-9393-27-3

Castillo, J., Pérez-López, R., Sarmiento, A.M., Nieto, J.M., 2012. Evaluation of organic substrates to enhance the sulfate-reducing activity in phosphogypsum. Sci. Total Environ. 439, 106–113. https://doi.org/10.1016/j.scitotenv.2012.09.035

Chen, T., Yan, Z.-A., Xu, D., Wang, M., Huang, J., Yan, B., Xiao, X., Ning, X., 2020. Current situation and forecast of environmental risks of a typical lead-zinc sulfide tailings impoundment based on its geochemical characteristics. J. Environ. Sci. https://doi.org/10.1016/j.jes.2020.03.010

Coertze, R.J., 2011. The regulation of radioactive waste in South Africa. North-West

University (Potchefstroom Campus), South Africa.

Cortina, J.-L., Lagreca, I., De Pablo, J., Cama, J., Ayora, C., 2003. Passive In Situ Remediation of Metal-Polluted Water with Caustic Magnesia: Evidence from Column Experiments. Environ. Sci. Technol. 37, 1971–1977. https://doi.org/10.1021/es026018m

Council for Geoscience, 2003. Simplified Geology Map South Africa, Lesotho and Swaziland. Johannesburg.

Cravotta III, C.A., Trahan, M.K., 1999. Limestone drains to increase pH and remove dissolved metals from acidic mine drainage. Appl. Geochemistry 14, 581–606. https://doi.org/10.1016/S0883-2927(98)00066-3

Cui, H., 2015. Beneficiation of Rare Earth Elements Bearing Ancylite. University of Colorado.

Dawson, J.B., Hinton, R.W., 2003. Trace-element content and partitioning in calcite, dolomite and apatite in carbonatite, Phalaborwa, South Africa. Mineral. Mag. 67, 921–930. https://doi.org/10.1180/0026461036750151

Dawson, J.B., Steele, I.M., Smith, J. V., Rivers, M.L., 1996. Minor and trace element chemistry of carbonates, apatites and magnetites in some African carbonatites. Mineral. Mag. 60, 415–425. https://doi.org/10.1180/minmag.1996.060.400.03

de Ronde, C.E.J., Kamo, S.L., 2000. An Archcean arc-arc collisional event: a short-lived (ca 3 Myr) episode, Weltevreden area, Barberton greenstone belt, South Africa. J. African Earth Sci. 30, 219–248.

Department of Environmental Affairs, 2013. National Environmental Management: Waste Act (Act No 59 of 2008): Regulation 634, 635 and 636, Government Gazette Staatskoernat. South Africa.

Department of Environmental Affairs, 2009. Environmental Management Framework for the Olifants and Letaba Rivers Catchment Areas (OLEMF) Volume 1 : Environmental Management Framework Report. Pretoria.

Department of Water Affairs and Forestry, S.A., 2004. Olifants Water Managment Area: Internal Strategic Perspective, Water Management.

Dold, B., 2017. Acid rock drainage prediction: A critical review. J. Geochemical Explor. 172, 120–132. https://doi.org/10.1016/j.gexplo.2016.09.014

Doye, I., Duchesne, J., 2003. Neutralisation of acid mine drainage with alkaline industrial residues: laboratory investigation using batch-leaching tests. Appl. Geochemistry 18, 1197–1213. https://doi.org/10.1016/S0883-2927(02)00246-9

DWAF, 2003. Groundwater Resource Assessment [WWW Document]. Dep. Water Aff. For. URL http://noframe.data.dirisa.org/sarva/themefolder/theme_groundwater/data-1 (accessed 11.4.20).

DWAF, 1998. 1:500 000 Hydrogeological Map 2330 Phalaborwa. Petroria.

European Union, 2017. Study on the review of the list of Critical Raw Materials Criticality Assessments. Brussels. https://doi.org/10.2873/876644

Fan, H.-R., Yang, K.-F., Hu, F.-F., Liu, S., Wang, K.-Y., 2016. The giant Bayan Obo REE-Nb-Fe deposit, China: Controversy and ore genesis. Geosci. Front. 7, 335–344. https://doi.org/10.1016/J.GSF.2015.11.005

Fan, H.R., Yang, K.F., Hu, F.F., Liu, S., Wang, K.Y., 2016. The giant Bayan Obo REE-Nb-Fe deposit, China: Controversy and ore genesis. Geosci. Front. 7, 335–344. https://doi.org/10.1016/j.gsf.2015.11.005

Foskor, 2018. Foskor Intergrated Report for the Year Ended 31 March 2018. Phlaborwa.

FOSKOR, 2018. Foskor integrated report 2018. Phalaborwa.

Gambogi, J., 2019. USGS Rare earths. U.S. Geol. Surv. Miner. Commod. Summ. Febr. 2019 1, 2.

Gambogi, J., 2016. RARE EARTHS [ADVANCE RELEASE] RaRe eaRths Legislation and Government Programs.

GARD (Global Acid Rock Drainage), 2014. GARDGuide [WWW Document]. Int. Netw. Acid Prev. Guid. 2014. URL http://www.gardguide.com/index.php?title=Main_Page (accessed 1.27.20).

Giebel, J.R., Gauert, C.D.K., Costin, G., 2016. Rare earth minerals in the lower

part of the Palabora Carbonatite Complex, South Africa. Miner. Resour. a Sustain. World. Proc. 13th SGA Bienn. Meet. 1009–1013. https://doi.org/10.13140/RG.2.1.3957.3523

Giebel, R.J., 2019. The petrogenesis of carbonatites: Mineral variations and effects on the REE mineralization. Eberhard Karls Universität Tübingen.

Giebel, R.J., Gauert, C.D.K., Marks, M.A.W., Costin, G., Markl, G., 2017. Multi-stage formation of REE minerals in the Palabora Carbonatite Complex, South Africa. Am. Mineral. 102, 1218–1233. https://doi.org/10.2138/am-2017-6004

Giebel, R.J., Marks, M.A.W., Gauert, C.D.K., Markl, G., 2019. A model for the formation of carbonatite-phoscorite assemblages based on the compositional variations of mica and apatite from the Palabora Carbonatite Complex, South Africa. Lithos 324–325, 89–104. https://doi.org/10.1016/j.lithos.2018.10.030

Golder Associates, 2019. Draft Consolidated Environmental Management Report.

Golder Associates, 2013. Draft Consolidated Environmental Management Report. Phalaborwa.

Golder Associates, 2012. Numerical Groundwater Model for the Mine Complex. Phase 4 - Impact Analysis. Johannesburg.

Gomez-Arias, A., Castillo, J., Van Heerden, E., Vermeulen, D., 2016. Use of alkaline mine waste as treatment for acid drainage. Min. Meets Water – Conflicts Solut. 931–936.

Gomez-Arias, A., Castillo, J., Welman-Purchase, M.D., Posthumus, J.J., Van Heerden, E., 2015. Evidences of effective treatment of alkaline mine drainage with BaCO3, in: Brown, A., Bucknam, C., Burgess, J., Carballo, M., Castendyk, D., Figueroa, L., Kirk, L., McLemore, V., McPhee, J., O'Kane, M., Seal, R., Wiertz, J., Williams, D., Wilson, W., Wolkersdorfer, C. (Eds.), 10th ICARD | IMWA 2015 Conference – Agreeing on Solutions for More Sustainable Mine Water Management. Santiago de Chile, p. paper 303. https://doi.org/ISBN 978-956-9393-27-3

Gomez-Arias, A., Yesares, L., Castillo, J., Welman-Purchase, M., Vermeulen, D.,

2019. Limitations of current protocols to predict groundwater contamination from alkaline mine, in: Gómez Hernández, J.J., Andreo Navarro, B. (Eds.), Groundwater Management and Governance. Coping with Uncertainty. Spanish Chapter of the International Association of Hydrogeologists (AIH-GE), Malaga, p. 695. https://doi.org/ISBN 978-84-938046-3-3

Groves, D.I., Vielreicher, N.M., 2001. The Phalabowra (Palabora) carbonatite-hosted magnetite-copper sulfide deposit, South Africa: an end-member of the iron-oxide copper-gold-rare earth element deposit group? Miner. Depos. 36, 189–194. https://doi.org/10.1007/s001260050298

Hanekom, H.J., Van Staden, C.M.V.H., Smit, P.J., Pike, D.R., 1965. The Geology of the Palabora Igneous Complex. South African Geological Survey, Pretoria.

Hansen, H.K., Rojo, A., Ottosen, L.M., 2005. Electrodialytic remediation of copper mine tailings. J. Hazard. Mater. 117, 179–183. https://doi.org/10.1016/j.jhazmat.2004.09.014

Haque, N., Hughes, A., Lim, S., Vernon, C., 2014. Rare Earth Elements: Overview of Mining, Mineralogy, Uses, Sustainability and Environmental Impact. Resources 3, 614–635. https://doi.org/10.3390/resources3040614

Harmer, R., 2000. Mineralisation of the Phalaborwa complex and the carbonatite connection in iron oxide Cu-Au-U-REE deposits, in: Perter, T.M. (Ed.), Hydrothermal Iron Oxide, Copper-Gold and Related Deposits: A Global Perspective. PGC Publishing, Adelaide, pp. 331–340.

Harmer, R.E., Nex, P.A.M., 2016. Rare earth deposits of Africa. Episodes 39, 381–406. https://doi.org/10.18814/epiiugs/2016/v39i2/95784

Hatch, G.P., 2011. Leading Contenders for New Sources of Supply. Technology.

Heinrich, E.W.M., 1970. The Palabora carbonatitic complex - A unique copper deposit. Can. Mineral. 10, 585–598.

Hiller, E., Petrák, M., Tóth, R., Lalinská-Voleková, B., Jurkovič, Ľ., Kučerová, G., Radková, A., Šottník, P., Vozár, J., 2013. Geochemical and mineralogical characterization of a neutral, low-sulfide/high-carbonate tailings impoundment, Markušovce, eastern Slovakia. Environ. Sci. Pollut. Res. 20, 7627–7642. https://doi.org/10.1007/s11356-013-1581-5

Hlabela, P., Maree, J., Bruinsma, D., 2007. Barium Carbonate Process for Sulphate and Metal Removal from Mine Water. Mine Water Environ. 26, 14–22. https://doi.org/10.1007/s10230-007-0145-7

Holmes, A., Cahen, L., 1957. Geochronologie Africaine: 1956-Resultats acquis au let juillet 1956. Académie R. des Sci. Colon. Cl. des Sci. natarelles Mddicales 8, 1–169.

Hornig-Kjarsgaard, I., 1998. Rare Earth Elements in Sovitic Carbonatites and their Mineral Phases. J. Petrol. 39, 2105–2121. https://doi.org/10.1093/petroj/39.11-12.2105

Hu, L., Wu, H., Zhang, L., Zhang, P., Wen, Q., 2017. Geotechnical Properties of Mine Tailings. J. Mater. Civ. Eng. 29, 04016220-1-04016220–10. https://doi.org/10.1061/(ASCE)MT.1943-5533.0001736

Huang, G., Liu, C., Zhang, Y., Chen, Z., 2020. Groundwater is important for the geochemical cycling of phosphorus in rapidly urbanized areas: a case study in the Pearl River Delta. Environ. Pollut. 260, 114079. https://doi.org/10.1016/j.envpol.2020.114079

Hubert, E., Wolkersdorfer, C., 2015. Establishing a conversion factor between electrical conductivity and total dissolved solids in South African mine waters. Water SA 41, 490–500. https://doi.org/10.4314/wsa.v41i4.08

Humsa, T.Z., Srivastava, R.K., 2015. Impact of Rare Earth Mining and Processing on Soil and Water Environment at Chavara , Kollam , Kerala : A case study. Procedia Earth Planet. Sci. 11, 566–581. https://doi.org/10.1016/j.proeps.2015.06.059

Ibrahim, H.A., El-Sheikh, E.M., 2011. Bioleaching Treatment of Abu Zeneima Uraniferous Gibbsite Ore Material for Recovering U, REEs, Al and Zn. Res. J. Chem. Sci. 1, 55–66.

Inprocon, 2013. Bosveld Phosphate water balance assessment. Pretoria.

Jaguin, J., Boulvais, P., Poujol, M., Bosse, V., Paquette, J.-L., Vilbert, D., 2013. Albitization in the Antimony Line, Murchison Greenstone Belt (Kaapvaal Craton): A geochemical and geochronological investigation. Lithos 168–169, 124–143. https://doi.org/10.1016/j.lithos.2013.01.010

Jowitt, S., Werner, T., Weng, Z., Mudd, G., 2018. Recycling and secondary sources of the rare earth elements REE Resource, in: Goldschmidt-AGU Fall Meeting Abstracts. Boston.

K2C, 2014. Kruger to Canyons Biosphere Region: Annual Report 2013-2014, Kruger to Canyons. Pretoria. www.kruger2canyons.org.

Kanazawa, Y., Kamitani, M., 2006. Rare earth minerals and resources in the world, in: Journal of Alloys and Compounds. https://doi.org/10.1016/j.jallcom.2005.04.033

Kings, S., 2014. Bosveld Phosphates pollutes Kruger rivers, again. Mail Guard.

Krishnamurthy, N., Gupta, C.K., 2015. Extractive metallurgy of rare earths, second edi. ed. CRC Press, Boca Raton.

Kruse, N., Hawkins, C., López, D.L., Johnson, K., 2019. Recovery of an Acid Mine Drainage-Impacted Stream Treated by Steel Slag Leach Beds. Mine Water Environ. 38, 718–734. https://doi.org/10.1007/s10230-019-00636-y

Lèbre, É., Corder, G.D., Golev, A., 2017. Sustainable practices in the management of mining waste: A focus on the mineral resource. Miner. Eng. 107, 34–42. https://doi.org/10.1016/j.mineng.2016.12.004

Linde, G.F., 2013. A HOLISTIC HYDROGEOLOGICAL ENVIRONMENTAL SITE RISK ASSESSMENT METHODOLOGY FOR THE FERTILISER INDUSTRY IN SOUTH AFRICA. University of the Free State.

Lowe, D. onald R., Byerly, G.R., 1999. Geologic evolution of the Barberton greenstone belt and vicinity. The Geological Society of America,Inc., Boulder.

Lowe, D.R., 1994. Accretionary history of the Archean Barberton Greenstone Belt (3.55-3.22 Ga), southern Africa. Geology 22, 1099. https://doi.org/10.1130/0091-7613(1994)022<1099:AHOTAB>2.3.CO;2

Macías, F., Pérez-López, R., Caraballo, M.A., Cánovas, C.R., Nieto, J.M., 2017. Management strategies and valorization for waste sludge from active treatment of extremely metal-polluted acid mine drainage: A contribution for sustainable mining. J. Clean. Prod. 141, 1057–1066. https://doi.org/10.1016/j.jclepro.2016.09.181

Madugalla, T.B.N.S., Pitawala, H.M.T.G.A., Karunaratne, D.G.G.P., 2014. Use of Carbonatites in the Production of Precipitated Calcium Carbonate: A Case Study from Eppawala, Sri Lanka. Nat. Resour. Res. 23, 217–229. https://doi.org/10.1007/s11053-013-9222-8

Mainganye, D., Ojumu, T., Petrik, L., 2013. Synthesis of Zeolites Na-P1 from South African Coal Fly Ash: Effect of Impeller Design and Agitation. Materials (Basel). 6, 2074–2089. https://doi.org/10.3390/ma6052074

Maiti, A., Basu, J.K., De, S., 2012. Experimental and kinetic modeling of As(V) and As(III) adsorption on treated laterite using synthetic and contaminated groundwater: Effects of phosphate, silicate and carbonate ions. Chem. Eng. J. 191, 1–12. https://doi.org/10.1016/j.cej.2010.01.031

Maleke, M., Valverde, A., Vermeulen, J.-G., Cason, E., Gomez-Arias, A., Moloantoa, K., Coetsee-Hugo, L., Swart, H., van Heerden, E., Castillo, J., 2019. Biomineralization and Bioaccumulation of Europium by a Thermophilic Metal Resistant Bacterium. Front. Microbiol. 10, 81. https://doi.org/10.3389/fmicb.2019.00081

Mbombela, 2014. Water Affairs sues over toxic spillage. News24.

Meyer, F.M., Robb, L.J., Reimold, W.U., de Bruiyn, H., 1994. Contrasting low- and high-Ca granites in the Archean Barberton Mountain Land, Southern Africa. Lithos 32, 63–76. https://doi.org/10.1016/0024-4937(94)90021-3

Milačič, R., Zuliani, T., Ščančar, J., 2012. Environmental impact of toxic elements in red mud studied by fractionation and speciation procedures. Sci. Total Environ. 426, 359–365. https://doi.org/10.1016/j.scitotenv.2012.03.080

Milani, L., Bolhar, R., Frei, D., Harlov, D.E., Samuel, V.O., 2017. Light rare earth element systematics as a tool for investigating the petrogenesis of phoscorite-carbonatite associations, as exemplified by the Phalaborwa Complex, South Africa. Min. Depos. 1105–1125. https://doi.org/10.1007/s00126-016-0708-2

Millán-Becerro, R., Pérez-López, R., Macías, F., Cánovas, C.R., 2020. Design and optimization of sustainable passive treatment systems for phosphogypsum leachates in an orphan disposal site. J. Environ. Manage. 275. https://doi.org/10.1016/j.jenvman.2020.111251

Millán-Becerro, R., Pérez-López, R., Macías, F., Cánovas, C.R., Papaslioti, E.-M., Dolores Basallote, M., 2019. Assessment of metals mobility during the alkaline treatment of highly acid phosphogypsum leachates. Sci. Total Environ. 660, 395–405. https://doi.org/10.1016/j.scitotenv.2018.12.305

Mohapatra, D.P., Kirpalani, D.M., 2017. Process effluents and mine tailings: sources, effects and management and role of nanotechnology. Nanotechnol. Environ. Eng. 2, 12. https://doi.org/10.1007/s41204-016-0011-6

Moncur, M.C., Jambor, J.L., Ptacek, C.J., Blowes, D.W., 2009. Mine drainage from the weathering of sulfide minerals and magnetite. Appl. Geochemistry 24, 2362–2373. https://doi.org/10.1016/j.apgeochem.2009.09.013

Moodley, I., Sheridan, C.M., Kappelmeyer, U., Akcil, A., 2018. Environmentally sustainable acid mine drainage remediation: Research developments with a focus on waste/by-products. Miner. Eng. 126, 207–220. https://doi.org/10.1016/j.mineng.2017.08.008

Moore, M., Davis, D.W., Robb, L.J., Jackson, M.C., Grobler, D.F., 1993. Archean rapakivi granite-anorthosite-rhyolite complex in the Witwatersrand basin hinterland, southern Africa. Geology 21, 1031–1034. https://doi.org/10.1130/0091-7613(1993)021<1031:ARGARC>2.3.CO;2

Moukodi, G.P., 2008. Hydrogeochemical determination of the salt load from copper mine waste in the Bushveld Igneous Complex. University of the Free State.

Moukodi, G.P., Usher, B.H., Surmon, M., 2009. Hydrogeochemical Characterisation of. Waste Manag. 766–771.

Msila, X., Labuschagne, F., Barnard, W., Billing, D.G., 2016. Radioactive nuclides in phosphogypsum from the lowveld region of South Africa. S. Afr. J. Sci. Volume 112. https://doi.org/10.17159/sajs.2016/20150102

Orris, G.J., Grauch, R.I., 2002. Rare earth element mines, deposits, and occurrences. Open-File Rep. 02-189 174.

Oster, S., 1982. The Diffusion of Innovation among Steel Firms: The Basic Oxygen Furnace. Bell J. Econ. 13, 45. https://doi.org/10.2307/3003429

Ouakibi, O., Hakkou, R., Benzaazoua, M., 2014. Phosphate carbonated wastes

used as drains for acidic mine drainage passive treatment. Procedia Eng. 83, 407–414. https://doi.org/10.1016/j.proeng.2014.09.049

Owen, R., Madari, N., 2009. Baseline Report on The Hydrogeology of the Limpopo Basin : Country studies from Mozambique , South Africa and a contribution to the Challenge Program on Water and Food Project 17 Livelihoods : Managing risk , mitigating drought and improving water product.

Pålsson, B.I., Martinsson, O., Wanhainen, C., Fredriksson, A., 2014. Unlocking Rare Earth Elements from European apatite- iron ores. Fist Eur. Rare Earth Resour. Conf. 1, 241–251.

Paradis, M., Duchesne, J., Lamontagne, A., Isabel, D., 2006. Using red mud bauxite for the neutralization of acid mine tailings: a column leaching test. Can. Geotech. J. 43, 1167–1179. https://doi.org/101139/T06-071

Parbhakar-Fox, A., Lottermoser, B.G., 2015. A critical review of acid rock drainage prediction methods and practices. Miner. Eng. 82, 107–124. https://doi.org/10.1016/j.mineng.2015.03.015

Parbhakar-Fox, A.K., Edraki, M., Walters, S., Bradshaw, D., 2011. Development of a textural index for the prediction of acid rock drainage. Miner. Eng. 24, 1277–1287. https://doi.org/10.1016/j.mineng.2011.04.019

Parkhurst, D.L., Appelo, C.A.J., 1999. USER' S GUIDE TO PHREEQC (VERSION 2)— A COMPUTER PROGRAM FOR SPECIATION , AND INVERSE GEOCHEMICAL CALCULATIONS. Denver.

Peelman, S., Kooijman, D., Sietsma, J., Yang, Y., 2018. Hydrometallurgical Recovery of Rare Earth Elements from Mine Tailings and WEEE. J. Sustain. Metall. 4, 367–377. https://doi.org/10.1007/s40831-018-0178-0

Pérez-López, R., Álvarez-Valero, A.M., Nieto, J.M., 2007. Changes in mobility of toxic elements during the production of phosphoric acid in the fertilizer industry of Huelva (SW Spain) and environmental impact of phosphogypsum wastes. J. Hazard. Mater. 148, 745–750. https://doi.org/10.1016/j.jhazmat.2007.06.068

Pérez-López, R., Álvarez-Valero, A.M., Nieto, J.M., Sáez, R., Matos, J.X., 2008. Use of sequential extraction procedure for assessing the environmental impact at

regional scale of the São Domingos Mine (Iberian Pyrite Belt). Appl. Geochemistry 23, 3452–3463. https://doi.org/10.1016/j.apgeochem.2008.08.005

Pérez-López, R., Castillo, J., Sarmiento, A.M., Nieto, J.M., 2011. Assessment of phosphogypsum impact on the salt-marshes of the Tinto river (SW Spain): Role of natural attenuation processes. Mar. Pollut. Bull. 62, 2787–2796. https://doi.org/10.1016/j.marpolbul.2011.09.008

Pérez-lópez, R., Nieto, J.M., De, J.D., Bolívar, J.P., 2015. Environmental tracers for elucidating the weathering process in a phosphogypsum disposal site : Implications for restoration. J. Hydrol. 529, 1313–1323. https://doi.org/10.1016/j.jhydrol.2015.08.056

Poujol, M., Robb, L.J., 1999. New U-Pb zircon ages on gneisses and pegmatite from south of the the Murchison greenstone belt, South Africa. South African J. Geol. 102, 93–97.

Poujol, M., Robb, L.J., Anhaeusser, C.R., Gericke, B., 2003. A review of the geochronological constraints on the evolution of the Kaapvaal Craton, South Africa. Precambrian Res. 127, 181–213. https://doi.org/10.1016/S0301-9268(03)00187-6

Poujol, M., Robb, L.J., Respaut, J.-P., Anhaeusser, C.R., 1996. 3.07-2.97 Ga greenstone belt formation in the northeastern Kaapvaal Craton; implications for the origin of the Witwatersrand Basin. Econ. Geol. 91, 1455–1461. https://doi.org/10.2113/gsecongeo.91.8.1455

Pufahl, P.K., Groat, L.A., 2017. Sedimentary and Igneous Phosphate Deposits: Formation and Exploration: An Invited Paper. Econ. Geol. 112, 483–516. https://doi.org/10.2113/econgeo.112.3.483

Qureshi, A., Jia, Y., Maurice, C., Öhlander, B., 2016. Potential of fly ash for neutralisation of acid mine drainage. Environ. Sci. Pollut. Res. 23, 17083–17094. https://doi.org/10.1007/s11356-016-6862-3

Rauret, G., López-Sánchez, J.F., Sahuquillo, A., Rubio, R., Davidson, C., Ure, A., Quevauviller, P., 1999. Improvement of the BCR three step sequential extraction procedure prior to the certification of new sediment and soil

reference materials. J. Environ. Monit. 1, 57–61. https://doi.org/10.1039/a807854h

Reischmann, T., 1995. Precise U/Pb age determination with baddeleyite (ZrO2), a case study from the Phalaborwa igneous complex, South Africa. South African J. Geol. 98, 1–4.

René, M., 2018. History of Uranium Mining in Central Europe, in: Awwad, N.S. (Ed.), Uranium - Safety, Resources, Separation and Thermodynamic Calculation. Intechopen, London, pp. 1–20. https://doi.org/10.5772/intechopen.71962

Robb, L.J., Brandl, G., Anhaeusser, C.R., Poujol, M., 2006. Archaean Granitoid Intrusions. Geol. South Africa 57–71.

Robbins, E.I., Nord, G.L., Savela, C.E., Eddy, J.I., Livi, K.J.T., Gullett, C.D., Nordstrom, D.K., Chou, I.-M., Briggs, K.M., 1996. Microbial and mineralogical analysis of aluminum-rich precipitates that occlude porosity in a failed anoxic limestone drain, Monongalia County, West Virginia, in: 13th Annual International Pittsburgh Coal Conference. Pittsburgh, pp. 761–767.

Rodgers, K., Hursthouse, A., Cuthbert, S., 2015. The Potential of Sequential Extraction in the Characterisation and Management of Wastes from Steel Processing: A Prospective Review. Int. J. Environ. Res. Public Health 12, 11724–11755. https://doi.org/10.3390/ijerph120911724

Rötting, T.S., Ayora, C., Carrera, J., 2007. Chemical and Hydraulic Performance of " Dispersed Alkaline Substrate " (Das) for Passive Treatment of Acid Mine Drainage With High Metal Concentrations. Water 3, 1–5.

Rötting, T.S., Caraballo, M.A., Serrano, J.A., Ayora, C., Carrera, J., 2008a. Field application of calcite Dispersed Alkaline Substrate (calcite-DAS) for passive treatment of acid mine drainage with high Al and metal concentrations. Appl. Geochemistry 23, 1660–1674. https://doi.org/10.1016/j.apgeochem.2008.02.023

Rötting, T.S., Thomas, R.C., Ayora, C., Carrera, J., 2008b. Passive Treatment of Acid Mine Drainage with High Metal Concentrations Using Dispersed Alkaline Substrate. J. Environ. Qual. 37, 1741–1751.

https://doi.org/10.2134/jeq2007.0517

Roux, E.H., de Jager, D.H., du Plooy, J.H., Nicotra, A., van der Linde, G.J., de Waal, P., 1989. Phosphate in South Africa. J. South African Inst. Min. Metall. 89, 129–139.

Rubinos, D.A., Barral, M.T., 2013. Fractionation and mobility of metals in bauxite red mud. Environ. Sci. Pollut. Res. 20, 7787–7802. https://doi.org/10.1007/s11356-013-1477-4

Ruttenberg, K.C., 1992. Development of a sequential extraction method for different forms of phosphorus in marine sediments. Limnol. Oceanogr. 37, 1460–1482. https://doi.org/10.4319/lo.1992.37.7.1460

Saadaoui, E., Ghazel, N., Ben Romdhane, C., Massoudi, N., 2017. Phosphogypsum: potential uses and problems–a review. Int. J. Environ. Stud. 74, 558–567. https://doi.org/10.1080/00207233.2017.1330582

SABS, 2015. SANS 241-1 : 2015 SOUTH AFRICAN NATIONAL STANDARD Drinking water Part 1 : Microbiological , physical , aesthetic, 2nd ed. SABS Standards Division.

Sheppard, M.I., 1980. The Environment Behaviour of Uranium and Thorium. At. Energy Canada Ltd. 51.

Simandl, G.J., Paradis, S., 2018. Carbonatites: related ore deposits, resources, footprint, and exploration methods. Appl. Earth Sci. Trans. Inst. Min. Metall. 127, 123–152. https://doi.org/10.1080/25726838.2018.1516935

Simmons, J., Ziemkiewicz, P., Black, D.C., 2002. Use of steel slag leach beds for the treatment of acid mine drainage. Mine Water Environ. 21, 91–99. https://doi.org/10.1007/s102300200024

Skousen, J., Zipper, C.E., Rose, A., Ziemkiewicz, P.F., Nairn, R., McDonald, L.M., Kleinmann, R.L., 2017. Review of Passive Systems for Acid Mine Drainage Treatment. Mine Water Environ. 36, 133–153. https://doi.org/10.1007/s10230-016-0417-1

Smiciklas, I., Jovic, M., Sljivic-Ivanovic, M., Milenkovi, A., Smiljanic, S., 2015. Metals speciation in bauxite residue with implications to its use as an

immobilisation agent, in: Bauxite Residue Valorisation and Best Practices. KU Leuven, Leuven, pp. 241–248.

Smuda, J., Dold, B., Spangenberg, J.E., Friese, K., Kobek, M.R., Bustos, C.A., Pfeifer, H.R., 2014. Element cycling during the transition from alkaline to acidic environment in an active porphyry copper tailings impoundment, Chuquicamata, Chile. J. Geochemical Explor. 140. https://doi.org/10.1016/j.gexplo.2014.01.013

South Africa, 1989. The Environment Conservation Act (No. Act 73 of 1989). Pretoria, South Africa.

Southwood, M., Cairncross, B., 2017. The Minerals of Palabora, Limpopo Province, South Africa 7529. https://doi.org/10.1080/00357529.2017.1331398

Standards Australia, 1997. AS 4439.3 - Wastes , sediments and contaminated soils Part 3 : Preparation of leachates — Bottle leaching procedure. Council of Standard Australia, Australia. https://doi.org/ISBN 0 7337 0830 7

Stettler, E.H., De Beer, J.H., Blom, M.P., 1989. Crustal domains in the northern Kaapvaal craton as defined by magnetic lineaments. Precambrian Res. 45, 263–276. https://doi.org/10.1016/0301-9268(89)90065-X

Steyl, G., 2011. Deliverable 8 : Consolidate Phase II ESKOM-SASOL PHASE II Sustainable Salt Sinks.

Stumm, W., Morgan, J.J., 1973. Aquatic Chemistry: An Introduction Emphasizing Chemical Equilibria in Natural Waters., second edi. ed. Wiley-Interscience, New York.

Surender, D., 2009. Active Neutralisation and Amelioration of Acid Mine Drainage with Fly ash. University of Western Cape.

Sverdrup, H.U., 1990. The kinetics of base cation release due to chemical weathering. Lund Univ. Press. Lund.

Taneez, M., Hurel, C., 2019. A review on the potential uses of red mud as amendment for pollution control in environmental media. Environ. Sci. Pollut. Res. 26, 22106–22125. https://doi.org/10.1007/s11356-019-05576-2

Torres, E., Lozano, A., Macías, F., Gomez-Arias, A., Castillo, J., Ayora, C., 2018.

Passive elimination of sulfate and metals from acid mine drainage using combined limestone and barium carbonate systems. J. Clean. Prod. 182, 114–123. https://doi.org/10.1016/j.jclepro.2018.01.224

Uken, R., Watkeys, M.K., 1997. An interpretation of mafic dyke swarms and their relationship with major mafic magmatic events on the Kaapvaal Craton and Limpopo Belt. South African J. Geol. 100, 341–348.

USEPA, 1998. TCLP : Toxicity Characteristic Leaching Procedure and Characteristic Hazardous Wastes, United States Environmental Protection Agency. Washington DC.

Usher, B.H., Cruywagen, L.-M., de Necker, E., Hodgson, F.D.I., 2003. On-site and Laboratory Investigations of Spoil in Opencast Collieries and the Development of Acid-Base Accounting Procedures. Institute for Groundwater Studies, Bloemfontein.

Valderrama, L., Santander, M., Paiva, M., Rubio, J., 2011. Modified-three-product column (3PC) flotation of copper-gold particles in a rougher feed and tailings. Miner. Eng. 24, 1397–1401. https://doi.org/10.1016/j.mineng.2011.05.007

Valverde, A., Cason, E.D., Gómez-Arias, A., Bozkale, D., Govender, D., Riddell, E., Cowan, D., 2020. Pollution shapes the microbial communities in river water and sediments from the Olifants River catchment, South Africa. Arch. Microbiol. https://doi.org/10.1007/s00203-020-02035-2

van Heerden, E., Castillo, J., Gomez-Arias, A., Posthumus, R., Van der Hoven, W.G., 2015. Mine drainage remediation using barium carbonate dispersed alkaline substrate 80.

Vegter, J.R., 2003. HYDROGEOLOGY OF GROUNDWATER REGION 19 LOWVELD. Pretoria.

Vergara, R., 2018. PRELIMINARY ECONOMIC ASSESSMENT FOR THE MATAMULAS RARE EARTHS PROJECT IN COMPLIANCE WITH THE JORC CODE. QUANTUM Min.

Verwoerd, W.J., 1993. Update on carbonatites of South Africa and Namibia. South African J. Geol. 96, 75–95.

Vielreicher, N.M., Groves, D.I., Vielreicher, R.M., 2000. The Phalaborwa (Palabora) Deposit and his Potential Connection to Iron-Oxide Copper-Gold Deposits of Olympic Damp Type, in: Porte, T.M. (Ed.), Hydrothermal Iron Ore Copper-Gold & Related Deposits: A Global Perspective. PGC Publishing, Adelaide, pp. 321–329.

Vierrether, C.W., Cornell, W.L., 1993. Ri 9453 Rare-Earth Occurrences in the Pea Ridge Tailings.

Wall, F., Zaitsev, A.N., 2004. Phoscorites and Carbonatites from MAntle to Mine: The Key Example of the Kola Alkaline Province. Mineralogical Society of Great Britain & Ireland, London.

Watzlaf, G.R., 2004. TREATMENT OF HIGH-FLOW, LOW-IRON MINE DRAINAGE WITH A SEMI-PASSIVE SYSTEM. J. Am. Soc. Min. Reclam. 2004, 1962–1973. https://doi.org/10.21000/JASMR0401962

Watzlaf, G.R., Kairies, C.L., Schroeder, K.T., Danehy, T., Beam, R., 2002. Quantitative Results from the Flushing of Four Reducing and Alkalinity-Producing Systems, in: 23rd Annual West Virginia Surface Mine Drainage Task Force Symposium. Morgantown, WV, USA. p. 11.

Watzlaf, G.R., Schroeder, K.T., Kairies, C.L., 2000. Long-term performance of anoxic limestone drains. Mine Water Environ. 19, 98–110. https://doi.org/10.1007/BF02687258

Weber, P.A., Hughes, J.B., Conner, L.B., Lindsay, P., Smart, R.S.C., 2006. Short-term acid rock drainage characteristics determined by paste pH and kinetic NAG testing: Cypress prospect, New Zealand. 7th Int. Conf. Acid Rock Drain. 2006, ICARD - Also Serves as 23rd Annu. Meet. Am. Soc. Min. Reclam. 3, 2289–2310. https://doi.org/10.21000/jasmr06022289

WHO, 2011. Guidelines for Drinking-water Quality, 4th ed. World Health Organization.

Wilkin, R.T., Barnes, H.L., 1997. Formation processes of framboidal pyrite. Geochim. Cosmochim. Acta 61, 323–339. https://doi.org/10.1016/S0016-7037(96)00320-1

Woolley, A.R., 2001. Alkaline Rocks and Carbonatites of the World: Part 3 Africa.

The Geological Society, London.

Wu, F.-Y., Yang, Y.-H., Li, Q.-L., Mitchell, R.H., Dawson, J.B., Brandl, G., Yuhara, M., 2011. In situ determination of U–Pb ages and Sr–Nd–Hf isotopic constraints on the petrogenesis of the Phalaborwa carbonatite Complex, South Africa. Lithos 127, 309–322. https://doi.org/10.1016/J.LITHOS.2011.09.005

Yeheyis, M.B., Shang, J.Q., Yanful, E.K., 2009. Long-term evaluation of coal fly ash and mine tailings co-placement: A site-specific study. J. Environ. Manage. 91, 237–244. https://doi.org/10.1016/j.jenvman.2009.08.010

Zeh, A., Gerdes, A., Barton, J.M., 2009. Archean Accretion and Crustal Evolution of the Kalahari Craton—the Zircon Age and Hf Isotope Record of Granitic Rocks from Barberton/Swaziland to the Francistown Arc. J. Petrol. 50, 933–966. https://doi.org/10.1093/petrology/egp027

Zhang, B., Liu, C., Li, C., Jiang, M., 2014. A novel approach for recovery of rare earths and niobium from Bayan Obo tailings. Miner. Eng. 65, 17–23. https://doi.org/10.1016/j.mineng.2014.04.011

ZHENG, Q., WU, W., BIAN, X., 2017. Investigations on mineralogical characteristics of rare earth minerals in Bayan Obo tailings during the roasting process. J. Rare Earths 35, 300–308. https://doi.org/10.1016/S1002-0721(17)60913-X

Ziemkiewicz, P.F., Skousen, J.G., Simmons, J., 2003. Long-term Performance of Passive Acid Mine Drainage Treatment Systems. Mine Water Environ. 22, 118–129. https://doi.org/10.1007/s10230-003-0012-0

SUPPLEMENTATY MATERIALS

APPENDIX A. SUPPLEMENTARY MATERIAL OF CHAPTER 4

APPENDIX A.1. SEQUENTIAL EXTRACTION PROTOCOL.

The steps of the chemical extractions performed in triplicate to composites of each of the main lithologies from PIC waste rock dumps (B-carbonatite, T-carbonatite, phoscorite, feldspathic pyroxenite and mica-pyroxenite) as well as to composite of East tailing and a composite of Selati tailing are displayed in the table below. Additionally, pseudo-total digestions (with aqua regia) were performed in triplicate to composites of each sector of the tailings, as well as to each of the main lithologies.

Protocol	
Step 1 **(carbonates)**	1 g of dry sample was placed in a 50 ml polypropylene centrifuge tube, 40 ml of 0.11 mol/L acetic acid was added and the tubes were shaken in disk rotator at 40 rpm for 16 h at room temperature. Thereafter, the solid residue was separated by centrifugation at 5000 rpm for 20 minutes and the supernatant was extracted. the solid was washed with distilled water. The supernatant and the washings were decanted into polyethylene tubes and stored at 4°C for further analysis. The results are referred as fraction 1 (F1).

Step 2 **(Sulphides)**	The residues from Step 1 underwent chemical digestion using 40 ml of 0.1 mol/l hydroxylamine hydrochloride (adjusted to pH of around 2 by adding HNO_3). Again, the extraction was performed as described in Step 1 and the results are referred as fraction 2 (F2)
Step 3 **(Fe Oxides)**	The residue from Step 2 was digested using 10 ml of 8.8 mol/l H_2O_2 (pH 2.0–3.0) added carefully into the tubes. The tubes were covered and the contents react for 1 h at room temperature, then opened and digested at 85°C in a water bath until the level of the volume is reduced around 2–3 mL. This step was performed twice. After cooling, 50 ml of 1 mol/l ammonium acetate (adjusted to pH 2 by adding HNO_3) was added to the residue, which was extracted as described in Step 1. The results are referred as fraction 3 (F3).
Step 4 **(Silicates)**	10 ml of aqua regia (a mixture of 12 mol/l HCl and 15.8 mol/l HNO_3 in the ratio 3:1) was added to the residue from step 3 and digested for 24 h inside fume hood. Then, it was boiled on a hot plate for 1 h at 100°C.

APPENDIX A.2. CHEMICAL ANALYSIS OF THE SEQUENTIAL EXTRACTION:

The supernatants of the sequential extractions were analysed using: 1) inductively coupled plasma-mass spectrometry (ICP-MS) NexIon 2000b (PerkinElmer), for minor cations and rare earth elements; 2) inductively coupled plasma-optical emission spectrometry (ICP-OES) Prodigy XP (Teledyne Leeman), for mayor cations; and 3) High Performance Liquid Chromatography (HPLC) Shimadzu prominence, for anions. Certified multi-elements standard solutions (analytical grade) from Merck and Sigma were used for calibration, as well as for quality control. The standards run at the beginning, after every batch of 20 samples and at the end of the analysis. The samples were diluted with ultrapure water. An aliquot of the ultrapure water was included as blank, along with an aliquot of each of the reagents used during the sequential extraction. Detection limits were calculated by average and standard deviations from 10 blanks. The detection limits ranged from 0.10 mg/l to 0.02 mg/l for ICP-OES; from 0.005 µg/L to 0.0005 µg/L for ICP-MS; and from 0.5 mg/l to 0.0500 mg/l for HPLC analyses. The average measurement error was estimated to be below 1%. In addition, 20 subsamples were also analyzed by an accredited laboratory at the Institute for Groundwater Studies at the University of Free Sate in order to validate the results.

APPENDIX A.3. DATA TABLES

Table A. 1. Summary of EPMA analyses on main lithologies from PIC WRDs (% oxide). Basic statistic parameters (minimum, maximum, mean and standard deviation).

(% oxide)	Y_2O_3	La_2O_3	Ce_2O_3	Pr_2O_3	Nd_2O_3	Sm_2O_3	Eu_2O_3	Gd_2O_3	Tb_2O_3	Dy_2O_3	Ho_2O_3	Er_2O_3	Tm_2O_3	Yb_2O_3	Lu_2O_3
Fluorapatite in Phoskorites (n = 34)															
Min	0.0000	0.0160	0.1560	nd	nd	nd	nd	nd	nd	nd	nd	nd	nd	nd	nd
Max	0.0720	0.2690	0.6130	1.9870	0.9900	0.1690	0.0750	0.1490	nd	nd	0.0890	0.2580	0.0740	0.0390	nd
Mean	0.0270	0.1400	0.3400	0.1490	0.2150	0.0630	0.0200	0.0410	nd	nd	0.0130	0.1380	0.0130	0.0030	nd
Std. Dsv.	0.0220	0.0630	0.1330	0.4470	0.2160	0.0390	0.0220	0.0340	nd	nd	0.0290	0.0800	0.0200	0.0100	nd
fluorapatite in transgressive carbonatite (n = 10)															
Min	0.0080	0.0620	0.2200	nd	nd	0.0170	nd	nd	nd	nd	nd	nd	nd	nd	nd
Max	0.1230	0.3190	0.8960	0.1680	0.5030	0.2110	0.0810	nd	0.0280	0.1310	0.1050	nd	0.0310	0.0500	0.0390
Mean	0.0500	0.1780	0.4690	0.0860	0.2580	0.0930	0.0310	nd	0.0050	0.0380	0.0180	nd	0.0110	0.0130	0.0080
Std. Dsv.	0.0370	0.0830	0.2240	0.0570	0.1910	0.0640	0.0310	nd	0.0100	0.0560	0.0390	nd	0.0110	0.0200	0.0150
calcite in trangressive carbonatite (n = 6)															
Min	nd	nd	nd	nd	nd	nd	nd	nd	nd	nd	nd	nd	nd	nd	nd
Max	0.0030	0.9670	1.0180	0.0550	0.1030	0.0360	0.0350	0.0360	0.1060	0.1020	0.0600	0.2290	0.0170	0.0030	0.0900
Mean	0.0010	0.2440	0.2780	0.0150	0.0390	0.0130	0.0150	0.0160	0.0350	0.0380	0.0210	0.0570	0.0060	0.0010	0.0320
Std. Dsv.	0.0010	0.4180	0.4320	0.0230	0.0390	0.0150	0.0140	0.0150	0.0440	0.0420	0.0240	0.0990	0.0080	0.0010	0.0380
dolomite in trangressive carbonatite (n = 8)															
Min	nd	nd	nd	nd	nd	nd	nd	nd	nd	nd	nd	nd	nd	nd	nd
Max	0.0780	0.2300	0.1640	0.0710	0.0160	0.0150	0.0330	0.0200	nd	0.0440	0.0750	nd	0.0220	0.0460	0.0390
Mean	0.0190	0.0940	0.0500	0.0220	0.0060	0.0050	0.0120	0.0060	nd	0.0110	0.0290	nd	0.0080	0.0150	0.0140
Std. Dsv.	0.0300	0.0920	0.0690	0.0290	0.0070	0.0060	0.0130	0.0080	nd	0.0180	0.0300	nd	0.0100	0.0170	0.0160
magnetite in transgressive carbonatite (n=5)															
Min	nd	nd	nd	nd	nd	nd	nd	nd	nd	nd	nd	nd	nd	nd	nd
Max	0.0150	0.0180	nd	0.0800	0.0250	0.0000	0.0020	0.0110	nd	nd	0.0370	nd	nd	0.0410	nd
Mean	0.0050	0.0080	nd	0.0330	0.0090	0.0000	0.0010	0.0050	nd	nd	0.0170	nd	nd	0.0170	nd
Std. Dsv.	0.0070	0.0080	nd	0.0370	0.0110	0.0000	0.0010	0.0050	nd	nd	0.0160	nd	nd	0.0170	nd
ilmenite in transgressive carbonatite (n=4)															
Min	nd	nd	nd	nd	nd	nd	nd	nd	nd	nd	nd	nd	nd	nd	nd
Max	0.0180	nd	nd	0.0130	0.0150	0.0100	0.0170	0.0260	nd	nd	0.0570	nd	nd	0.0130	nd
Mean	0.0070	nd	nd	0.0040	0.0060	0.0030	0.0070	0.0110	nd	nd	0.0270	nd	nd	0.0050	nd
Std. Dsv.	0.0080	nd	nd	0.0060	0.0070	0.0050	0.0080	0.0120	nd	nd	0.0230	nd	nd	0.0060	nd
feldspathic pyroxenite (n=13)															
Min	nd	nd	nd	nd	nd	nd	nd	nd	nd	nd	nd	nd	nd	nd	nd
Max	0.0280	0.0320	nd	0.0590	0.0200	0.0370	0.0410	0.0340	nd	0.0610	0.0690	nd	0.0190	0.0440	nd
Mean	0.0052	0.0025	nd	0.0067	0.0056	0.0028	0.0051	0.0065	nd	0.0047	0.0142	nd	0.0021	0.0034	nd
Std. Dsv.	0.0092	0.0089	nd	0.0175	0.0063	0.0103	0.0128	0.0106	nd	0.0169	0.0225	nd	0.0055	0.0122	nd

Table A.1. Continuation

(% oxide)		Y_2O_3	La_2O_3	Ce_2O_3	Pr_2O_3	Nd_2O_3	Sm_2O_3	Eu_2O_3	Gd_2O_3	Tb_2O_3	Dy_2O_3	Ho_2O_3	Er_2O_3	Tm_2O_3	Yb_2O_3	Lu_2O_3
mica-pyroxenite (n=8)																
Min	nd	nd	nd	nd	nd	nd	nd	nd	nd	nd	nd	nd	nd	nd	nd	
Max	0.0280	nd	0.0400	0.0370	0.0410	0.0340	0.0390	0.0230	nd	nd	0.0400	nd	0.0040	0.0570	nd	
Mean	0.0101	nd	0.0050	0.0065	0.0086	0.0043	0.0049	0.0063	nd	nd	0.0131	nd	0.0005	0.0083	nd	
Std. Dsv.	0.0117	nd	0.0141	0.0134	0.0139	0.0120	0.0138	0.0091	nd	nd	0.0166	nd	0.0014	0.0199	nd	
monazite in transgressive carbonatite (n = 1)																
PMC15-6		0.0720	16.3660	25.8890	1.9840	7.6400	1.8730	0.8000	0.9350	nd	0.0350	0.1740	0.2480	0.0000	0.0330	nd
monazite in banded carbonatite (n = 4)																
Min		nd	16.5740	30.1970	2.1000	8.7460	1.9500	0.8960	1.2260	nd	nd	nd	nd	nd	nd	nd
Max		0.0440	23.5730	34.4280	2.4560	8.9090	2.2920	0.9630	2.0370	nd	0.0830	0.0100	0.0420	nd	0.0570	nd
Mean		0.0233	21.6055	32.9352	2.3193	8.8253	2.1673	0.9375	1.7275	nd	0.0377	0.0033	0.0205	nd	0.0190	nd
Std. Dsv.		0.0185	3.2109	1.9421	0.1576	0.0762	0.1543	0.0296	0.3579	nd	0.0384	0.0047	0.0172	nd	0.0269	nd
parisite in transgressive carbonatite (n = 1)																
PMC15-7		nd	13.849	29.735	2.737	11.596	1.283	0.859	1.75	nd	0.18	0.219	0.253	nd	0.088	0.064
anzaite in transgressive carbonatite (n = 3)																
Min		1.2050	3.3460	19.4680	2.6150	13.2900	3.2380	2.0960	3.7690	nd	0.3700	nd	nd	nd	0.0180	nd
Max		2.8720	7.5230	28.9460	3.4760	16.7960	4.8240	2.8960	5.2120	nd	0.7880	0.0680	0.2460	nd	0.1340	nd
Mean		2.0188	5.1454	24.2118	3.1180	15.1174	3.9864	2.5160	4.4240	nd	0.5992	0.0272	0.1234	nd	0.0698	nd
Std. Dsv.		0.7465	1.9554	4.2387	0.4114	1.5750	0.7149	0.3600	0.6589	nd	0.1913	0.0333	0.1100	nd	0.0533	nd
bastnasite in transgressive carbonatite (n = 4)																
Min		0.0080	15.6130	34.9150	3.1580	10.9450	2.9180	1.0760	4.6480	nd	nd	nd	nd	nd	nd	nd
Max		0.1300	23.9490	39.6770	4.5160	15.1090	3.7510	1.7980	5.4480	nd	0.0850	0.0640	nd	nd	nd	nd
Mean		0.0618	19.3333	37.0137	3.7122	12.9980	3.2168	1.4137	4.9553	nd	0.0352	0.0213	nd	nd	nd	nd
Std. Dsv.		0.0517	3.4874	1.9880	0.5903	1.7033	0.3786	0.2966	0.3520	nd	0.0381	0.0302	nd	nd	nd	nd
allanite in transgressive carbonatite (n = 8)																
Min		0.0040	3.2630	8.1120	0.8740	4.5790	1.0880	0.2470	1.3030	nd	nd	nd	0.0820	nd	nd	nd
Max		0.2420	6.6900	11.8750	1.2270	5.9960	1.4940	0.3730	1.5590	nd	0.0550	0.0470	0.2620	nd	0.0770	nd
Mean		0.0946	4.9526	10.2230	1.0436	5.0500	1.2312	0.2988	1.4539	nd	0.0174	0.0147	0.1684	nd	0.0195	nd
Std. Dsv.		0.0902	1.2146	1.5556	0.1244	0.5370	0.1615	0.0466	0.0993	nd	0.0233	0.0180	0.0639	nd	0.0300	nd

nd: no detected

Table A. 2. Average concentration of main elements in WRDs and tailings, determined by sequential extraction (fractions: F1, F2, F3 and F4) and Pseudo-total digestion (PT).

mg/kg		Al	Ba	Ca	Cu	F	Fe	K	Mg	Mn	Na	Ni	P	S	Si	Sr	Th	Ti	U	Zr
B-carb	**F1**	<1	168.9	76078	15.1	na	0.6	227.0	2085	155.2	823.9	1.30	<100	790.9	96.3	702.4	<0,01	na	<0,01	<0,01
	F2	15.0	165.5	68462	3.4	<0,01	821.2	34.5	3194	176.2	62.8	<0,1	<100	320.0	88.8	1144.0	na	na	<0,01	na
	F3	126.9	110.9	83002	1594.9	<0,01	1391.0	76.0	16457	335.4	1115.8	8.00	na	2478.1	1108.0	1310.2	na	na	<0,01	na
	F4	234.0	39.0	7766	607.8	<0,01	50950.8	110.8	5744	131.0	<0,1	17.00	na	2210.8	202.0	115.4	na	na	27.75	na
	PT	386.8	300.5	138345	1764.3	<0,01	46752.8	299.3	20168	809.8	736.4	19.00	22203.5	5817.3	305.8	2391.1	16.9	321.2	1.57	1.37
T- carb	**F1**	<1	55.1	76373	37.7	na	0.6	109.3	2171	120.8	893.2	2.16	<100	4049.6	82.5	675.6	<0,01	na	<0,01	<0,01
	F2	38.2	51.1	62446	3.2	<0,01	1164.5	18.7	4418	183.6	<0,1	2.10	<100	848.5	66.1	1066.7	na	na	<0,01	na
	F3	185.0	22.0	82034	2334.4	<0,01	359.3	47.0	40278	464.5	1100.8	10.13	na	3715.2	102.9	1248.1	na	na	<0,01	na
	F4	135.3	4.3	15805	83.3	<0,01	26921.5	7.8	659	31.3	<0,1	<0,1	na	1006.3	309.3	317.0	na	na	<0,01	na
	PT	261.3	79.8	133539	1498.3	<0,01	23563.5	46.8	28316	486.8	155.3	5.25	23442.5	8570.3	268.5	2250.6	71.4	253.7	21.86	0.99
F-pyrox	**F1**	151.4	11.1	433	11.0	67.6	213.1	412.8	180	7.8	46.6	0.50	<100	648.4	28.0	15.4	<0,01	1.7	0.06	<0,01
	F2	201.2	6.1	1921	3.3	<0,01	195.0	93.3	537	5.3	88.6	0.71	3736.6	467.3	225.5	70.6	0.2	13.4	0.24	0.07
	F3	169.0	4.9	1563	107.8	<0,01	146.9	158.2	758	4.0	4326.0	2.12	5608.5	<30	152.6	63.0	<0,01	17.1	0.01	0.01
	F4	454.1	12.4	335	6.4	<0,01	1034.1	<0,1	2149	11.1	181.9	1.84	<100	<30	14.5	4.4	2.3	61.7	0.17	0.52
	PT	1224.2	46.7	5456	176.5	<0,01	2550.7	<0,1	8118	50.3	764.9	5.21	9084.0	<30	34.8	167.8	5.6	103.7	0.98	1.94
Phoscor	**F1**	99.0	94.8	5264	2.2	94.4	<0,1	873.1	30705	12.0	194.4	0.47	<100	302.7	118.7	49.8	<0,01	19.3	0.16	<0,01
	F2	494.7	278.2	2567	7.5	<0,01	786.2	221.4	6976	43.5	99.8	2.25	4074.6	690.4	404.0	37.3	<0,01	10.3	0.26	0.01
	F3	686.2	47.1	3933	1.4	<0,01	125.0	514.2	9295	16.8	5364.3	5.41	7475.0	<30	382.6	63.6	0.1	28.0	0.01	0.01
	F4	18259.6	438.7	19614	42.5	<0,01	21297.1	6471.1	112426	161.3	812.7	83.34	45707.0	793.3	16.3	308.9	60.3	95.2	4.01	0.54
	PT	19927.2	629.7	30737	55.5	<0,01	21629.2	8428.6	165656	234.8	1082.8	80.76	52188.5	2716.7	20.2	433.4	58.2	152.6	4.76	0.67
M-pyrox	**F1**	119.4	88.5	1928	345.2	107.2	480.1	2768.3	2351	40.2	113.3	5.88	<100	284.6	203.5	58.7	<0,01	7.4	0.10	<0,01
	F2	483.3	37.0	2531	84.6	<0,01	903.6	1009.1	2487	12.7	114.7	4.47	4630.8	<30	492.6	58.4	0.1	10.0	0.40	0.02
	F3	286.9	45.9	2374	5793.0	115	93.4	2376.3	3180	10.9	4562.8	12.33	1754.9	2350.4	309.5	50.1	<0,01	20.4	0.02	1.62
	F4	12428.3	275.2	11807	1180.2	<0,01	104460.1	6327.2	84543	320.1	841.6	193.30	24187.5	2167.8	15.3	232.7	34.0	110.8	3.34	0.58
	PT	12989.4	109.0	17156	6196.3	<0,01	92345.1	11134.9	90722	305.4	1143.9	143.46	29757.8	6514.8	22.2	359.9	33.2	159.9	4.24	0.80
East tailing	**F1**	2.8	129.4	19717	104.9	8.8	<0,1	393.9	4439	152.9	147.9	1.47	<100	1321.3	1.9	582.3	<0,01	26.0	<0,01	<0,01
	F2	42.9	111.1	17128	93.7	<0,01	784.2	40.8	9152	146.2	139.6	3.30	<100	1149.6	114.6	483.7	0.2	64.0	0.16	0.01
	F3	6.8	13.3	308	265.2	<0,01	20.5	99.8	2032	6.3	4909.4	3.95	3178.8	677.5	87.4	6.6	<0,01	1.2	0.00	<0,01
	F4	6525.5	219.3	13025	567.8	<0,01	116194.6	<0,1	78812	607.8	3953.2	127.09	18702.0	1502.7	22.1	309.6	159.7	80.9	46.52	0.89
	PT	3772.4	77.9	49885	587.8	<0,01	146715.9	<0,1	110131	1010.4	1770.3	144.47	20912.0	3536.7	29.6	1327.5	206.0	204.4	61.25	0.74
Selai tailing	**F1**	77.1	52.4	2314	34.9	119.2	427.8	1519.8	5074	23.9	70.5	2.18	<100	<30	129.3	33.6	<0,01	8.8	0.02	<0,01
	F2	429.8	44.4	3156	24.1	<0,01	803.7	430.0	2923	15.3	104.4	3.44	4197.4	731.6	595.8	62.6	0.4	16.4	0.72	0.12
	F3	360.2	7.9	2908	27.3	<0,01	114.8	645.2	4178	12.8	4135.2	5.16	6115.8	<30	360.3	62.6	0.1	30.3	0.64	0.02
	F4	9572.9	114.8	7196	42.3	<0,01	22055.8	3618.3	68897	181.5	880.8	65.56	9621.0	<30	15.3	100.1	34.4	468.8	5.35	0.63
	PT	10122.6	191.9	14675	134.0	<0,01	22755.6	6109.8	84070	237.3	1221.6	66.72	18047.0	992.7	19.4	233.5	30.7	195.3	4.98	0.20

B-carb: banded carbonatite; T-carb: transgressive carbonatite; F-pyrox: feldspathic pyroxenite; P-pyrox: pegmatoide pyroxenite; M-pyrox: Mica pyroxenite; Phoscor: phoscorite; na: not analysed

Table A. 3. Average concentration of rare earth elements (REE) in waste rock dumps and tailings, determined by the sequential extraction.

mg/kg	Fraction	Sc	Y	La	Ce	Pr	Nd	Sm	Eu	Gd	Tb	Dy	Ho	Er	Tm	Yb	Lu
B-carb	F1	0.028	0.988	1.124	2.060	0.204	1.390	0.256	0.116	0.202	0.000	0.000	0.090	0.000	0.074	0.030	0.010
	F2	0.048	7.518	20.298	22.452	1.100	9.156	1.322	0.420	2.012	0.184	0.284	0.234	0.368	0.078	0.156	0.054
	F3	1.947	20.920	106.322	297.237	38.787	175.160	35.092	6.122	20.300	10.260	7.822	1.037	3.785	0.000	0.855	0.100
	F4	5.875	6.300	43.100	64.150	0.000	36.625	12.750	2.775	19.800	1.500	1.800	0.000	1.350	0.000	0.875	1.200
	PT	5.674	36.946	204.870	507.974	45.869	232.005	51.013	11.713	51.343	8.213	16.901	1.804	8.239	0.352	2.521	0.816
T-carb	F1	0.020	0.384	0.534	0.994	0.368	0.500	0.076	0.064	0.018	0.000	0.000	0.078	0.000	0.048	0.018	0.010
	F2	0.150	10.602	35.614	71.120	5.788	34.218	5.970	1.246	5.156	1.604	1.478	0.358	0.664	0.004	0.310	0.062
	F3	0.202	10.162	42.910	126.165	22.932	76.472	15.702	2.675	9.055	4.785	2.577	0.550	0.890	0.000	0.480	0.047
	F4	5.525	15.525	112.950	290.775	19.075	160.350	34.700	6.375	26.375	8.400	5.925	0.600	5.050	0.300	1.125	0.975
	PT	4.650	32.442	257.965	663.990	65.194	302.110	60.213	11.621	49.984	8.431	15.467	2.064	5.778	0.415	1.871	0.280
F-pyrox	F1	0.000	0.405	2.126	5.366	0.553	2.244	0.488	0.122	0.694	0.069	0.257	0.038	0.061	0.005	0.022	0.002
	F2	0.193	5.342	38.234	85.230	11.166	47.541	8.849	1.693	6.810	0.572	1.957	0.230	0.488	0.032	0.157	0.016
	F3	0.076	4.713	28.635	62.831	8.434	34.953	6.723	1.307	5.309	0.448	1.550	0.183	0.393	0.027	0.128	0.014
	F4	0.188	0.287	4.473	11.520	1.055	4.082	0.711	0.154	0.681	0.062	0.224	0.028	0.045	0.005	0.022	0.002
	PT	0.704	7.662	92.375	231.245	22.557	90.594	15.614	3.541	17.250	1.506	5.643	0.692	1.183	0.107	0.500	0.035
Phoscor	F1	0.001	0.493	2.789	4.313	0.711	3.148	0.687	0.162	0.845	0.079	0.306	0.044	0.082	0.008	0.044	0.004
	F2	0.196	4.169	11.497	24.333	3.376	15.248	3.372	0.791	3.247	0.345	1.350	0.169	0.328	0.023	0.116	0.011
	F3	0.003	7.758	70.796	179.378	19.806	86.044	15.914	3.482	17.896	1.494	5.470	0.675	1.121	0.100	0.454	0.033
	F4	2.818	34.247	345.668	941.984	96.866	419.689	82.313	16.644	83.692	7.267	25.613	3.237	5.430	0.481	2.198	0.151
	PT	2.495	42.717	387.259	1058.168	106.622	465.068	94.068	18.797	93.859	8.171	30.403	3.708	6.310	0.567	2.544	0.181

B-carb: banded carbonatite; T-carb: transgressive carbonatite; F-pyrox: feldspathic pyroxenite; P-pyrox: pegmatoide pyroxenite; M-pyrox: Mica pyroxenite; Phoscor: phoscorite;

Table A.3. Continuation

mg/kg	Fraction	Sc	Y	La	Ce	Pr	Nd	Sm	Eu	Gd	Tb	Dy	Ho	Er	Tm	Yb	Lu
M-pyrox	F1	0.000	0.059	0.254	0.616	0.064	0.303	0.063	0.013	0.090	0.008	0.020	0.005	0.008	0.000	0.002	0.000
	F2	0.268	6.597	28.582	63.318	8.558	37.757	7.846	1.632	6.728	0.608	2.166	0.264	0.536	0.036	0.179	0.018
	F3	0.008	5.035	52.315	129.565	14.017	57.870	10.619	2.340	11.658	1.002	3.673	0.450	0.752	0.067	0.301	0.021
	F4	3.145	23.173	241.879	632.053	65.182	270.995	55.452	10.967	53.615	4.685	17.157	2.097	3.750	0.325	1.531	0.109
	PT	2.881	28.757	283.508	715.385	73.833	305.525	56.447	12.670	63.292	5.483	20.640	2.575	4.366	0.393	1.764	0.128
South tailing	F1	0.000	0.129	0.373	0.860	0.100	0.460	0.119	0.030	0.155	0.016	0.063	0.012	0.021	0.003	0.012	0.001
	F2	0.459	7.051	29.435	67.977	9.374	40.558	8.308	1.745	7.051	0.669	2.405	0.305	0.615	0.051	0.225	0.030
	F3	0.247	8.698	42.542	96.665	13.920	61.782	12.346	2.382	9.660	0.818	2.773	0.334	0.714	0.049	0.239	0.027
	F4	2.883	9.116	95.040	257.301	26.214	108.310	18.993	4.157	20.724	1.768	6.631	0.813	1.416	0.136	0.628	0.048
	PT	3.093	17.529	165.384	436.826	45.812	191.123	34.920	7.794	38.697	3.455	12.866	1.637	2.842	0.265	1.236	0.091
East tailing	F1	0.006	6.092	22.560	59.768	6.416	29.146	5.747	1.591	7.194	0.693	2.8220	0.417	0.791	0.077	0.384	0.032
	F2	0.075	2.479	7.968	16.423	2.205	10.055	1.811	0.431	1.505	0.144	0.604	0.055	0.127	0.008	0.049	0.004
	F3	0.000	0.177	1.015	3.008	0.295	1.282	0.258	0.066	0.269	0.027	0.114	0.017	0.028	0.003	0.015	0.001
	F4	5.321	21.597	189.973	523.129	54.914	225.704	38.500	9.319	41.453	3.921	15.681	2.063	3.897	0.399	2.030	0.155
	PT	5.220	31.986	228.401	633.382	64.986	274.301	51.314	11.521	51.304	4.885	19.949	2.628	4.998	0.496	2.442	0.190

B-carb: banded carbonatite; T-carb: transgressive carbonatite; F-pyrox: feldspathic pyroxenite; P-pyrox: pegmatoide pyroxenite; M-pyrox: Mica pyroxenite; Phoscor: phoscorite;

Table A. 4. Content of REE in PIC tailings based on REE minerals and REE-bearing minerals abundances and their REO concentrations from SEM compositional maps and SEM-EDS analyses

East tailing	Abundance (%)	REO (%)	Ore grade (kgREO/T)
fluorapatite	9	1.2	1.08
calcite	40	0.8	3.2
dolomite	13	0.3	0.39
ilmenite	0.5	0.107	0.00535
magnetite	9	0.095	0.0855
Diopside	20	0.085	0.17
monazite	0.3	64.87	2.019
SUM			6.87695
Selati tailing	Abundance (%)	REO (%)	Ore grade (kgREO/T)
fluorapatite	15	1.08	1.62
calcite	5	0.8	0.4
dolomite	1	0.3	0.03
ilmenite	0.5	0.107	0.005
magnetite	1	0.095	0.0095
Diopside	31	0.085	0.2635
monazite	<0.1	64.87	<0,673
SUM			2.32835

Table A. 5. Details of East and Selati tailing's REE abundance and monetary value according to the sequential extraction protocol.

	East tailing							Selati tailing						
	Sum (mg/kg)	Sum (kg REE/t)	REO/REE ratio (wt)	Sum (kg REO/t)	RMB/kg	$/kg	M$ in East Tailing	Sum (mg/kg)	Sum (kg REE/t)	REO/REE ratio (wt)	Sum (kg REO/t)	RMB/kg	$/kg	M$ in Selati Tailing
Y	30.35	0.0303	1.2699	0.0385	20	2.84	65.7	24.99	0.0250	1.2699	0.0317	20	2.84	256.9
La	221.52	0.2215	1.1734	0.2599	11.75	1.6685	260.2	167.39	0.1674	1.1734	0.1964	11.75	1.669	934.0
Ce	602.33	0.6023	1.1713	0.7055	11.5	1.633	691.2	422.80	0.4228	1.1713	0.4952	11.5	1.633	2304.8
Pr	63.83	0.0638	1.1703	0.0747	320	45.44	2036.7	49.61	0.0496	1.1703	0.0581	320	45.44	7518.6
Nd	266.19	0.2662	1.1664	0.3105	292.5	41.535	7737.4	211.11	0.2111	1.1664	0.2462	292.5	41.54	29148.2
Sm	46.32	0.0463	1.1596	0.0537	12.5	1.775	57.2	39.77	0.0398	1.1596	0.0461	12.5	1.775	233.3
Eu	11.41	0.0114	1.1579	0.0132	210	29.82	236.3	8.31	0.0083	1.1579	0.0096	210	29.82	818.1
Gd	50.42	0.0504	1.1526	0.0581	169.5	24.069	839.3	37.59	0.0376	1.1526	0.0433	169.5	24.07	2972.1
Tb	4.79	0.0048	1.1762	0.0056	4125	585.75	1978.3	3.27	0.0033	1.1762	0.0038	4125	585.8	6423.0
Dy	19.22	0.0192	1.1477	0.0221	1825	259.15	3430.2	11.87	0.0119	1.1477	0.0136	1825	259.2	10064.1
Ho	2.55	0.0026	1.1455	0.0029	367.5	52.185	91.5	1.46	0.0015	1.1455	0.0017	367.5	52.19	249.6
Er	4.84	0.0048	1.1435	0.0055	157.5	22.365	74.3	2.77	0.0028	1.1435	0.0032	157.5	22.37	201.7
Tm	0.49	0.0005	1.1421	0.0006				0.24	0.0002	1.1421	0.0003			
Yb	2.48	0.0025	1.1387	0.0028				1.10	0.0011	1.1387	0.0013			
Lu	0.19	0.0002	1.1372	0.0002				0.11	0.0001	1.1372	0.0001			
Sum	1326.91	1.3269		1.5539			17598.5	982.40	0.9824		1.1507	23.50	3.29	61124.3

Table A. 6. Details of East and Selati tailing's REE abundance and monetary value according to the geochemical/mineralogical semi-quantification.

	East tailing				Selati tailing			
	%REO	kg REO/ton	$/kg	M$ in East Tailing	%REO	kg REO/ton	$/kg	M$ in Selati Tailing
Y	2.48	0.17	2.840	290.6	2.76	0.06	2.840	516.2
La	16.73	1.15	1.669	1151.6	17.07	0.40	1.669	1876.6
Ce	45.40	3.12	1.633	3059.1	43.04	1.00	1.633	4630.8
Pr	4.81	0.33	45.440	9013.5	5.05	0.12	45.440	15106.5
Nd	19.98	1.37	41.535	34242.2	21.40	0.50	41.535	58565.0
Sm	3.46	0.24	1.775	253.1	4.01	0.09	1.775	468.7
Eu	0.85	0.06	29.820	1045.9	0.84	0.02	29.820	1643.8
Gd	3.74	0.26	24.069	3714.3	3.77	0.09	24.069	5971.7
Tb	0.36	0.02	585.750	8755.3	0.33	0.01	585.750	12905.2
Dy	1.42	0.10	259.150	15180.6	1.18	0.03	259.150	20220.9
Ho	0.19	0.01	52.185	405.1	0.15	0.00	52.185	501.4
Er	0.36	0.02	22.365	328.9	0.27	0.01	22.365	405.2
Tm	0.04	0.00			0.02	0.00		
Yb	0.18	0.01			0.11	0.00		
Lu	0.01	0.00			0.01	0.00		
Sum	100.00	6.88		77440.2	100.00	2.33		122812.0

APPENDIX B. SUPPLEMENTARY MATERIAL OF CHAPTER 5

APPENDIX B.1. SAMPLING POINTS DESCRIPTION AND LOCATION

For this study, 60 rock samples (approx. 1 to 12 kg/each) were collected from the Waste rock dumps (WRD) that stores the barrens from the Cooper Open Pit (COP), as well as from the WRD that collects the barrens from the Northern Pyroxenite Mine (NPM). Tailing samples were collected from up to 2m-deep trench (approx. 5 kg/each) from 16 sampling locations, with shovels and soil samplers. All the tailings located in the eastern most part of Phalaborwa Complex collect the carbonatite froth-flotation from the Cu beneficiation, hereinafter referred to as East tailing (ET) and subdivided in four sections (i.e. N, S, E and W). The tailings generated in the phosphate plant have been accumulated in two tailing dams divided by Selati River at the southernmost area of Phalaborwa Complex. They are referred herein as Selati tailing N (STN) and Selati tailing S (STS).

Table B. 1. List of the sites considered in the present study and brief description of the type of samples collected from each Waste Rock Dump (WRD-COP and WRD-NPM), as well as from each tailing (i.e. East Tailing (ET) and Selati Tailing (ST)).

Site	location	description
WRD-COP 1	23°59.979' S 31°08.882' E	rocks collected from North COP
WRD-COP 2	24°00.481' S 31°08.763' E	rocks collected from West COP
WRD-COP 3	24°00.800' S 31°08.692' E	rocks collected from South COP
WRD-COP 4	24°00.269' S 31°09.679' E	rocks collected from East COP
WRD-NPM 1	23°57.982' S 31°07.175' E	rocks collected from East NPM
WRD-NPM 2	23°58.084' S 31°06.645' E	rocks collected from West NPM
ET-W 1	24°00.803' S 31°09.608' E	newest tailing from top
ET-W 2	24°00.504' S 31°10.898' E	newest tailing in contact with soil
ET-E 1	24°00.355' S 31°11.793' E	dry tailing from the bottom of the pond
ET-E 2	24°00.161' S 31°11.702' E	dry tailing from the bottom of the pond
ET-E 3	24°00.585' S 31°11.710' E	slurry freshly poured
ET-S 1	24°00.932' S 31°11.127' E	dry tailing
ET-S 2	24°00.507' S 31°11.177' E	dry old tailing
ET-S 3	24°00.619' S 31°11.362' E	wet new tailing
ET-N 1	24°00.463' S 31°11.161' E	dry new tailing
ET-N 2	24°00.328' S 31°10.806' E	dry old tailing
ET-N 3	23°59.794' S 31°10.539' E	dry old tailing
ET-N 4	23°59.391' S 31°10.562' E	slurry freshly poured
ET-N 5	23°59.482' S 31°11.141' E	dry old tailing
ET-N 6	24°00.164' S 31°11.407' E	dry old tailing
ST-S 1	24° 2.470'S 31° 5.999'E	fresh tailing
ST-S 2	24° 2.795'S 31° 5.855'E	old dry green tailing
ST-S 3	24° 2.675'S 31° 5.063'E	tailing from 2m pit section
ST-S 4	24° 1.887'S 31° 5.029'E	fresh tailing from pipe
ST-N 1	24° 0.098'S 31° 6.357'E	fresh tailing
ST-N 2	23°59.710'S 31° 6.026'E	old dry tailing

APPENDIX B.2. WASTE TOXICITY CLASSIFICATION ACCORDING TO NATIONAL AND INTERNATIONAL REGULATIONS

South African regulation stipulates the use of AS-4439 (Standards Australia, 1997) for solid wastes and contaminated soils to assess the suitability of wastes for disposal in a landfill. The results have been compared with the South African Leachable Concentration Thresholds (LCT) for landfill disposal of waste (Department of Environmental Affairs, 2013), which are similar to international thresholds, such as the Australian EPA 448.3 (Bulletin, 2007) (Table B.2). However, certain elements such as V, SO_4, Sb, Mn, Co and Cl have been added to the South African thresholds for landfill disposal (Department of Environmental Affairs, 2013). In addition, the total concentration (TC) of the pollutants present in the solid wastes have been assessed and compared with South African total concentration thresholds (TCT) (Department of Environmental Affairs, 2013), similar to the Australian EPA-B and EPA-C described in EPA 448.3 (Bulletin, 2007). Both the leachable and total concentration thresholds (LCT and TCT) are considered for the classification of wastes in South Africa (Department of Environmental Affairs, 2013). Each element has four LTC thresholds; LTC0, LTC1, LTC2 and LTC3, and three TC thresholds; TCT0, TCT1 and TCT2. Each waste can be classified according to the highest threshold overcame by any of the elements assessed (Table B.2). In order to identify each group easily, and following the Department of Environmental Affairs (2013) criteria, the wastes have been classified as follows:

- Type 0 waste (Unsuitable for landfill disposal): wastes with any element above LTC3 or TCT2. This waste is not allowed for landfill and “must be treated and re-assessed in terms of the Norms and Standards for Assessment of Waste Landfill Disposal.
- Type 1 waste (Extremely hazardous): wastes with any element between LTC2 and LTC3 and between TCT1 and TCT2.This waste may be disposed according to Class A landfill design, as described in DWAF (1998).
- Type 2 waste (hazardous): wastes with any element between LTC1 and LTC2 and all elements bellow or equal to TCT1. Dispose as Class B landfill design.
- Type 3 waste (non-hazardous): wastes with any element between LTC0 and LTC1 and all elements bellow or equal to TCT1. Dispose as Class C landfill design.

- Type 4 waste (inert): wastes with every element below or equal to LTC0 and TCT0. Dispose as Class D landfill design.

Table B. 2. National and international thresholds of leachable concentration and total concentration for waste classification.

	Leachable concentration thresholds (mg/L)							Total concentration thresholds (mg/kg)					
	South Africa[1]				Australia[2]		USA[3]	South Africa[1]				Australia[2]	
Thresholds	**LCT0**	**LCT1**	**LCT2**	**LCT3**	**EPA-C**	**EPA-B**	**TCLP**	**TCT0**	**TCT1**	**TCT2**	**EPA fill**	**EPA-C**	**EPA-B**
Ag	n.r.	n.r.	n.r.	n.r.	10	40	5	n.r.	n.r.	n.r.	10	180	720
As	0.01	0.5	1	4	0.7	2.8	5	5.8	500	2000	20	500	2000
B	0.5	25	50	200	n.r.	n.r.	n.r.	150	15000	60000	n.r.	n.r.	n.r.
Ba	0.7	35	70	280	n.r.	n.r.	100	62.5	6250	25000	n.r.	n.r.	n.r.
Cd	0.003	0.15	03	1.2	0.2	0.8	1	7.5	260	1040	3	100	400
Cl	300	15000	30000	120000	n.r.	n.r.	n.r.	n.r.	n.r.	n.r.	n.r.	n.r.	n.r.
Co	0.5	25	50	200	n.r.	n.r.	n.r.	50	5000	20000	n.r.	n.r.	n.r.
Cr	0.1	5	10	40	5.0	20	5	46000	800000	n.r.	1	500	2000
Cu	2	100	200	800	200	800	n.r.	16	19500	78000	100	5000	20000
F-	1.5	75	150	600	150	600	n.r.	100	10000	40000	450	10000	40000
Hg	0.006	0.3	0.6	2.4	0.1	0.4	0.2	0.93	160	640	1	75	300
Mn	0.5	25	50	200	n.r.	n.r.	n.r.	1000	25000	100000	n.r.	n.r.	n.r.
Mo	0.07	3.5	7	28	5.0	20	n.r.	40	1000	4000	40	1000	4000
Ni	0.07	3.5	7	28	2.0	8.0	n.r.	91	10600	42400	60	3000	12000
Pb	0.01	0.5	1	4	1.0	4.0	5	20	1900	7600	300	1500	6000
Sb	0.02	1	2	8	n.r.	n.r.	n.r.	10	75	300	n.r.	n.r.	n.r.
Se	0.01	0.5	1	4	1.0	4.0	1	10	50	200	10	50	200
SO_4	250	12500	25000	100000	n.r.	n.r.	n.r.	n.r.	n.r.	n.r.	n.r.	n.r.	n.r.
TDS	1000	12500	25000	100000	n.r.	n.r.	n.r.	n.r.	n.r.	n.r.	n.r.	n.r.	n.r.
V	0.2	10	20	80	n.r.	n.r.	n.r.	150	2680	10720	n.r.	n.r.	n.r.
Zn	5	250	500	2000	300	1200	n.r.	240	160000	640000	200	35000	140000

1: Australian Standard Leaching Procedure AS 4439.1, 4439.2 and 4439.3. Limits in R. 635 in Department of Environmental Affairs (DEA) Gazette 36784, South Africa.
2: AS 4439.2 and 4439.3 limits in Environmental protection Agency (EPA) Publication 448.3, Australia.
3: test Method 1311 in US - EPA Publication SW–846

APPENDIX B.3. ANALYTICAL DETAILS

APPENDIX B.3.1. ELEMENT ANALYSIS USING ICP-OES

Macro cations, micro cations and sulfate were analyzed by ICP-OES (Teledyne Prodigy). The list of elements analyzed is as follows: Ag, Al, As, B, Ba, Be, Ca, Cd, Co, Cr, Cu, Fe, K, Li, Mg, Mn, Mo, Na, Ni, Pb, S, Sb, Se, Si, Sn, Sr, U, V, Y, Zn

Standard preparation

All standards used for calibration were prepared using both single and multi-element Certified Reference Materials (CRM). Deionized water was used as the blank standard for calibration.

Trace elements: A 1000 ppm custom-made Ultraspec CRM in 5% HNO_3 was used to make a 100 ppm stock solution. Tenfold serial dilutions were made on the stock to prepare 10 ppm, 1 ppm, 0.1 ppm & 0.01 ppm standards for calibration. From the 10 ppm standard, a 20x dilution was made to make a 5 ppm standard which was then used to prepare 0.5 ppm, 0.05 ppm and 0.005 ppm calibration standards by serial dilution (10x). Calibration range of standards for trace elements: 0.005 ppm, 0.01 ppm, 0.05 ppm, 0.1 ppm, 0.5 ppm & 1 ppm. For the higher range of calibration: 1 ppm, 5 ppm, 10 ppm, 100 ppm.

Macro cations: A 10 000 ppm custom-made Ultraspec CRM in 5% HNO_3 was used to make a 400 ppm standard (1 mL of CRM in 24 mL of deionized water) and a 200 ppm standard (0.5 mL of CRM in 24.5 mL of deionized water). The 100 ppm standard is made by diluting the 400 ppm standard 4x.

Silicon: A 1000 ppm Ultraspec Si CRM – $(NH_4)_2SiF_6$ 99.999% pure in H_2O/Tr.HF – was used to prepare a 100 ppm stock solution. From this stock, a 10x serial dilution was made to make 10 ppm and 1 ppm calibration

standards. A 5x dilution was also made from the stock to get a 20 ppm calibration standard. The 5 ppm calibration standard was made by diluting the stock solution 20x. Calibration range of standards for Si: 1 ppm, 5 ppm, 10 ppm, and 20 ppm.

Sulfate: A 10 000 ppm Ultraspec Sulfate Ion (SO_4) CRM – Ultrapure Sulfuric Acid in H_2O – was used to make 1000 ppm, 100 ppm and 500 ppm standards. A serial 10x dilution was made to make the 1000 ppm and the 100 ppm. The 500 ppm was made by doing a 20x dilution. For the lower range of standards (10 ppm, 25 ppm, 50 ppm) – the 10 ppm was made by diluting the 100 ppm 10x, the 50 ppm was made by diluting the 500 ppm 10x and the 25 ppm was made by diluting the 100 ppm 4x. Calibration ranges: 100 ppm, 500 ppm, 1000 ppm (higher) and 10 ppm, 25 ppm, 50 ppm (lower).

Quality control

A group of quality control standards was used and made from CRMs. The method was set up to automatically do the specified quality control checks at every 12 samples. The following quality control standards were used:

- ***Trace elements*:** a 0.5 ppm and 0.05 ppm QC standard check
- ***Macro cations*:** a 100 ppm and 10 ppm QC standard check
- ***Silicon*:** a 5 ppm QC standard check
- ***Sulfate*:** a 100 ppm QC standard check

Instrument setup

The plasma conditions were set as follows:
Auxiliary flow: 0.5 LPM
Coolant flow: 18 LPM
Nebulizer flow: 34 PSI
Pump flow: 30 RPM
RF Power: 1.1 kW

Purge: Low
The auto-sampler uptake rate was set at 50 seconds.

Method selection

A method was created with all the desired elements and set-up to automatically analyze the specified elements by default. The number of integrations per sample were set to 3, axial time to 30s and radial time to 10s.

Powering Instrument and running samples:

- After ensuring that there was sufficient gas and the instrument had been appropriately setup, the plasma was ignited using the AUTOSTART button.
- The system was let to stabilize for approximately 30 minutes before the commencement of the run.
- A calibration was then performed with each daily run of the samples. The method was set up to automatically run the calibration for all the specified elements.
- A run list was set up on Excel with the samples to be copied into the instrument.
- Once the calibration was completed, a calibration summary was saved and the calibration standards deselected in order to begin with the sample run.
- Using the pre-set run list from Excel, the samples to be analyzed were then loaded and quality control checks set up after every 12 samples analyzed. Intermediate sample checks were also done throughout the sample run.
- Upon completion of the analyses, the results were exported into a .CSV file.

APPENDIX B.3.2. DETERMINATION OF ORTHOPHOSPHATE AND CHLORIDE

The instrument used for determination of orthophosphate and chloride is the discrete analyzer *Easy Chem 200.* This instrument makes measurements based on the Beer Lambert's law that absorbance is directly proportional to the concentration of the solution.

The standards used for the calibration were 5 mg/l KH_2PO_4 and 5 mg/l of NaCl, the instrument dilutes that standard to make a calibration, with dilutions % of 0.0, 2.0, 5.0, 10.0, 17.5, 25.0, 50.0, 75.0, 100.0. Samples are prepared by filtering through *Whatman number 2* to remove suspended solids and then poured into a 2ml cup for analysis. To ensure validity of results a quality control standard of 3 mg/l Orthophosphate and chloride is also measured, prepared from KH_2PO_4 and primary salt (NaCl).

APPENDIX B.3.3. DETERMINATION OF FLUORIDE

The SPADNS colorimetric method is based on the reaction between fluoride and a zirconium-dye lake, that produces a red color, the higher the concentration of fluoride, the less red the solution becomes. The instruments used for determination of fluoride is *HACH DR3900 spectrophotometer*.

Samples are prepared by filtering through *Whatman number 2* to remove suspended solids and then 10 ml of the sample is poured into a test tube. The sample is then allowed to react with 2 ml of the SPADNS fluoride reagent for 1 minute and then measured by *HACH DR3900 spectrophotometer.* To ensure validity of results a quality control standard of 1 mg/l Fluoride is also measured, prepared from potassium fluoride.

APPENDIX B.4. DATA TABLES

Table B. 3. Simplified mineralogical distribution of acid consuming and acid producing minerals of PIC's Waste (wt.%). Including banded carbonatite (B-carb), transgressive carbonatite (T-carb), pegmatoidal pyroxenite (P-pyrox), micaceous pyroxenite (M-pyrox), feldspathic pyroxenite (F-pyrox), phoscorite (Phosc), East tailings (ETN, ETW, ETE and ETS) and Selati tailings (STN and STS). Content has been estimated X-ray diffraction (XRD) and complemented by petrographic microscopy, scanning electron microscope (SEM) coupled with electron microprobe analyses (EPMA) for rock samples and silicon drift detector (SDD) for tailing samples.

Samples	calcite	dolomite	diopside	phlogopite	microcline	apatite	pyrite	chalcopyrite
B-carb	69.68	7.12	ND	ND	ND	ND	ND	0.10
T-carb	46.25	1.32	ND	16.98	ND	ND	ND	0.05
M-pyrox	ND	ND	25.15	54.85	ND	ND	ND	0.03
P-pyrox	ND	ND	22.38	34.71	ND	12.45	ND	0.02
F-pyrox	ND	ND	16.98	5.06	54.9	3.16	ND	0.01
Phosc	1.6	ND	ND	8	ND	70.4	ND	0.03
ETN	40	13	4	7	ND	9	0.3	0.5
ETW	52	10	7	7	ND	8	0.3	0.5
ETE	35	7	6	7	ND	9	0.3	0.4
ETS	33	22	ND	8	ND	9	0.3	0.5
STN	7	2	24	43	1	16	0.2	0.6
STS	3	1	38	39	2	15	0.2	0.6

Table B. 4. Acid Rock Drainage Index (ARDI) of transgressive carbonatite (T-carb), banded carbonatite (B-carb), feldspathic pyroxenite (F-pyrox), pegmatoidal pyroxenite (P-pyrox), Syenite, mica-pyroxenite (M-pyrox), phoscorite (Phosc), East tailing south sector (ETS), East tailing north sector (ETN), East tailing west sector (ETW), East tailing east sector (ETE), Selati tailing north (STN) and Selati tailing south (STS).

Parameters		T-carb	B-carb	F-pyrox	P-pyrox	M-pyrox	Syenite	Phosc	ETS	ETN	ETW	ETE	STN	STS
A	Me	0.05	0.13	0.001	0.1	0.01	0	X	X	X	X	X	X	0.001
	Mi	0.04	0.1	0.01	0.11	0.01	0.03	0.1	0.09	0.095	0.08	0.1	0.1	0.03
B	Me	10	10	0	0	0	0	X	X	X	X	X	X	0
	Mi	10	10	10	10	4	10	8	8	8	8	5	5	10
C	Me	0	5	0	0	2	0	X	X	X	X	X	X	0
	Mi	2.5	5	5	5	2.6	5	2.5	2.5	2.5	2.5	4	4	5
D	Me	-2	-3	0	0	3	0	X	X	X	X	X	X	0
	Mi	-2	-4	0	0	1	0	-3	-4	-3	-2	-1.5	-1	0
E	Me	-1	-2	0	0	2	0	X	X	X	X	X	X	0
	Mi	-1.2	-1.9	0.1	0.1	1	-2.5	-2.5	-2.9	-2.4	-2	-2	-2	0.1
Sum		16.39	19.33	15.111	15.31	15.131	15.62	12.53	5.1	3.69	5.195	6.58	5.6	6.1
Average		1.64	1.93	1.51	1.53	1.51	1.56	1.25	0.51	0.37	0.52	0.66	0.56	0.61
X_{Me}		7.05	10.13	0.00	0.10	0.00	7.01	0.00	x	x	x	x	x	x
Y_{Mi}		9.34	9.20	15.11	15.21	15.13	8.61	12.53	5.10	3.69	5.20	6.58	5.60	6.10
ARDI*		**8.20**	**9.67**	**7.56**	**7.66**	**7.57**	**7.81**	**6.27**	**5.10**	**3.69**	**5.20**	**6.58**	**5.60**	**6.10**

*Final ARDI score classification (Parbhakar-Fox et al., 2011):

-1 to -10	Acid neutralizing capacity
0 to 10	Not acid forming/acid neutralizing capacity
11 to 20	Not acid forming
21 to 30	Potentially acid forming
31 to 40	Acid forming
41 to 50	Extremely acid forming

Table B. 5. Neutralization potential (NP) calculations for transgressive carbonatite (T-carb), banded carbonatite (B-carb), feldspathic pyroxenite (F-pyrox), pegmatoidal pyroxenite (P-pyrox), Syenite, mica-pyroxenite (M-pyrox), phoscorite (Phosc), East tailing S, East tailing N, East tailing W, East tailing E, Selati tailing N and Selati tailing S.

Samples	FIZZ	0h	2h	22h		24h		NaOH (0,1N) (mL)	total HCL (mL)	Modified NP (kg CaCO3/t)	NP deviation (kg CaCO3/t)
	rate	HCl 1N (ml)	HCl 1N (ml)	pH	HCl 1N (ml)	pH	HCl 1N (ml)				
T-carb	High	3	2	7.78	215	5.27	2	8.2	27.8	679.6	19.6
B-carb	High	3	2	7.76	27.3	4.03	0.9	10.8	33.2	800.6	23.1
East tailing S	High	3	2	7.67	7.7	5.10	1.5	7.4	14.2	335.7	11.6
East tailing N	High	3	2	7.66	9.7	5.32	1.7	7.4	16.3	389.9	3.0
East tailing W	High	3	2	8.05	21.7	4.20	1	11.5	27.7	662.9	11.9
East tailing E	High	3	2	7.65	6	5.06	1.5	9.4	12.5	289.0	1.9
Selati tailing N	Moderate	2	2	2.34	0	2.53	0	18.2	4.0	54.6	2.1
Selati tailing S	Moderate	2	2	2.36	0	2.53	0	16.3	4.0	59.2	0.6
F-pyrox	none	1	1	2.08	0	2.22	0	15.1	2.0	12.3	0.2
P-pyrox	Moderate	2	2	2.85	0.5	2.45	0	16.2	4.5	72.0	2.2
Syenite	none	1	1	1.96	0	2.10	0	15.9	2.0	10.2	0.2
M-Pyrox	none	1	1	2.73	0.6	2.45	0	14.2	2.4	25.4	1.9
Phosc	Slight	2	1	4.86	3.3	2.85	0.3	21.5	6.7	112.8	2.0

Table B. 6 Mean Pseudo-total concentration in mg/kg of PIC's waste, including transgressive carbonatite (T-carb), banded carbonatite (B-carb), feldspathic pyroxenite (F-pyrox), pegmatoidal pyroxenite (P-pyrox), Syenite, mica-pyroxenite (M-pyrox), phoscorite (Phosc), East tailing and Selati tailing.

mg/kg	B-carb	T-carb	F-pyrox	P-pyrox	Syenite	M-pyrox	Phoscorite	East tailing	Selati tailing
Al	375.875	358.470	975.672	17680.304	6007.276	8955.461	19539.552	6578.109	10439.937
As	50.800	33.600	3.510	6.814	2.163	11.074	14.700	8.038	8.533
B	2.000	1.340	7.529	12.148	6.477	7.460	8.054	24.891	14.222
Ba	484.315	132.470	34.439	780.252	33.392	113.024	858.743	472.962	219.449
Br	0.000	0.000	8.629	8.787	4.012	7.220	9.400	20.112	17.182
Ca	235307.585	236657.570	4251.307	13908.628	934.459	23371.496	31377.537	30474.190	15573.804
Co	31.500	28.125	1.567	119.857	4.166	18.318	32.246	63.445	25.334
Cr	0.000	0.000	3.728	1.584	5.286	41.266	120.908	31.475	81.558
Cu	2221.105	2458.525	128.597	14804.206	39.847	1.933	53.651	1031.604	128.618
Fe	53163.510	28445.810	1589.072	198855.907	13415.582	13018.325	22208.252	116999.341	23402.106
K	448.230	182.700	664.341	19361.409	760.869	5600.274	8079.822	169.373	6213.340
Li	0.000	0.000	0.711	4.660	9.867	8.115	5.456	2.334	3.892
Mg	27480.085	47525.090	3624.074	111439.465	8227.547	73682.651	159400.803	94435.505	81071.669
Mn	797.815	800.170	28.278	585.469	108.505	182.446	233.587	913.199	233.552
Mo	0.000	0.000	0.419	0.403	1.010	0.491	0.758	1.767	0.578
Na	2002.430	1993.910	4643.050	5994.995	5151.856	5269.931	6471.193	9150.026	5190.879
Ni	26.300	14.385	5.170	392.626	13.433	39.344	91.475	135.812	76.334
Pb	51.125	0.000	9.116	17.278	9.662	10.049	11.635	24.969	11.306
S	5799.892	9619.525	1115.733	8113.033	0.000	1492.667	1786.400	4651.100	731.600
Sb	0.000	0.000	0.027	0.000	0.025	0.017	0.018	0.040	0.020
Se	4.825	4.125	4.173	7.674	2.809	17.463	25.045	11.278	12.339

Table B.6. Continuation

mg/kg	B-carb	T-carb	F-pyrox	P-pyrox	Syenite	M-pyrox	Phoscorite	East tailing	Selati tailing
Si	1495.080	560.745	420.664	1045.161	326.666	996.640	921.633	226.060	1100.676
Sr	3271.923	3307.425	153.453	320.743	6.345	479.160	459.589	1382.267	258.860
Th	37.487	52.162	2.504	39.300	30.685	28.947	60.431	159.926	34.890
Ti	130.498	124.902	94.009	142.641	580.533	154.597	152.892	296.354	524.349
U	27.750	0.000	0.486	4.075	1.581	3.642	4.451	46.686	6.726
V	37.250	6.500	1.933	227.125	14.411	13.378	12.094	126.577	22.502
Zn	38.570	54.260	3.016	12.370	5.889	4.950	5.679	6.169	5.742
Zr	0.000	0.000	0.603	3.673	0.851	0.760	0.557	0.897	0.766

Table B. 7. ABACUS calculations based on paste pH, NAG, S% and NP. Interpretation based on NNP of 1) transgressive carbonatite, 2) banded carbonatite 3) East tailing S, 4) East tailing N, 5 East tailing W, 6) East tailing E, 7) Selati tailing N, 8) Selati tailing S, 9) feldspathic pyroxenite, 10) pegmatoidal pyroxenite, 11) Syenite, 12) Micaceous pyroxenite and 13) phoscorite.

Site Name	Initial pH	Final pH	Acid Potential (Open System)	Acid Potential (Closed System)	Base Potential	Net Neutralizing Potential (Open)	Net Neutralizing Potential (Closed)	Interpretation
1	8,693	9,833	7,744	15,488	679,625	671,881	664,137	Probably Excess Neutralizing Minerals
2	8,24	9,37	11,610	23,220	800,625	789,015	777,405	Probably Excess Neutralizing Minerals
3	8,39	7,353	2,312	4,625	335,667	333,354	331,042	Probably Excess Neutralizing Minerals
4	8,583	8,64	2,117	4,234	389,917	387,799	385,682	Probably Excess Neutralizing Minerals
5	8,53	8,78	2,25	4,5	662,917	660,667	658,417	Probably Excess Neutralizing Minerals
6	8,653	8,667	2,097	4,194	289	286,903	284,806	Probably Excess Neutralizing Minerals
7	9,097	6,5	0,312	0,625	54,583	54,271	53,958	Probably Excess Neutralizing Minerals
8	9,11	5,833	0,312	0,625	59,167	58,854	58,5417	Probably Excess Neutralizing Minerals
9	9,317	4,050	0,312	0,625	12,25	11,937	11,625	Verify with other tests
10	9,273	7,347	14,687	29,375	72	57,312	42,625	Probably Excess Neutralizing Minerals
11	9,483	4,95	0,312	0,625	10,167	9,854	9,542	Verify with other tests
12	9,723	5,393	0,312	0,625	25,417	25,104	24,792	Probably Excess Neutralizing Minerals
13	8,82	5,383	0,312	0,625	112,833	112,521	112,208	Probably Excess Neutralizing Minerals

Table B. 8. ABACUS interpretations based on initial and final pH, Net Neutralization Potential (NNP), Neutralization Potential Ratio (NPR), as well as S%-NPR correlations. ABACUS verdict is based on ABA index, the higher the index, the higher the risk to produce acid drainage. of 1) transgressive carbonatite, 2) banded carbonatite 3) East tailing S, 4) East tailing N, 5 East tailing W, 6) East tailing E, 7) Selati tailing N, 8) Selati tailing S, 9) feldspathic pyroxenite, 10) pegmatoidal pyroxenite, 11) Syenite, 12) Micaceous pyroxenite and 13) phoscorite.

Site Number	pH values	Net Neutralizing Potential	NPR (Open System)	NPR (Closed System)	%S and NPR Method(Soregali and Lawrence,1997)	ABA INDEX	VERDICT
1	Lower Acid Risk	Probably Excess Neutralizing Minerals	No Acid Potential	No Acid Potential	Too little S to create sustained acidity	-1	Do Further Testing
2	Lower Acid Risk	Probably Excess Neutralizing Minerals	No Acid Potential	No Acid Potential	Confirm with other testing	-2	Do Further Testing
3	Lower Acid Risk	Probably Excess Neutralizing Minerals	No Acid Potential	No Acid Potential	Too little S to create sustained acidity	-19	Very Low Risk
4	Lower Acid Risk	Probably Excess Neutralizing Minerals	No Acid Potential	No Acid Potential	Too little S to create sustained acidity	-18	Very Low Risk
5	Lower Acid Risk	Probably Excess Neutralizing Minerals	No Acid Potential	No Acid Potential	Too little S to create sustained acidity	-19	Very Low Risk
6	Lower Acid Risk	Probably Excess Neutralizing Minerals	No Acid Potential	No Acid Potential	Too little S to create sustained acidity	-18	Very Low Risk
7	Lower Acid Risk	Probably Excess Neutralizing Minerals	No Acid Potential	No Acid Potential	Too little S to create sustained acidity	-11	Very Low Risk
8	Lower Acid Risk	Probably Excess Neutralizing Minerals	No Acid Potential	No Acid Potential	Too little S to create sustained acidity	-11	Very Low Risk
9	Medium Risk Acid Generation	Verify with other tests	No Acid Potential	No Acid Potential	Too little S to create sustained acidity	-12	Very Low Risk
10	Lower Acid Risk	Probably Excess Neutralizing Minerals	No Acid Potential	Acid under certain conditions	confirm with other testing	-2	Do Further Testing
11	Medium Risk Acid Generation	Verify with other tests	No Acid Potential	No Acid Potential	Too little S to create sustained acidity	-12	Very Low Risk
12	Medium Risk Acid Generation	Probably Excess Neutralizing Minerals	No Acid Potential	No Acid Potential	Too little S to create sustained acidity	-12	Very Low Risk
13	Medium Risk Acid Generation	Probably Excess Neutralizing Minerals	No Acid Potential	No Acid Potential	Too little S to create sustained acidity	-12	Very Low Risk

APPENDIX C. SUPPLEMENTARY MATERIAL OF CHAPTER 6

APPENDIX C.1. FIGURES

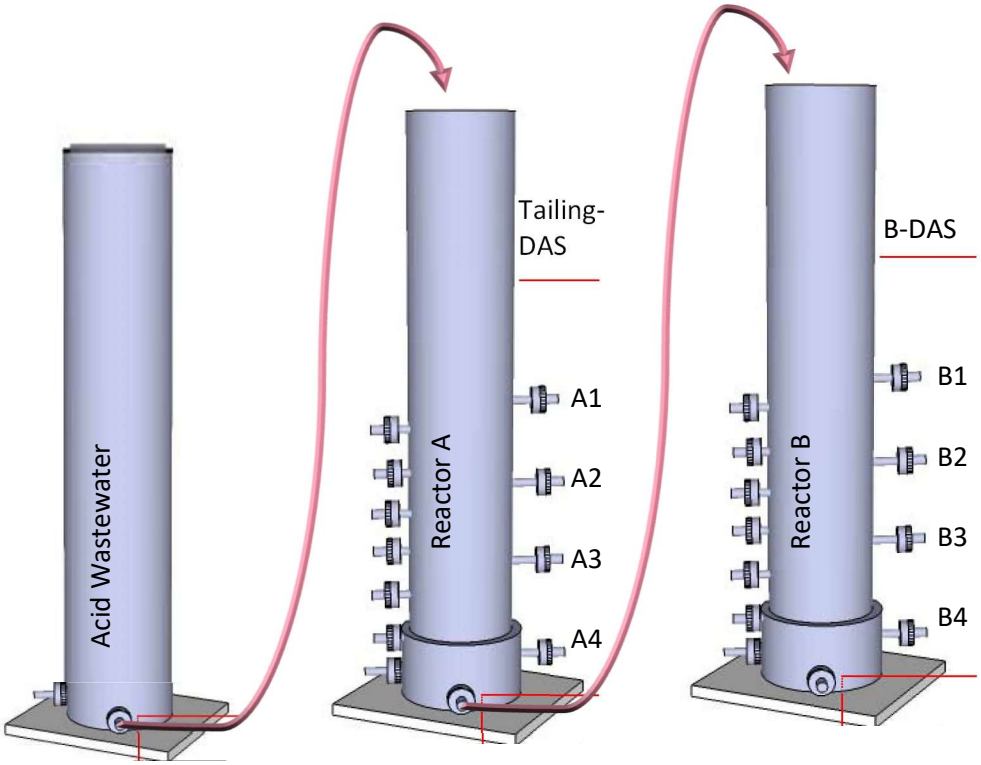

Figure C. 1. Set up of the Dispersed alkaline substrate (DAS) system at lab-scale. Reactors A is filled with a mixture of the woodchips and the material collected in East tailing (from the Cu plant). Reactor B is filled with a mixture of woodchips and witherite ($BaCO_3$) following BDAS system design, as especified in van Heerden et al., 2015.

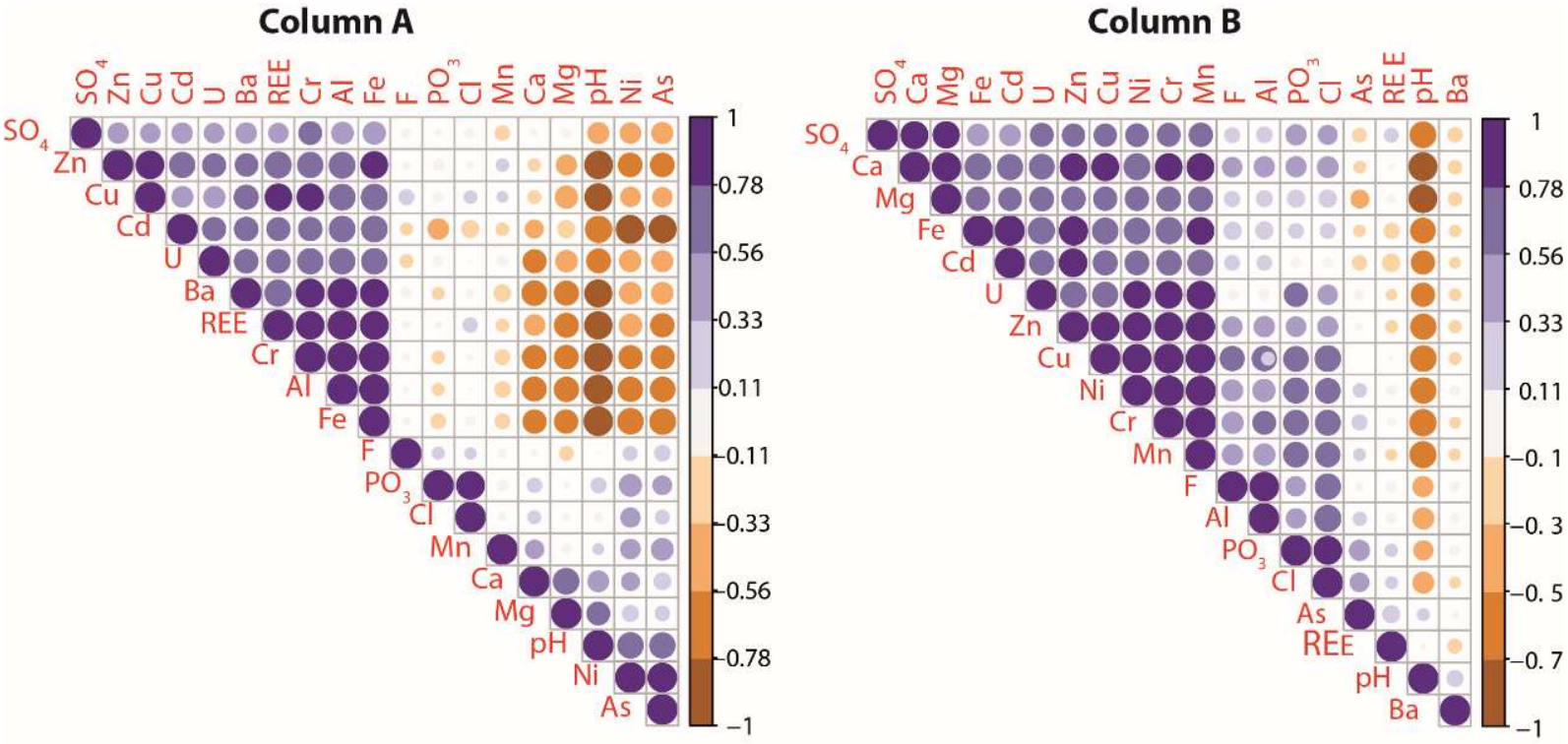

Figure C. 2. Correlation analysis plots of the physicochemical parameters of the water in column A and B. Blue circles represent positive correlations and red circles represent negative correlations. Colour intensity and circle size are proportional to the correlation coefficients, which are shown in the legend to the right of each plot.

APPENDIX C.2. DATA TABLES

Table C. 1. Pseudototal concentration of rare earth elements (in mg/L) in each of the sampling ports of the lab-scale reactor, average from week 1 to 6. Note that "A outlet" is also to be considered as the inlet of column B.

Sampling ports	Ce	Dy	Er	Eu	Gd	Ho	La	Lu	Nd	Pr	Sc	Sm	Tb	Tm	Y	Yb
Inlet A	1.476	0.133	0.150	0.094	0.248	0.024	1.286	0.042	1.293	0.168	0.246	0.403	0.093	0.139	0.833	0.119
A Port 1	1.325	0.045	0.146	0.122	0.438	0.078	1.202	0.057	1.263	0.378	0.237	0.508	0.128	0.032	0.764	0.141
A Port 2	0.308	0.000	0.091	0.052	0.100	0.065	0.197	0.050	0.194	0.209	0.157	0.175	0.089	0.030	0.130	0.098
A Port 3	0.135	0.000	0.081	0.040	0.045	0.062	0.070	0.048	0.040	0.214	0.138	0.121	0.079	0.030	0.001	0.088
A Port 4	0.134	0.011	0.075	0.041	0.046	0.059	0.061	0.048	0.045	0.183	0.130	0.114	0.079	0.031	0.000	0.086
A Outlet	0.141	0.000	0.085	0.040	0.043	0.062	0.064	0.049	0.030	0.205	0.132	0.116	0.078	0.029	0.000	0.087
B Port 1	0.147	0.030	0.076	0.067	0.049	0.069	0.090	0.061	0.108	0.141	0.140	0.120	0.083	0.030	0.036	0.099
B Port 2	0.098	0.032	0.079	0.062	0.051	0.069	0.070	0.060	0.082	0.125	0.134	0.118	0.080	0.030	0.029	0.094
B Port 3	0.090	0.036	0.077	0.066	0.067	0.069	0.067	0.059	0.080	0.106	0.133	0.118	0.077	0.032	0.028	0.093
B Port 4	0.091	0.036	0.077	0.063	0.070	0.069	0.066	0.060	0.077	0.108	0.132	0.115	0.078	0.032	0.027	0.093
B Outlet	0.104	0.047	0.083	0.065	0.068	0.061	0.062	0.057	0.081	0.102	0.133	0.118	0.084	0.034	0.014	0.095

Table C. 2. Sequential extraction performed to the tailing before the interaction, 5 samples collected at the end of the experiment from column A (A1 to A5, from top to bottom) and 5 from column B (B1 to B5, from top to bottom).

Element (mg/kg)	Fraction	Tailing	A1	A2	A3	A4	A5	B1	B2	B3	B4	B5
Al	F1	2.8	862.4	1220.7	733.7	1147.0	1179.7	1057.3	6.5	bdl	bdl	bdl
	F2	42.9	1063.6	934.8	1289.0	5030.4	2222.1	3251.6	532.1	2.1	bdl	bdl
	F3	6.8	11.3	18.3	63.0	108.3	52.6	71.2	bdl	bdl	bdl	bdl
	F4	6525.5	6324.2	11563.2	19265.9	19262.3	20471.9	10785.6	6243.5	1983.4	769.3	488.0
As	F1	0.939	4.253	2.387	5.147	1.373	0.893	bdl	bdl	bdl	0.907	bdl
	F2	0.573	bdl	bdl	bdl	4.013	0.627	1.267	bdl	bdl	bdl	bdl
	F3	0.122	bdl	bdl	bdl	bdl	bdl	0.183	bdl	bdl	bdl	bdl
	F4	6.405	6.667	11.333	10.867	9.000	4.733	bdl	bdl	bdl	bdl	bdl
B	F1	bdl	8.92	6.85	4.67	19.44	17.39	22.32	6.87	12.16	15.61	16.72
	F2	0.426	7.93	3.72	bdl	15.93	6.87	22.80	4.45	6.81	5.99	1.69
	F3	10.060	4.95	3.13	3.33	7.77	6.83	5.02	4.88	22.57	15.23	11.78
	F4	14.405	574.20	470.43	467.73	327.27	439.90	34.33	0.27	bdl	bdl	bdl
Ba	F1	129.4	2.9	4.2	3.8	3.3	4.9	26.7	2.1	2.6	95.7	73.8
	F2	111.1	4.9	1.6	18.4	43.7	53.4	83.5	115.9	155.5	3117.8	445.1
	F3	13.3	1.8	1.9	0.5	bdl	bdl	36.8	43.4	128.3	409.2	422.2
	F4	219.3	1113.2	1063.4	1214.2	989.0	1557.2	2593.0	4288.4	4843.2	4077.8	5460.5
Be	F1	na.	63.1	41.3	14.0	60.7	77.1	66.8	43.5	42.3	41.6	84.4
	F2	na.	3905.2	5159.1	2473.6	0.0	266.9	bdl	165.3	42.4	38.0	38.4
	F3	na.	41.3	40.7	40.9	38.9	37.8	38.0	38.1	34.4	34.0	34.5
	F4	na.	bdl	bdl	bdl	bdl	bdl	50269.9	10969.8	2554.4	1070.3	606.8
Ca	F1	19717	35565	37504	50967	41181	47109	55946	4891	978	745	6709
	F2	17128	60513	16618	7442	45012	31263	28479	69720	45720	26336	19354
	F3	308	583	632	971	1359	1108	1026	3133	332	2099	435
	F4	13025	51491	103737	175048	155101	234226	28977	40248	58713	37820	981

Table C.2. Continuation

Element (mg/kg)	Fraction	Tailing	A1	A2	A3	A4	A5	B1	B2	B3	B4	B5
Cd	F1	0.011	0.067	0.000	0.027	0.120	0.053	0.253	0.067	0.160	0.280	0.093
	F2	<0,002	0.133	0.320	0.107	0.147	0.147	1.133	0.960	0.947	0.800	0.547
	F3	0.011	0.083	0.167	0.000	0.250	0.317	0.433	0.100	0.550	0.500	0.367
	F4	0.272	15.533	12.600	12.767	8.433	11.267	0.933	0.267	0.067	0.467	bdl
Co	F1	1.013	1.267	1.253	1.520	8.840	8.187	11.507	7.427	5.587	7.587	38.627
	F2	1.789	1.440	2.760	5.040	2.840	2.227	5.707	9.027	23.160	39.147	12.600
	F3	1.388	14.000	8.083	9.767	6.900	7.817	5.433	7.183	5.700	5.683	4.217
	F4	59.255	77.600	67.700	69.867	51.533	74.200	0.767	bdl	bdl	bdl	bdl
Cr	F1	0.194	0.613	0.867	0.960	3.120	3.413	4.373	2.227	2.147	1.880	4.827
	F2	0.233	17.427	31.813	14.933	1.867	1.933	10.973	3.787	3.680	3.627	2.627
	F3	0.086	1.783	1.867	2.633	1.833	1.667	7.217	2.567	1.833	2.017	1.783
	F4	30.963	52.467	61.067	179.867	168.567	216.867	255.600	123.867	61.133	31.533	24.133
Cu	F1	104.94	56.93	85.51	89.29	106.29	143.59	674.93	5.03	1.29	0.00	48.96
	F2	93.73	43.37	58.75	94.99	102.59	132.65	1030.55	1088.19	562.64	293.21	144.00
	F3	265.19	491.07	381.58	221.85	135.32	186.13	62.43	87.90	2.55	4.42	44.93
	F4	567.75	336.63	494.03	899.87	688.23	1221.47	457.83	744.43	649.80	582.20	392.53
F	F1	8.8	2413	2400	2413	3480	5147	5880	2360	2320	2440	24160
	F2	bdl	6480	10200	20267	16000	10453	12280	10760	9880	13400	8760
	F3	bdl	1450	1700	2100	2250	2467	7350	3500	4350	4300	270
	F4	bdl	3467	15780	35867	28900	24867	19600	17800	7200	5600	1500
Fe	F1	bdl	53.1	32.0	6.9	10.9	33.4	15.5	3.6	3.7	3.6	6.8
	F2	784.2	3933.1	3115.5	1322.4	1749.1	733.3	7994.4	173.9	17.8	10.2	7.6
	F3	20.5	4.0	4.3	4.2	4.6	4.4	4.4	4.3	4.1	4.1	4.2
	F4	116195	135555	120796	130606	80728	120290	27702	11113	4022	1980	1039

Table C.2. Continuation

Element (mg/kg)	Fraction	Tailing	A1	A2	A3	A4	A5	B1	B2	B3	B4	B5
K	F1	394	817	1034	707	1437	1021	4103	2875	2268	2459	2710
	F2	41	493	2244	4279	1603	926	3109	2464	813	510	250
	F3	100	615	569	1316	1406	1371	1081	845	269	232	270
	F4	bdl	2845	2976	4658	3421	5318	184	144	122	234	74
Li	F1	bdl	3.933	3.253	2.347	1.960	2.587	5.227	bdl	bdl	bdl	bdl
	F2	0.097	bdl	bdl	bdl	3.533	0.813	0.293	0.333	bdl	bdl	bdl
	F3	0.062	bdl	bdl	bdl	bdl	bdl	bdl	bdl	bdl	bdl	bdl
	F4	2.139	0.267	0.467	2.433	1.067	2.500	bdl	bdl	bdl	bdl	bdl
Mg	F1	4439	2158	3848	3523	3409	2425	6970	4827	4228	3640	24954
	F2	9152	472	1213	2657	2498	1998	2726	5729	21070	34508	8539
	F3	2032	348	419	1156	991	1268	336	602	415	541	170
	F4	78812	15109	18422	32976	30591	56808	566	817	435	342	122
Mn	F1	152.88	36.55	45.45	63.69	49.92	66.27	344.53	112.29	56.05	21.55	554.97
	F2	146.20	27.03	32.23	42.83	82.65	84.41	227.96	535.83	830.44	910.49	674.63
	F3	6.28	3.78	4.57	9.45	8.93	10.22	10.37	18.00	0.17	0.07	19.15
	F4	607.84	725.20	687.97	849.53	693.27	1081.87	96.57	190.37	446.47	952.83	332.57
Mo	F1	0.008	1.973	2.213	2.040	2.947	1.187	5.400	0.827	2.533	0.880	1.787
	F2	0.073	0.373	0.347	0.080	0.627	0.533	0.987	0.267	1.040	0.800	0.600
	F3	0.418	0.967	0.817	0.900	1.733	1.150	1.433	1.017	1.383	1.150	0.750
	F4	1.268	64.333	50.667	53.000	80.333	56.667	0.367	bdl	1.133	0.300	0.133
Na	F1	148	1945	2267	1822	2532	2513	6036	1859	1283	1495	1432
	F2	140	534	460	712	1945	1015	1319	1483	727	502	271
	F3	4909	739	850	987	790	967	893	1202	917	1009	1001
	F4	3953	1491	2910	3808	3184	3259	708	645	809	823	583

Table C.2. Continuation

Element (mg/kg)	Fraction	Tailing	A1	A2	A3	A4	A5	B1	B2	B3	B4	B5
Ni	F1	1.47	2.51	2.56	2.59	6.67	5.44	13.01	9.33	8.01	10.27	42.05
	F2	3.30	2.69	4.92	4.61	1.84	1.73	6.24	9.24	23.67	46.85	13.00
	F3	3.95	8.67	6.82	6.62	5.12	6.63	4.15	4.28	3.08	3.60	3.35
	F4	127.09	121.40	101.10	112.10	78.47	106.43	3.43	3.17	0.43	1.27	1.53
P	F1	bdl	4388	7788	8983	9409	bdl	bdl	20697	16036	15676	bdl
	F2	bdl	bdl	bdl	bdl	bdl	bdl	bdl	61536	95331	113309	55419
	F3	3179	2338	2617	3175	bdl	bdl	bdl	9452	7413	12532	bdl
	F4	18702	22840	34123	46393	39270	49325	27133	33233	48920	34830	4677
Pb	F1	bdl	2.720	0.640	1.480	1.880	0.200	1.893	0.200	0.427	0.053	0.560
	F2	<0,01	4.053	1.733	0.000	1.707	0.987	1.773	1.147	1.413	0.600	1.827
	F3	0.201	0.817	0.367	2.483	0.417	0.783	0.467	0.200	1.917	0.100	0.817
	F4	24.768	66.867	58.333	55.200	39.700	48.667	bdl	bdl	0.267	bdl	1.267
S	F1	1321	105161	106579	105189	72635	39310	80773	30789	9320	4769	7167
	F2	1150	130711	36314	10157	9182	4328	13015	15693	8005	3011	2846
	F3	678	2299	2033	2598	1633	1522	2994	3774	2345	1457	886
	F4	1503	6903	8666	15018	13278	19418	2861	3883	5588	3800	2044
Sb	F1	na.	5.08	5.40	6.97	8.33	4.03	2.15	2.60	3.24	3.29	5.59
	F2	na.	1.03	3.65	0.77	3.96	bdl	0.05	0.69	0.47	0.67	0.03
	F3	na.	1.27	5.65	3.00	4.10	5.00	3.18	4.52	4.68	3.85	1.87
	F4	na.	73.00	63.67	42.33	50.00	91.33	bdl	bdl	2.50	9.07	5.67
Se	F1	2.01	0.17	0.25	1.89	21.23	21.57	13.40	11.87	11.47	20.17	29.17
	F2	0.50	0.03	13.83	8.96	0.00	4.15	2.15	1.71	3.29	9.31	5.16
	F3	0.05	13.48	19.57	11.30	17.27	13.03	17.03	15.85	22.10	10.92	9.10
	F4	8.72	bdl	bdl	bdl	bdl	bdl	bdl	1.83	1.30	bdl	bdl

Table C.2. Continuation

Element (mg/kg)	Fraction	Tailing	A1	A2	A3	A4	A5	B1	B2	B3	B4	B5
Si	F1	1.9	579.2	270.7	188.1	146.5	152.3	270.6	140.2	138.1	140.3	124.6
	F2	114.6	1346.8	1129.8	907.2	386.8	345.1	1612.7	168.4	107.7	103.6	71.7
	F3	87.4	280.1	336.8	343.7	107.0	133.0	427.1	582.5	605.9	608.5	675.8
	F4	22.1	174.9	2501.1	10020.8	9414.8	6383.1	5860.2	4255.8	894.5	325.0	41.1
Sn	F1	na.	37.7	46.6	65.2	49.5	63.4	333.7	108.4	53.7	20.4	1102.4
	F2	na.	25.7	30.6	40.9	81.6	82.9	223.7	527.2	1230.5	1456.2	667.0
	F3	na.	3.5	4.3	9.0	8.5	9.8	9.9	17.4	bdl	0.0	18.6
	F4	na.	681.0	649.2	806.5	658.1	1030.2	90.7	181.1	427.2	912.1	316.9
Sr	F1	582.3	284.1	350.0	541.6	374.7	388.2	127.2	14.4	4.4	11.2	28.7
	F2	483.7	489.8	470.6	534.6	967.2	746.4	548.5	319.7	176.3	148.9	88.9
	F3	6.6	21.8	24.3	37.5	30.0	27.1	42.3	33.4	10.5	25.7	51.5
	F4	309.6	602.7	1026.5	2206.8	2324.3	3235.2	1921.9	1136.6	624.7	399.4	187.3
U	F1	bdl	bdl	bdl	bdl	bdl	bdl	bdl	bdl	bdl	19.38	2.75
	F2	0.16	bdl	bdl	bdl	bdl	0.93	2.25	bdl	5.13	412.13	70.20
	F3	bdl	bdl	bdl	bdl	bdl	bdl	4.78	3.74	24.58	80.35	86.41
	F4	46.52	97.52	65.10	57.48	46.37	82.43	270.33	289.07	252.59	323.38	160.19
V	F1	0.01	37.25	47.21	67.52	59.40	72.07	349.24	117.32	61.67	27.96	1096.6
	F2	0.31	30.37	42.57	52.92	79.40	84.47	233.97	530.25	1224.1	1442.20	667.63
	F3	0.36	11.43	12.20	17.02	16.08	17.32	17.32	24.85	6.65	6.47	25.75
	F4	125.90	834.53	772.53	928.30	742.27	1141.60	103.53	186.37	433.00	928.77	320.87
Zn	F1	bdl	6.67	6.47	6.23	10.91	17.19	74.31	2.81	1.37	1.75	3.57
	F2	bdl	4.23	3.75	5.57	14.37	18.24	104.57	101.65	19.91	4.29	6.69
	F3	1.57	3.63	2.95	1.18	0.78	1.72	1.35	0.57	0.33	bdl	0.58
	F4	4.60	90.80	81.83	102.90	68.23	118.77	72.00	141.93	168.47	129.53	167.47

bdl: below detection limit; na: not analysed

APPENDIX C.3. SEM-EDS IMAGES

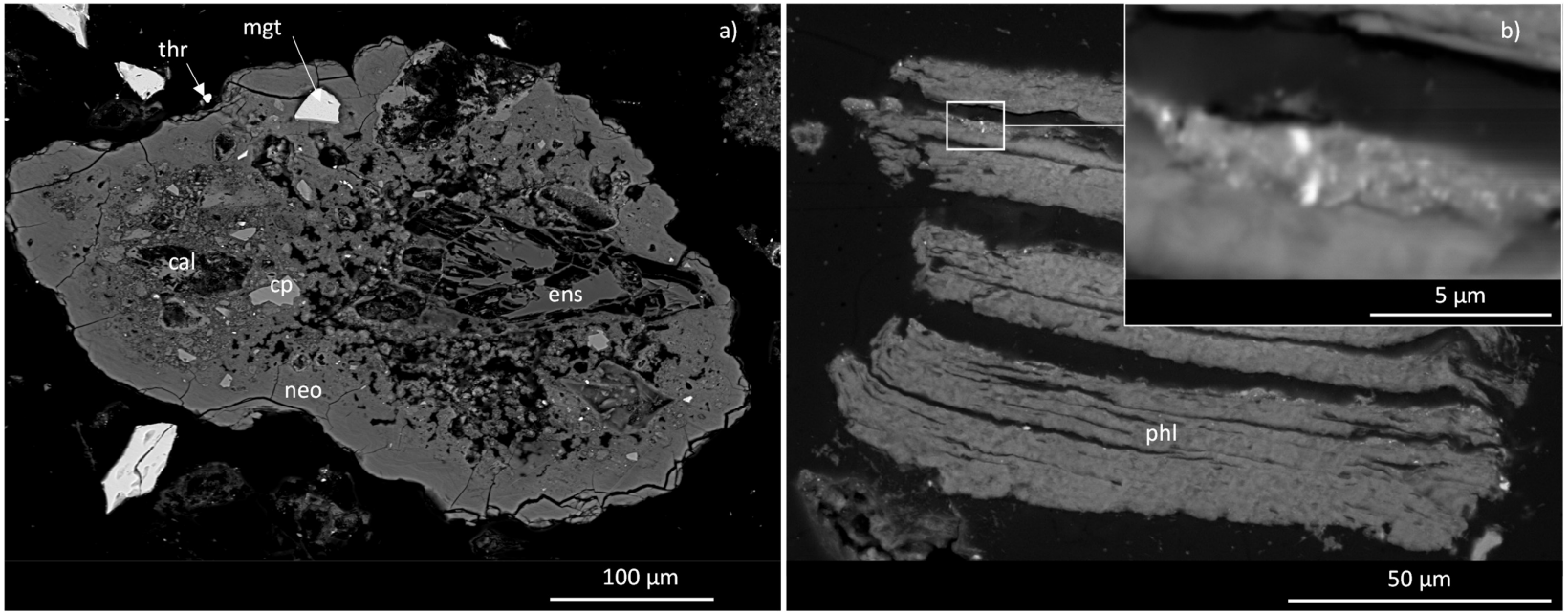

Figure C. 3. Scanning electron microscope (SEM) images from the top of column A showing a) Polimictic and heterometric fragment of rock forming minerals including magnetite (mgt), chalcopyrite (cp), enstatite (ens) and calcite (cal) embedded by a newly-formed botroids of Ca-Al-halide-phosphate (neo); and b) aggregate of newly formed Fe-Cr oxyhydroxide in the interlayers of exfoliation of the phlogopite.

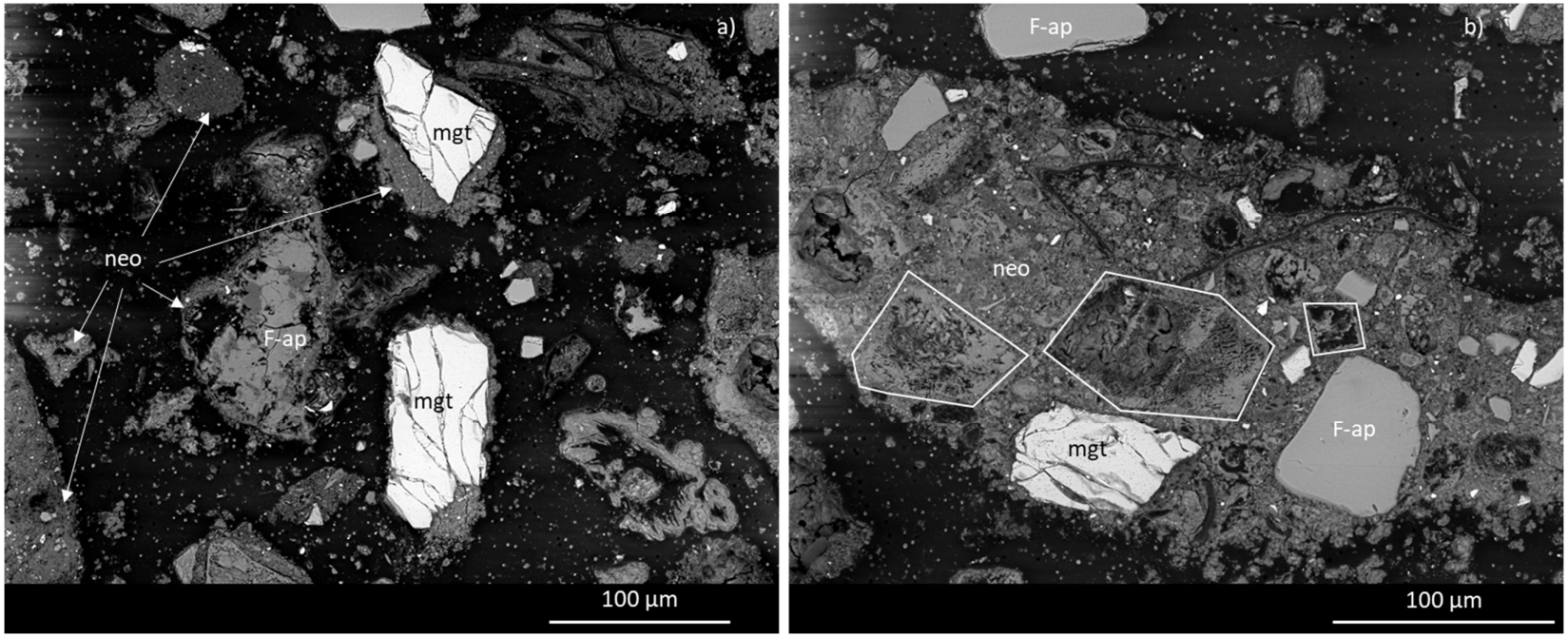

Figure C. 4. Scanning electron microscope (SEM) images from the middle of column A showing newly-formed Ca-Al-F phosphate (neo) embedding fragments of magnetite (mgt) and fluorapatite (F-ap) in images a) and b); and pseudomorph Ca-Al-F phosphates of dissolved calcites retaining their crystal forms (marked in white).

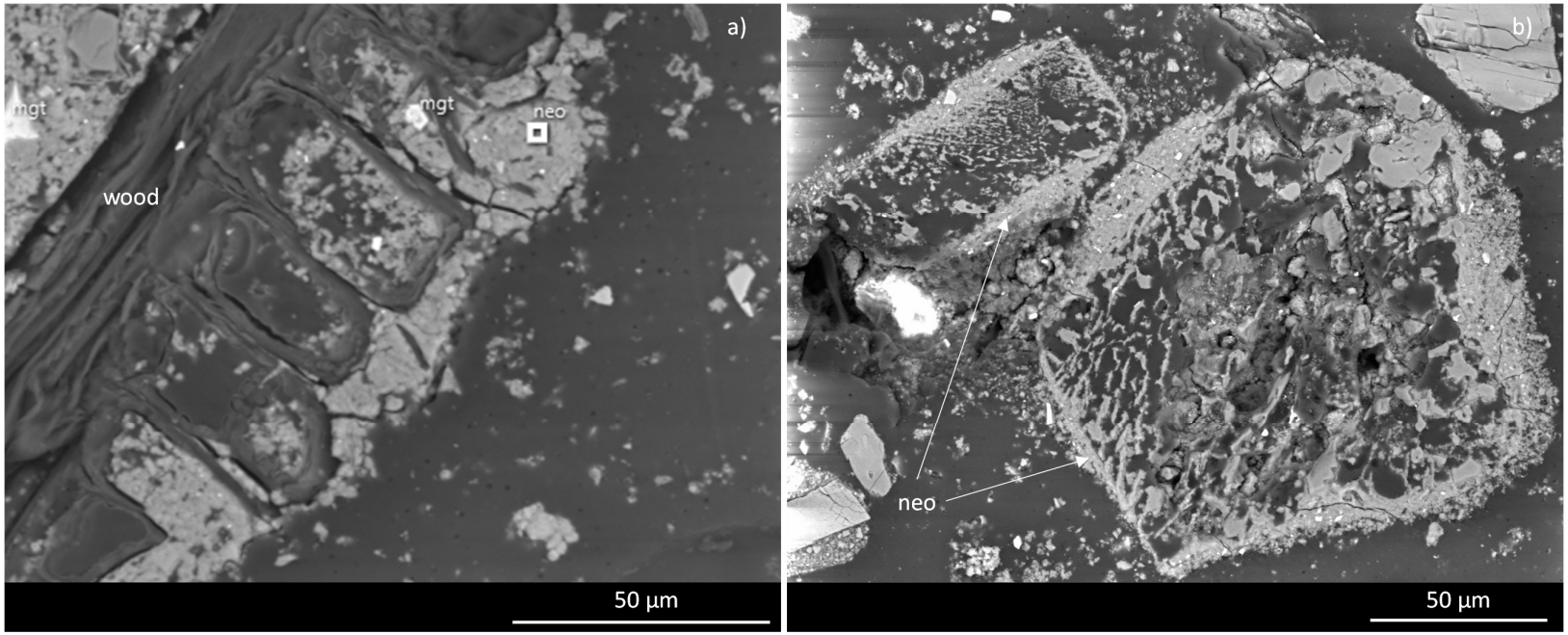

Figure C. 5. Scanning electron microscope (SEM) images from the bottom of column A showing a) Newly-formed Ca-Al-F phosphate (neo) filling open spaces and encapsulating a wood fragment, embedding fragments of magnetite (mgt); and b) pseudomorph Ca-Al-F phosphates of dissolved calcites retaining their crystal forms.

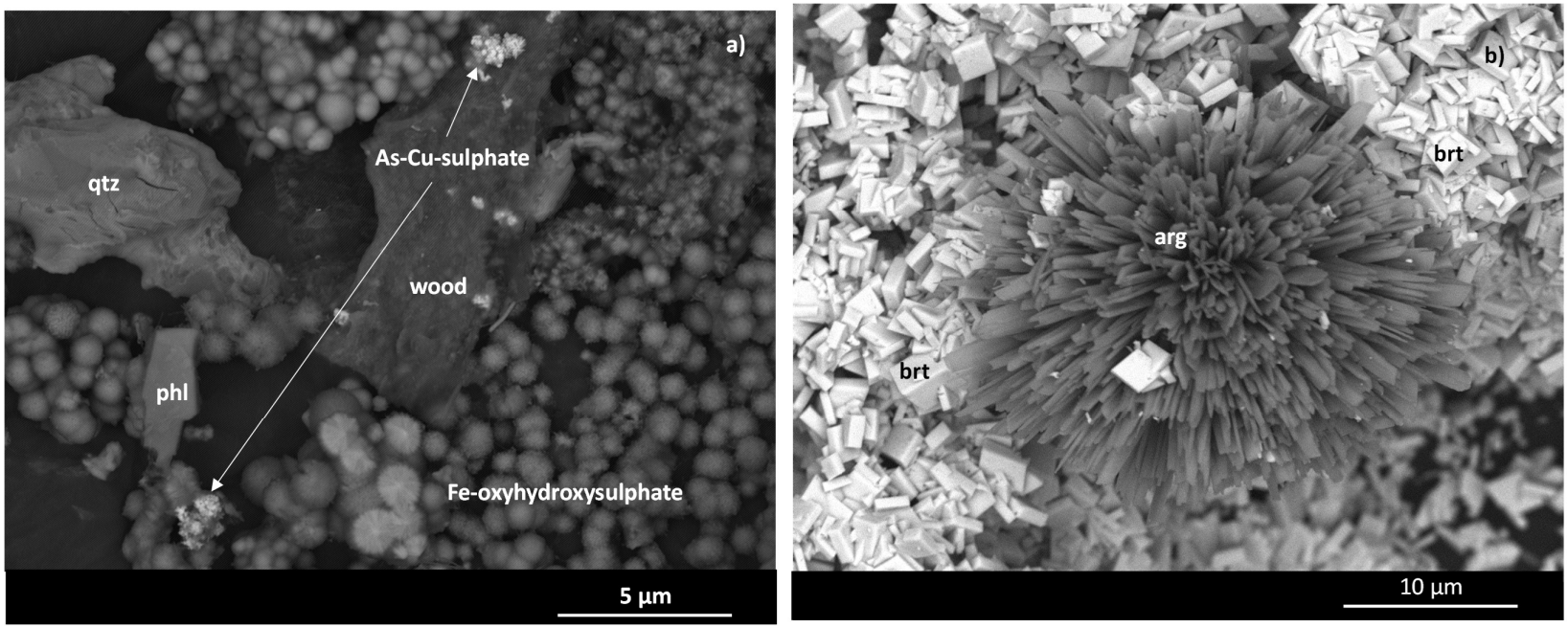

Figure C. 6. Scanning electron microscope (SEM) image of carbon coated sample from the top of column B showing a) relict fragments of quartz and phlogopite, as well as radial aggregates of newly formed Fe-oxyhydroxysulfate and fine-grained skeletal As-Cu-sulphate growing on both the wood and the Fe-oxyhydroxysulfate; and b) newly formed minerals such as radial aragonite (arg) aggregate included in a matrix formed by euhedral barite (brt) crystals.

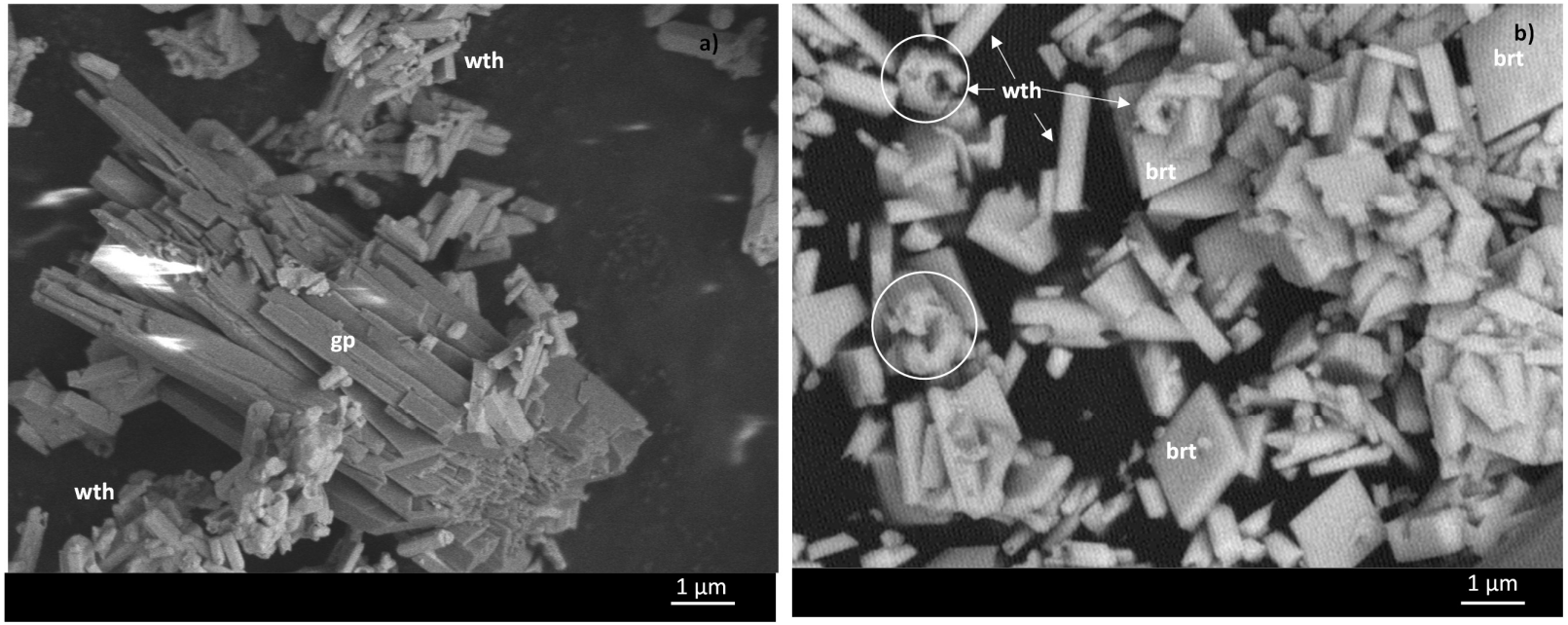

Figure C. 7. Scanning electron microscope (SEM) image of a) uncoated sample from the middle of column A showing newly formed gypsum aggregate associated to undissolved witherite (wth) crystals; and b) newly formed euhedral and subhedral barite crystals with witherite (wth) crystal showing dissolution marks (circles).